Field Testing and Load Rating of a Steel-Girder Highway Bridge

by

Peter Schönwetter, B.S.

Thesis

Presented to the Faculty of the Graduate School

of The University of Texas at Austin

in Partial Fulfillment

of the Requirements

for the Degree of

Master of Science in Engineering

The University of Texas at Austin

May 1999

Field Testing and Load Rating of a Steel-Girder Highway Bridge

APPROVED BY

SUPERVISING COMMITTEE:

_____

Karl H. Frank

_____

Joseph A. Yura

The best thing
about banging your head
against a brick wall,
is that it feels
really, really good
when you stop.

-unknown

ACKNOWLEDGMENTS

I would like to thank Dr. Karl Frank and Dr. Joseph Yura for their guidance during the course of this research project. In particular, the field testing portion of this project would not have been possible without their expert help and advice. I would also like to thank Dr. Sharon Wood for her insight on the structural concrete aspects of this project and for her patient advice on graduate school and graduate research.

This thesis would not have been completed without the abundant help of Dr. Howard Liljestrand. His enthusiasm for graduate research and his dedication to his students are equaled only by his expertise and his patience.

I would like to thank David Jauregui and Loyl Bussell for all of their tireless help. They built, carried, calculated, drove, instrumented, listened, load tested, soldered, and lost sleep at every opportunity to make sure that the field tests were done right. In addition, I would like to thank Nicole Garcia, Dave McIlrath, Norm Grady, Blanca Velázquez, Mike Cooper, and Michelle Parsley for lending a hand when a hand was needed.

I would also like to thank the staff of the Ferguson Structural Engineering Laboratory, especially Ray Madonna for letting me root through his abundantly-stocked drawers of electronic parts without too much fuss, and Laurie Golding for her patience and understanding. They both knew just what I needed, and how to find it.

In addition, I would like to thank the Texas Department of Transportation for sponsoring this research project. In particular, thank you to Mike Lynch and Wayne Clendennan for providing plenty of support and enthusiasm.

Finally, I would like to thank my parents, Heribert and Patricia Schönwetter, and the rest of my extended family, for all of their love and support.

May 7, 1999

Field Testing and Load Rating of a Steel-Girder Highway Bridge

by

Peter Schönwetter, M.S.E.

The University of Texas at Austin, 1999

Supervisor: Karl H. Frank

The load rating of a highway bridge is often underestimated by engineering analysis. A method is presented for improving the load rating of a continuous-span concrete-slab-on-steel-girder highway bridge through field testing. Bonded foil-type strain gages and an electronic data acquisition system were used to evaluate the neutral axis locations, composite behavior, moment distribution behavior, and noncomposite deck flexure in the bridge. Data was recorded at thirty gage locations during a series of crawl-speed dynamic tests. As a result, the bridge's AASHTO LFD operating and inventory load ratings were both improved by a factor of 1.25.

CONTENTS

CHAPTER 1
Introduction

In recent years, the Texas Department of Transportation (TxDOT) has become concerned over the condition of many of the older highway bridges in Texas. Engineering analysis and load rating calculations indicate that many of these bridges are not capable of carrying modern vehicle loads. To reduce the risk of a catastrophic failure, many of these bridges have been posted with load restrictions. Others have been closed to traffic. The detours, repairs, and new construction caused by the postings and closures have resulted in significant expense to the public and to industry.

In 1996, an informal survey conducted by TxDOT indicated that there were hundreds of bridges with insufficient load ratings under TxDOT's jurisdiction. In an attempt to reduce the number of bridges on this list, TxDOT sponsored a research project through the Ferguson Structural Engineering Laboratory at the University of Texas at Austin. The goal of this project was to develop a method for load testing many types of highway bridges in order to more accurately assess their load capacity. As part of TxDOT's load testing project, a load test was performed on a concrete-slab-on-steel-girder highway bridge, the results of which are presented herein.

1.1 A Comparison of Design Calculations and Load Rating Calculations

The decision to post or close a bridge is often based on the results of a load rating calculation. This rating is determined by comparing the moments, shears, and stresses caused by a heavy vehicle with the available capacity of the bridge. Similar to load rating procedures, standard bridge design codes present methods for calculating the moments, shears, and stresses in the bridge and for calculating the available capacity of the bridge. Since most engineers are already familiar with the methods presented in the design codes, they often use these same methods during a rating analysis. In fact, design and rating calculations are so similar that even the vehicles used for rating are design trucks, such as the AASHTO HS-20-44 and HS-25-44 vehicles.

The rating-as-design method has some advantages. Since the same loads and same analysis techniques are used for rating old bridges and for designing new ones, the engineer can directly compare the capacity of an older bridge with the capacity of a replacement design. This helps to simplify the decision to replace the bridge, repair it, or leave it alone. However, this method may result in overly conservative load ratings, since the design vehicles and design codes only approximate the actual loading, condition, and capacity of the bridge.

There is one major difference between design calculations and load rating calculations. For load rating calculations, the bridge is already in place. The existence of the bridge presents an advantage over design calculations, since design calculations must make do with assumptions as to what loads the bridge will carry and how the bridge will behave under those loads. Load testing can be used to determine the exact load carrying behavior of the bridge and possibly improve its load rating.

Several research studies have shown that the calculations used in design often underestimate the actual strength of a bridge, and that the rating of a bridge can be improved through nondestructive load testing (Bakht and Jaeger 1990; Chajes et al. 1997; Commander 1989; Pinjarkar et al. 1990). As a result of these research studies, the practice of improving bridge load ratings through load testing has recently become very popular. Several states, including Alabama, Florida and New York, have developed organized load testing programs in order to reduce the number of posted and closed bridges on their highways.

1.2 Types of Load Testing

There are two methods of testing used to load rate bridges: diagnostic tests and proof tests. The AASHTO Manual for Condition Evaluation of Bridges (1994b, 47) defines a diagnostic test as a test "performed to determine the effect on various components of a known load on the structure." A proof test is defined as a test to "directly determine the maximum live load that the bridge can carry safely."

Proof tests are inherently riskier than diagnostic tests, in the sense that the bridge structure may be permanently damaged by an excessive proof load. The advantage of a

successful proof test is that it determines the exact capacity of the bridge. There is no room for argument when the load in question has actually been carried by the bridge. Proof tests are not very useful for understanding the behavior of the bridge, because they focus only on the weight of the test vehicle. Strain and deflection data are usually not measured during a proof test.

Diagnostic tests measure strain and deflection in the bridge to evaluate the bridge's response to a known load. The measured data can be compared directly to the results of a structural analysis. Therefore, diagnostic tests are useful for understanding the load carrying behavior of a bridge and adjusting the bridge's load rating. However, the data from a diagnostic test only applies to loads equal to and less than the load used during testing. It is dangerous to extrapolate an understanding of the bridge's load bearing behavior to heavier loads, and a sudden or even catastrophic failure may result.

The load tests performed during the course of this research project were diagnostic tests, because our goal was to better understand the bridge's behavior. Furthermore, proof tests were not performed in an effort to reduce the risk of damaging the bridge.

1.3 Methods of Structural Analysis and Load Rating

There are three methods of structural analysis that can be used to design a bridge or evaluate a bridge's behavior. They are the allowable stress design method (ASD), the load factor design method (LFD), and the load and resistance factor design method (LRFD). The AASHTO Manual (1994b, 50) introduces the ASD method as follows:

> The allowable or working stress method constitutes a traditional specification to provide structural safety. The actual loadings are combined to produce a maximum stress in a member which is not to exceed the allowable or working stress. The latter is found by taking the limiting stress of the material and applying an appropriate factor of safety.

The AASHTO Manual also introduces the LFD method as follows:

> The load factor method is based on analyzing a structure subject to multiples of the actual loads (factored loads). Different factors are applied to each type of load which reflect the uncertainty inherent in the load calculations. The rating is determined such that the effect of the factored loads does not exceed the strength of the member.

To summarize, the ASD method compares the actual loads on the bridge against an allowable level of stress in each member, while the LFD method compares factored loads against the load resisting strength of each member.

A newer method for structural design and analysis is the LRFD method. The LRFD method is an extension of the LFD method. In the LRFD method the strength of each member is modified by a resistance factor to account for the uncertainty inherent in the strength calculations. Although this method has been adopted by the American Institute of Steel Construction (AISC 1994) and the American Concrete Institute (ACI-318 1995) for some time now, AASHTO has issued a LRFD specification (1994a) only recently. Consequently, the full provisions of the AASHTO LRFD code are only

starting to be used in practice, and the AASHTO Manual does not specifically address the LRFD method of design and rating.

The Big Creek Relief Bridge was built in 1954. Because of its age, the bridge was probably designed using the ASD method. However, the ASD method is no longer used in the practice of bridge design or load rating. The AASHTO LFD method (1992) was chosen for use in this research study, because of its current widespread acceptance by highway bridge design engineers. The LFD method was also chosen, because it often results in an improved load rating for the bridge, over the ASD method.

In this study, the AASHTO LFD method was modified by using the AASHTO LRFD provisions for moment distribution, shear distribution, and live load placement. The provisions in the AASHTO LRFD code represent the results of a wider and more recent body of accepted research, in comparison with the AASHTO LFD code. The provisions in the AASHTO LRFD code also make use of a larger set of variables in assessing the behavior of the bridge.

1.4 Inventory and Operating Ratings

In the ASD and LFD methods of bridge rating, the bridge is assigned two load ratings: inventory and operating. The inventory rating describes the level of load that the bridge can sustain for an indefinite length of time without suffering damage. The operating rating describes the maximum load that the bridge can carry, with the expectation that repeated exposure to the operating load will shorten the lifespan of the bridge. Both inventory and operating ratings were calculated for the Big Creek Relief Bridge as part of this study.

1.5 Sources of Additional Strength

The goal of load testing is to improve a bridge's load rating to avoid the expensive remedies of posting, closing, or replacing the bridge. The bridge's load rating is improved by identifying sources of additional strength that were not considered or were underestimated in the standard rating procedure. Then those additional strengths are included in a revised rating calculation.

In a slab-on-girder highway bridge, additional strength may be provided by unintended composite action between the girders and the deck, greater lateral moment and shear distribution across the superstructure, noncomposite flexure of the deck, and flexural participation of the curb and parapet. The load tests performed on the Big Creek Relief Bridge focused on gathering data to evaluate these potential sources of additional strength and improving the load rating of the bridge.

The following sections present an overview of these four sources of additional strength, but they are far from comprehensive. Further information on highway bridge behavior, design, and analysis can be found in Bridge Engineering, by Tonias (1995).

1.5.1 Additional Strength Due to Unintended Composite Action

Unintended composite action is the result of bonding between the top flange of a steel girder and the underside of the cast-in-place concrete deck. The steel-concrete bond allows for the transfer of longitudinal shear forces between the girder and the deck, resulting in composite flexure. A composite girder is stiffer and stronger than a similar noncomposite girder and is able to carry higher vehicle loads, thereby improving the load rating of the bridge.

The presence of unintended composite action can be evaluated by locating the neutral axis of the girder. The neutral axis location is found by measuring strain at several points through the depth of the cross section. Since bridge girders are supposed to remain elastic under both service loads and field test loads, the strain in the girder varies linearly from the top of the girder to the bottom. There is exactly one point where the strain is zero. By definition, this point is the location of the neutral axis.

In a noncomposite girder, the neutral axis is located at the center of gravity of the steel girder alone. If the girder is acting compositely with the deck, then the neutral axis is located above the center of gravity of the steel girder, closer to the deck. The neutral axis location provides a clear indication of the presence or absence of unintended composite behavior.

The girders on the Big Creek Relief Bridge were not designed to behave compositely and, therefore, did not contain shear studs or any other mechanical means of

transferring shear between the deck and the girders. However, the top flange of each girder was embedded in the deck. Because of the large bond surface provided by the embedded flanges, the possibility that some or all of the girders were behaving in a composite manner was investigated during the load tests.

1.5.2 Additional Strength Due to Load Distribution

Load distribution refers to the ability of the bridge superstructure to disperse a vehicle's load among all of the girders in the superstructure. It is caused by interaction between all of the elements of the superstructure as the girders nearest to the truck deflect under the vehicle's load. The result is a lateral spreading of the load among all of the girders, with the largest portions of the load carried by the girders underneath the truck and smaller portions of the load carried by the girders farther away. The largest fraction of the truck's weight applied to a girder is referred to as the load distribution factor for that girder.

Most design codes use a set of equations to determine the distribution factor for each girder, and each load case. Two examples are: the AASHTO Standard Specifications for Highway Bridges (1992) and the AASHTO LRFD Bridge Design Specifications (1994a). These codes divide bridge girders into two categories, interior and exterior, and provide equations for determining the distribution factors for positive moment, negative moment, and shear. Most of the distribution factor equations are empirical in nature and are based on the physical properties of the deck and girder materials, as well as geometric variables such as the deck thickness, the girder spacing, and the girder depth.

Standard load rating calculations are performed using the distribution factor equations from the design codes. However, the distribution factors specified by the design codes have been shown to be conservative in many cases (Tonias 1995, 125). Instead of relying on the design code estimates, load testing may reveal that the bridge is more efficient at distributing moments and shears. By modifying the load rating calculations to account for the actual distribution behavior of the bridge, the bridge's load rating may change.

The lateral moment distribution behavior of a bridge can be evaluated by measuring the strain on the bottom flange of each girder while the bridge is under load. If each of the girders has the same section properties, then the distribution of strain among the girders is analogous to the distribution of moment in the bridge. If the girders have varying section properties, then more calculations are necessary to convert the measured strain distribution into moment distribution. In either case, the ratio of the moment in one girder to the sum of the moments in all of the girders is the lateral moment distribution factor for that girder.

The lateral moment distribution behavior of the Big Creek Relief Bridge was evaluated, because it was likely to result in an improvement in the bridge's load rating. Unlike other sources of additional strength, lateral moment distribution occurs in every bridge. Improving the bridge's load rating is a matter of assessing the degree of lateral moment distribution, rather than diagnosing whether it is or is not present.

The standard load rating calculations showed that the shear strength of the bridge was more than adequate. Therefore, load testing to determine the actual shear distribution behavior of the bridge was unnecessary. The bridge's high shear strength was not surprising, because the girders are rolled-steel sections. As with most rolled sections, their shear capacity is much greater than their moment capacity, in the sense that the truck weight necessary to cause a shear failure is much greater than the truck weight necessary to cause a flexural failure. This condition is typical of most steel girder highway bridges with rolled sections, when subject to common truck loads.

1.5.3 Additional Strength Due to Noncomposite Flexure of the Deck

In the design or load rating of a noncomposite highway bridge, it is assumed that the girders resist the entire live load moment. However, when the bridge girders flex under load the deck flexes along with them. The flexure in the deck produces a moment which helps to resist the weight of the truck, thereby reducing the moment applied to the girders. Since the deck and the girders are not bonded together, each element flexes about its own neutral axis. By accounting for the portion of the applied moment that is resisted by the deck, the load rating of the bridge may improve.

Noncomposite flexure of the deck can be evaluated by comparing the total moment applied by the test truck with the total moment measured in the girders. When the total applied moment is greater than the sum of the moments measured in the girders, the difference can be attributed to the moment in the deck. The moment applied by the test truck can be determined through static analysis by modeling the entire superstructure of the bridge as one flexural member. The moments in the girders can be measured using the procedure described in section 1.5.2, above, for measuring lateral moment distribution. In fact, a study of the lateral moment distribution in a noncomposite bridge is not complete without considering noncomposite deck flexure because the difference between the applied moment and the measured moment must be explained. Noncomposite flexure of the deck is the most likely explanation for the difference.

An investigation of the noncomposite flexure of the deck is not necessary on a composite bridge. In this case, the deck is considered to be part of the top flange of each girder, so the flexure of the deck is already included in the flexure of the girders.

1.5.4 Additional Strength Due to Flexure of the Curb and Parapet

Reinforced concrete curbs and parapets are often tied into the bridge deck, or even cast at the same time as the deck, forming a strong connection. Although the flexural strength contribution from these elements is not usually considered during design, composite behavior between the parapet, curb, and deck can significantly increase the flexural strength of the bridge. These elements can behave like girders, attached to the top of the deck instead of the underside, and participate in resisting live load.

Evaluating the strength contribution of a curb and parapet can be done in two ways. First, the curb can be considered to increase the effective area of the deck, working compositely with the exterior girder. By instrumenting the exterior girder and determining the location of the neutral axis, the participation of the curb can be confirmed. Alternately, the curb and parapet can be considered as an additional exterior girder and instrumented similarly to the real girders. Composite behavior of the parapet

can then be determined from the location of its neutral axis. This may indicate that the parapet is acting as an additional girder.

1.6 Scope and Organization

In this thesis, an analytical load rating and an experimental load rating are determined for a four-span-continuous concrete-slab-on-steel-girder highway bridge. The evaluation considers only the flexural capacity of the bridge. Emphasis is placed on the evaluation of the lateral load distribution and the sources of additional strength for the bridge. Equipment and procedures for conducting a load test on the bridge are presented and evaluated. A physical description of the bridge is presented in Chapter 2. Chapter 3 contains a standard load rating calculation using the AASHTO LFD method. Chapter 4 contains a description of the test setup, including the test instrumentation and its placement, a description of the test vehicles, and a discussion of the field testing procedure. The results of the field test are presented in Chapter 5. Chapter 6 contains a revised load rating of the bridge, based on the field test results. A discussion of the reliability of extrapolating the field test results is also presented in Chapter 6. The conclusions of this study are presented in Chapter 7. Finally, two appendices are included. A discussion of measurement error in the data acquisition system and the numerical methods used to evaluate the field test data is presented in Appendix A, and an explanation of the data acquisition system's hardware and software is presented in Appendix B.

CHAPTER 2
Bridge Description

After examining several candidate bridges, the Big Creek Relief Bridge was chosen for this load test. Located on State Highway 6, just south of Marlin, Texas, this bridge spans the flood-relief wash for nearby Big Creek. It is a steel girder bridge with a reinforced concrete deck and a reinforced concrete substructure. The bridge was built in 1954, using salvaged steel for the girders, and carried two lanes of traffic (one in each direction) until it was taken out of service in January of 1997. At that time, Route 6 was rerouted over a new prestressed concrete bridge that runs parallel to the Big Creek Relief Bridge to the east.

The Big Creek Relief Bridge was ideal for the load testing project because the bridge's decommissioning allowed for extensive load testing without disrupting the traffic flow on Route 6. The bridge was also chosen because the wash provided easy access to the underside of the superstructure. In addition, the noncomposite girders, continuous spans, and large curbs made this bridge a likely candidate for an improved rating through load testing. Plans for the bridge were available from the Texas Department of Transportation (TxDOT), and test vehicles were available from the nearby TxDOT Office in Marlin. A preliminary analysis showed that the weight capacity of the trucks was sufficient to effect a substantial loading on the bridge. Also, the scales at a local feed store were available for determining the trucks' axle weights. The only problems with the test site were the occasional flooding of the wash and the long ninety-minute drive from Austin to Marlin.

2.1 Bridge Geometry

The Big Creek Relief Bridge consists of one 2-span continuous unit and four 4-span continuous units, running in an approximate north-south direction. The northernmost 4-span unit was chosen for load testing. Figure 2-1 shows a plan view of the roadway and substructure. Figure 2-2 shows an east elevation of the bridge.

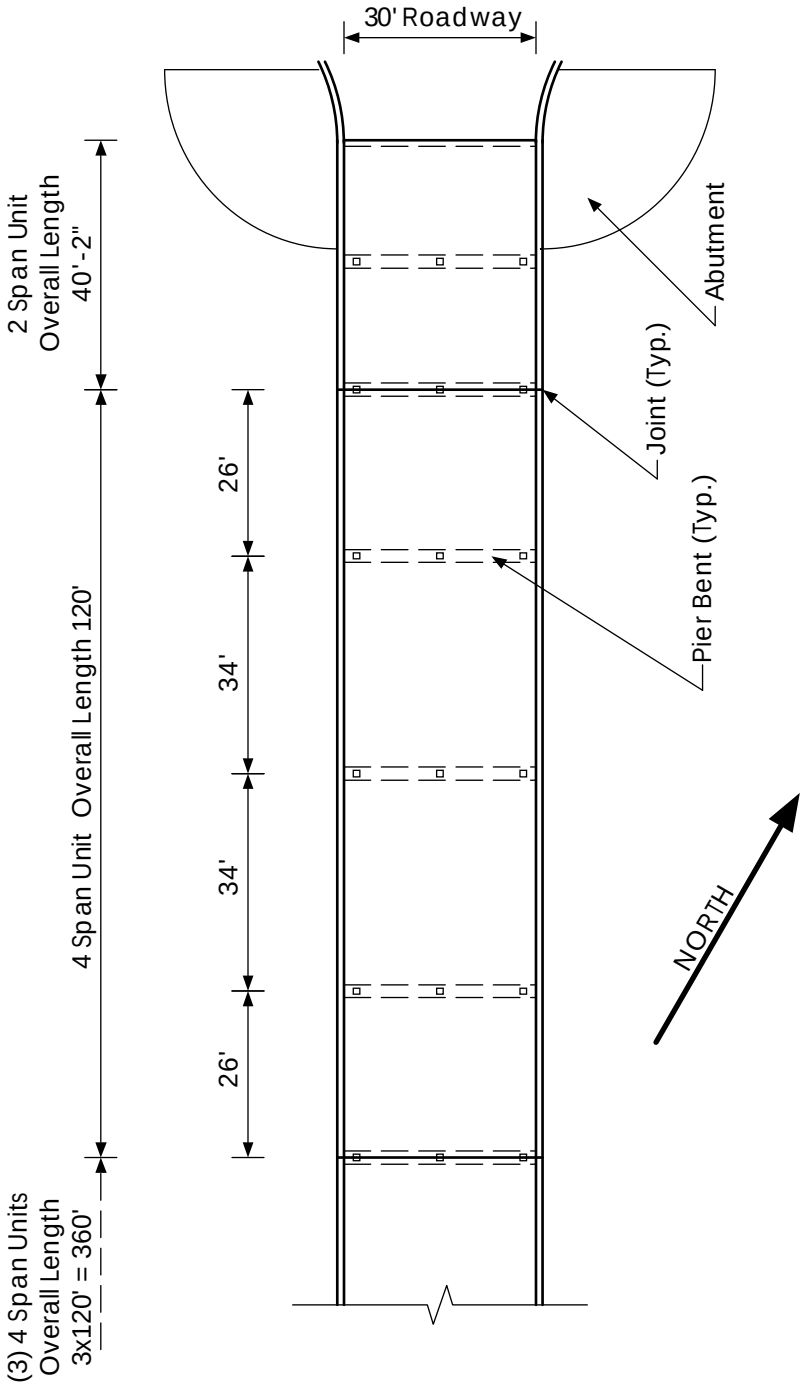

Figure 2-1 Plan View of the Roadway and Substructure

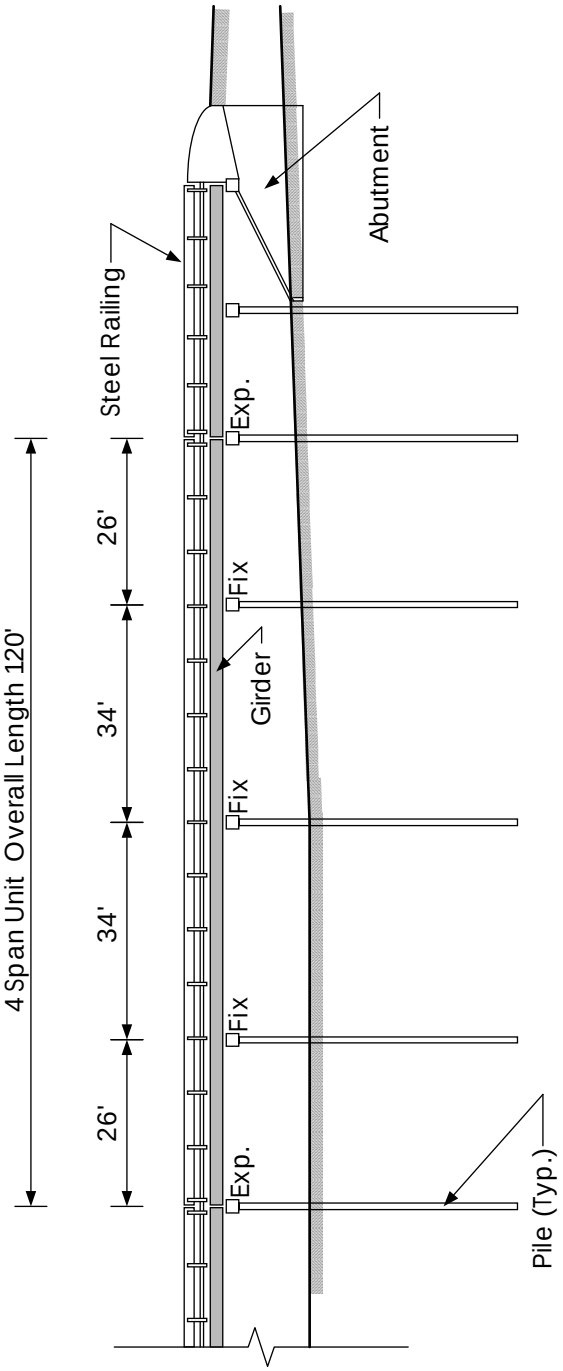

Figure 2-2 East Elevation of the Bridge

The nominal lengths of the four continuous spans are 26 feet, 34 feet, 34 feet, and 26 feet, respectively. The roadway is 30 feet wide and carries two lanes of traffic. In cross section, the bridge contains five identical steel girders, spaced evenly at 6.5 feet center-to-center. Figure 2-3 shows a cross section of the superstructure.

2.1.1 Girders

The girders are Bethlehem Steel section CB-21-59#. This section is no longer produced, but it is similar to the current AISC wide flange section W21x62, except for slightly thinner flanges on the CB-21-59# section. A 5" by 5/16" by 6'-6" cover plate is welded to the top and bottom flanges of the girders at the center bearing location. Figure 2-4 shows a half elevation of the girders, including the bearing locations, cover plates, diaphragms, construction joints, and splices. Figure 2-5 shows a cross section of the girders and cover plates, including the nominal section dimensions, areas, and moments of inertia. Figure 2-6 shows a plan view of a cover plate, including the bearing spacers and weld details.

The cover plates increase the stiffness of the girders by 28 percent near the center bearing. To simplify the analysis procedure, the cover plates were ignored during moment and shear calculations. This change in stiffness results in a slight reduction in negative moment at the center bearing, and a slight increase in positive moment in the adjacent spans. Since the 6-foot-6-inch long cover plates comprise only 5.4 percent of the beam's length, the error introduced by neglecting the plates during moment calculations was assumed to be negligible.

The girders were measured to confirm their dimensions. Figure 2-7 shows the as-measured dimensions for three different cross sections. In the figure, Section A is located at the end of an exterior girder, and Sections B and C are located on interior girders, near a diaphragm. Precise measurements of the top flange width, top flange thickness, and girder depth were not made because the top flange was embedded in the concrete deck.

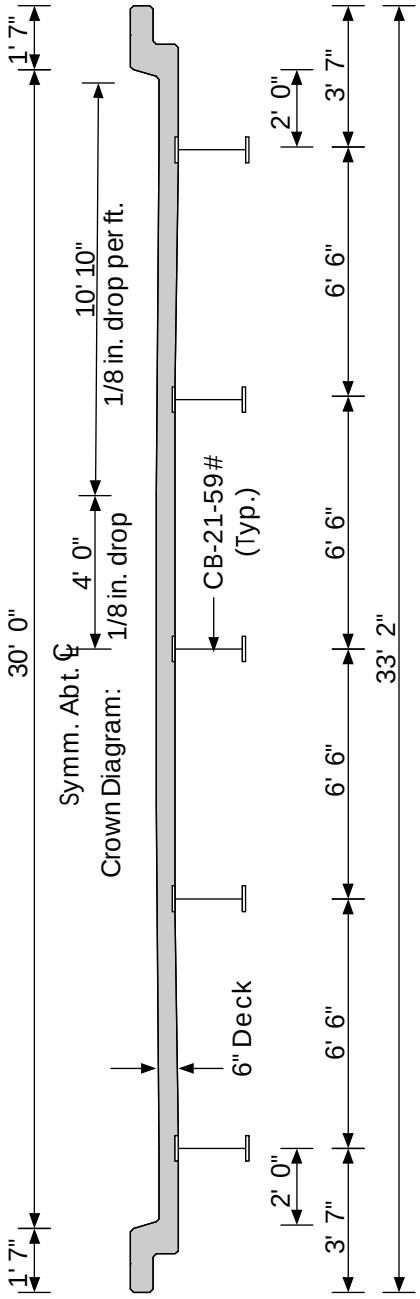

Figure 2-3 Cross Section of the Superstructure

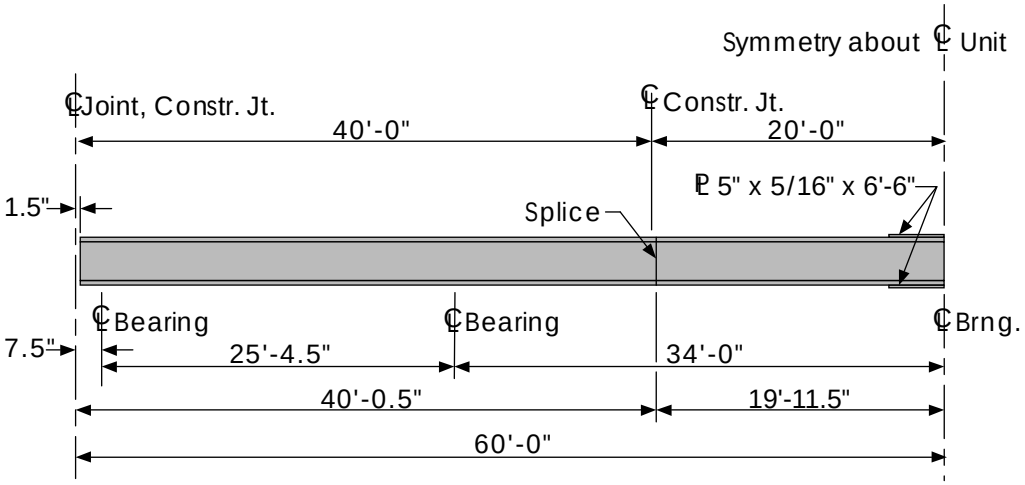

Figure 2-4 Half Girder Longitudinal Elevation

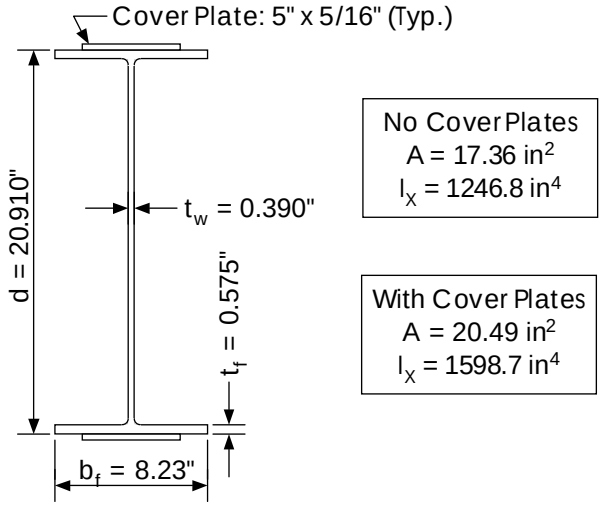

Figure 2-5 Girder Cross Section, Showing the Nominal Dimensions and Section Properties

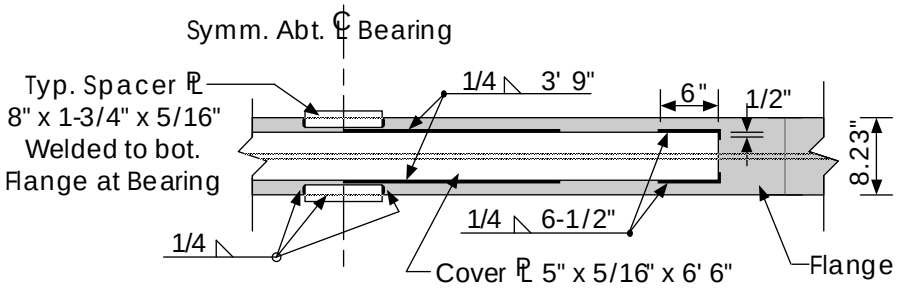

Figure 2-6 Detail of a Cover Plate

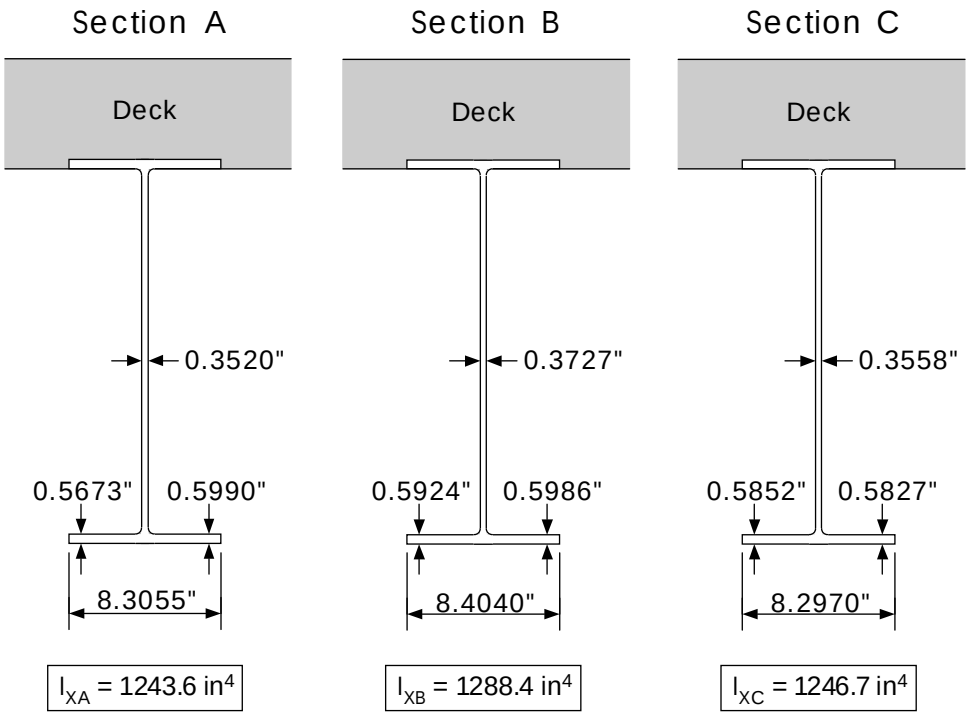

Figure 2-7 Girder Cross Sections, Showing the As-Measured Section Dimensions and the Calculated Moments of Inertia

The moment of inertia was calculated for all three cross sections. The average thickness of the bottom flange was used for both the top and bottom flanges, because the top flange thickness could not be measured. In addition, the nominal depth was used in place of a measured depth.

For all three sections, the moment of inertia varied very little from the nominal value. The results are shown in Table 2-1 and in Figure 2-7, above. The close agreement between the as-measured and nominal section properties suggests that the girders on the bridge are the specified section, and that slight changes in the section dimensions do not affect the girder stiffness. Therefore, the nominal section properties were used for all of the analysis and rating calculations.

	Moment of Inertia (in^4)	**Variation from Nominal**
Nominal	1246.8	-----
Section A	1243.6	-0.26 %
Section B	1288.4	+3.34 %
Section C	1246.7	-.01 %

Table 2-1 Nominal vs. Measured Moment of Inertia

2.1.2 Deck

The reinforced concrete deck is 6 inches thick and is cast even with the bottom face of the top flanges. The main reinforcement in the deck is three sets of #5 bars, placed perpendicular to the direction of traffic. Figure 2-8 shows two details of the transverse reinforcement in the deck. A cross section of the deck, including a crown diagram, is shown in Figure 2-3, above.

An 18-inch curb is placed on both sides of the bridge. There is a sectional steel railing bolted to the curb. The curb and deck were placed at the same time, and they are connected with reinforcing bars, forming a continuous unit. Figure 2-9 shows a cross section detail of an exterior girder, curb, and railing, including transverse reinforcement.

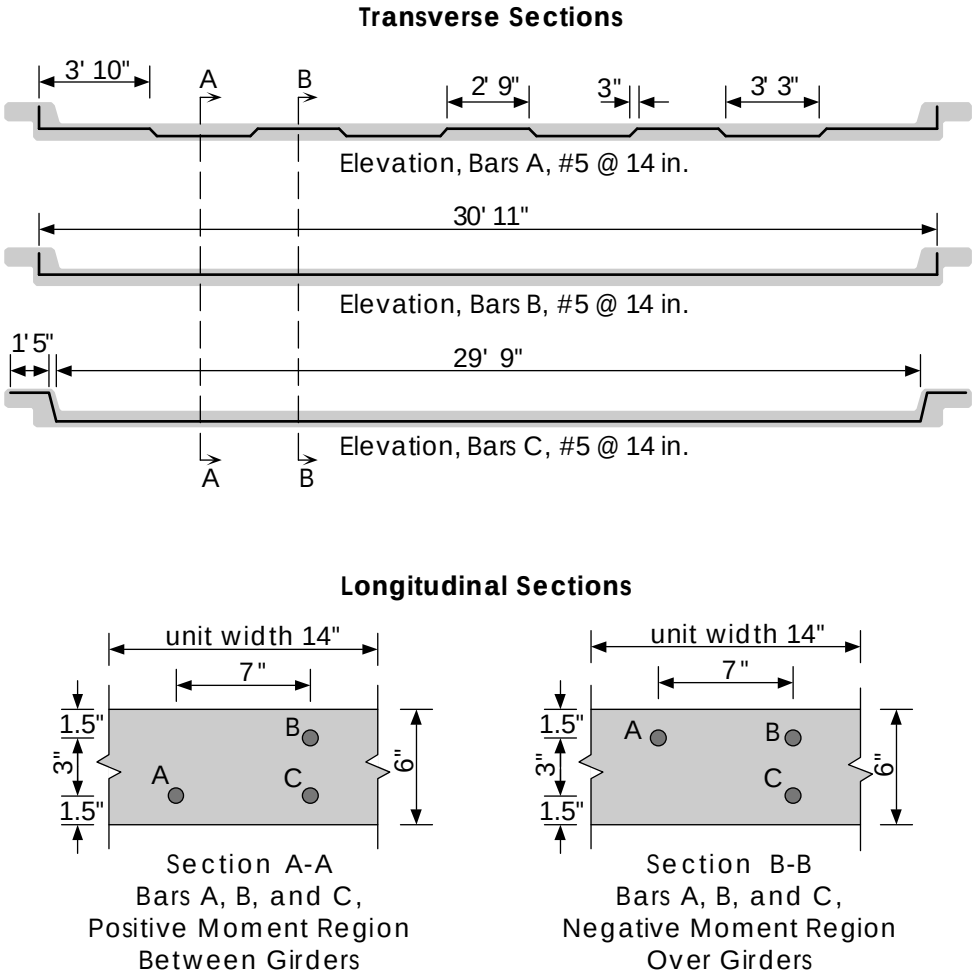

Figure 2-8 Details of the Main Transverse Reinforcement in the Concrete Bridge Deck

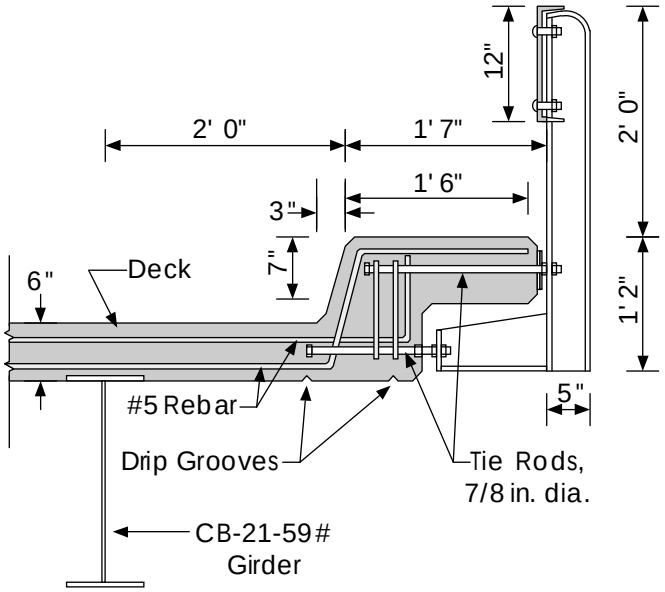

Figure 2-9 Detail of an Exterior Girder, Curb and Railing

2.1.3 Joints and Bearings

Each four span unit contains two construction joints. A reinforced concrete diaphragm is located at each of the construction joints. Diaphragms are also located at the ends of each girder, at the expansion joints. Figure 2-10 shows a detail of a construction joint and diaphragm, and Figure 2-11 shows a detail of an expansion joint and diaphragm.

Each girder is supported by the substructure at five bearing locations. On each of the five girders, the three center bearings are fixed. Figure 2-12 shows a detail of a fixed bearing. These bearings allow the girder to rotate, but prevent translation in all directions.

The two end bearings are expansion bearings. Figure 2-13 shows a detail of an expansion bearing. The ends of the girders rest on the bearings but are not tied down, so the girder ends are free to translate. Large vertical and lateral movements are confined by steel plates in the expansion shoe.

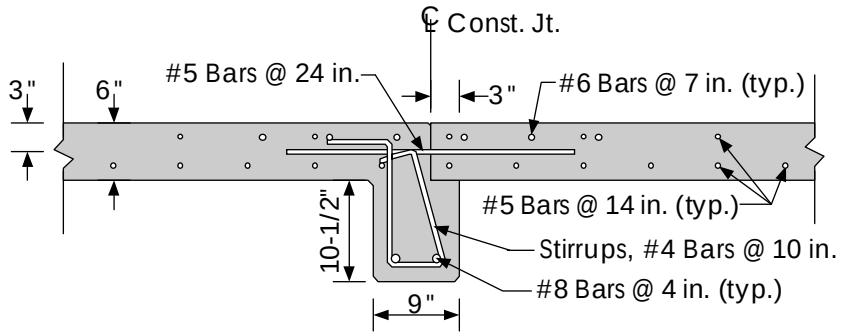

Figure 2-10 Detail of a Construction Joint and Diaphragm

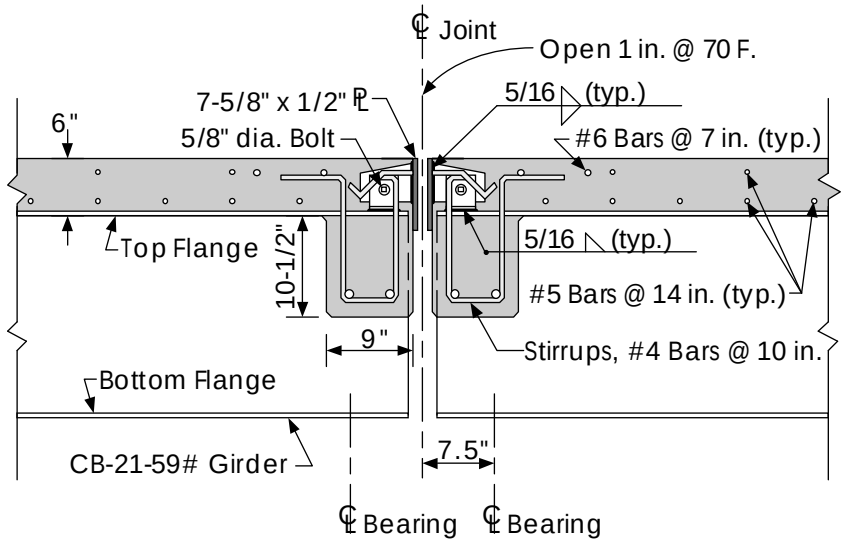

Figure 2-11 Detail of an Armored Expansion Joint

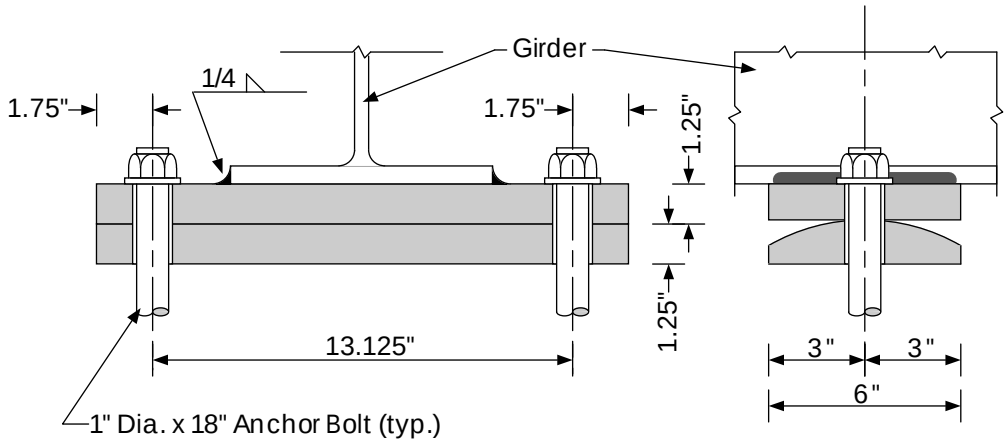

Figure 2-12 Detail of a Fixed Bearing

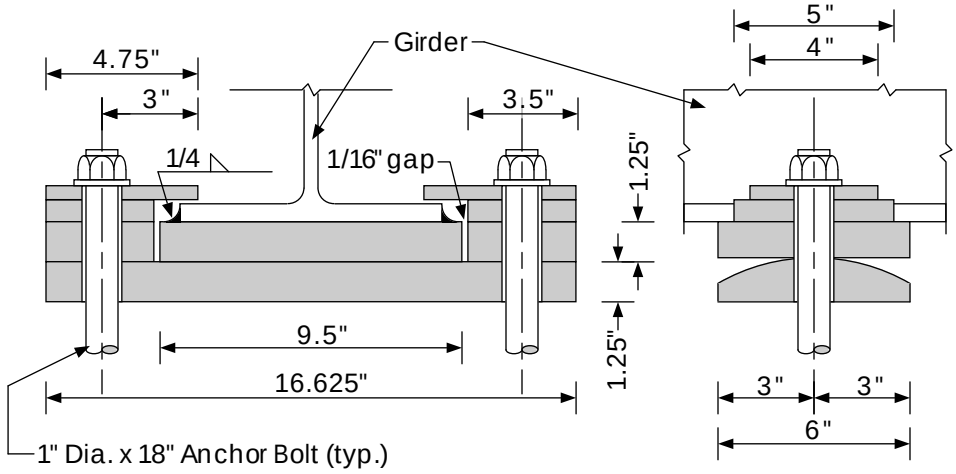

Figure 2-13 Detail of an Expansion Bearing

2.1.4 Substructure

The pile caps are 30 inches wide and 30 feet long. Their depth varies from 30 inches at the end to 31.5 inches in the middle, forming a crown profile. The caps are supported by three reinforced concrete piles, each 16 inches square and driven to a depth of about 35 feet. The piles are spaced at 11 feet center to center in each bent. An elevation of a pile bent, including reinforcement, is shown in Figure 2-14. The main reinforcement in the pile caps is 8 #9 bars, 4 on the top and 4 on the bottom of the pile cap. They are confined with 'U' stirrups made from #4 bars.

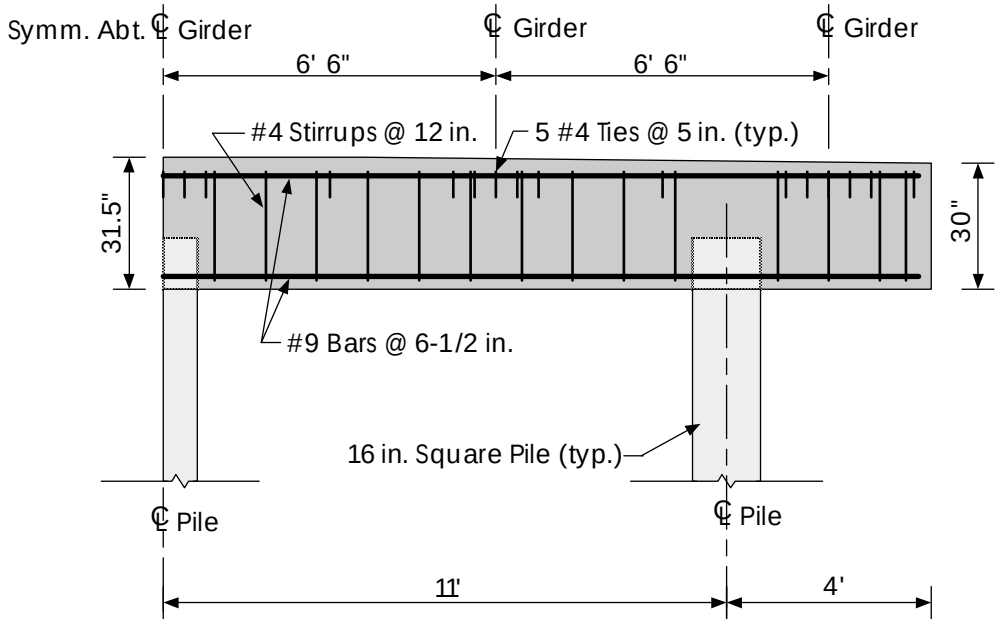

Figure 2-14 Half Elevation of Pile Bent

2.2 Material Properties

The plans for the Big Creek Relief Bridge do not include detailed information about the strength of the structural steel, rebar, or concrete. Until material specimens were cut out of the bridge and tested, the strengths of the steel and concrete were estimated using the AASHTO Manual for Condition Evaluation of Bridges (1994b). This manual contains tables of material properties for older grades of steel or concrete. For unknown grades of steel or concrete, the AASHTO Manual estimates the strength and other material properties, based on the year the material was produced.

2.2.1 Girders

The age of the structural steel in the Big Creek Relief Bridge was difficult to determine. Although the bridge was built in 1954, the rolled steel girders were salvaged from a bridge previously in place at the site. The existing plans for the Big Creek Relief Bridge did not specify when the girders were fabricated or when the older bridge was built.

The CB-21-59# sections are mentioned in the AISC Iron and Steel Beams catalog (1953). This reference contains tables of the many different steel sections produced before mill standardization began in 1953. The AISC Catalog attributes the CB-21-59# section to the Carnegie Brothers & Co. 1934 mill catalog of rolled steel shapes. The date of the Carnegie Catalog suggests that the girders were produced in the early to mid 1930's. For rolled steel sections produced between 1905 and 1936, the AASHTO Manual suggests using a yield strength of 30 ksi.

As a result of the uncertainty in the origin and properties of the CB-21-59# sections, two specimens were flame cut from the bottom flanges of the girders after the load testing was completed. David Jauregui, then a Graduate Research Assistant at the University of Texas at Austin, performed tensile coupon tests on each the specimens. Mr. Jauregui confirmed that the yield strength of the steel was, in fact, 30 ksi. As a result, this value was used in the analysis and load rating calculations.

2.2.2 Cover Plates, Joints, and Bearings

The cover plates, bearings, and expansion joints were fabricated in 1954. The yield strength of these components was estimated to be 33 ksi, based on the tables in the AASHTO Manual. No material testing was performed to confirm this estimate.

2.2.3 Rebar

The rebar in the bridge deck and substructure is specified in the plans as 'intermediate grade.' For rebar of unknown or intermediate grades placed in or after 1954, the AASHTO Manual suggests using a yield strength of 40 ksi. No material testing was performed to confirm this estimate.

2.2.4 Concrete

The plans for the bridge specify 'Class A' concrete for the deck and substructure. The AASHTO Manual estimates the compressive strength of the concrete to be 2500 psi. This designation is applied to all concrete built before 1959.

A Schmidt Hammer was used, unsuccessfully, to determine the actual strength of the concrete on the bridge. Sixty readings were taken on the underside of the deck. The result was a very high concrete strength of 7000 psi. This value is likely to be too high, because the hammer readings were taken against the exposed surface of the deck. For older concrete, a half-inch layer should be removed before using the Schmidt Hammer, to avoid testing the drier, harder, surface material. The "inner" concrete retains more moisture, and has a lower ultimate strength. Because of the uncertainty in the Schmidt Hammer measurements, the AASHTO estimate of 2500 psi. was used in the analysis of the bridge.

2.3 Site Description

Prior to selection, the test site was inspected in the summer of 1996. Due to a severe drought that season, the ground underneath and around the bridge was firm and stable. In addition, most of the debris and foliage had been cleared from the site during the construction of the replacement bridge. Figure 2-15 is a photo of the west elevation

of the bridge, looking toward the south end. The replacement bridge can be seen, partially, in the background of the photo.

The bridge site was considered excellent for load testing, because the ground underneath the bridge was dry and devoid of stream channels, roadways, debris, or other obstacles. In addition, the clearance between the ground and the bottom of the girders was low, averaging about eleven feet. The low clearance allowed easy access to the underside of the bridge, using extension ladders. Finally, easy vehicle access to the underside of the bridge was possible, because the embankment sloped gently to grade beyond the steep concrete abutments.

Figure 2-15 West Elevation of the Bridge

The instrumentation and load testing of the Big Creek Relief Bridge did not begin until February of 1997, six months after the initial inspection. By this time, winter rain had softened the ground under the bridge considerably. Moreover, the firm soil had been replaced by a deep pool of mud.

The original plan for installing the instrumentation on the bridge depended on using extension ladders to reach the girders and the underside of the deck. However, the ladders would not work in the newly-formed mud. To provide stable footings for the ladders, two wooden platforms were constructed. Figure 2-16 is a photo of one of the platforms.

Each platform consisted of four sheets of 3/4-inch thick plywood, supported by nine wooden boxes. The plywood sheets were nailed down to prevent slipping. The result was a 4-foot by 32-foot platform, that provided a stable working surface while conforming to the shape of the ground beneath it. To prevent shifting and slipping of the extension ladders, short pieces of 2 by 4 were nailed to the top surface of the platforms.

Figure 2-16 Platform Used for Accessing the Underside of the Bridge

The wash underneath the bridge provided flood relief for nearby Big Creek. At one point during the instrumentation process, there was six feet of standing water underneath the bridge, and therefore no work was performed that day. In anticipation of this possibility, the platforms were chained to the substructure with 1/4-inch thick cable, so that they would not float away. This example reinforces the need to study the flood history of a bridge site prior to the start of instrumentation and testing.

CHAPTER 3

Initial Load Rating and Analysis

A linear-elastic structural analysis of the Big Creek Relief Bridge was performed to determine the moments in the girders resulting from the application of various live and dead load combinations. Calculations were performed for rating purposes and for comparing the moments produced by the field test vehicle with the moments produced by the rating vehicle.

The rating calculations and analysis of the bridge presented here consider only the moments developed in the bridge's girders. The calculations for shear are not presented, because an analysis of the shear capacity of the girders showed the girders to be more than adequate. Like most rolled-steel sections, the bridge girders had ample web material for resisting shear.

3.1 Analysis Method for Calculating Moments in the Bridge

The actual load resisting behavior of the bridge is complex and three-dimensional. To simplify the analysis, the bridge was analyzed as a single "design girder," using the continuous line-girder model shown in Figure 3-1.

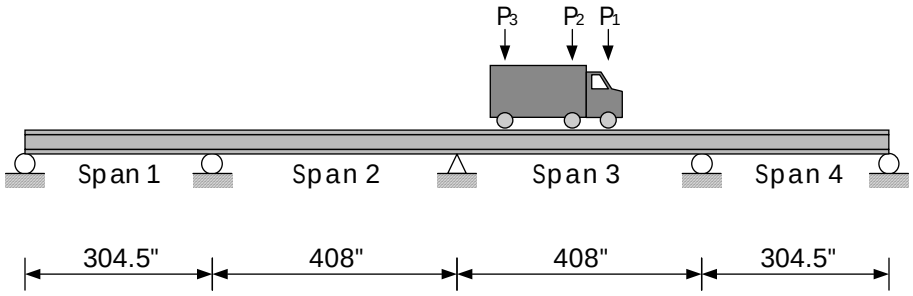

Figure 3-1 The "Design Girder," Including a Typical Live Load

A typical vehicle live load is shown on the design girder in Figure 3-1. The loads P_1, P_2, and P_3 represent the weight of each of the vehicle's axles. In addition to the

concentrated axle loads, uniform live loads and dead loads were applied to the line-girder model as part of the analysis.

The effect of axial load was neglected in the analysis by modeling only one of the bearings as restrained in the horizontal direction. In reality, bearings 2, 3, and 4 were fixed against horizontal translation. The additional stiffness provided by the cover plates at bearing 3 was also ignored in the analysis, and the girder was assumed to have a uniform moment of inertia of 1246.8 inches^4 along its entire length. These approximations were assumed to have a negligible effect on the calculated moments.

A spreadsheet was used to determine moment diagrams for the design girder, for both live load and dead load. The moments in the design girder were calculated for one-hundred positions on each span, using the moment distribution method and statics. The positions of the live loads were adjusted manually to determine a moment envelope and identify the maximum live load positive moment and maximum live load negative moment along the length of the design girder.

3.2 HS-20 LFD Load Rating

The five girders on the Big Creek Relief Bridge were load rated for moment, using the AASHTO HS-20 design vehicle and the provisions of the AASHTO LFD (1992) specification. As part of the rating procedure, inventory and operating ratings were determined using Equation 3-1, the following AASHTO LFD rating equation:

$$RF = \frac{C - A_1 \cdot D}{A_2 \cdot L_{DF+I}} \qquad (3\text{-}1)$$

where

RF is the AASHTO LFD rating factor,

C is the capacity of the girder, in kip∿inches,

D is the dead load moment in the girder, in kip∿inches,

L_{DF+I} is the live load moment in the girder, including the effects of lateral moment distribution and impact, in kip∿inches,

A_1 is the LFD rating coefficient for dead load, 1.3 for both inventory and operating ratings, and

A_2 is the LFD rating coefficient for live load, 1.3 for operating rating and 2.17 for inventory rating.

Rating factors greater than one indicate an acceptable rating, because the girder's remaining capacity to resist live load is greater than the live load applied. Rating factors less than one indicate that the bridge is not capable of safely supporting the applied load. In the latter case, the bridge is typically posted with weight restrictions or closed to traffic.

Many locations on the bridge were investigated to determine the lowest rating factor. These included bearings 2, 3, and 4 for negative moment and points along spans 2 and 3 for positive moment. The combination of dead load moment, live load moment, and moment capacity that produced the lowest rating factor according to Equation 3-1 was taken as the rating for the bridge.

3.2.1 Dead Load

The weight of the various elements of the superstructure was tabulated and distributed evenly among the five girders. Table 3-1 shows a summary of the areas, unit weights, and dead load contributions for the girders, deck, wearing surface, curbs, railings, and railing posts. The total area of the girders was taken as the area of the CB-21-59 section multiplied by five for the five girders. The area of the deck was found by multiplying the width of the deck, 29.66 feet, by the thickness of the deck, 0.5 feet. The area of the wearing surface was found by multiplying the width of the wearing surface, 29.66 feet, by the assumed thickness of the wearing surface, 0.167 feet, or 2 inches. The area of the curbs was taken as the area of the structural concrete not covered by the wearing surface. The area of the railings was taken as the area of the channel sections. The area of the railing posts was determined by smearing the volume of all of the posts evenly along the bridge.

The unit weight of the steel girders, steel railings, and steel railing posts was taken as 0.490 kips per foot^3. The unit weight of the concrete deck and curbs was taken

as 0.150 kips per foot^3. The unit weight of the wearing surface was taken as 0.120 kips per foot^3, corresponding to the unit weight of asphalt.

Component	Area (feet^2)	Unit Weight (kips per foot^3)	Linear Weight (kips per foot)
Girders	0.603	0.490	0.295
Deck	14.83	0.150	2.225
Wearing Surface	4.943	0.120	0.593
Curbs	2.917	0.150	0.438
Railings	0.084	0.490	0.041
Railing Posts	0.041	0.490	0.020
Total Dead Load Applied to the Superstructure	---	---	**3.612**
Dead Load Applied to each Line Girder (Total / 5)	---	---	**0.722**

Table 3-1 Summary of Dead Loads

Table 3-1 shows that the total dead load applied to the superstructure was 3.612 kips per foot. Dividing by five, the dead load applied to each girder was 0.722 kips per foot. A dead load moment diagram for each of the girders was calculated using the line girder dead load of 0.722 kips per foot.

Figure 3-2 shows the unfactored dead load moment diagram for each girder. The moment diagram is unfactored because it does not include the AASHTO dead load rating factor of 1.3. The maximum dead load positive moments were 435 kip-inches near the middle of spans 2 and 3, and 367 kip-inches near the middle of spans 1 and 4. The maximum dead load negative moments were -869 kip-inches at bearing 3, and -767 kip-inches at bearings 2 and 4. The dead load moment diagram was the same for all five girders.

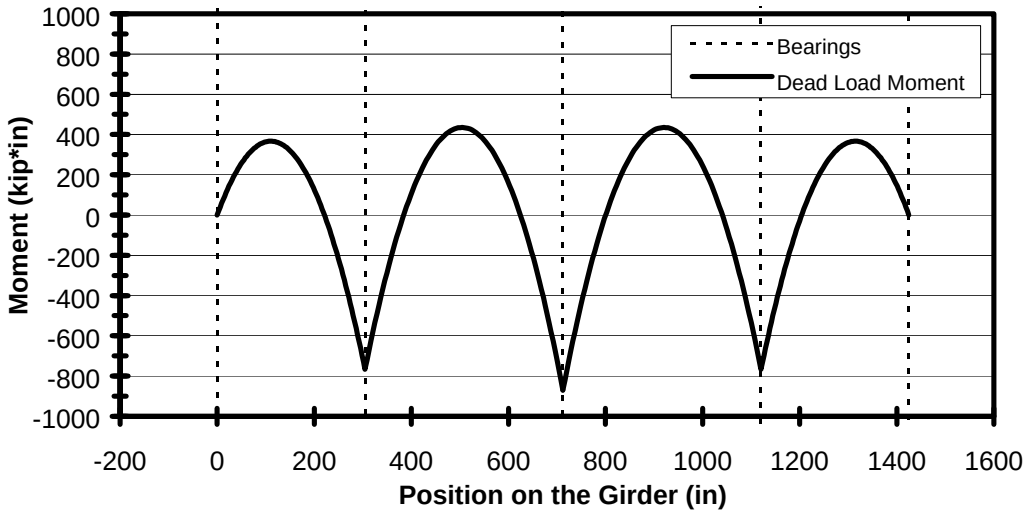

Figure 3-2 Unfactored Dead Load Moment Diagram for Each Girder

Moment rating calculations compare the dead load moment and live load moment at a cross section against that cross section's moment capacity. When the largest live load and dead load moments occur at the same location, this location is the cross section used for rating, because it produces the lowest rating factor. However, when the locations of maximum live load and dead load moment do not coincide, the location with the lowest rating factor must be determined by trial and error. This was the case for the positive moment regions of the Big Creek Relief Bridge.

Table 3-2 shows the dead load moments used for rating. In the positive moment region, the lowest rating factors were found to occur near the location of maximum dead load moment, using trial and error. On spans 2 and 3, the dead load moment used for rating was 431 kip∽inches, 0.99 times the maximum dead load moment. The difference of 1 percent between the maximum dead load moment and the dead load moment used for rating indicates that the trial and error process produced a negligible improvement in the accuracy of the rating calculations. The maximum moments for both dead load and live load could have been used, instead.

Case	Dead Load Moment (kip-inches)
Positive Moment on Spans 2 and 3	431
Negative Moment at Bearing 3	-869
Negative Moment at Bearings 2 and 4	-767

Table 3-2 Dead Load Moments Used for Rating

In the negative moment region, the maximum dead load and live load moments occurred at the same location. Therefore, the maximum negative dead load and live load moments were used for rating at bearings 2, 3, and 4.

3.2.2 Design Live Load

The AASHTO HS-20 truck and lane loadings were both considered in determining the live load moment envelope for the design girder. Figure 3-3 shows a diagram of the HS-20 truck load, and Figure 3-4 shows a diagram of the HS-20 lane load. The truck load and the lane load were separately applied to the design girder.

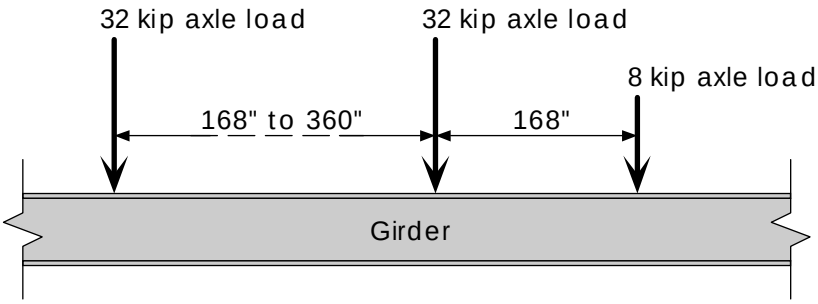

Figure 3-3 HS-20 Truck Load

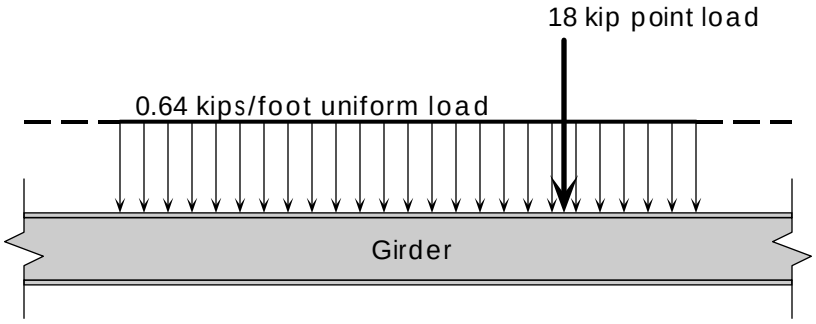

Figure 3-4 HS-20 Lane Load for Positive Moment

When the HS-20 truck load was applied to the design girder, the spacing of the 32-kip axles was adjusted to produce a maximum load effect. For positive moment on spans 2 and 3, the shortest possible spacing of 168 inches produced the maximum moment effect. For negative moment at bearings 2 and 4, an axle spacing of 264 inches produced the maximum effect. For negative moment at bearing 3, an axle spacing of 288 inches produced the maximum effect.

When the HS-20 lane load was applied to the design girder, the uniform load was placed on the portions of the girder where it contributed to a maximum load effect. Maximum moments resulted from a "checkered" load placement, where alternate spans were loaded for positive moment and adjoining spans were loaded for negative moment. Following the provisions of the AASHTO LFD code, one 18-kip load was placed on the appropriate span to produce maximum positive moment effects, and two 18-kip loads were placed on adjoining spans to produce maximum negative moment effects.

The HS-20 unfactored moment envelope for the design girder is shown in Figure 3-5. The moment envelope is unfactored because it does not include the AASHTO live load rating factors of 1.3 or 2.17. For every position on the bridge, the HS-20 truck loading controlled since it produced the largest positive moment and negative moment.

For highway bridges, a lane load often produces the maximum live load negative moment. However, this was not the case for the Big Creek Relief Bridge. The HS-20 lane load produced a moment at bearing 3 that was only 0.93 times the moment produced

by the HS-20 truck load. In all other cases, the HS-20 lane load produced moments that were less than 0.93 times the moments produced by the HS-20 truck load.

The HS-20 truck load produced larger moments than the HS-20 lane load because the span lengths on the Big Creek Relief Bridge were very short. On longer span bridges, the center and rear axles of the HS-20 truck can not be placed far enough apart to produce the maximum moment effect, because they are limited to a spacing of 360 inches. The two 18-kip concentrated loads from the HS-20 lane load are not subject to this constraint, so they produce a larger negative moment effect on most longer span bridges.

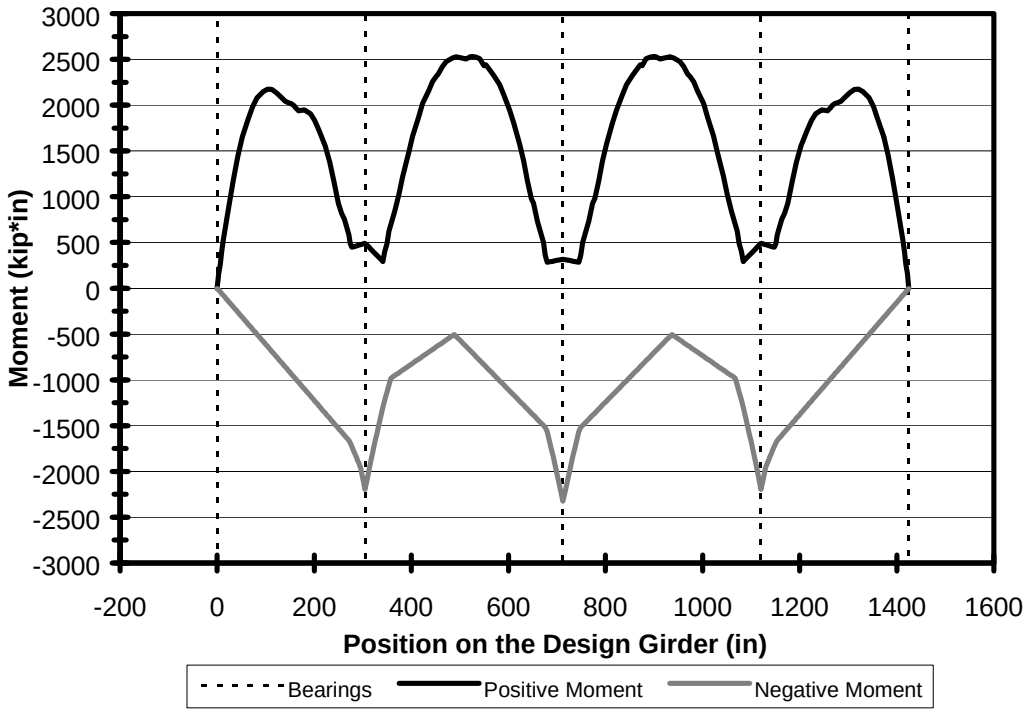

Figure 3-5 HS-20 Unfactored Live Load Moment Envelope for the Design Girder

The maximum live load positive moment is 2532 kip-inches and occurs at 526 inches on span 2 and at 899 inches on span 3. Figure 3-6 shows a diagram of the design girder with the HS-20 truck's axle loads in the position corresponding to maximum live

load positive moment on span 2. The truck is facing to the right in Figure 3-6 and in similar figures to follow.

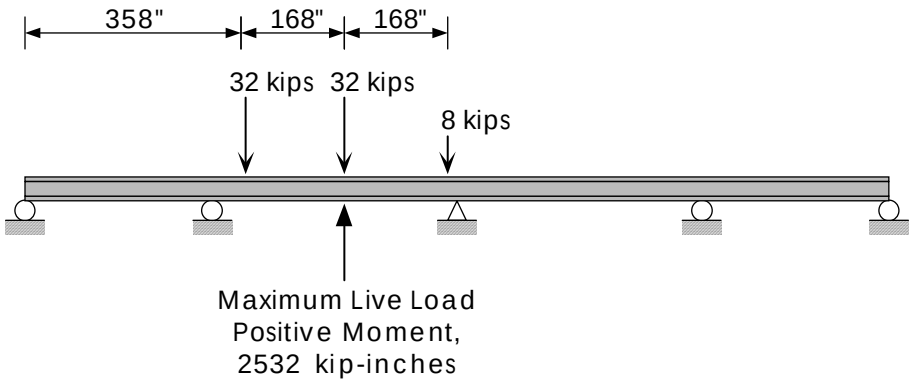

Figure 3-6 HS-20 Truck Position for Maximum Live Load Positive Moment on Span 2

The maximum live load negative moment is -2324 kip-inches and occurs at bearing 3. Figure 3-7 shows a diagram of the design girder with the HS-20 truck's axle loads in the position corresponding to maximum live load negative moment at bearing 3.

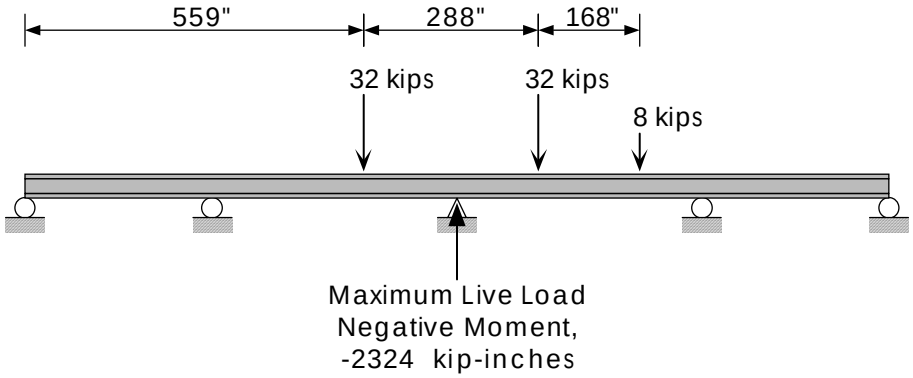

Figure 3-7 HS-20 Truck Position for Maximum Live Load Negative Moment at Bearing 3

There was a cover plate on the girder at bearing 3 which increased the capacity of the girder at that location. Because of the increased capacity, the lowest rating for

negative moment did not occur at bearing 3. The live load negative moment at bearings 2 and 4 was -2196 kip~inches, approximately 0.95 times the live load negative moment at bearing 3. However, unlike bearing 3, there were no cover plates at bearings 2 and 4, so the moment capacity at these locations was lower than the moment capacity at bearing 3. Because of the large live load and lower capacity, the rating for negative moment at bearings 2 and 4 was lower than the rating for negative moment at bearing 3. Figure 3-8 shows a diagram of the bridge with the HS-20 truck's axle loads in the position corresponding to maximum live load negative moment at bearing 2.

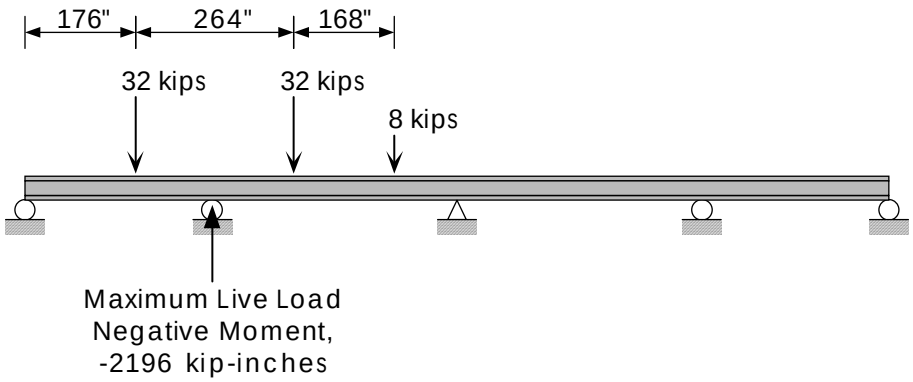

Figure 3-8 HS-20 Truck Position for Maximum Live Load Negative Moment at Bearing 2

3.2.3 Moment Distribution and Impact

The unfactored live load moment envelope determined in section 3.2.2, above, does not include the effects of lateral moment distribution or impact. A distributed live load plus impact moment envelope for each girder was determined by scaling the live load moment envelope for the design girder by the lateral moment distribution factors and impact factor specified in the AASHTO LRFD (1994a) code.

Following the provisions of the AASHTO LRFD code, the bridge was divided into 12 foot wide design lanes. Because the bridge had a 30-foot wide roadway, two design lanes fit on the bridge. Therefore, the AASHTO LRFD equations for two design lanes were used to determine the lateral moment distribution factors for each girder.

The AASHTO LRFD code differentiates between exterior and interior girders. Equation 3-2 shows the formula used to determine the lateral moment distribution factor for the interior girders:

$$MDF_{int} = 0.075 + \left(\frac{S}{9.5}\right)^{0.6} \cdot \left(\frac{S}{L}\right)^{0.2} \cdot \left(\frac{K_g}{12 \cdot L \cdot t_s^{\,3}}\right)^{0.1} \qquad (3\text{-}2)$$

where

MDF_{int} is the lateral moment distribution factor for an interior girder,

S is the girder spacing, in feet,

L is the span length, in feet,

t_s is the thickness of the slab, in inches, and

K_g is a longitudinal stiffness parameter, in inches^4.

The value of K_g was determined using Equation 3-3:

$$K_g = n \cdot \left(I + A \cdot e_g^{\,2}\right) \qquad (3\text{-}3)$$

where

n is the modular ratio between girder and deck materials,

I is the moment of inertia of the girder, in inches^4,

A is the area of the girder, in inches^2, and

e_g is the distance between the centers of gravity of the girder and the deck, in inches.

Table 3-3 shows the values of S, L, t_s, n, I, A, and e_g used to determine the lateral moment distribution factors for the Big Creek Relief Bridge. The value of L depended on the moment effect under consideration. For positive moment on each span, L was taken as the length of the span under consideration. For negative moment at a bearing, L was taken as the average length of the adjoining spans.

Variable	Value
Girder Spacing, S	6.5 feet
Span Length, L, for Positive Moment on Spans 1 and 4	25.375 feet
Span Length, L, for Positive Moment on Spans 2 and 3	34 feet
Span Length, L, for Negative Moment at Bearing 2	29.688 feet
Span Length, L, for Negative Moment at Bearing 3	34 feet
Slab Thickness, t_s	6 inches
Modular Ratio, n	12
Moment of Inertia, I	1246.8 inches^4
Girder Area, A	17.36 inches^2
Offset Distance, e_g	12.88 inches

Table 3-3 Variables Used to Determine the AASHTO LRFD Lateral Moment Distribution Factors for the Interior Girders

For all locations on the bridge, the value of K_g was found to be:

$$K_g = 12 \cdot \left(1246.8 + 17.36 \cdot (12.88)^2\right) = 49521 \text{ inches}^4$$

For positive moment on spans 1 and 4, the value of MDF_{int} was found to be:

$$MDF_{int} = 0.075 + \left(\frac{6.5}{9.5}\right)^{0.6} \cdot \left(\frac{6.5}{25.375}\right)^{0.2} \cdot \left(\frac{49521}{12 \cdot 25.375 \cdot 6^3}\right)^{0.1} = 0.664$$

For positive moment on spans 2 and 3, and for negative moment at bearing 3, the value of MDF_{int} was found to be:

$$MDF_{int} = 0.075 + \left(\frac{6.5}{9.5}\right)^{0.6} \cdot \left(\frac{6.5}{34}\right)^{0.2} \cdot \left(\frac{49521}{12 \cdot 34 \cdot 6^3}\right)^{0.1} = 0.615$$

For negative moment at bearings 2 and 4, the value of MDF_{int} was found to be:

$$MDF_{int} = 0.075 + \left(\frac{6.5}{9.5}\right)^{0.6} \cdot \left(\frac{6.5}{29.688}\right)^{0.2} \cdot \left(\frac{49521}{12 \cdot 29.688 \cdot 6^3}\right)^{0.1} = 0.637$$

The AASHTO LRFD lateral moment distribution factors for the exterior girders are based on the values for the interior girders. Following the AASHTO LRFD code, the moment distribution factors for the exterior girders were determined using Equation 3-4:

$$MDF_{ext} = MDF_{int} \cdot \left(0.77 + \frac{d_e}{9.1}\right) \qquad (3\text{-}4)$$

where

MDF_{ext} is the lateral moment distribution factor for an exterior girder, and

d_e is the distance between the center of the exterior beam and the interior edge of the curb or traffic barrier, in feet.

The distance between the center of the exterior girder and the curb face was exactly 2 feet, as shown in Figure 2-3. Therefore, the value of d_e was taken as 2 feet. This is the minimum value allowed by the AASHTO LRFD code.

For positive moment on spans 1 and 4, the value of MDF_{ext} was found to be:

$$MDF_{ext} = 0.664 \cdot \left(0.77 + \frac{2}{9.1}\right) = 0.657$$

For positive moment on spans 2 and 3, and for negative moment at bearing 3, the value of MDF_{ext} was found to be:

$$MDF_{ext} = 0.615 \cdot \left(0.77 + \frac{2}{9.1} \right) = 0.608$$

For negative moment at bearings 2 and 4, the value of MDF_{ext} was found to be:

$$MDF_{ext} = 0.637 \cdot \left(0.77 + \frac{2}{9.1} \right) = 0.630$$

Table 3-4 presents a summary of the AASHTO LRFD lateral moment distribution factors for the bridge. In all cases, the lateral moment distribution factors were larger for the interior girders than the exterior girders, so the interior girders controlled the rating of the bridge. Therefore, the values for MDF_{int} were used to determine the live load moments used for rating.

Case	Interior Girders	Exterior Girders
Positive Moment, Spans 1 and 4	0.664	0.657
Positive Moment, Spans 2 and 3	0.615	0.608
Negative Moment, Bearings 2 and 4	0.637	0.630
Negative Moment, Bearing 3	0.615	0.608

Table 3-4 Two Design Lane AASHTO LRFD Moment Distribution Factors, Used for the HS-20 Rating Calculations

The AASHTO LRFD code specifies using an impact factor of 1.33 to approximate the magnitude of the dynamic effects associated with live load. This value was used, along with the interior girder moment distribution factors, to determine the live

load moments used for rating. Figure 3-9 shows the unfactored live load moment envelope for an interior girder, including the effects of lateral moment distribution and impact. The unfactored dead load moment diagram for an interior girder is also shown in the figure. The moment envelopes are unfactored because they do not include the AASHTO rating factors of 1.3 for dead load and 1.3 or 2.17 for live load. The maximum live load positive moments were 2071 kip‿inches on spans 2 and 3 and 1921 kip‿inches on spans 1 and 4. The maximum live load negative moments were -1901 kip‿inches at bearing 3 and -1861 kip‿inches at bearings 2 and 4.

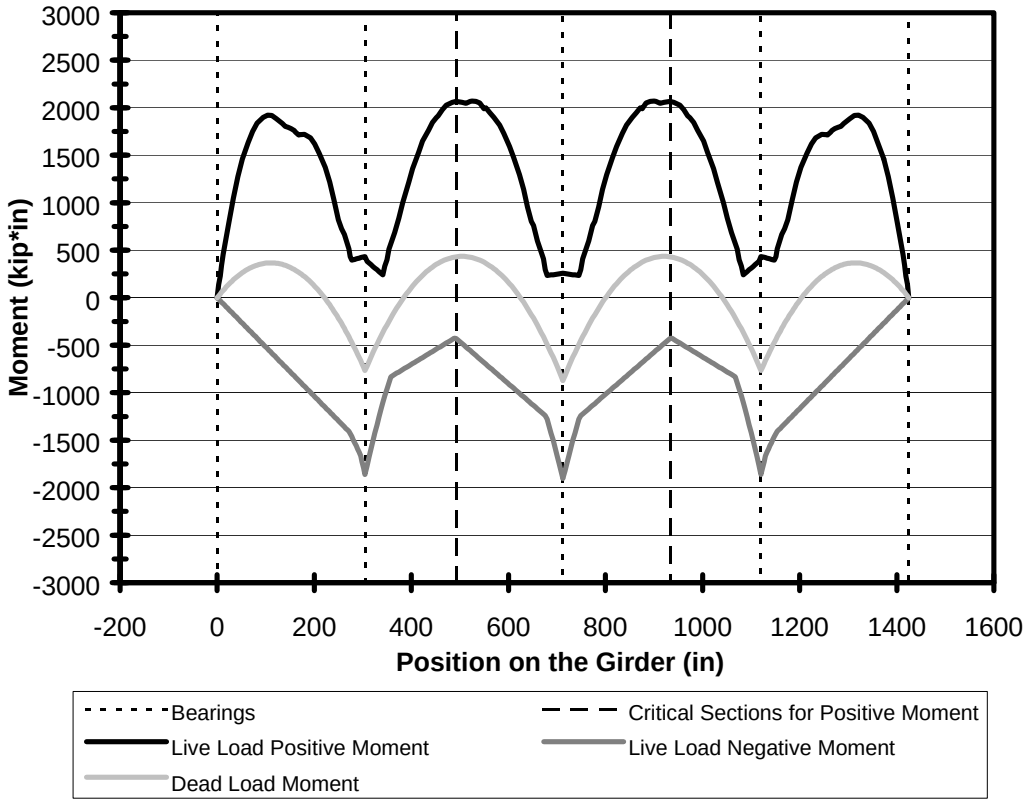

Figure 3-9 Unfactored Live Load Moment Envelope for an Interior Girder, Including Lateral Moment Distribution and Impact

Moment rating calculations compare the dead load moment and live load moment at a cross section against that cross section's moment capacity. When the largest

live load and dead load moments occur at the same location, this location is the cross section used for rating, because it produces the lowest rating factor. However, when the locations of maximum live load and dead load moment do not coincide, the location with the lowest rating factor must be determined by trial and error. This was the case for the positive moment regions of the Big Creek Relief Bridge.

Table 3-5 shows the live load moments for an interior girder, including moment distribution and impact, used for rating. In the positive moment region, the lowest rating factors were found to occur near the location of maximum live load moment, using trial and error. On spans 2 and 3, the live load moment used for rating was 2067 kip-inches, 0.99 times the maximum live load moment. The difference of 1 percent between the maximum live load moment and the live load moment used for rating indicates that the trial and error process produced a negligible improvement in the accuracy of the rating calculations. The maximum moments for both dead load and live load could have been used, instead.

Case	Live Load Moment (kip-inches)
Positive Moment on Spans 2 and 3	2067
Negative Moment at Bearing 3	-1901
Negative Moment at Bearings 2 and 4	-1861

Table 3-5 Live Load Moments for an Interior Girder, Including Moment Distribution and Impact, Used for Rating

The locations of lowest rating are called the "critical sections" of the bridge. For negative moment, the critical sections were located at bearings 2, 3, and 4. For positive moment, the critical sections were located at 492 inches and 933 inches, on spans 2 and 3, respectively. The critical sections for positive moment are shown in Figure 3-8, above, along with the bearing locations.

3.2.4 Capacity

As a result of its age, the Big Creek Relief Bridge was probably designed using the Allowable Stress Design (ASD) method. In the ASD method, the girders in the bridge are designed so that the flexural stress does not exceed 0.55 times the yield strength of the steel under "service load."

However, in the AASHTO LFD rating procedure, the capacity of the girder is expressed as an ultimate strength, and the design load is a factored load. In this case, the girders are typically designed to resist their full plastic moment. In order to develop the full plastic moment, the webs and flanges of the girders must be "compact" enough to avoid local buckling failures and each flange must be suitably braced to avoid a lateral torsional buckling failure of the whole section.

The ability of the CB-21-59 section to develop the full plastic moment was checked. First, the capacity of the CB-21-59 girders was determined using Equation 3-5:

$$M_p = F_y \cdot Z \qquad (3\text{-}5)$$

where

M_p is the plastic moment capacity of the girder, in kip~inches,

F_y is the yield strength of the steel, in ksi, and

Z is the plastic section modulus of the girder, in inches^3.

For a yield strength of 30 ksi in the steel and a plastic section modulus of 135.8 inches^3, the plastic moment capacity of the girders was found using Equation 3-5 as follows:

$$M_p = 30 \cdot 135.8 = 4074 \ \text{kip} \cdot \text{inches}$$

In the cover plated region at bearing 3, the yield strength of the cover plates was 33 ksi. Each cover plate had an area of 1.56 inches^2 and its centroid was 10.61 inches away from the centroid of the girder. Therefore, the plastic section modulus of each cover plate was 16.55 inches^3. The plastic moment capacity of the cover plated section was found using equation 3-5 as follows:

$$M_p = 4074 + 2 \cdot (33 \cdot 16.55) = 5166 \ \text{kip} \cdot \text{inches}$$

The plastic moment capacity of the girders was found to be 4074 kip-inches. In the cover plated region, the plastic moment capacity was found to be 5166 kip-inches.

Next, the flange local buckling, web local buckling, and lateral torsional buckling capacity of the CB-21-59 girders were all checked using the provisions of the AASHTO LFD code. Equation 3-6 was used to check the flange local buckling capacity of the girder, and Equation 3-7 was used to check the web local buckling capacity of the girder:

$$\frac{b'}{t_f} \le \frac{2055}{\sqrt{F_y}} \tag{3-6}$$

$$\frac{h}{t_w} \le \frac{19230}{\sqrt{F_y}} \tag{3-7}$$

where

b' is the width of the projecting flange element, in inches,
t_f is the flange thickness, in inches,
F_y is the yield strength of the steel, in psi,
h is the clear distance between flanges, in inches, and
t_w is the web thickness, in inches.

For a flange width of 8.230 inches, a flange thickness of 0.575 inches, and a yield strength of 30 ksi, the flange local buckling capacity of the girders was checked using Equation 3-6 as follows:

$$\frac{\frac{1}{2} \cdot 8.230}{0.575} = 7.16 \le 11.86 = \frac{2055}{\sqrt{30{,}000}}$$

For a girder depth of 20.901 inches, a flange thickness of 0.575 inches, and a web thickness of 0.390 inches, and a yield strength of 30 ksi, the web local buckling capacity of the girders was checked using equation 3-7 as follows:

$$\frac{(20.910 - 2 \cdot 0.575)}{0.390} = 50.67 \le 111.0 = \frac{19230}{\sqrt{30{,}000}}$$

These calculations show that the flanges and web of the CB-21-59 section are compact.

For positive flexure, the compression flange was continuously laterally braced, because the top flange was embedded in the concrete deck. For negative flexure, however, the compression flange was laterally braced only at the bearings. The adequacy of the lateral bracing of the compression flange to resist lateral torsional buckling under negative flexure was checked using Equation 3-8:

$$\frac{L_b}{r_y} \le \frac{\left(3.6 - 2.2 \cdot \frac{M_1}{M_n}\right) \cdot 10^6}{F_y} \qquad (3\text{-}8)$$

where

L_b is the laterally unbraced length of the girder, in inches,

r_y is the radius of gyration of the steel section, with respect to the horizontal axis, in inches,

M_1 is the smaller moment at the end of the unbraced length, in kip∽inches,

M_n is the moment capacity of the girder, in kip∽inches, and

F_y is the strength of the steel, in psi.

L_b was taken to be 408 inches, the length of spans 2 or 3, because there were no lateral braces present on the bridge. The full plastic moment capacity of 4074 kip∽inches was used for M_n. The value of M_1 was taken as zero, because the unbraced length extended to the end of the girder. 30 ksi was used for the yield strength of the girder. The lateral bracing of the compression flange in the negative moment region was checked using Equation 3-8 as follows:

$$\frac{408}{1.68} = 243 \text{ is not} \leq 120 = \frac{\left(3.6 - 2.2 \cdot \frac{0}{4074}\right) \cdot 10^6}{30{,}000}$$

This calculation shows that the CB-21-59 section did not satisfy the lateral bracing requirement. Therefore, the section was insufficiently laterally braced and could not develop the full plastic moment.

Due to insufficient lateral bracing, the girders could not develop the full plastic moment. As a result, the capacity of the girders was assumed to be the yield moment. The actual capacity of the girders was probably somewhere between the plastic moment and the yield moment. However, an investigation of the exact yield capacity of the girders was beyond the scope of this thesis.

The yield moment of the girders was defined as the moment causing yielding of the outer fiber of the flanges. The yield moment was determined using Equation 3-9:

$$M_y = F_y \cdot S \qquad (3\text{-}9)$$

where

M_y is the yield moment capacity of the girder, in kip∽inches,

F_y is the yield strength of the steel, in ksi, and

S is the elastic section modulus of the girder, in inches^3.

The elastic section modulus of the girder was determined by dividing the moment of inertia of the girder by the distance from the neutral axis of the girder to the outer fiber of the flanges. For a moment of inertia of 1246.8 inches^4, a distance of 10.455 inches, and a yield strength of 30 ksi, the yield moment of the girder was calculated using Equation 3-9 as follows:

$$M_y = 30 \cdot \frac{1246.8}{10.455} = 3578 \ \text{kip} \cdot \text{inches}$$

The yield moment was found to be 3578 kip∿inches, 0.88 times the full plastic moment. In addition, cover plates were welded to the girders near bearing 3. Each cover plate had an area of 1.56 inches^2 and a yield strength of 33 ksi. The distance from the neutral axis to the extreme fiber of the cover plates was 10.768 inches. The moment of inertia of the cover plated section was 1598.7 inches^4. The yield moment of the cover plated section was determined by calculating the moment causing yield in the cover plate and the moment causing yield in the flange, respectively, using Equation 3-9 as follows:

$$M_y = 33 \cdot \frac{1598.7}{10.768} = 4899 \ \text{kip} \cdot \text{inches} \qquad \text{yield in cover plate}$$

$$M_y = 30 \cdot \frac{1598.7}{10.455} = 4587 \ \text{kip} \cdot \text{inches} \qquad \text{yield in flange}$$

The yield moment of the cover plated section was 4587 kip∿inches and was controlled by yielding of the outer fiber of the flanges. Table 3-6 presents a summary of the yield and plastic moment capacities of the girders.

	Yield Moment Capacity (kip∿in)	**Plastic Moment Capacity (kip∿in)**
Without Cover Plates	3578	4074
With Cover Plates	4587	5166

Table 3-6 Yield Moment and Plastic Moment Capacity of the Girders

3.2.5 Rating Calculations

AASHTO LFD inventory and operating ratings were determined using Equation 3-1, above, for positive moment on spans 2 and 3, negative moment at bearing 3, and negative moment at bearings 2 and 4. The overall lowest rating factor was taken as the rating factor for the bridge. Table 3-7 shows the live load moment, dead load moment, and capacity used to determine the rating factor for each case.

Case	Yield Moment Capacity (kip∽inches)	Dead Load Moment (kip∽inches)	Live Load Moment (kip∽inches)
Positive Moment, Spans 2 and 3	3578	431	2067
Negative Moment, Bearing 3	-4587	-869	-1901
Negative Moment, Bearings 2 and 4	-3578	-767	-1861

Table 3-7 Summary of Rating Moments

Using Equation 3-1, the inventory and operating ratings for positive moment on spans 2 and 3 were determined as follows:

$$RF = \frac{(3578) - 1.3 \cdot (431)}{2.17 \cdot (2067)} = 0.673 \qquad \text{inventory rating factor}$$

$$RF = \frac{(3578) - 1.3 \cdot (431)}{1.3 \cdot (2067)} = 1.123 \qquad \text{operating rating factor}$$

The inventory and operating ratings for negative moment at bearing 3 were determined as follows:

$$RF = \frac{(-4587) - 1.3 \cdot (-869)}{2.17 \cdot (-1901)} = 0.838 \qquad \text{inventory rating factor}$$

$$RF = \frac{(-4587) - 1.3 \cdot (-869)}{1.3 \cdot (-1901)} = 1.399 \qquad \text{operating rating factor}$$

The inventory and operating ratings for negative moment at bearings 2 and 4 were determined as follows:

$$RF = \frac{(-3578) - 1.3 \cdot (-767)}{2.17 \cdot (-1861)} = 0.639 \qquad \text{inventory rating factor}$$

$$RF = \frac{(-3578) - 1.3 \cdot (-767)}{1.3 \cdot (-1861)} = 1.067 \qquad \text{operating rating factor}$$

The AASHTO HS-20 LFD rating of the Big Creek Relief Bridge was controlled by negative moment at bearings 2 and 4 on the interior girders. The inventory rating factor of 0.639 indicated that the bridge could not carry traffic loads equivalent to the HS-20 vehicle for an indefinite period of time, and the operating rating factor of 1.067 suggested that HS-20 loads would just barely be permissible, on a short-term or a permit basis. In summary, the rating analysis indicated that the bridge had a deficient load rating and that load posting or closure was required.

Bridge ratings are often expressed as a multiple of the rating vehicle's designation. Since the inventory rating factor for the bridge was 0.639 and the HS-20 vehicle was used to apply the live load, the bridge had a HS-12.8 inventory rating. Similarly, the operating rating for the bridge was HS-21.3. Table 3-8 presents a summary of the HS-20 ratings for the bridge.

If the plastic moment capacity for the bridge was used instead of the yield moment capacity, the inventory rating for the bridge would have been 0.762 and the operating rating would have been 1.272. This is an improvement of 1.19 times the yield capacity results. The rating would still have been controlled by the negative moment at bearings 2 and 4.

	Rating Factor	**HS-20 Rating**
Inventory Level	0.639	HS-12.8
Operating Level	1.067	HS-21.3

Table 3-8 AASHTO HS-20 LFD Load Rating of the Big Creek Relief Bridge, Controlled by Negative Moment at Bearings 2 and 4 on the Interior Girders

3.3 Line Girder Analysis of the Test Vehicle Loading

A 10 cubic yard dump truck was used to load the bridge during the field tests. An analysis of the moments produced by the 10 cubic yard (c.y.) truck was performed to determine a moment envelope and several moment influence lines. The moment envelope was used to compare the moments produced by the 10 c.y. truck with the moments produced by the HS-20 vehicle, used for rating. The moment influence lines were determined to compare the results of the analysis with the field test data. In order to develop the moment influence lines, moment distribution and impact factors for the 10 c.y. truck were also determined. This section presents the results of the moment envelope, lateral moment distribution factor, and moment influence line calculations.

3.3.1 Design Live Load

Figure 3-10 shows a diagram of the 10 c.y. truck's axle loads. The truck had 3 axles, weighing 11.24 kips, 19.54 kips, and 19.54 kips, respectively, from front to back. The distance between the front axle and the center axle was 151 inches, and the distance between the center axle and the rear axle was 53 inches.

The 10 c.y. moment envelope for the design girder, including the AASHTO LRFD two-lane moment distribution factors and impact, is shown in Figure 3-11. For comparison, the moment envelope for the HS-20 vehicle is also shown in the figure. At every position on the design girder, the HS-20 vehicle produced a larger moment than the 10 c.y. truck.

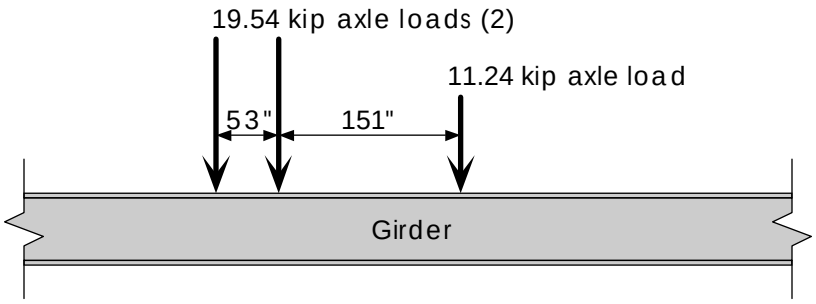

Figure 3-10 10 Cubic Yard Truck Load

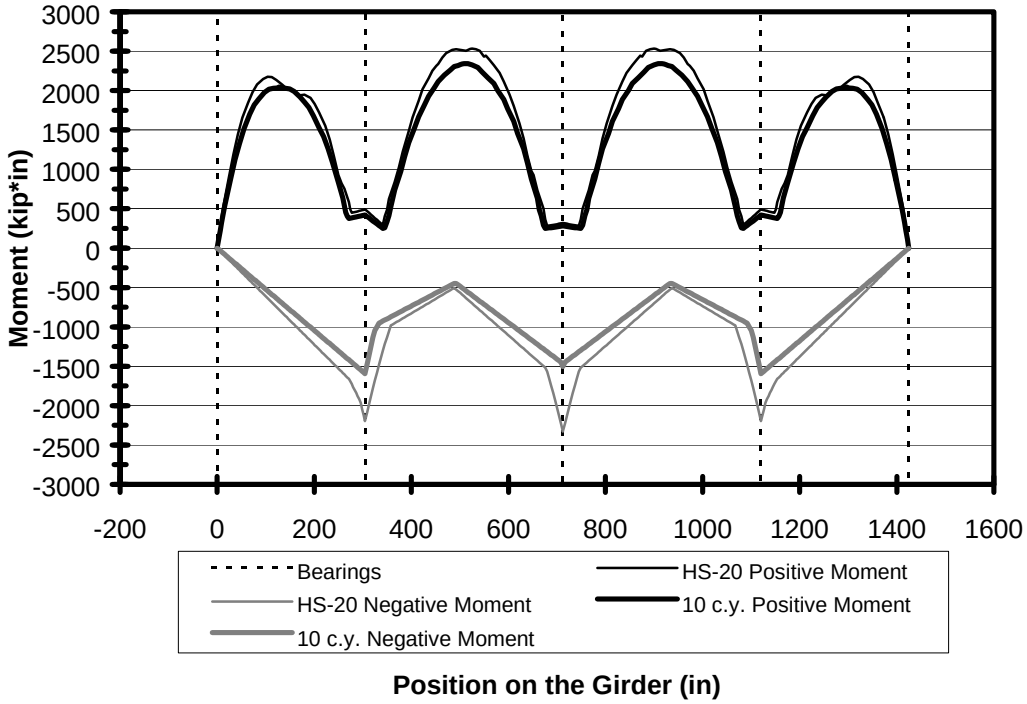

Figure 3-11 10 Cubic Yard Truck and HS-20 Design Vehicle Live Load Moment Envelopes for the Design Girder

The maximum live load positive moment produced by the 10 c.y. truck was 2341 kip~inches and occurred at 515 inches on span 2 and at 910 inches on span 3. Figure 3-12 shows a diagram of the design girder with the 10 c.y. truck's axle loads in the position corresponding to maximum live load positive moment on span 3. In Figure 3-12 and similar figures to follow, the truck is facing to the right.

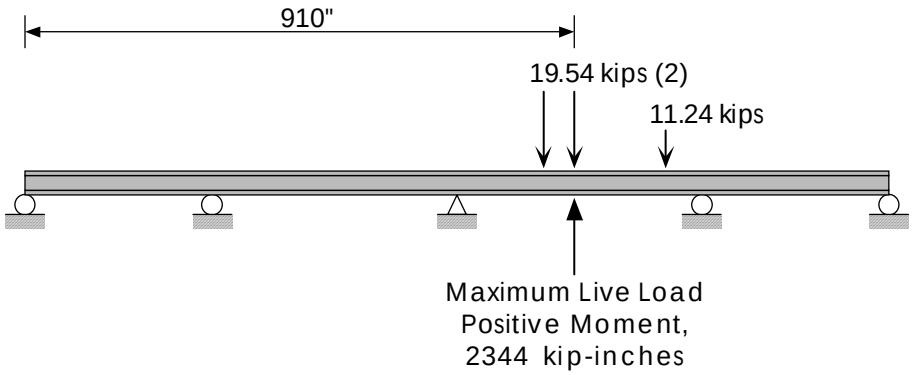

Figure 3-12 10 c.y. Truck Position for Maximum Live Load Positive Moment on Span 3

The maximum live load negative moment produced by the 10 c.y. truck was -1593 kip-inches and occurred at bearings 2 and 4. Figure 3-13 shows a diagram of the design girder with the 10 c.y. truck's axle loads in the position corresponding to maximum live load negative moment at bearing 2.

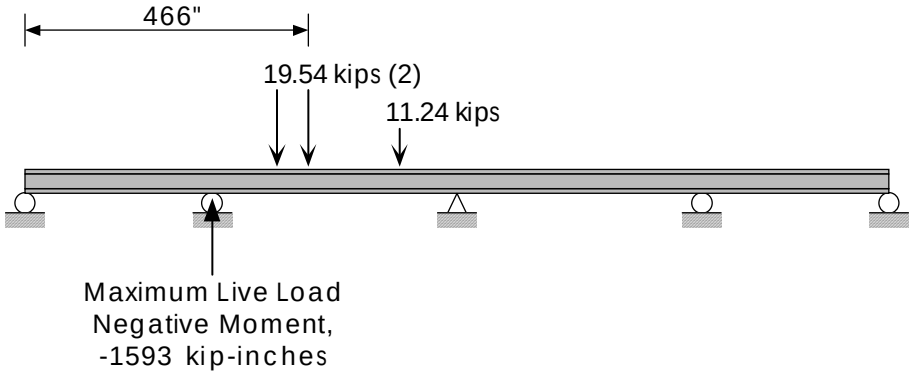

Figure 3-13 10 c.y. Truck Position for Maximum Live Load Negative Moment at Bearing 2

The live load negative moment at bearing 3 produced by the 10 c.y. truck was -1502 kip-inches, which is 0.94 times the maximum live load negative moment. Figure 3-14 shows a diagram of the design girder with the 10 c.y. truck's axle loads in the position corresponding to maximum live load negative moment at bearing 3.

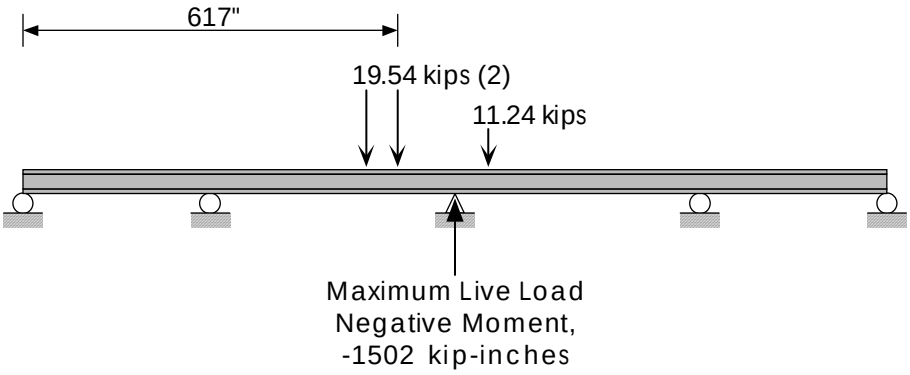

Figure 3-14 10 c.y. Truck Position for Maximum Live Load Negative Moment at Bearing 3

Table 3-9 presents the maximum live load moments in the design girder produced by the 10 c.y. truck and the HS-20 vehicle. The results in Table 3-9 show that, in the positive moment regions, the 10 c.y. truck was capable of producing moment magnitudes similar to the HS-20 vehicle. However, in the negative moment regions, the response produced by the 10 c.y. truck, due to its short wheelbase, was only 0.65 to 0.73 times the response produced by the HS-20 vehicle.

The results in Table 3-9 include the AASHTO two-lane moment distribution factors and impact factor, but the field tests were conducted with just one 10 c.y. truck, moving slowly. Therefore, in Table 3-9, the 10 c.y. truck's maximum moments do not correspond with the actual maximum moments recorded during the field tests. A comparison of the maximum moments recorded during the field tests and the HS-20 maximum moments from Table 3-9 is presented in Chapter 6, along with a discussion on extrapolating the test data.

Case	10 c.y. Design Moment (kip-in)	HS-20 Design Moment (kip-in)	Ratio of 10 c.y. to HS-20
Positive Moment, Spans 2 and 3	2344	2532	0.93
Negative Moment, Bearing 3	-1502	-2324	0.65
Negative Moment, Bearings 2 and 4	-1593	-2196	0.73

Table 3-9 Comparison of Maximum Live Load Moments Produced by the 10 Cubic Yard Truck and the HS-20 Truck, Including the AASHTO Two-Lane Moment Distribution Factors and Impact

3.3.2 Field Test Lateral Moment Distribution and Impact Factors

The field tests were performed using only one 10 c.y. truck. Therefore, the AASHTO LRFD moment distribution factors for one design lane and one vehicle were used to model the lateral moment distribution behavior of the bridge. This approach differs from the HS-20 load rating calculations, where the lateral moment distribution factors for two design lanes were used.

The AASHTO LRFD code differentiates between exterior and interior girders. Equation 3-10 shows the formula used to determine the lateral moment distribution factor for an interior girder, assuming one design lane. In Equation 3-10, the term inside the brackets includes the effect of a multiple presence factor of 1.2, used in design to account for the probability of two trucks crossing the bridge at one time. However, the effects of multiple presence are not applicable to the field tests, because the field tests were performed in a controlled environment, in which only one truck was placed on the bridge. To remove the effect of the multiple presence factor, the (1/1.2) term was added to the end of Equation 3-10:

$$MDF_{int} = \left[0.06 + \left(\frac{S}{14}\right)^{0.4} \cdot \left(\frac{S}{L}\right)^{0.3} \cdot \left(\frac{K_g}{12 \cdot L \cdot t_s^{\,3}}\right)^{0.1} \right] \cdot \frac{1}{1.2} \qquad (3\text{-}10)$$

where

MDF_{int} is the moment distribution factor for an interior girder,

S is the girder spacing, in feet,

L is the span length, in feet,

t_s is the thickness of the slab, in inches, and

K_g is a longitudinal stiffness parameter, in inches^4.

The value of K_g was determined using equation 3-3, as shown in section 3.2.1, above. The values of S, L, and t_s used to determine the lateral moment distribution factors for the 10 c.y. truck were the same values used to determine the lateral moment distribution factors for the HS-20 truck. These values are summarized in Table 3-3, above.

For positive moment on spans 1 and 4, the value of MDF_{int} was found to be:

$$MDF_{int} = \left[0.06 + \left(\frac{6.5}{14}\right)^{0.4} \cdot \left(\frac{6.5}{25.375}\right)^{0.3} \cdot \left(\frac{49521}{12 \cdot 25.375 \cdot 6^3}\right)^{0.1}\right] \cdot \frac{1}{1.2} = 0.446$$

For positive moment on spans 2 and 3, and for negative moment at bearing 3, the value of MDF_{int} was found to be:

$$MDF_{int} = \left[0.06 + \left(\frac{6.5}{14}\right)^{0.4} \cdot \left(\frac{6.5}{34}\right)^{0.3} \cdot \left(\frac{49521}{12 \cdot 34 \cdot 6^3}\right)^{0.1}\right] \cdot \frac{1}{1.2} = 0.403$$

For negative moment at bearings 2 and 4, the value of MDF_{int} was found to be:

$$MDF_{int} = \left[0.06 + \left(\frac{6.5}{14}\right)^{0.4} \cdot \left(\frac{6.5}{29.688}\right)^{0.3} \cdot \left(\frac{49521}{12 \cdot 29.688 \cdot 6^3}\right)^{0.1}\right] \cdot \frac{1}{1.2} = 0.422$$

For single vehicle loading, the AASHTO LRFD lateral moment distribution factors for the exterior girders are based on the “lever rule.” Figure 3-15 shows the lateral position of the 10 c.y. truck, used to determine the lateral moment distribution

factor for the exterior girder. The centroid of the truck's outer wheel was placed 2 feet from the curb, as specified in the AASHTO LRFD code.

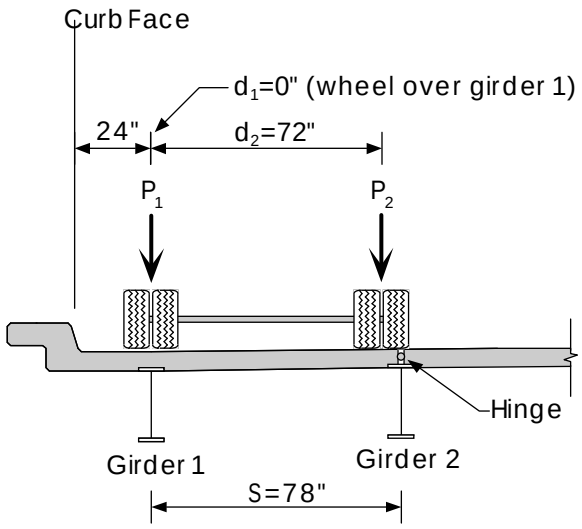

Figure 3-15 Position of the 10 Cubic Yard Truck's Rear Axle for Determining the Exterior Girder Lateral Moment Distribution Factor, Using the "Lever Rule"

In applying the lever rule, the deck was modeled as having a hinge over the interior girder. The lateral moment distribution factor was determined by calculating the percentage of the live load that was resisted by the exterior girder, according to a static analysis. For the truck position shown in Figure 3-15, the LRFD lateral moment distribution factor for the exterior girders was calculated using Equation 3-11:

$$MDF_{ext} = \tfrac{1}{2} \cdot \left(\frac{S - d_1}{S} + \frac{S - d_2}{S} \right) \qquad (3\text{-}11)$$

where

MDF_{ext} is the LFD moment distribution factor for the exterior girder,

S is the girder spacing, in inches,

d_1 is the distance from the exterior girder to the exterior wheel, in inches, and

d_2 is the distance from the exterior girder to the interior wheel, in inches.

For d_1 equal to zero, d_2 equal to 72 inches, and S equal to 78 inches, the LRFD moment distribution factor for the exterior girders was determined as follows:

$$MDF_{ext} = \tfrac{1}{2} \cdot \left(\frac{78-0}{78} + \frac{78-72}{78} \right) = 0.538$$

Table 3-10 presents a summary of the AASHTO LRFD lateral moment distribution factors for the 10 c.y. truck on the bridge. In all cases, the lateral moment distribution factors for the exterior girders, determined using the lever rule, were larger than the lateral moment distribution factors for the interior girders.

Case	Interior Girders	Exterior Girders
Positive Moment, Spans 1 and 4	0.446	0.538
Positive Moment, Spans 2 and 3	0.403	0.538
Negative Moment, Bearings 2 and 4	0.422	0.538
Negative Moment, Bearing 3	0.403	0.538

Table 3-10 Single-Lane AASHTO LRFD Moment Distribution Factors for the 10 c.y. Truck

The effects of impact were assumed to be negligible in the analysis of the 10 c.y. truck, because the truck was driven across the bridge at about 4 miles per hour during the field tests. This speed was too slow to produce dynamic effects in the bridge. Therefore, an impact factor of 1.00 was used to determine moment influence lines for the 10 c.y. truck for comparison with the field test data.

3.3.3 Moment Influence Lines

Moment influence lines were determined for the 10 c.y. truck at the two locations where instrumentation was placed during the field tests: 316 inches in the negative moment region near bearing 2 and 908 inches in the positive moment region on span 3. Line girder, exterior girder, and interior girder moment influence lines were determined. The line girder moment influence lines were determined by applying the 10 c.y. truck load to the design girder. The exterior and interior moment influence lines were determined by scaling the line girder moment influence line by the appropriate lateral moment distribution factors, determined in section 3.3.2, above.

Figure 3-16 shows the moment influence lines for the negative moment region at 316 inches. The exterior girder moment influence line was calculated using a lateral moment distribution factor of 0.538. The interior girder moment influence line was calculated using a lateral moment distribution factor of 0.422. An impact factor of 1.00 was used in both cases.

Figure 3-17 shows the moment influence lines for the positive moment region at 908 inches. The exterior girder moment influence line was calculated using a lateral moment distribution factor of 0.538. The interior girder moment influence line was calculated using a lateral moment distribution factor of 0.403. An impact factor of 1.00 was used in both cases.

The interior and exterior girder moment influence lines from Figures 3-16 and 3-17 were used to predict the results of the field tests and properly set up the test instrumentation, as described in Chapter 4. Furthermore, the line girder moment influence lines were used to determine the extent of noncomposite flexural participation in the deck, by comparing the calculated moment influence lines to the sum of the measured moments in each girder. This procedure is presented in Chapter 6.

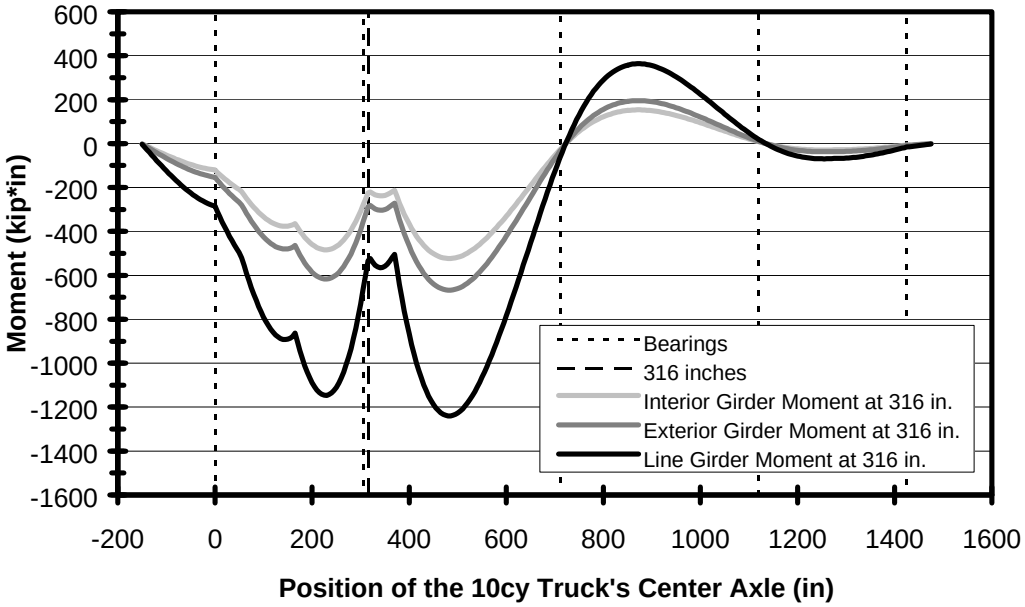

Figure 3-16 Line, Exterior, and Interior Girder Moment Influence Lines at 316 Inches, for the 10 Cubic Yard Truck

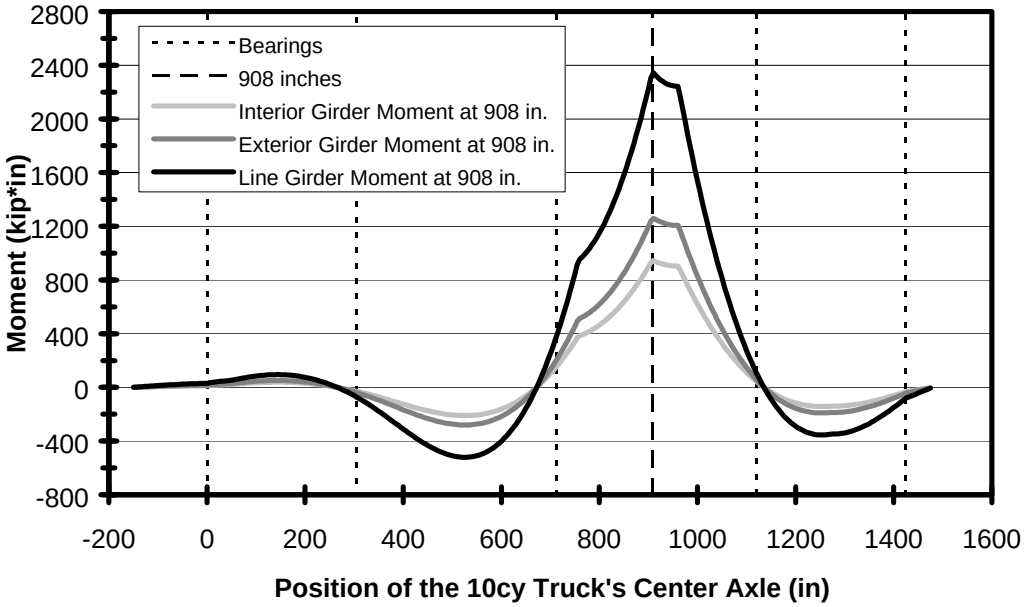

Figure 3-17 Design, Exterior, and Interior Girder Moment Influence Lines at 908 Inches, for the 10 Cubic Yard Truck

3.4 Comparison of Moment Distribution Factors

For the load rating calculations, presented in section 3.2, above, the AASHTO LRFD moment distribution factors were used to approximate the lateral moment distribution behavior of the bridge. However, there are other methods for approximating the distribution behavior of the bridge, such as the AASHTO LFD method, and finite element analysis. In this section, the AASHTO LRFD moment distribution factors, calculated in section 3.2.3, above, are compared with the moment distribution factors given by the AASHTO LFD code and the moment distribution factors given by a finite element analysis using BRUFEM, a bridge analysis program. The effect of the various moment distribution factors on the load rating of the bridge is also presented.

3.4.1 AASHTO LFD vs. AASHTO LRFD

The lateral moment distribution factor equations given in the AASHTO LFD code have fewer variables, and therefore, are simpler to apply than the equations given in the AASHTO LRFD code. Equation 3-12 was used to determine the LFD axle load moment distribution factor for the interior girders on the Big Creek Relief Bridge, for two design lanes:

$$MDF_{int} = \tfrac{1}{2} \cdot \left(\frac{S}{5.5} \right) \qquad (3\text{-}12)$$

where

S is the spacing between girders, in feet.

Using a girder spacing of 6.5 feet, the value of MDF_{int} was found to be:

$$MDF_{int} = \tfrac{1}{2} \cdot \left(\frac{6.5}{5.5} \right) = 0.591$$

This value was used for positive flexure and negative flexure on every span and at every bearing.

The AASHTO LFD lateral moment distribution factors for the exterior girders are based on the "lever rule." Figure 3-18 shows the lateral positions of the HS-20 trucks, used to determine the lateral moment distribution factor for the exterior girder.

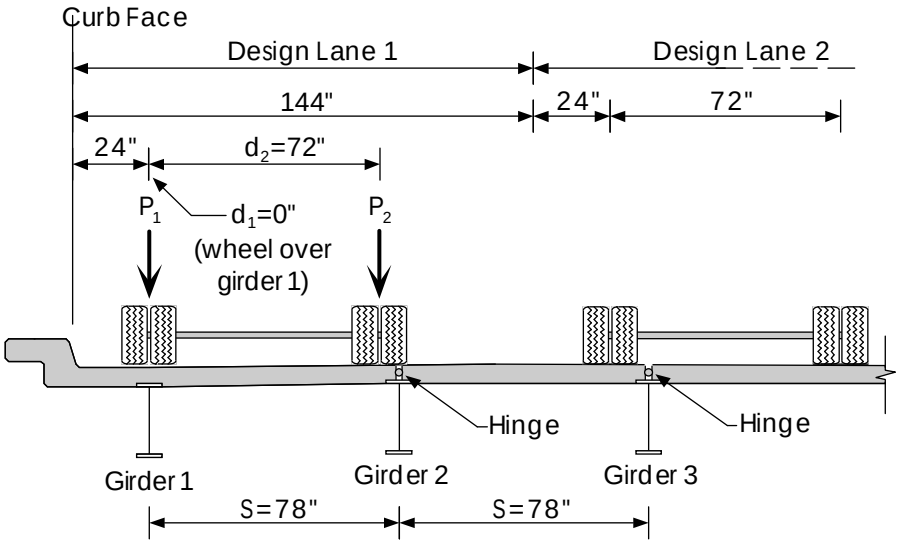

Figure 3-18 Position of HS-20 Trucks for Determining the Two-Lane AASHTO LFD Exterior Girder Moment Distribution Factor, Using the "Lever Rule"

Two HS-20 trucks were used to calculate the lateral moment distribution factor, because two 12 foot wide design lanes fit on the bridge. For the truck in the first design lane, the centroid of the truck's outer wheel was placed 2 feet from the curb, as specified in the AASHTO LFD code. For the second design lane, the truck was placed as close as possible to girder 1, while remaining in the design lane. Because the girder spacing was shorter than the width of the design lane and the deck was modeled as hinged over the interior girders, the position of the second vehicle had no effect on the moment distribution factor for the exterior girder.

The AASHTO LFD moment distribution factor for the exterior girders was calculated using Equation 3-13:

$$MDF_{ext} = \tfrac{1}{2} \cdot \left(\frac{S - d_1}{S} + \frac{S - d_2}{S} \right) \qquad (3\text{-}13)$$

where

MDF_{ext} is the LFD moment distribution factor for the exterior girder,

S is the girder spacing, in inches,

d_1 is the distance from the exterior girder to the exterior wheel, in inches, and

d_2 is the distance from the exterior girder to the interior wheel, in inches.

For d_1 equal to zero, d_2 equal to 72 inches, and S equal to 78 inches, the LFD moment distribution factor for the exterior girders was determined as follows:

$$MDF_{ext} = \tfrac{1}{2} \cdot \left(\frac{78-0}{78} + \frac{78-72}{78} \right) = 0.538$$

Table 3-11 shows a comparison of the AASHTO LFD and LRFD moment distribution factors for two design lanes. In all cases, the LFD lateral moment distribution factors were lower than the corresponding LRFD lateral moment distribution factors.

During the rating procedure, shown in section 3.2, the two-lane AASHTO LRFD lateral moment distribution factors were used. In the rating analysis, the lowest rating factor corresponded to negative moment at bearings 2 and 4 on an interior girder. For comparison, if the AASHTO LFD moment distribution factors had been used in the rating calculations in section 3.2, the inventory and operating ratings for the bridge would have increased by a factor of 1.077 (= 1/0.928, from Table 3-11).

Case	AASHTO LFD	AASHTO LRFD	Ratio of LFD / LRFD
Interior Girders			
Positive Moment on Spans 1 and 4	0.591	0.664	0.890
Positive Moment on Spans 2 and 3	0.591	0.615	0.961
Negative Moment at Bearings 2 and 4	0.591	0.637	0.928
Negative Moment at Bearing 3	0.591	0.615	0.961
Exterior Girders			
Positive Moment on Spans 1 and 4	0.538	0.657	0.819
Positive Moment on Spans 2 and 3	0.538	0.608	0.885
Negative Moment at Bearings 2 and 4	0.538	0.630	0.854
Negative Moment at Bearing 3	0.538	0.618	0.885

Table 3-11 Comparison of AASHTO LFD and LRFD Lateral Moment Distribution Factors for Two Design Lanes

The moment distribution factors provided by both the AASHTO LFD and LRFD codes are approximate in nature. In fact, the commentary to the AASHTO LRFD code (1994b, C4.6.2.2.1) states that "correction factors dealing with 5 percent adjustments were thought to imply misleading levels of accuracy in an approximate method." Considering this implied level of accuracy, the difference between the AASHTO LFD rating and the AASHTO LRFD rating was negligible.

3.4.2 Finite Element Analysis vs. AASHTO LRFD

A study of the moment distribution behavior of the Big Creek Relief Bridge was also performed by Jauregui (1999). As part of Jauregui's study, a set of moment distribution factors for the bridge were determined using the finite element analysis program BRUFEM. The results of Jauregui's study are shown in Table 3-12.

Case	BRUFEM	AASHTO LRFD	Ratio of BRUFEM / LRFD
Interior Girders			
Positive Moment on Spans 1 and 4	0.635	0.664	0.956
Positive Moment on Spans 2 and 3	0.610	0.615	0.992
Negative Moment at Bearings 2 and 4	0.618	0.637	0.970
Negative Moment at Bearing 3	0.635	0.615	1.033
Exterior Girders			
Positive Moment on Spans 1 and 4	0.435	0.657	0.662
Positive Moment on Spans 2 and 3	0.458	0.608	0.753
Negative Moment at Bearings 2 and 4	0.471	0.630	0.748
Negative Moment at Bearing 3	0.471	0.618	0.762

Table 3-12 Comparison of AASHTO LRFD Moment Distribution Factors for Two Design Lanes with BRUFEM Finite Element Analysis

For the interior girders, Jauregui's results showed excellent agreement with the AASHTO LRFD two-lane moment distribution factors. However, for the exterior girders, Jauregui's results were significantly lower. This discrepancy was probably due

to the conservative nature of the AASHTO LRFD equations, since the intent of the AASHTO LRFD code is to design the bridge's exterior girders for at least as much live load as the interior girders.

Rating analyses, however, are concerned with the actual behavior of the bridge. Therefore, the lower lateral moment distribution factors determined by Jauregui are appropriate, since they are based on the actual dimensions and behavior of the bridge. Indeed, for the negative moment regions of the exterior girders, the field test results agreed favorably with Jauregui's analysis. The results of the field tests are presented in detail in Chapter 5.

If Jauregui's results were used to load rate the bridge, the inventory and operating ratings for the bridge would have increased by a factor of 1.031 (= 1/0.970, from Table 3-12). A negligible increase, since the load rating was still controlled by negative moment at bearings 2 and 4 on the interior girders.

CHAPTER 4

Field Test Setup and Procedure

The Big Creek Relief Bridge was field tested on several occasions over a period of months. Each field test made use of a larger set of instrumentation and evaluated more aspects of the bridge's behavior. By the end of the field tests, thirty foil gages and five transducers (hereafter referred to collectively as "the gages") had been placed on the bridge, and two test vehicles had been used. This chapter focuses on the gages, test vehicle, and procedure used during the final field test, because the data collected during this test was used to load rate the bridge.

4.1 Instrumentation

Figure 4-1 shows a framing plan of the bridge, including the locations of the two cross sections that were instrumented. One cross section was located in a positive moment region near the middle of a span, and the other cross section was located in a negative moment region near a bearing. A grid is also shown in Figure 4-1. The origin of the grid is at the intersection of the centerline of bearing 1 and the centerline of girder 1. This grid is the basis for describing the positions of the gages and the test trucks.

Gages were placed as near to the locations of maximum moment as practically possible. The gages in the positive moment region were placed at 908 inches. This was the location of maximum live load positive moment, as determined by analysis. The negative moment gages were placed at 316 inches, near the point of maximum live load negative moment. The maximum live load negative moment occurred at 304.5 inches, at the location of bearing 2. However, at bearing 2, the lower flanges of the girders were welded to the fixed bearings (as shown above in Figure 2-12), causing a stress concentration in the flange. The gages in the negative moment region were placed 12 inches away from bearing 2 to avoid the stress concentration.

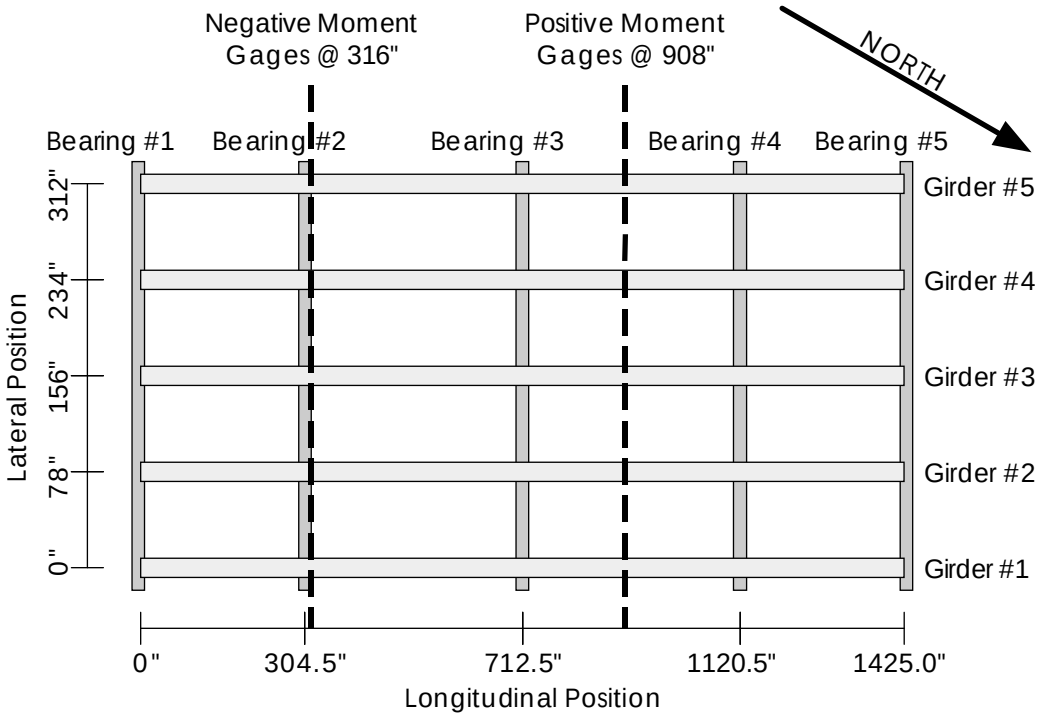

Figure 4-1 Plan View of the Girders and Bearings, Showing the Cross Sections Where Strain Instrumentation Was Placed

Three foil gages were placed on each of the girders. In addition, transducers were placed on the girders in the positive moment region. Figure 4-2 shows a detail of the foil gage and transducer placement on a typical girder. A total of thirty foil gages and five transducers were installed on the bridge.

Figures 4-3 and 4-4 show the labels used to identify the foil gages and transducers. The top flange foil gages were labeled with the prefix ST, where S stands for a foil strain gage and T stands for top. They were located on the underside of the top flange, 2 inches from the edge of the flange. The bottom flange foil gages were labeled with the prefix SB, where B stands for bottom. They were located on the top face of the bottom flange, 2 inches in from the edge of the flange. The mid-web foil gages were labeled with the prefix SM, where M stands for mid-depth. They were located at mid-depth of the web, 9.88 inches away from the inside face of each flange. The transducer positions were labeled with the prefix T. One strain transducer was placed on each girder

in the positive moment region. The transducers were located on the top face of the bottom flange, opposite from the foil gages.

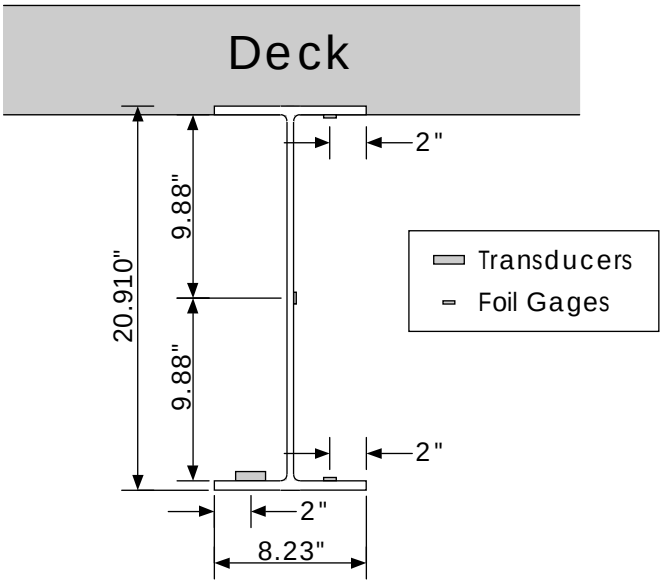

Figure 4-2 Detail of Gage and Transducer Placement

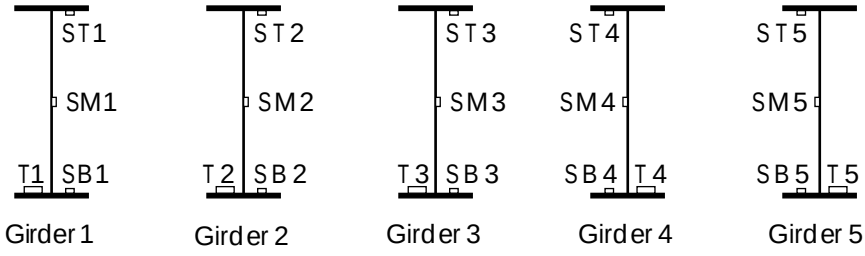

Figure 4-3 Strain Gage and Transducer Position Labels, for the Positive Moment Region at 908 inches

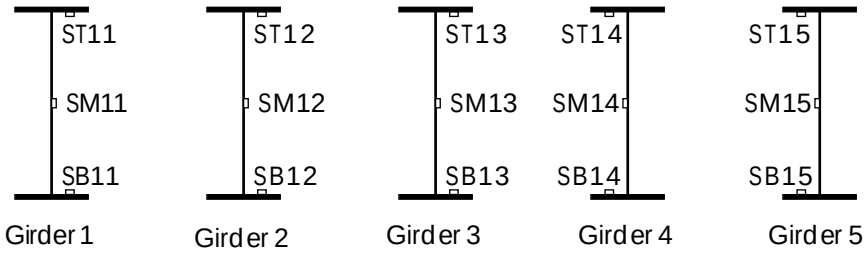

Figure 4-4 Strain Gage Position Labels, for the Negative Moment Region at 316 inches

The instrumentation was protected from the weather within practical limitations. The foil gages were permanently bonded to the bridge and sealed with a weatherproof coating. For additional protection from the elements, the foil gages were placed on the interior side of the girders. However, there was not enough room to place the transducers on the same side of the flange as the foil gages, so the transducers were placed on the more exposed side of the girders. This was acceptable, because the transducers were removable and because they were more weatherproof than the strain gages. The transducers were removed after testing and were not exposed to the weather for long periods of time.

4.1.1 Foil Gages

The foil gages had a 10 millimeter gage length, and a 2.5 millimeter gage width. The nominal resistance of the gages was 120 ohms, and they were temperature compensating. One meter long 3-wire leads were attached to the gages at the factory. The transverse sensitivity of the gages was -0.7 percent.

Before the foil gages were installed, the surface of the girders was prepared by removing the paint and rust, using a hand grinder. The exposed metal was polished by wet sanding with 600 grid sandpaper and acetone. Finally, the polished surface was cleaned with cotton swabs soaked in acetone.

The foil gages were bonded to the steel girders using an adhesive and catalyst. The adhesive was chosen because of its quick curing time and ease of installation. Butyl

rubber was used to insulate the exposed ends of the 3-wire leads. The gages were sealed with an acrylic coating to protect the gages from moisture and to insulate the lead wires. An exterior layer of silicone rubber was applied over the acrylic coating. The hardened silicone rubber anchored the lead wires to prevent pullout and protected the gages from abrasion and moisture.

4.1.2 Transducers

The removable strain transducers were manufactured by Bridge Weighing Systems, Inc., for the Texas Department of Transportation. They were part of a bridge fatigue assessment system, developed by the University of Texas in 1988 (Post et al. 1988) and were borrowed for use with this project. The transducers were studied to determine the feasibility of using strain transducers in lieu of foil gages during a field test.

A detail of a typical transducer is shown in Figure 4-5. The transducers had a seven inch gage length and contained four 350 ohm foil gages in a full-bridge configuration. Each of the foil gages was mounted on the inside surface of one of the four 23/64 inch holes drilled through the transducer. Two slots were cut through the holes in the transducer, to amplify the stress at the gage locations through bending of the center section. In addition, the full-bridge circuit in the transducers was four times more sensitive to strain than the quarter-bridge circuit used with the foil gages. This made the transducers much more sensitive to changes in strain than a foil gage.

The transducers were calibrated using a specially fabricated calibration bar (Post et al. 1988). The calibration bar, as shown in Figure 4-6, was 37 inches long and 0.375 inches thick, with a yield strength of 100 ksi. The width of the neck section was 2 inches, and the nominal cross sectional area of the bar was 0.75 square inches. The transducers were bolted to the side of the bar, using two holes drilled at a 7 inch spacing. Two strain gages were located in the center of the calibration bar, one on each side.

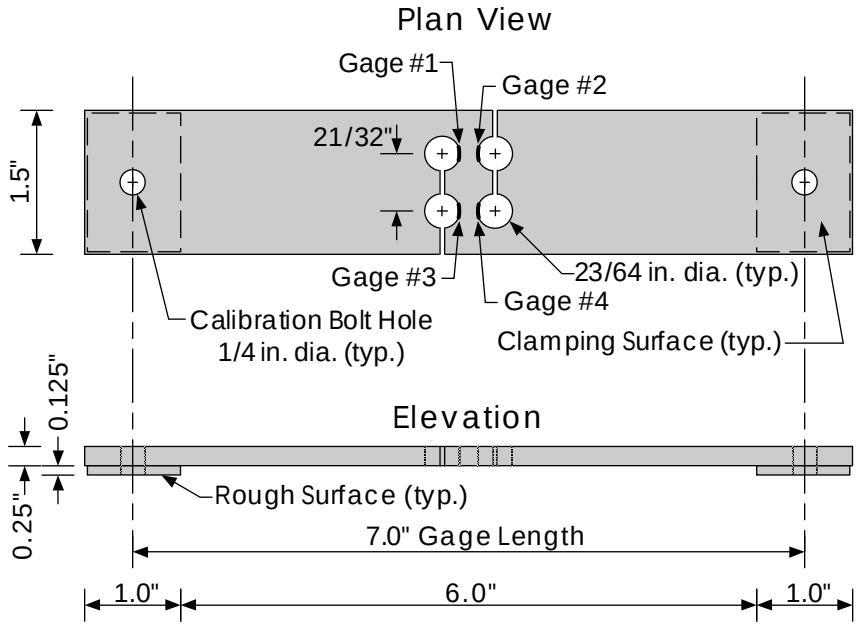

Figure 4-5 Detail of a Typical Strain Transducer

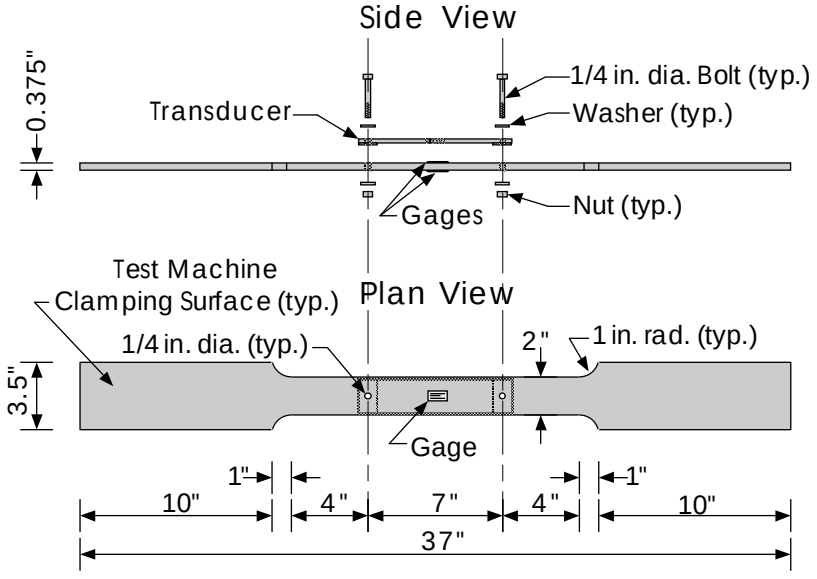

Figure 4-6 Detail of the Transducer Calibration Bar

The calibration bar was clamped in a universal test machine, and a transducer was attached to one side. The average tensile stress in the bar was cycled between zero and eight ksi, while the output from the transducer and the two strain gages was recorded. The output from the two strain gages was used to calculate the "apparent stress" in a plane passing through the mid-thickness of the transducer, since the transducer actually measured stress in its own plane, rather than in the plane of the surface to which it is attached.

The difference in surface stress between one side of the calibration bar and the other was approximately 16 percent, indicating that there was a significant amount of flexure in the calibration bar. The flexure was attributed to misalignment of the test machine fixtures and to out-of-straightness of the calibration bar. To cancel out the effects of flexure, three stress cycles were performed with the transducer on the front of the bar and three cycles were performed with the transducer on the back.

Figure 4-7 shows the calibration data from transducer UT1. This plot is typical of the calibration data from all of the transducers. A linear regression was performed to find a best-fit line for the data. The calibration factor for each transducer was taken as the slope of the best-fit line.

Table 4-1 presents the results of the calibration procedure, including the calibration factors, standard errors, and amplification factors for each transducer. The stress amplification in each transducer was calculated by dividing the transducer's calibration factor by the calibration factor of a quarter-bridge foil gage circuit (0.01819 millivolts per volt per ksi., for a foil gage with a gage factor of 2.11). In Table 4-1, the results show that the output from the transducers was amplified 6.65 to 8.36 times over the output of a foil gage in a quarter bridge circuit.

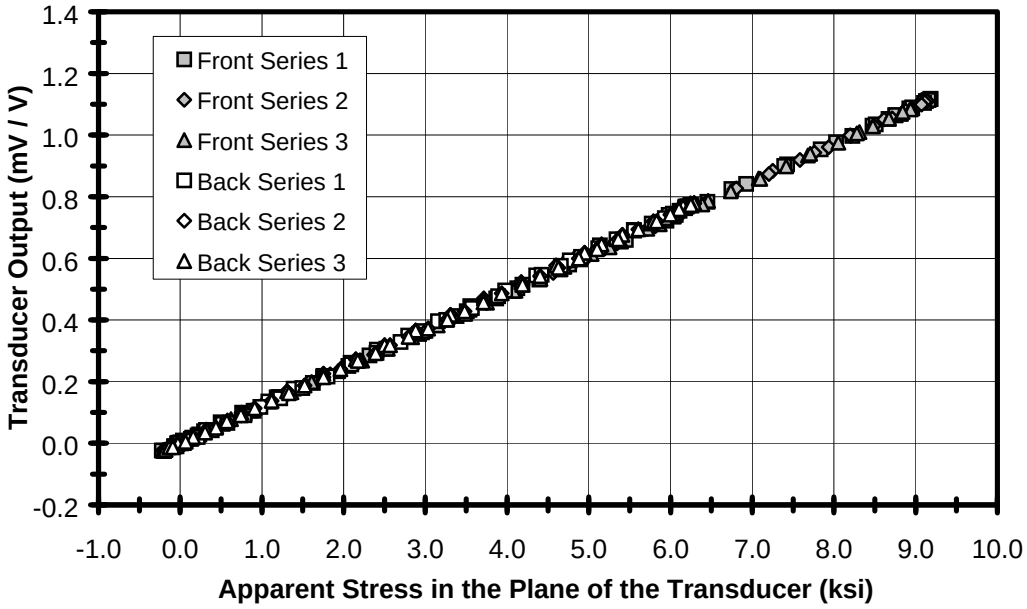

Figure 4-7 Sample Plot of Transducer Calibration Data

Transducer Name	Calibration Factor (mV/V per Ksi)	Standard Error	Amplification	Position
UT1	0.121	0.000218	6.65	T1
UT2	0.152	0.000291	8.36	T4
UT3	0.137	0.000281	7.53	T5
UT4	0.141	0.000302	7.75	T2
UT5	0.136	0.000313	7.48	T3

Table 4-1 Transducer Calibration Results and Positions

The position of each transducer on the bridge is also shown in Table 4-1. It was important to keep track of each transducer's position, because each transducer had a unique calibration factor. The transducer position labels T1 through T5 correspond with the transducer positions shown in Figure 4-3.

During the field tests, data from the transducers was collected to determine if the transducers were capable of reproducing the output of the foil gages. The test data showed that the transducers performed marginally. A detailed discussion of the field test results is presented in Chapter 5.

"Ease of installation" and "reusability" are often cited as advantages of using transducers instead of foil gages. However, for this field test, installation of the transducers required almost as much surface preparation as the installation of the foil gages. Before installing the transducers, the surface of the girders was prepared by removing the paint and rust, using a hand grinder. Then, the exposed metal was cleaned and degreased using paper towels and acetone. Finally, the transducers were attached to the steel girders with large C-clamps and hand tightened as firmly as possible. In short, the reusability of the transducers did not outweigh their installation effort and marginal performance.

4.2 Data Acquisition System

A computerized data acquisition system was used to record data during the field tests. An overview of the data acquisition system and its capabilities is presented in this section. Appendix B contains a detailed description of the data acquisition system hardware and the software used to control it.

The data acquisition system, and its accompanying hardware, was part of a bridge fatigue assessment system, developed by the University of Texas (Post et al. 1988). The system was borrowed from the Austin TxDOT office It was further modified for use with this project.

The heart of the data acquisition system was a Campbell Scientific model 21X datalogger. The 21X was capable of monitoring 8 channels of data and recording the data at a rate of 16 Hz. The 21X was powered by a 12-volt marine battery and controlled using a PC compatible laptop computer. The laptop computer was powered using a 120-volt AC gasoline generator.

The excitation for the foil gages and transducers was 5 volts. The excitation voltage was obtained from a 12-to-5-volt DC voltage reducer wired in parallel with the

21X unit. This technique is called “external excitation” because the gages do not draw current directly from the datalogger. Data from the gages was recorded on channels 1 through 7 of the 21X and the excitation voltage to the gages was recorded on channel 8.

For protection from the weather, the 21X and the DC voltage reducer were contained in a protective field case. The gages, the power supply, and the laptop were connected to the field case through “military style” amphenol connectors and weather resistant cables. The marine batteries used as the 12-volt DC source were also contained in separate protective cases.

During the load test, one battery was used to power the hardware in the field case and the gages, while the other battery was held in reserve. Because the field case had two power connections, the reserve battery could be switched in without interrupting power to the system.

While the transducers contained a full wheatstone bridge circuit, the foil gages comprised only one quarter of their bridge circuit. Full-bridge completion boxes (containing three 120 ohm resistors) were used to complete the bridge circuit for the foil gages. The completion boxes were installed on the bridge, using C-clamps. They were placed next to the foil gages to minimize the length of the wires in the wheatstone bridge circuit and reduce the errors caused by leadwire resistance.

A switch was used to record the longitudinal position of the truck in the test data. The switch was connected to channel 8 on the 21X and was operated by a person standing on the deck of the bridge. The truck’s position was recorded by interrupting the signal to channel 8 every time the truck’s front axle crossed a bearing. The other data channels were not affected by the interruption.

Figure 4-8 shows a picture of the various components of the data acquisition system. In the picture, the field case is shown in the upper right. The top of the field case is removed, and the 21X unit can be seen. The 12-to-5-volt DC reducer, inside the field case, is too small to be seen in the picture, but the eight amphenol connectors for the data cables are visible on the front of the field case. The battery boxes are shown in the upper left corner of the picture. Two of the full-bridge completion boxes are lying in front of the battery boxes, and all five transducers are shown in the foreground. For

scale, the transducers are eight inches long, and the field case measures twenty-five inches by ten inches by eleven inches.

Figure 4-8 Photo of The 21X Data Acquisition System

4.3 Test Vehicle

A 10 cubic yard truck from the TxDOT maintenance yard in Marlin was used to load rate the bridge. Figure 4-9 is a photo of the 10 cubic yard truck, and Figure 4-10 shows a diagram of the 10 cubic yard truck's wheelbase. The truck had three axles and a nominal weight of 50 kips. The distance from the front axle to the center axle was 151 inches. The center and rear axles were 53 inches apart.

Before the field test, the truck was loaded with gravel and weighed. A commercial grain scale was used for measuring the gross vehicle and axle weights. The actual weight of the test truck was 50.31 kips, very close to the nominal weight. Figure 4-10 shows the as-measured axle weights for the test truck.

Figure 4-9 10 Cubic Yard Test Truck

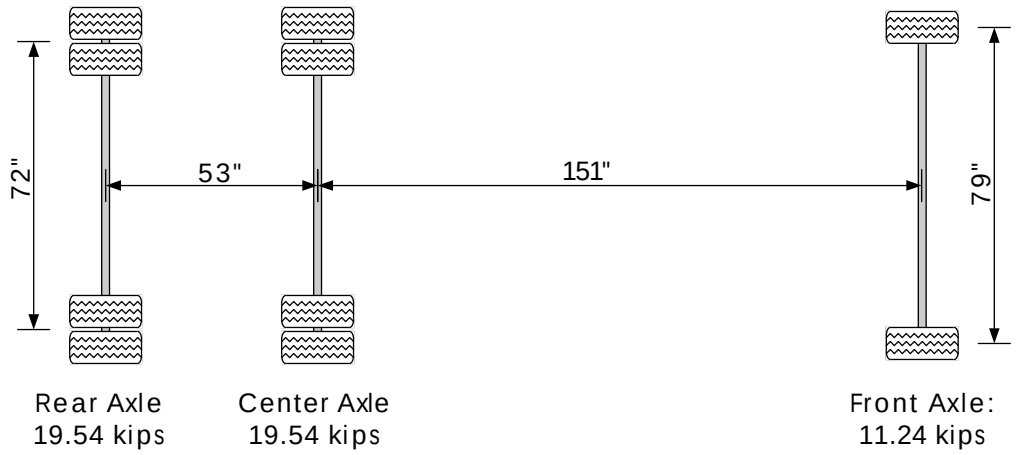

Figure 4-10 Test Truck Wheelbase Diagram

In addition, a 6 cubic yard truck was used during a preliminary field test. This truck was about half the weight of the 10 cubic yard truck, and had only two axles. The data collected with the 6 cubic yard truck was not used to load rate the bridge, because the response of the bridge under this truck's weight was too small.

4.4 Wheel Lines

The truck was placed in five lateral positions. Each position produced a maximum load effect in one of the girders. For each of the girders, the lateral positions were determined using the "lever rule," as specified in the AASHTO LRFD Bridge Design Specifications (1994a).

Figure 4-11 shows a cross section of the superstructure, including the rear axle positions for the five lateral truck positions used in this load test. The five lateral positions were labeled "wheel line 1" through "wheel line 5." On line 1, the truck was placed with the centerline of the right rear wheel directly over girder 1. For lines 2 through 4, the truck was placed straddling girders 2 through 4, respectively. For line 5, the truck was placed with the centerline of the left rear wheel on girder 5.

For the exterior girders, the load applied to the girder increases as the truck is positioned closer to the edge of the roadway. However, the AASHTO LRFD code limits the truck's lateral position by specifying that the centerline of the exterior wheel can not be placed closer than 2 feet from the edge of the curb face. This specification was adhered to during the load test.

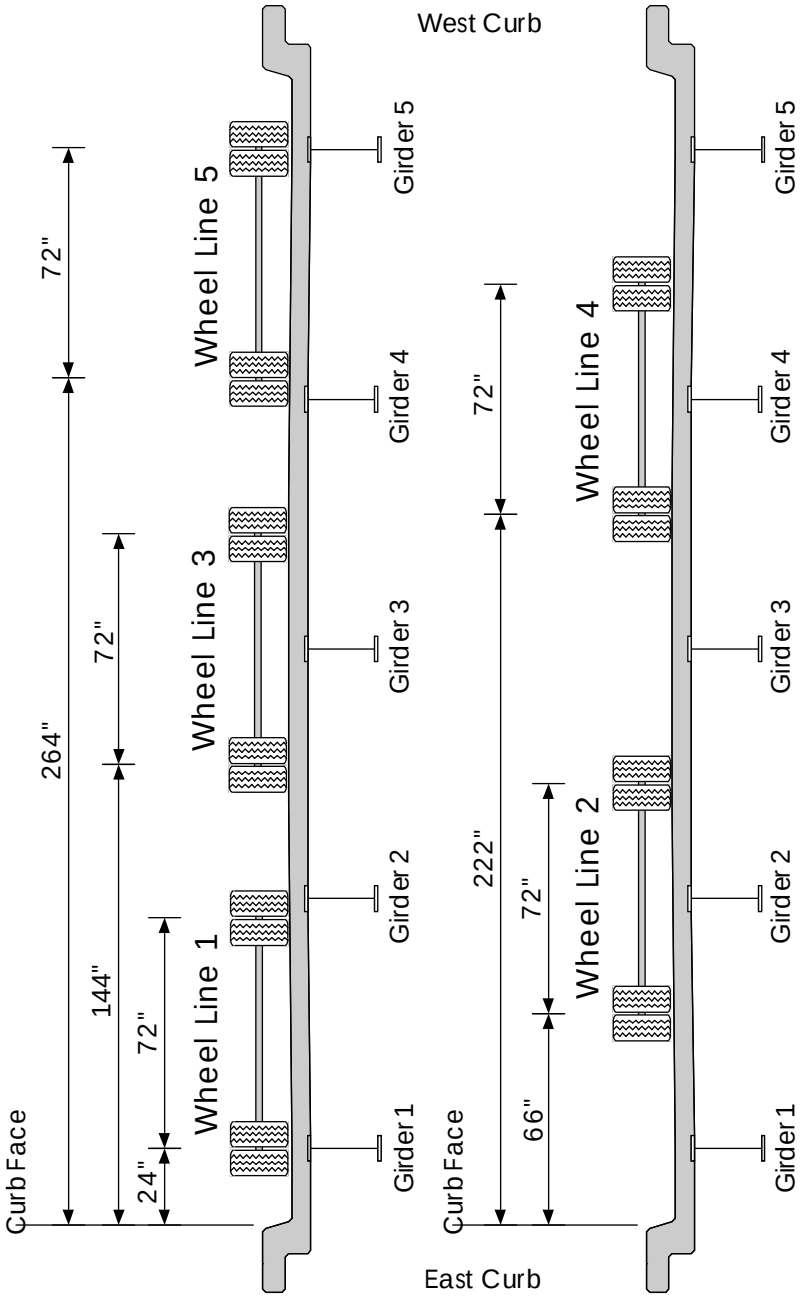

Figure 4-11 Deck Cross Section, Showing the Five Lateral Truck Positions Used During Field Testing

4.5 Roadway Preparation

Five wheel lines were painted on the bridge deck. As the truck moved across the bridge, the driver followed the lines to keep the truck in the same lateral position. From the driver's perspective, the easiest line to follow was a line drawn underneath the centerline of the front left wheel. An observer on the bridge deck watched to make sure that the truck stayed on the wheel line.

Five transverse lines were also drawn on the roadway, marking the position of each bearing. The observer on the bridge deck used a hand-held vehicle position switch to mark the truck's position in the data as the truck's front axle passed each bearing line. Figure 4-12 shows a plan view of the roadway, including the wheel lines and bearing lines. For reference, the centerline of each girder and the gage positions are also shown in the figure.

The wheel lines in Figure 4-12 do not line up with the wheel positions shown in Figure 4-11, because Figure 4-11 shows the 76-inch-wide rear axle. The wheel lines on the roadway were positioned for the 79-inch-wide front axle.

The wheel lines and bearing lines were marked on the roadway with spray paint. The endpoints of each of the lines were established using a tape measure. Chalk line was used to lay out the bearing lines, and a surveyor's transit was used to lay out the wheel lines. The bearing lines extended from curb to curb, to provide the greatest visibility for the person operating the vehicle position switch. The wheel lines began 25 feet before the first bearing and continued 40 feet beyond the last bearing. The extra long lines helped to line up the vehicle as it approached the test span and helped the driver keep the truck in line until the rear axle was off the bridge.

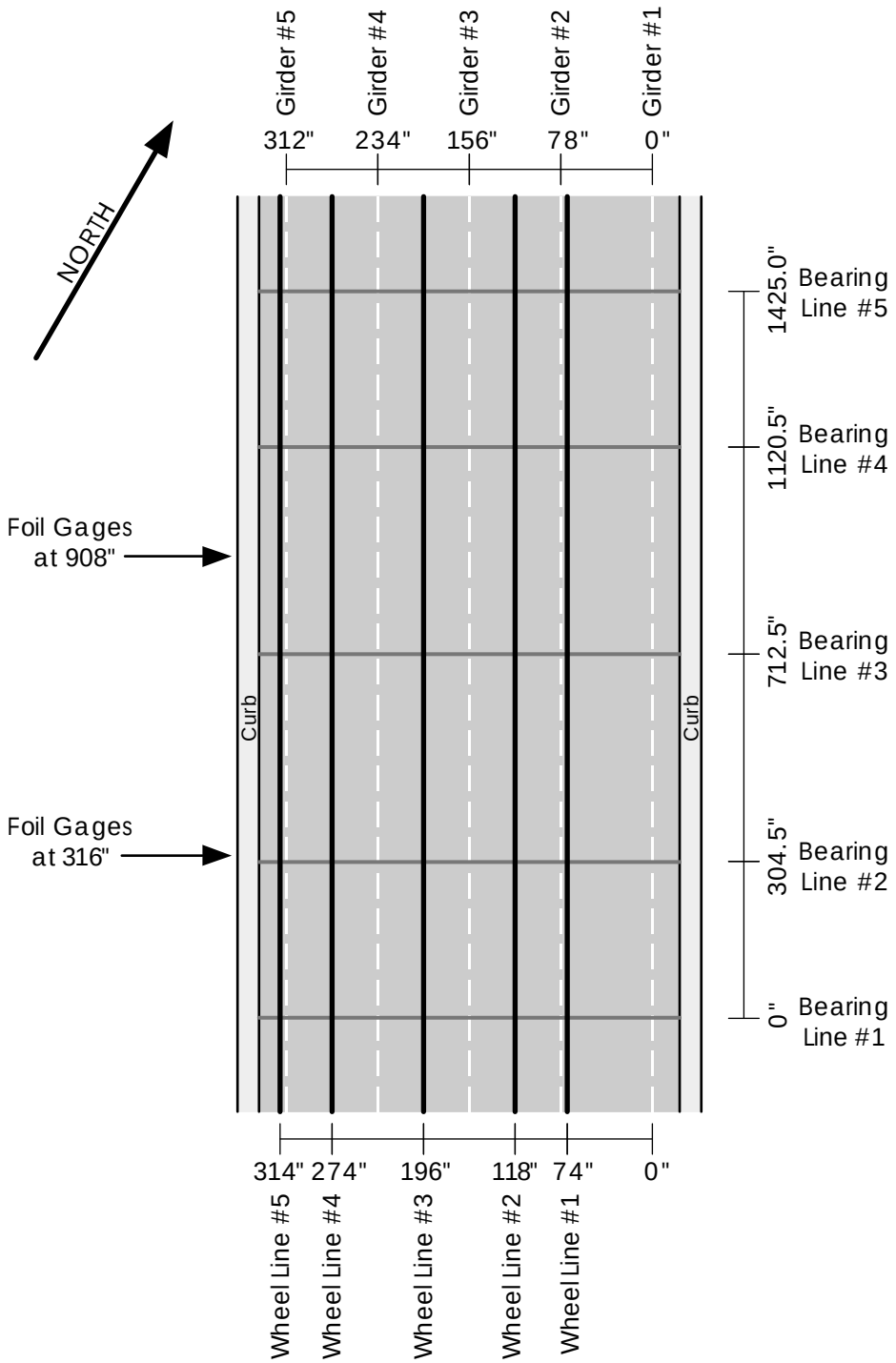

Figure 4-12 Plan View of the Wheel Lines and Bearing Lines

4.6 Test Schedule

The first step in discussing the test schedule is to define the terms "pass," "series," and "test." For this study, a pass was defined as one motion of the truck across the bridge. A series was defined as five passes, one on each wheel line, while data from a particular set of gages was recorded. Finally, a test was defined as a collection of several series. Table 4-2 shows a summary of each series performed during the field test.

Series	Purpose	Gages
	Negative Moment Region	
1	Neutral axis on girders 1 and 2.	Top flange, mid-web, and bottom flange foil gages on girders 1 and 2.
2	Neutral axis on girders 3 and 4.	Top flange, mid-web, and bottom flange foil gages on girders 3 and 4.
3	Neutral axis on girder 5 and negative moment distribution.	Top flange, mid-web, and bottom flange foil gages on girder 5 and bottom flange foil gages on girders 1 through 4.
	Positive Moment Region	
4	Neutral axis on girders 1 and 2.	Top flange, mid-web, and bottom flange foil gages on girders 1 and 2.
5	Neutral axis on girders 4 and 5.	Top flange, mid-web, and bottom flange foil gages on girders 4 and 5.
6	Neutral axis on girders 4 and 5. (Truck moving North to South.)	Top flange, mid-web, and bottom flange foil gages on girders 4 and 5.
7	Neutral axis on girder 3 and positive moment distribution.	Top flange, mid-web, and bottom flange foil gages on girder 5 and bottom flange foil gages on girders 1 through 4.

Table 4-2 Field Test Schedule

Many series were performed, because there were thirty foil gages on the bridge and only seven available channels on the data acquisition system. If a data acquisition

system with 30 channels had been available, then the strain data could have been gathered in just one series.

In all but one of the series, the truck was driven from south to north, with the exception of series 6. Consequently, the truck moved in the direction of traffic when it was on the east side of the bridge and against the direction of traffic when it was on the west side of the bridge. In series 6, however, the truck was driven from north to south to see if the behavior of girder 5 was affected by running the truck in the other direction. The test results indicated that girder 5 behaved consistently, regardless of the direction of the test truck.

In each pass, the speed of the truck was about 4 miles per hour. This slow speed allowed for the collection of many data points during the pass and minimized the dynamic response of the bridge.

4.7 Load Test Procedure

An outline of the load test procedure is presented in Table 4-3. By following this procedure, one pass was recorded every three and one-half minutes. It took about one minute to position the truck, fifteen seconds to zero the gages, forty-five seconds for the truck to cross the bridge, and one minute thirty seconds to download and label the data. There was a 10 minute interval between series. During this time, the data cables were connected to their new positions, and the gage output was monitored and inspected. Including the occasional repeat pass, each series took about 25 to 35 minutes to complete.

Step	Procedure
1	The laptop, generator, battery boxes, and the 21X field case were set up. The gages, completion boxes, and data cables were hooked up to the 21X field case. The axle weights of the truck were recorded and the truck was positioned on the appropriate wheel line at the starting end of the bridge.
2	The data acquisition program was uploaded to the 21X, and the output from the gages was checked for noise and drift. If there were problems, the connections were checked and fixed.
3	Once the system was working, the extra data cables and completion boxes were laid out in preparation for the next series.
4	The data channels on the 21X were zeroed.
5	The pass began as the truck started moving across the bridge.
6	When the front axle of the truck reached a position about 15 feet before the first bearing, recording of the data commenced.
7	As the front axle of the truck crossed each bearing line, the observer on the deck pressed the vehicle position switch for about a quarter of a second.
8	When the rear axle of the truck was about 15 feet beyond the last bearing, the deck manager signaled to the computer operator to stop recording data.
9	Data from the 21X was downloaded back to the laptop, and saved in a file.
10	The truck was positioned on the next wheel line at the starting end of the bridge, in preparation for the next pass.
11	The procedure repeated from step 4 until all of the passes in the series were complete.
12	When the series was completed, the data cables and completion boxes were connected to the appropriate gages for the next series, and the procedure was repeated from step 2.
13	When all of the series were completed, several backup copies of the data were saved on separate 3-1/2” floppy disks.
14	The computer, 21X field case, cables, completion boxes, battery boxes, and generator were disconnected and put away. The foil gages were left on the bridge, in case further testing was necessary.

Table 4-3 Load Test Procedure

CHAPTER 5

Test Results

During the field tests of the Big Creek Relief Bridge, strain data was recorded for the top flange, mid-web, and bottom flange of each girder, at ten different locations on the bridge, while the test truck was driven across the bridge at approximately 3 to 4 miles per hour. Five of the cross sections were located in a positive moment region near the middle of span 3. The other five cross sections were located in the negative moment region near bearing 2. A description of the field tests, including the placement of strain instrumentation and the testing procedure, is presented in Chapter 4.

The strain data was used to calculate the stresses and neutral axis offset at each cross section, as well as the moment in each girder and the corresponding moment distribution factor. The results of these calculations were used to determine the degree of composite behavior in each girder, at each of the instrumented cross sections, and also to determine the moment distribution behavior of the bridge in the positive moment and negative moment regions at 908 inches and 316 inches, respectively.

The test data, and the results of the ensuing calculations, are summarized in plots of stress, neutral axis offset, moment, and moment distribution factor vs. the position of the test truck. In these plots the position of the test truck is specified as the position of the truck's center axle. A description of the test truck, including its dimensions and axle weights is presented in Chapter 4. Explanations of the various plots, and the analysis methods used to create them, are presented in the Appendix.

In many of the following plots, the strain gages are referenced by a position label, such as SB1 or ST15. An explanation of the strain gage labels and positions is presented in Chapter 4, and a summary of the strain gage labels is provided in Table 5-1.

	Top Flange @ 908”	Mid Web @ 908”	Bottom Flange @ 908”	Top Flange @ 316”	Mid Web @ 316”	Bottom Flange @ 316”
Girder 1	ST1	SM1	SB1	ST11	SM11	SB11
Girder 2	ST2	SM2	SB2	ST12	SM12	SB12
Girder 3	ST3	SM3	SB3	ST13	SM13	SB13
Girder 4	ST4	SM4	SB4	ST14	SM14	SB14
Girder 5	ST5	SM5	SB5	ST15	SM15	SB15

Table 5-1 Strain Gage Labels

A diagnosis of the composite behavior at each cross section is presented in Section 5.1, and the neutral axis offset at each cross section is determined. The neutral axis results, along with strain data from the bottom flange gages, were used to determine the moment distribution behavior of the bridge. The moment distribution results are divided into two sections, 5.2 and 5.3. In Section 5.2, the moment distribution behavior of the girders alone is investigated. In Section 5.3, the additional moment resisted by the concrete deck, through noncomposite flexural participation, is considered, and moment distribution factors for both positive and negative flexure are determined.

In addition to the study of the behavior of the bridge, a feasibility study of a set of five removable strain transducers was conducted as part of this research project. The results of this feasibility study are presented in Section 5.4. The output of the transducers was examined to determine each transducer’s ability to replicate the data recorded by the strain gages. A description of the removable strain transducers, including their placement and specifications is presented in Chapter 4.

5.1 Composite Behavior of Individual Girders

The thirty strain gages were arranged in groups of three, to record strain data from the top flange, mid-web and bottom flange of the girders at ten cross sections. The strain data from each group was used to generate plots of stress and neutral axis offset vs. the test truck’s position. In the plots of stress vs. truck position, called stress influence

lines, all of the recorded data is shown. In the plots of neutral axis offset vs. truck position, only the neutral axis data corresponding to high levels of applied stress is shown. The rest of the neutral axis results were excluded, because they did not reflect the behavior of the girder under large loads. The methods used to convert the strain data into stress influence lines and neutral axis offsets are presented in the Appendix.

5.1.1 Girder 1, Positive Moment Region

Figure 5-1 is a plot of the stress influence lines for the positive moment region of girder 1, with the test truck on wheel line 1. The figure shows that this cross section behaved in a composite manner through the entire load test, because the stresses in the top and bottom flanges were of dissimilar magnitude. The bottom flange stress varied between -1.33 Ksi and 6.00 Ksi, while the top flange stress remained close to zero, indicating that the neutral axis was close to the top flange of the girder, not near the center of gravity of the steel section.

Figure 5-2 is a plot of neutral axis offset vs. truck position for girder 1. The data shown in Figure 5-2 confirms the composite behavior of the girder, because the neutral axis offset barely shifted during the test and because the results from all three gage pairs are similar. The data recorded in this load test was not sufficient for determining the exact cause of the slight downward drift in the neutral axis offset on span 3, but the variation was probably caused by changes in the effective width of the slab as the truck moved across the bridge.

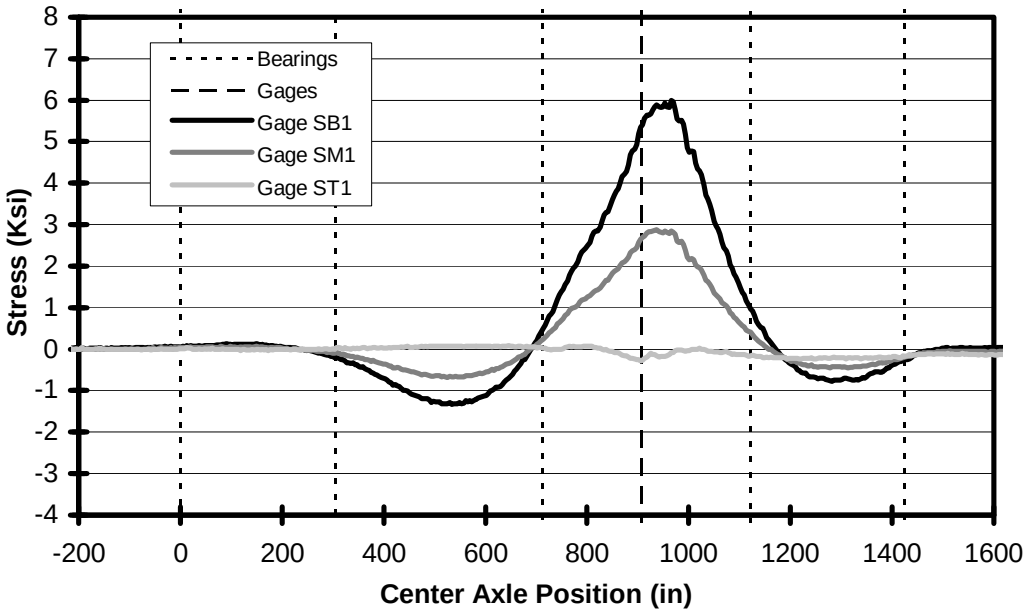

Figure 5-1 Stress Influence Lines for Girder 1, Wheel Line 1, Positive Moment Region at 908 inches

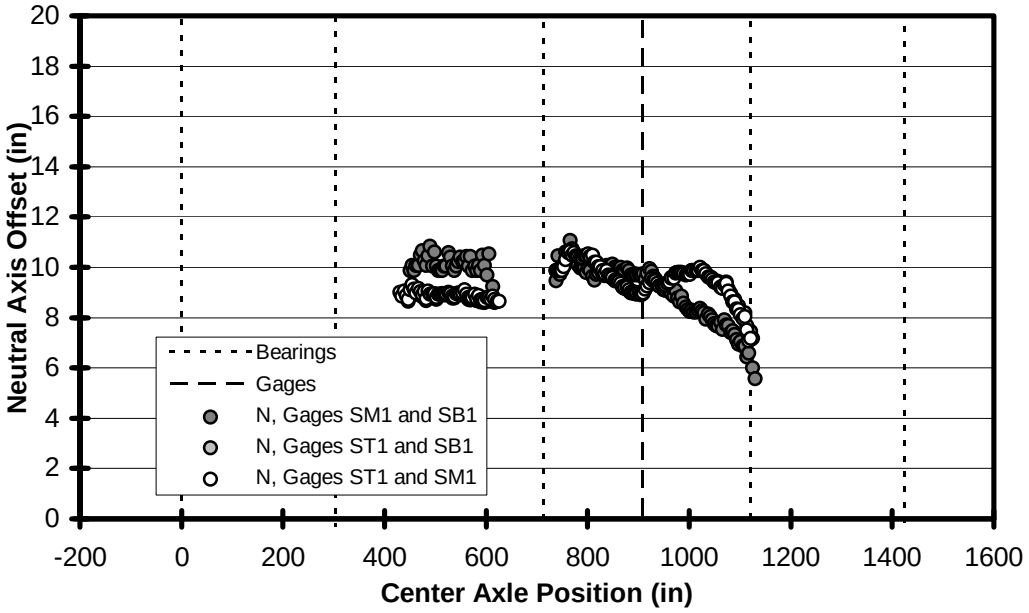

Figure 5-2 Neutral Axis Offset for Girder 1, Wheel Line 1, Positive Moment Region at 908 Inches

Figures 5-1 and 5-2 show that girder 1 continued to exhibit composite behavior when the tandem axles were on spans 2 and 4, even though there was a negative moment in the gaged cross section. The composite behavior under negative moment was possible, because the tensile stress in the deck remained below the tensile strength of the concrete.

A value for the neutral axis offset was determined by calculating the average value of the data from span 3 in Figure 5-2. In this case, the average value was found to be 9.36 inches. This places the neutral axis in the web of the girder, 0.52 inches below the inside surface of the top flange.

5.1.2 Girders 2, 3, and 4, Positive Moment Region

In the positive moment region, the response of each of the interior girders was similar enough to group their results together. Figures 5-3, 5-5, and 5-7 are plots of the stress influence lines for girders 2, 3, and 4, respectively. The truck was moving on wheel line 2 in Figure 5-3, on wheel line 3 in Figure 5-5, and on wheel line 4 in Figure 5-7. The figures show that each of the cross sections behaved in a composite manner when the test truck was on span 2, resulting in a mild negative moment to the gaged cross section. However, the composite behavior broke down under the large positive moment applied when the truck was on span 3. Under heavy load, the stresses in the top and bottom flanges were large and of similar magnitude while the stress at mid-web was small.

Figures 5-4, 5-6, and 5-8 show the neutral axis offset data for girders 2, 3, and 4, respectively. For clarity, the stress influence lines and neutral axis offset data for each girder are shown on the same page. The data shown in Figures 5-4, 5-6, and 5-8 illustrate the loss of composite behavior in each girder under heavy loading. The neutral axis offset starts near 9 inches, just as in girder 1, but quickly drops off to zero as the load increases and the girder and deck slip at their interface. The neutral axis offset continues to drop below the center of gravity of the steel as the cross section is unloaded and the girder and deck slip back into their ‘neutral’ position at their interface.

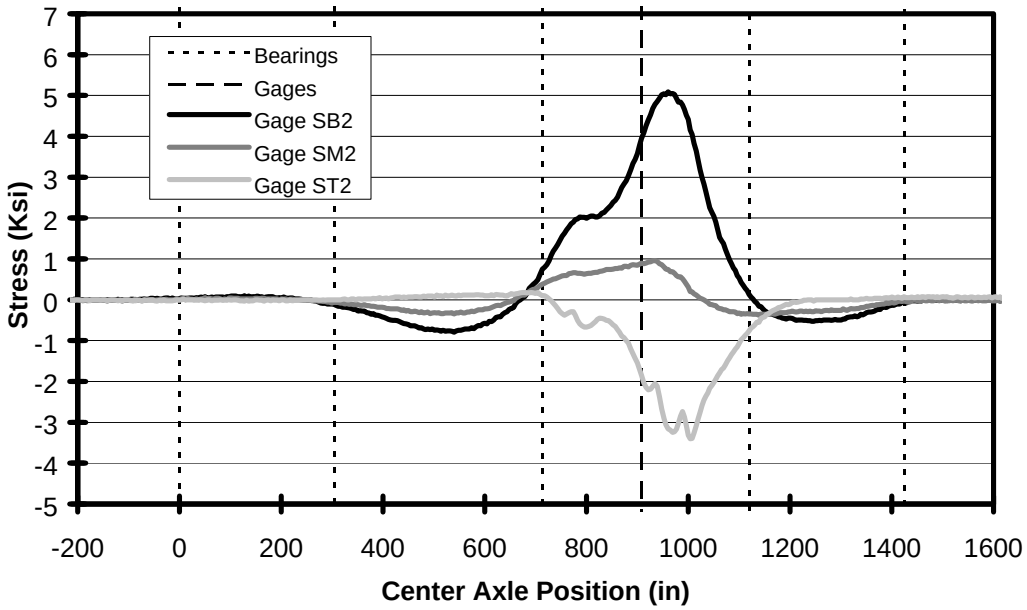

Figure 5-3 Stress Influence Lines for Girder 2, Wheel Line 2, Positive Moment Region at 908 Inches

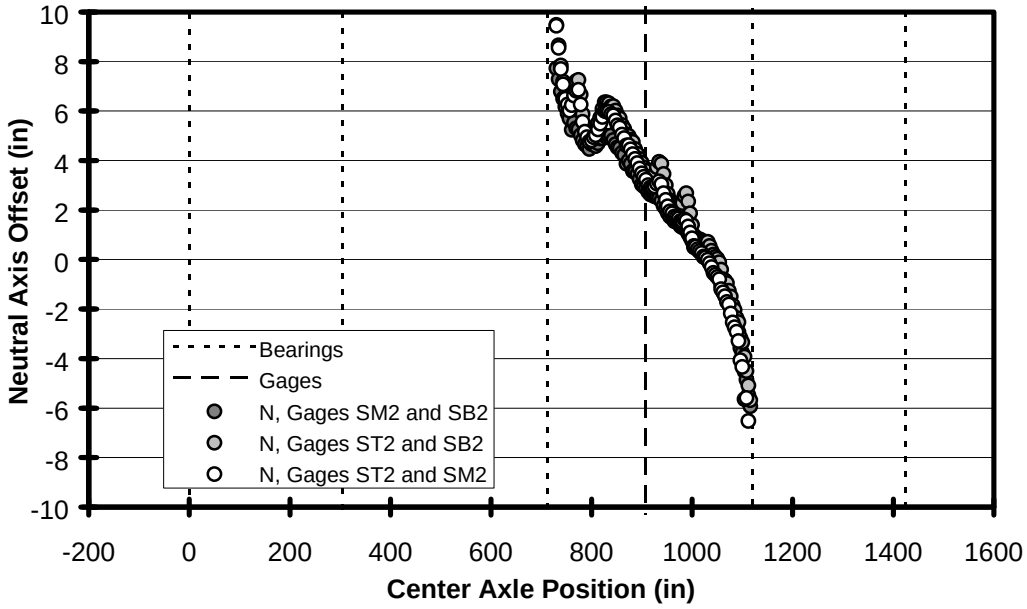

Figure 5-4 Neutral Axis Offset for Girder 2, Wheel Line 2, Positive Moment Region at 908 Inches

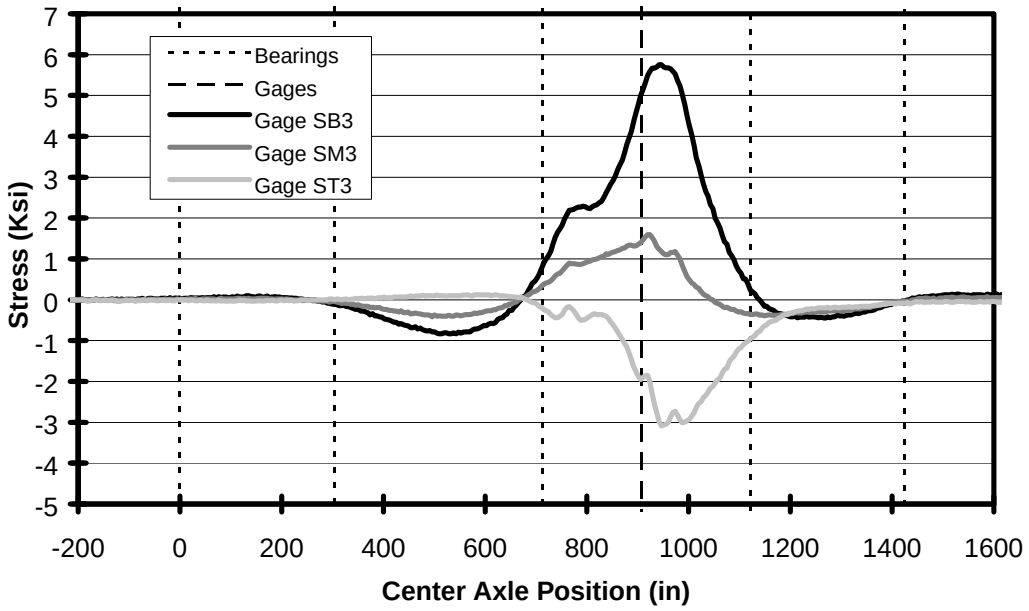

Figure 5-5 Stress Influence Lines for Girder 3, Wheel Line 3, Positive Moment Region at 908 Inches

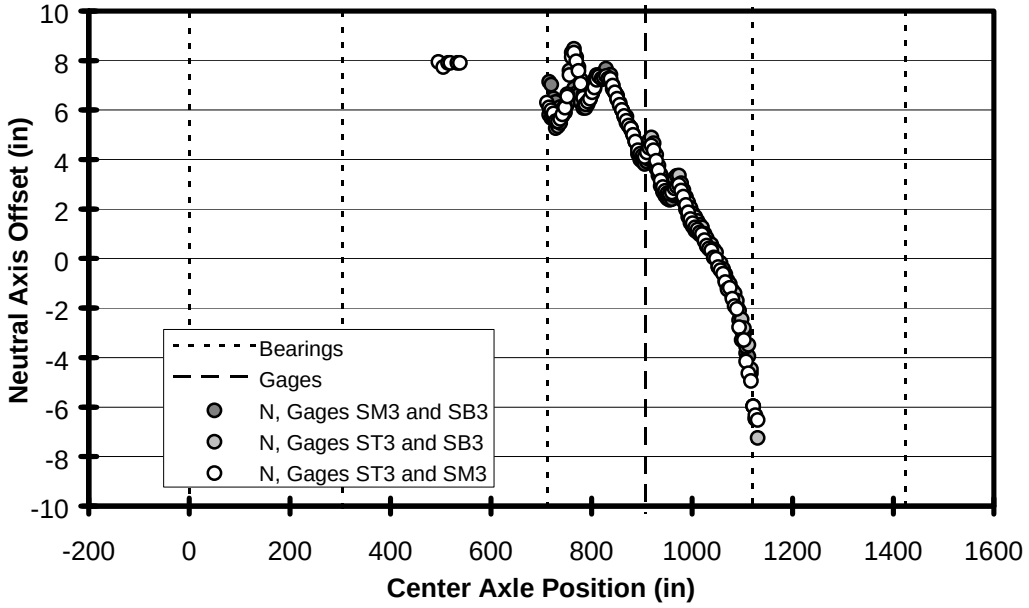

Figure 5-6 Neutral Axis Offset for Girder 3, Wheel Line 3, Positive Moment Region at 908 Inches

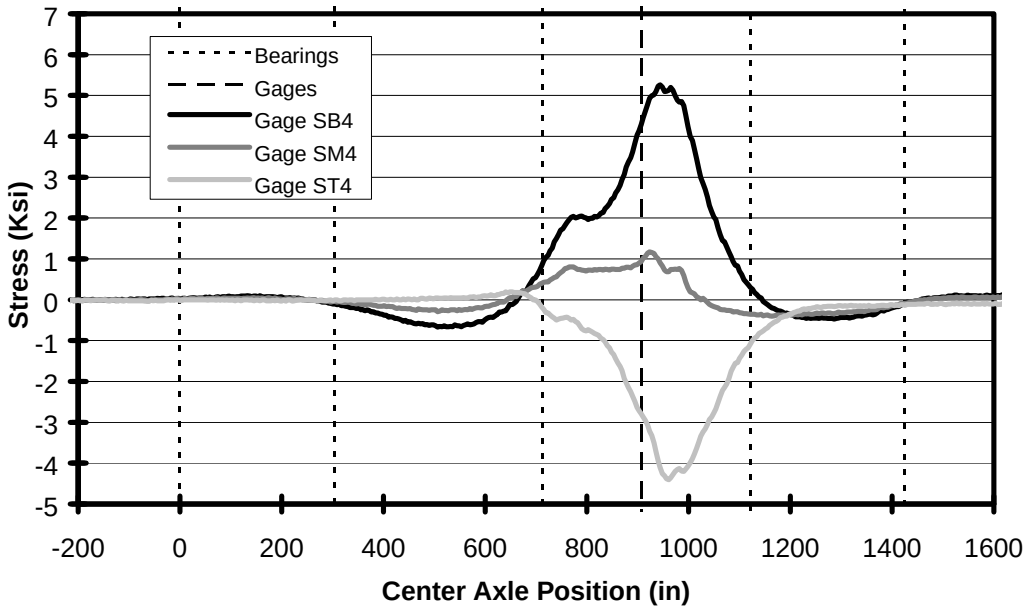

Figure 5-7 Stress Influence Lines for Girder 4, Wheel Line 4, Positive Moment Region at 908 Inches

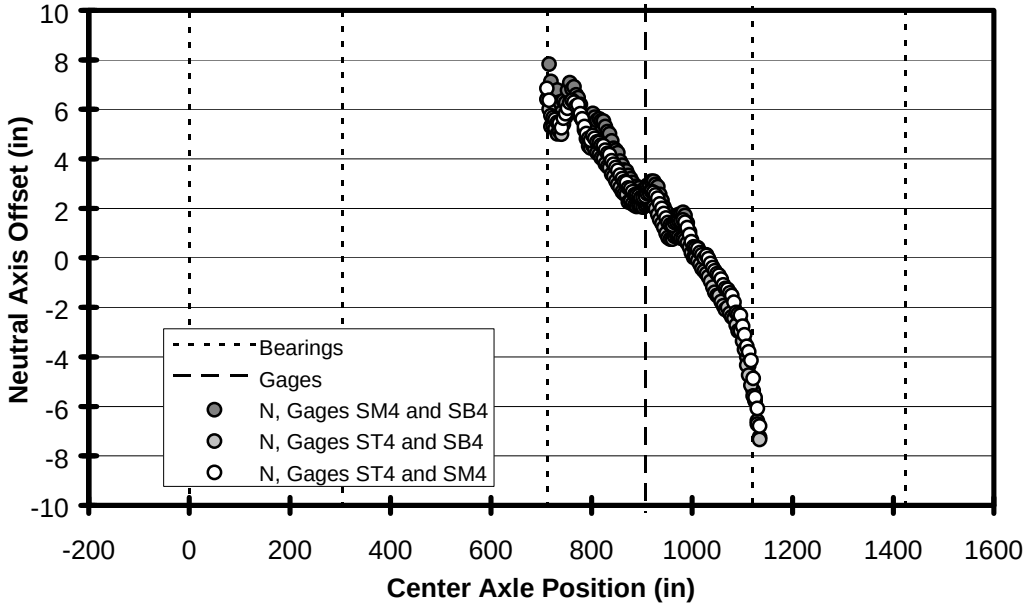

Figure 5-8 Neutral Axis Offset for Girder 4, Wheel Line 4, Positive Moment Region at 908 Inches

The radical slip in the neutral axis offset indicates that any composite behavior in girders 2, 3, and 4 is the result of friction alone and can not be relied on under heavy load. Therefore, the girders were assumed to be noncomposite for the purposes of analysis and rating. Moreover, their neutral axis offset was taken to be zero.

As a side note, the neutral axis offset plots show an interesting local effect. The neutral axis offset exhibits a 'peak' at 757 inches, 908 inches, and 961 inches. These locations correspond to the position of the truck's center axle as each axle on the test truck crossed over the gages. The peaks in the neutral axis offset were probably caused by increased friction at the interface between the girder and the deck as the weight of each axle pressed the deck and the girder together. The increased normal force temporarily prevented slip along the deck-girder interface, creating the illusion of composite behavior.

If the peaks in the neutral axis offset were caused by a local increase in the frictional force between the deck and the girder, then the peaks will only occur on noncomposite girders. There are no peaks in Figure 5-2, the neutral axis offset plot for girder 1, which acts in a composite manner.

5.1.3 Girder 5, Positive Moment Region

Figure 5-9 is a plot of the stress influence lines for the positive moment region of girder 5, with the test truck on wheel line 5. The figure shows that this cross section behaved in a composite manner when the test truck was on span 2 and applied a mild negative moment. The composite behavior continued on span 3 until the truck was about one-third of the way across the span. At that point, the composite behavior started to break down under the large positive moment. By the time the truck was two-thirds of the way across the span, the cross section was behaving noncompositely. The stresses in the top flanges and bottom flanges were large and of similar magnitude while the stress at mid-web was small.

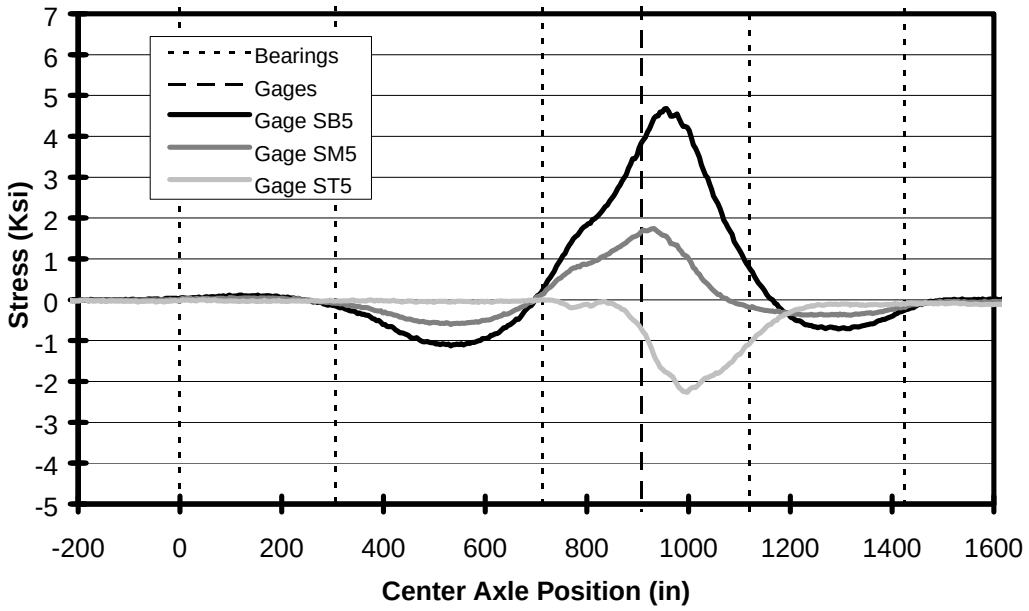

Figure 5-9 Stress Influence Lines for Girder 5, Wheel Line 5, Positive Moment Region at 908 Inches

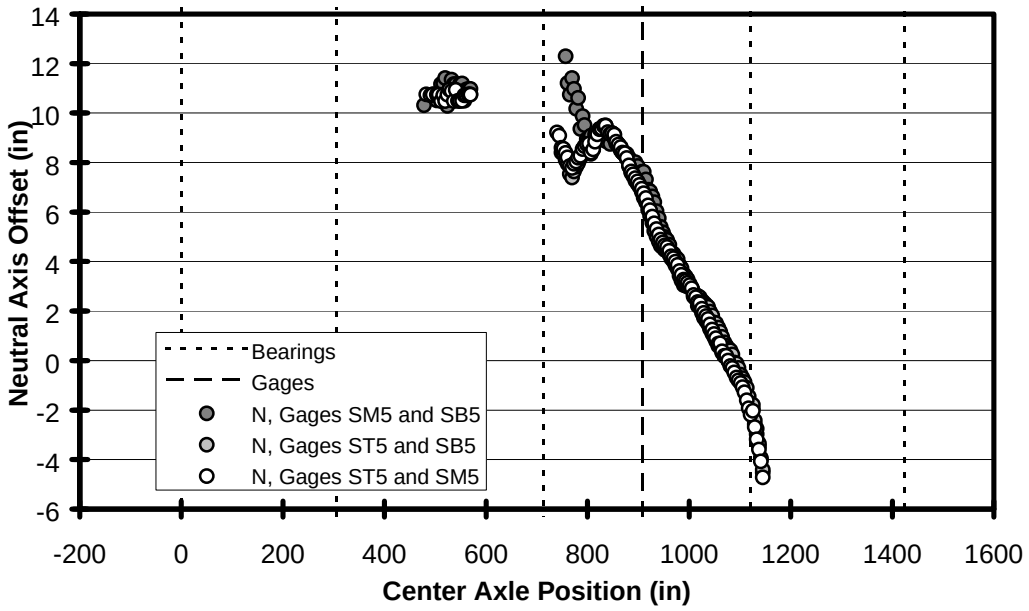

Figure 5-10 Neutral Axis Offset for Girder 5, Wheel Line 5, Positive Moment Region at 908 Inches

Figure 5-10 is a plot of neutral axis offset vs. truck position for girder 5. The results shown in Figure 5-10 illustrate the loss of composite behavior in girder 5. The neutral axis offset remained at 9 inches, until the truck reached the one-third point on the span. Then the neutral axis offset dropped toward zero as the truck continued across the span. Unlike girders 2, 3, and 4, the neutral axis offset did not drop far below zero by the time the truck exited span 3. Because of the large drop off in the neutral axis offset, girder 5 was assumed to be noncomposite for the purposes of analysis and rating.

Figure 5-10 does not exhibit the three peaks in the neutral axis offset at 757 inches, 908 inches, and 961 inches like the other noncomposite girders. This may be due to the differences in lateral truck position between the interior girder tests and the exterior girder tests. However, the data provided by the test instrumentation was not sufficient to determine why the peaks in neutral axis offset were not present.

5.1.4 Girders 1 through 5, Negative Moment Region

In the negative moment region, the response of each of the girders was similar enough to group their results together. Figures 5-11, 5-13, 5-15, 5-17 and 5-19 are plots of the stress influence lines for girders 1, 2, 3, 4, and 5, respectively. As with the results shown for the positive moment region, the test truck was moving on the wheel line closest to the girder. The figures show that each of the cross sections behaved in a noncomposite manner when the test truck was on spans 1 and 2 and the moment at bearing 2 was large. The stress influence lines for the top and bottom flanges are of similar magnitude, while the stress at mid-web was close to zero.

Figures 5-12, 5-14, 5-16, 5-18 and 5-20 show the neutral axis offset results for girders 1, 2, 3, 4, and 5, respectively. For clarity, the stress influence lines and neutral axis offset data for each girder are shown on the same page. The results shown in these five figures indicate that all five girders were behaving in a noncomposite manner, since the neutral axis offset remained close to zero most of the time. Therefore, for the purposes of analysis and rating, all five girders were assumed to act in a noncomposite manner in the negative moment region.

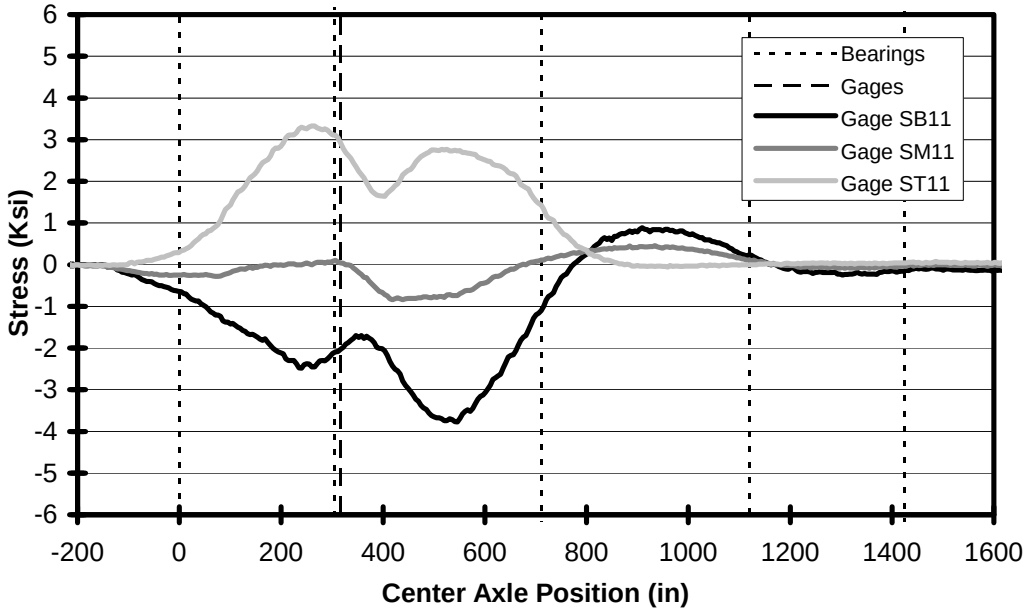

Figure 5-11 Stress Influence Lines for Girder 1, Wheel Line 1, Negative Moment Region

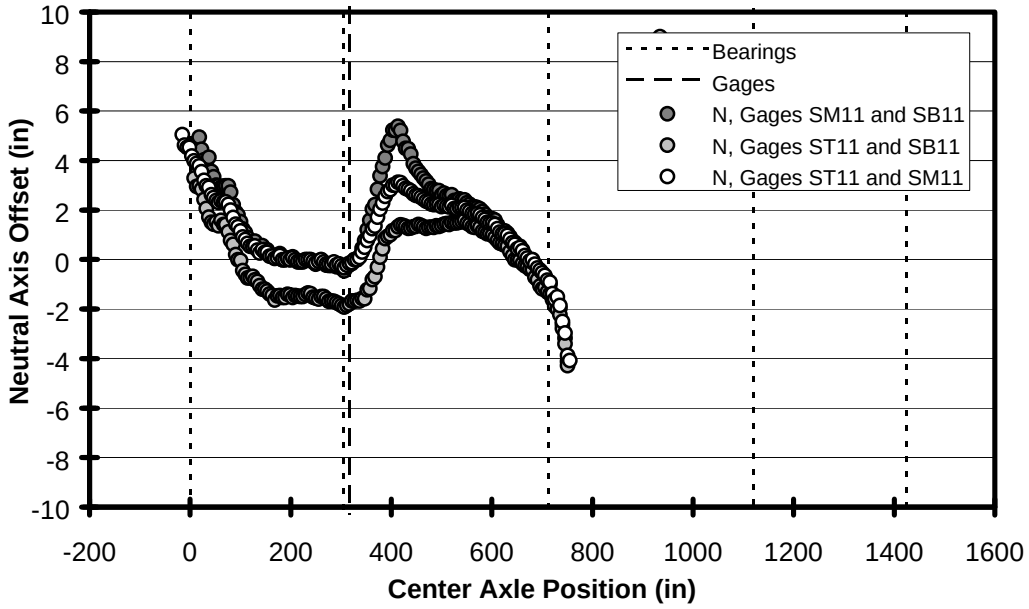

Figure 5-12 Neutral Axis Offset for Girder 1, Wheel Line 1, Negative Moment Region

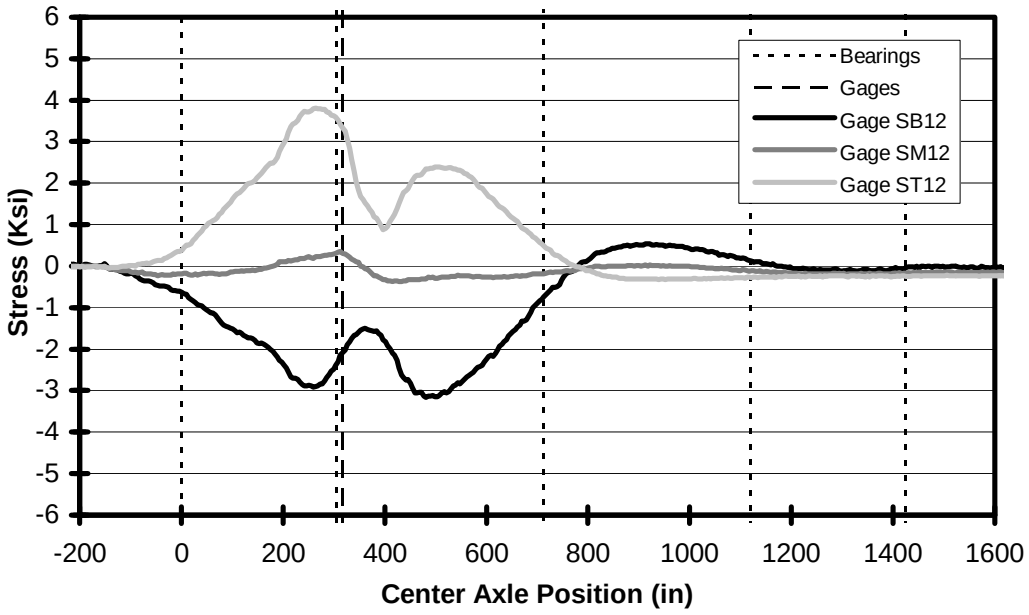

Figure 5-13 Stress Influence Lines for Girder 2, Wheel Line 2, Negative Moment Region

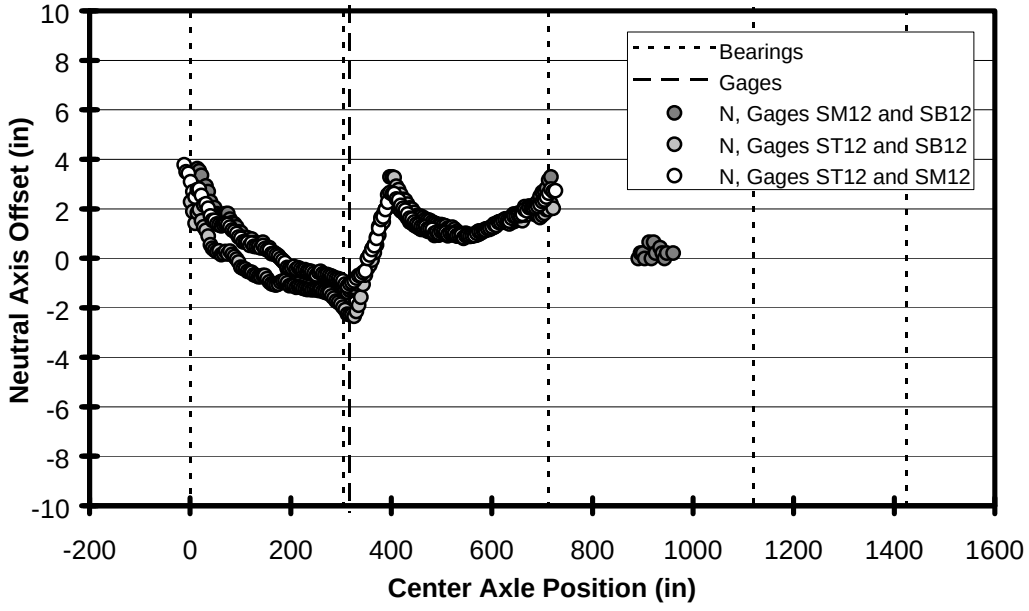

Figure 5-14 Neutral Axis Offset for Girder 2, Wheel Line 2, Negative Moment Region

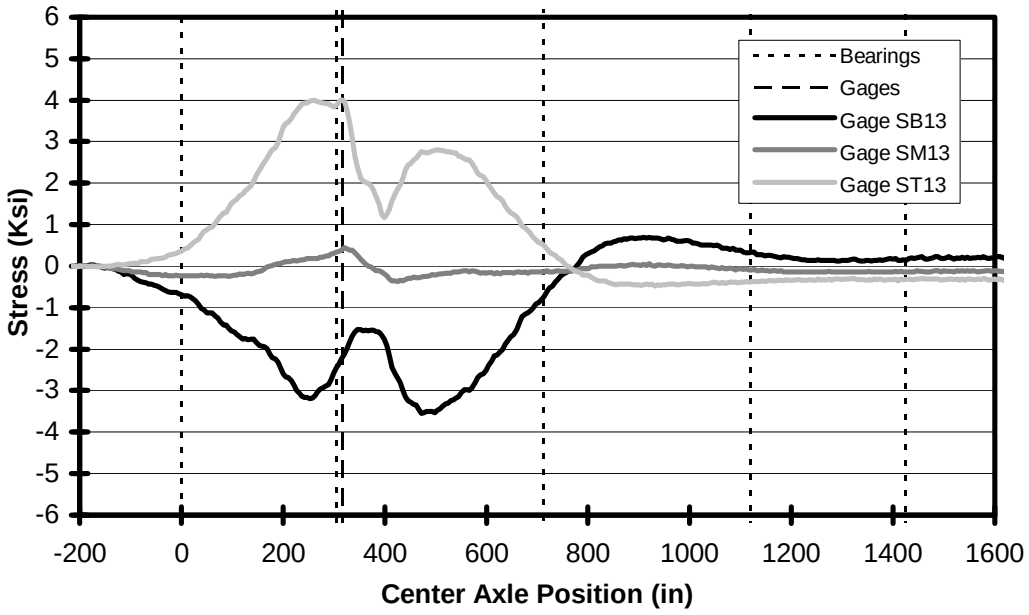

Figure 5-15 Stress Influence Lines for Girder 3, Wheel Line 3, Negative Moment Region

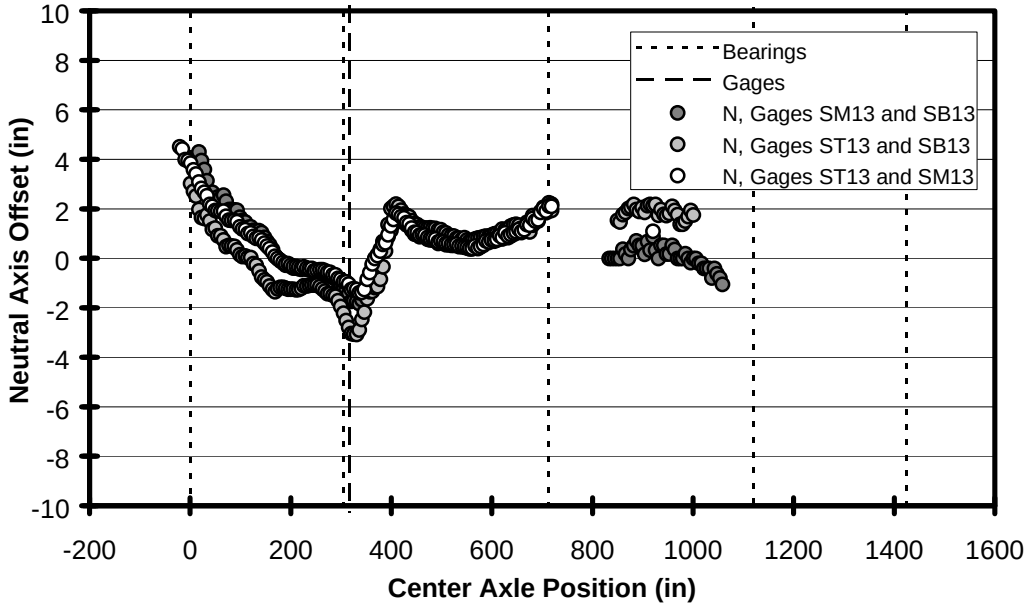

Figure 5-16 Neutral Axis Offset for Girder 3, Wheel Line 3, Negative Moment Region

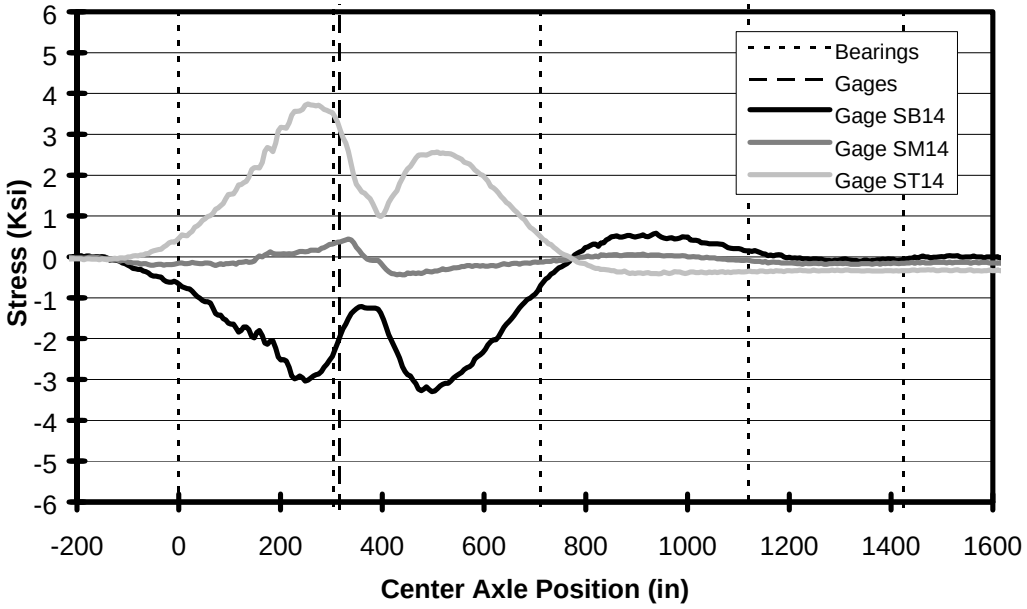

Figure 5-17 Stress Influence Lines for Girder 4, Wheel Line 4, Negative Moment Region

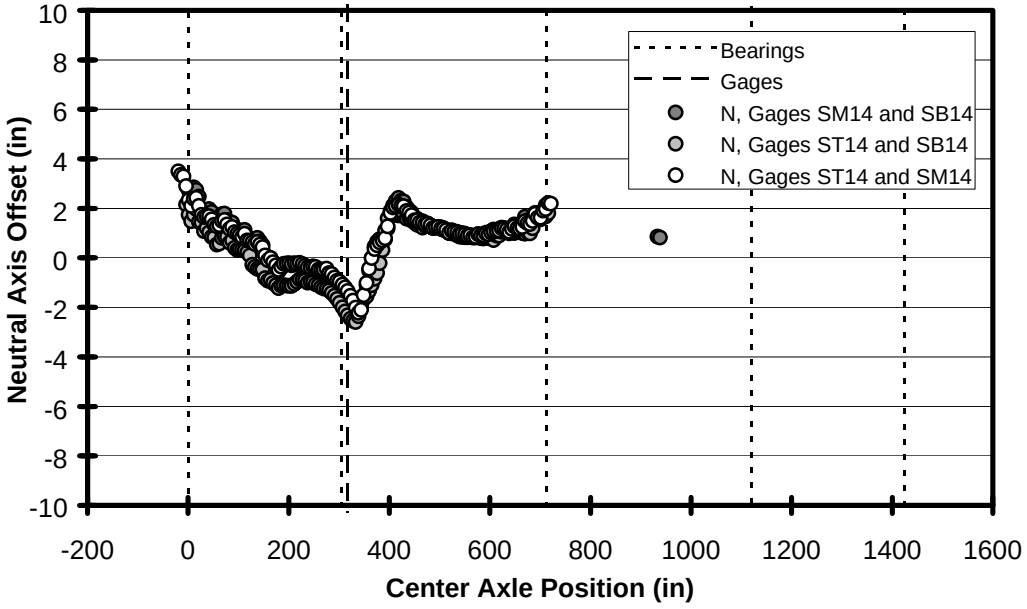

Figure 5-18 Neutral Axis Offset for Girder 4, Wheel Line 4, Negative Moment Region

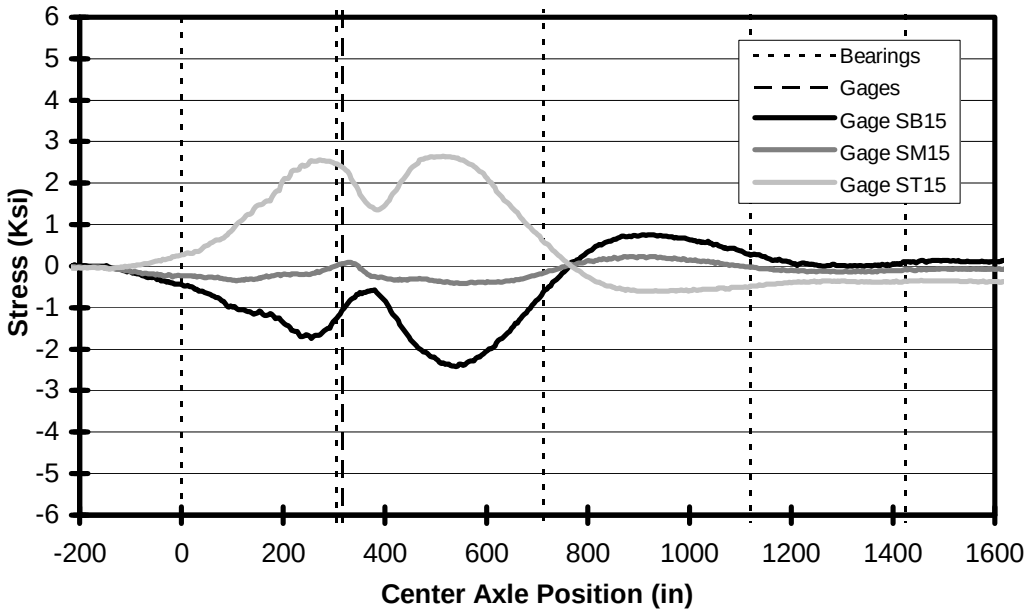

Figure 5-19 Stress Influence Lines for Girder 5, Wheel Line 5, Negative Moment Region

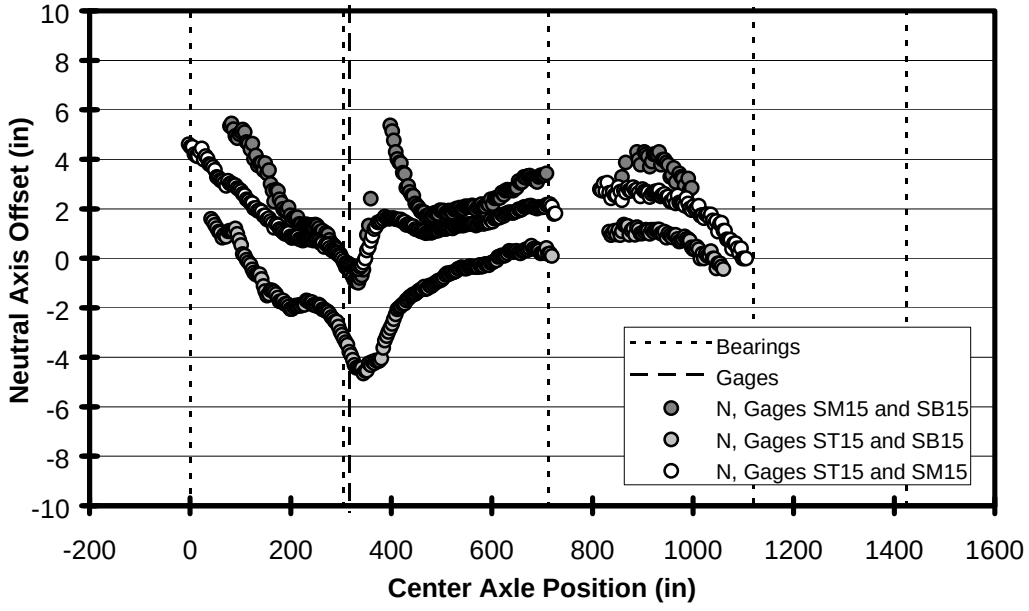

Figure 5-20 Neutral Axis Offset for Girder 5, Wheel Line 5, Negative Moment Region

In the middle of span 2, a 2 to 4 inch upward shift in the neutral axis offset is evident for each girder. This shift was most likely the result of increased friction between the girder and the deck, caused by an increase in the normal force at the deck-girder interface due to the weight of the truck. However, when the truck was not close to the gages at bearing 2, the normal force on the gaged cross sections was not as large, and the neutral axis remained at the center of gravity of the steel section.

The neutral axis offset results for girder 5, shown in Figure 5-20, are significantly more scattered than the results from the other four girders. Although the test data was not sufficient to reveal the cause of this anomaly, the data from repeat passes on this wheel line indicated that this phenomenon was consistent and repeatable. It is possible that this effect was caused by out-of-plane bending of the web of girder 5.

5.1.5 Summary of Composite Behavior

A summary of the composite behavior of the girders at each cross section is provided in Table 5-2. The test results indicated that all of the girders were behaving in a noncomposite manner, with the exception of the positive moment region of span 3 on girder 1. For the purposes of analysis and rating, the neutral axes of girders 2 through 5 were assumed to be located at the center of gravity of the steel section. However, for the positive moment regions of girder 1, the neutral axis was found to be 9.36 inches above the center of gravity of the steel section. In the negative moment regions of girder 1, the neutral axis was assumed to remain at the center of gravity of the steel section, just like the other girders.

Neutral Axis Offset (in)	Positive Moment Region at 908 Inches	Negative Moment Region at 316 Inches
Girder 1	9.36	0
Girders 2, 3, 4, and 5	0	0

Table 5-2 Neutral Axis Offsets for the Positive and Negative Moment Regions of Girders 1 through 5

5.2 Girder Moments and Girder Moment Distribution

The neutral axis offsets, determined above, and strain data from the bottom flanges of each girder were used to determine the moments and moment distribution factors in each girder. The procedure used to calculate moments and moment distribution factors from the strain data and neutral axis offsets is explained in the Appendix.

The results of the moment calculations are shown as plots of moment vs. truck position, or "moment influence lines." On the following pages, these plots are shown in color, because of the large number of moment influence lines on each plot. The plots of the moment distribution factors vs. truck position are shown in color as well. For clarity, the moment influence line plots and moment distribution factor plots for each wheel line are shown on the same page. Furthermore, in the plots of moment distribution factor vs. truck position, only the moment distribution factors corresponding to high levels of applied moment are shown. The rest of the results of the moment distribution factor calculations were excluded, because they did not reflect the behavior of the girder under large loads.

It is important to note that the moment contribution of the deck is not considered in this section. The additional moment resisted by noncomposite flexure of the deck is examined in detail in Section 5.3.

5.2.1 Positive Moment Region

In the positive moment region, the flexural behavior of the girders was similar, regardless of wheel line. Therefore, the results from each wheel line are presented together. Figures 5-21, 5-23, 5-25, 5-27, and 5-29 are plots of the moment influence lines for all five girders, with the test truck moving on wheel lines 1, 2, 3, 4, and 5, respectively. The figures show that, in general, the responses of the girders closest to the truck were larger than the responses of the other girders. However, the composite girder, girder 1, carried substantially more moment than the other girders. In Figure 5-21, the maximum moment in girder 1 was 1117 kip-inches, 1.56 times the next largest moment (716 kip-inches in girder 3, shown in Figure 5-25). In fact, when the truck was on wheel line 2 and the moment in girder 2 was at its peak, the composite behavior

of girder 1 produced so much moment that the moment in girder 1 was still 1.21 times larger than the moment in girder 2. This behavior is shown in Figure 5-23, when the maximum moment in girder 1 is 767 kip-inches and the maximum moment in girder 2 is 633 kip-inches.

The maximum moment in girder 5 was the lowest of all five girders, only 591 kip-inches. Even when the truck was on wheel line five, as shown in Figure 5-29, the moment in girder 4 was larger than the moment in girder 5. Although the test data was not sufficient to determine the cause of this behavior, the large moment in girder 4 was probably the result of the lateral position of the truck. On wheel line five, the exterior wheels were placed over girder 5, while the interior wheels were placed just 6 inches outside of girder 4. Thus, the weight of the truck was centered almost evenly between these two girders. Differences in the amount of friction along the deck-girder interfaces would be enough to allow girder 4 to carry as much moment as girder 5.

The moment distribution behavior for all five girders is shown in Figures 5-22, 5-24, 5-26, 5-28, and 5-30, with the test truck moving on wheel lines 1, 2, 3, 4, and 5, respectively. Each figure is placed on the same page as the corresponding plot of moment influence lines. In the figures, the moment distribution factors were plotted when the magnitude of the sum of the measured moments in the girders was larger than 1500 kip-inches.

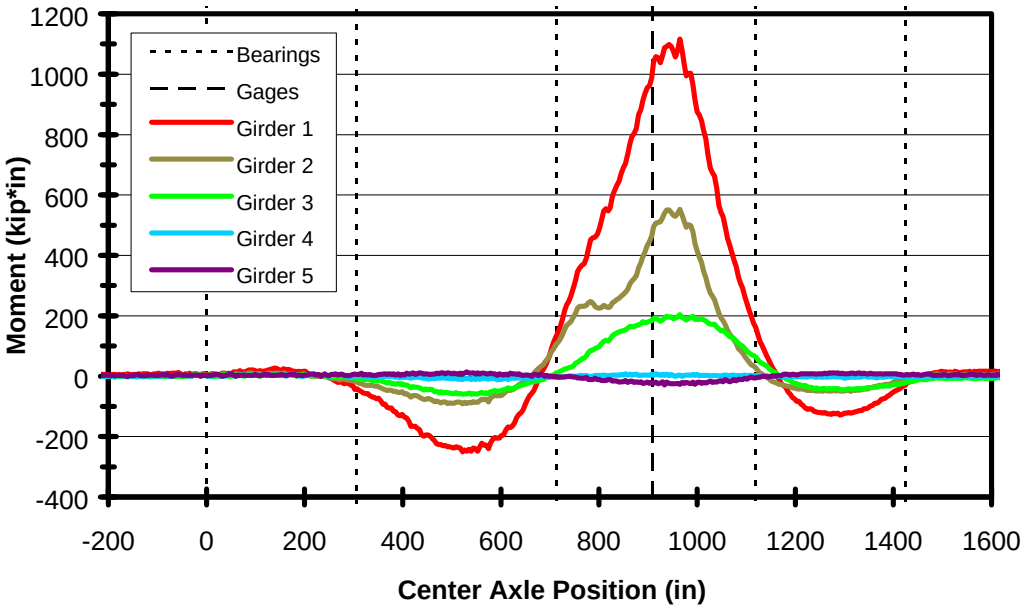

Figure 5-21 Moment Influence Lines, Wheel Line 1, Positive Moment Region

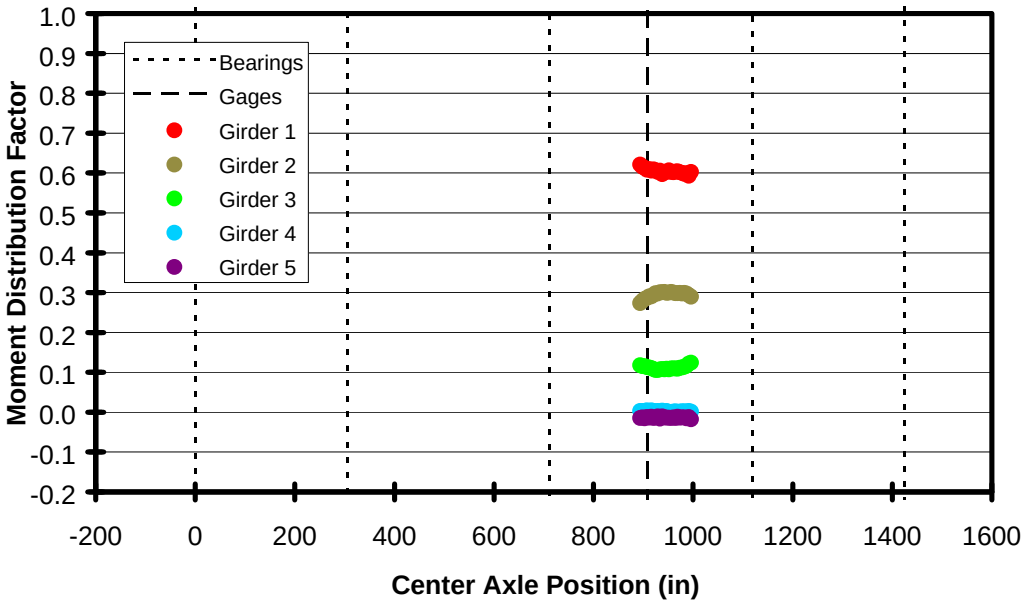

Figure 5-22 Moment Distribution Factors, Wheel Line 1, Positive Moment Region

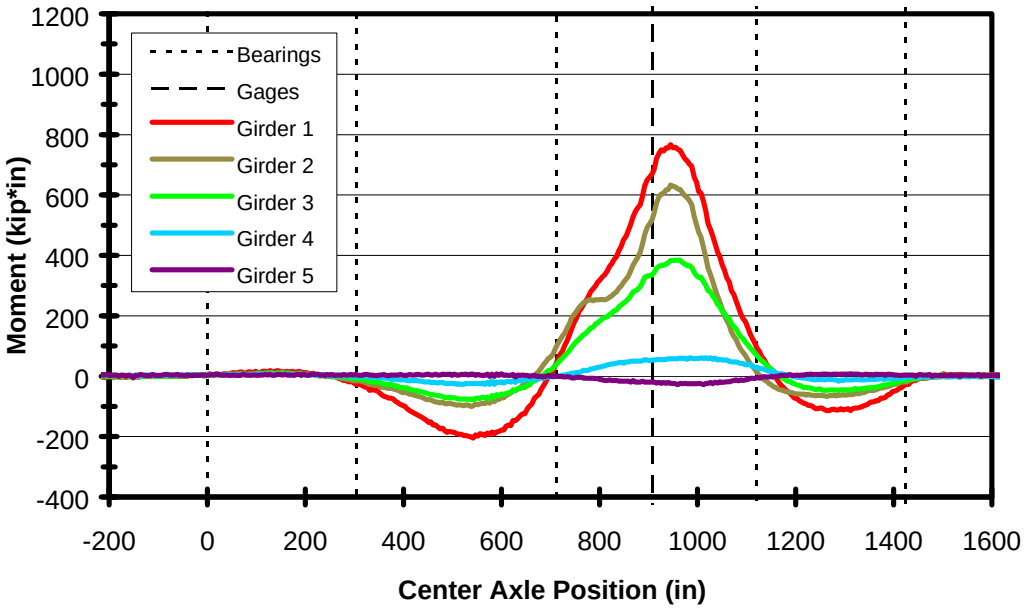

Figure 5-23 Moment Influence Lines, Wheel Line 2, Positive Moment Region

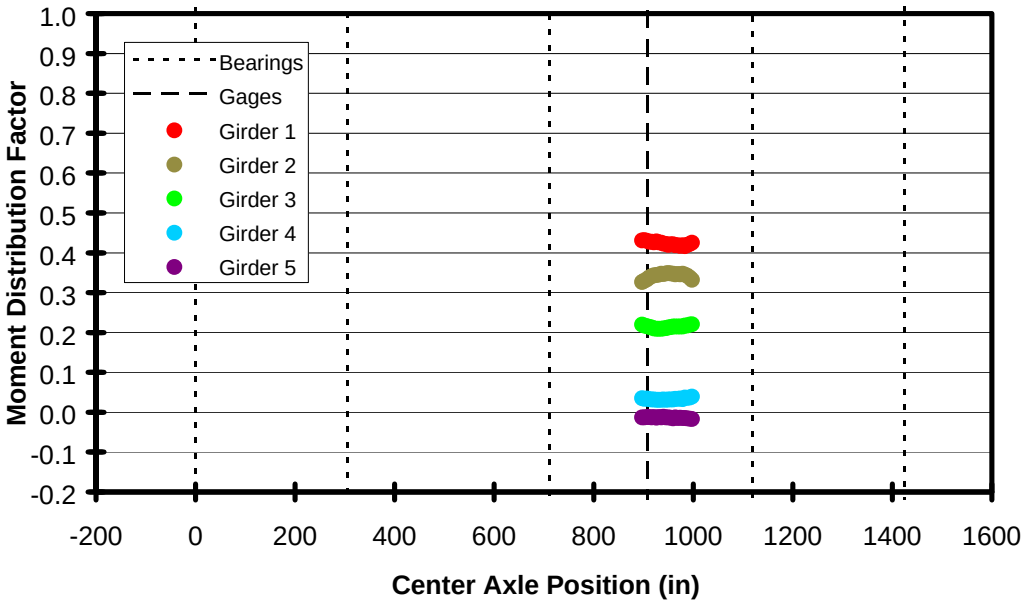

Figure 5-24 Moment Distribution Factors, Wheel Line 2, Positive Moment Region

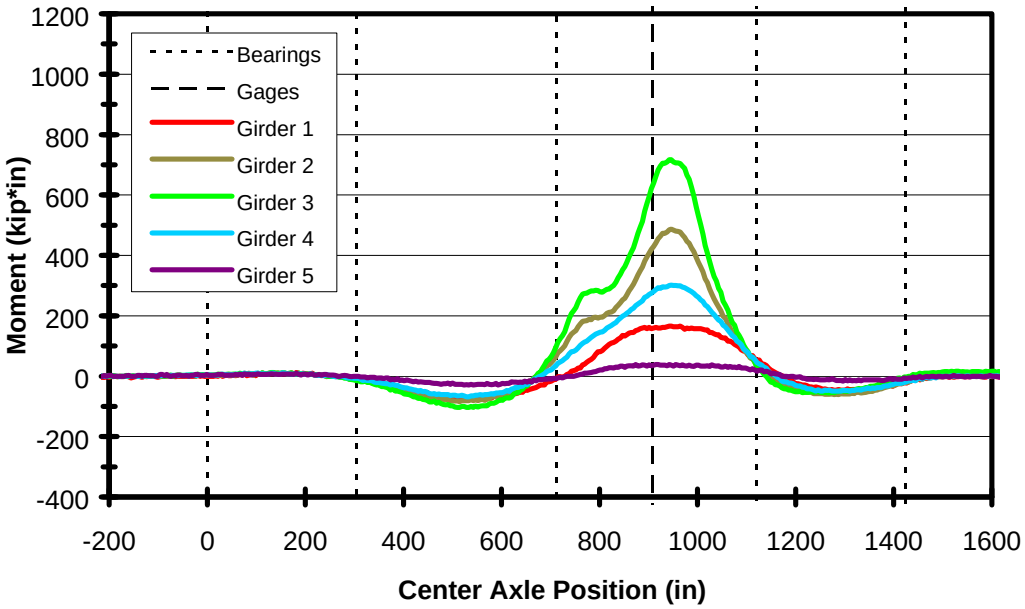

Figure 5-25 Moment Influence Lines, Wheel Line 3, Positive Moment Region

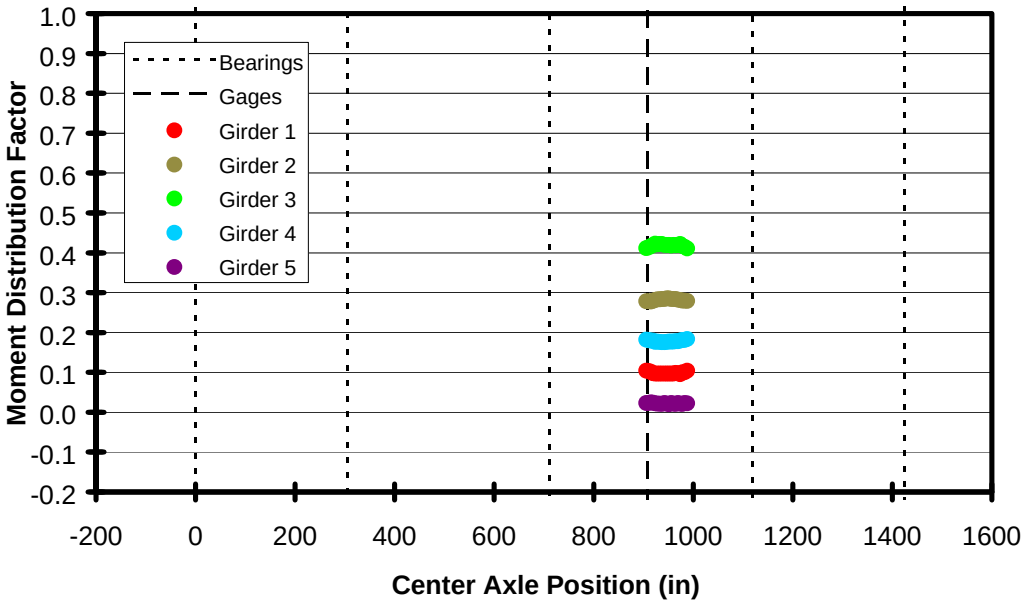

Figure 5-26 Moment Distribution Factors, Wheel Line 3, Positive Moment Region

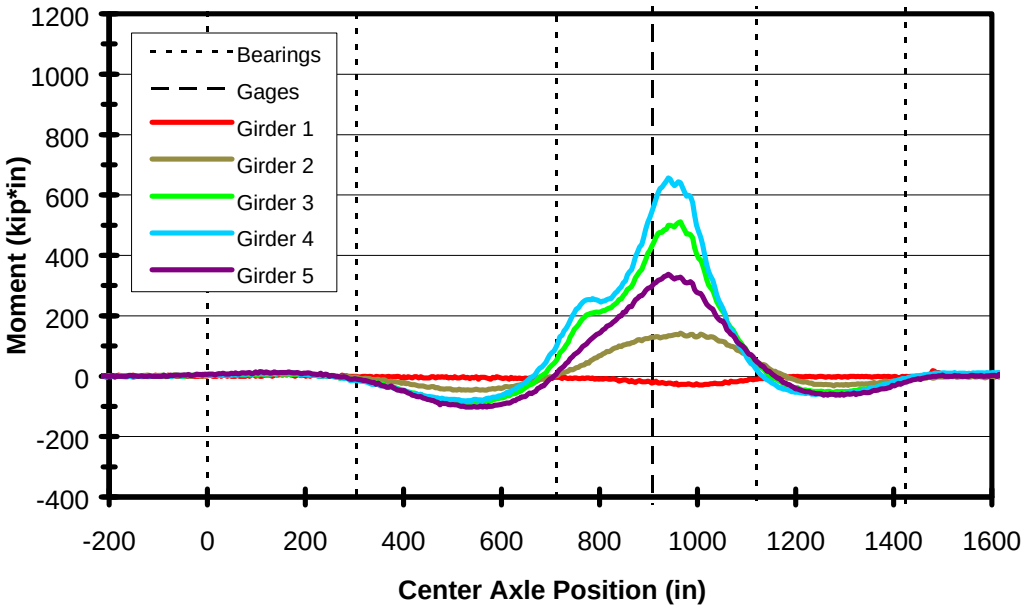

Figure 5-27 Moment Influence Lines, Wheel Line 4, Positive Moment Region

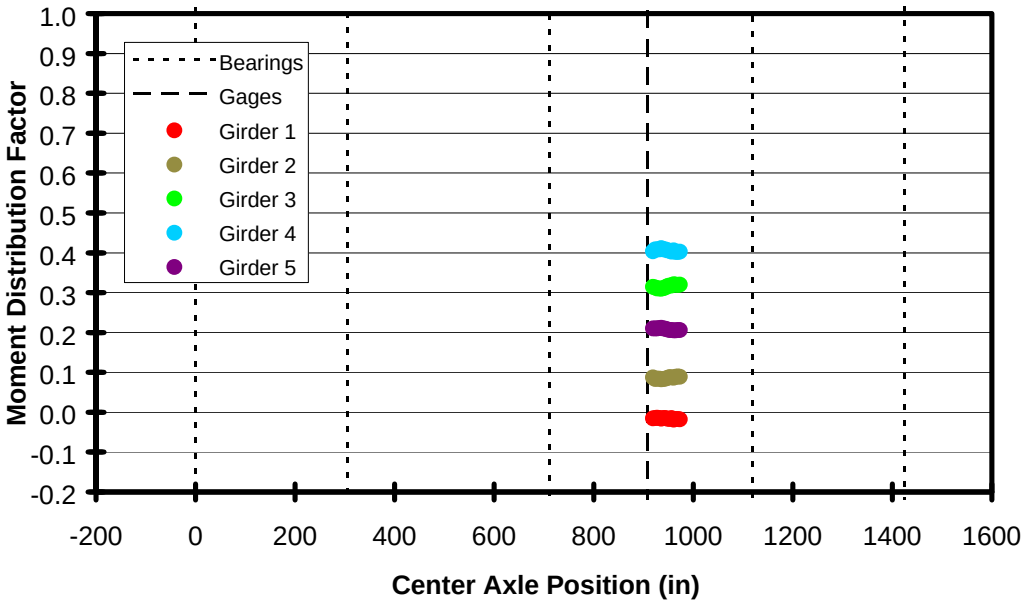

Figure 5-28 Moment Distribution Factors, Wheel Line 4, Positive Moment Region

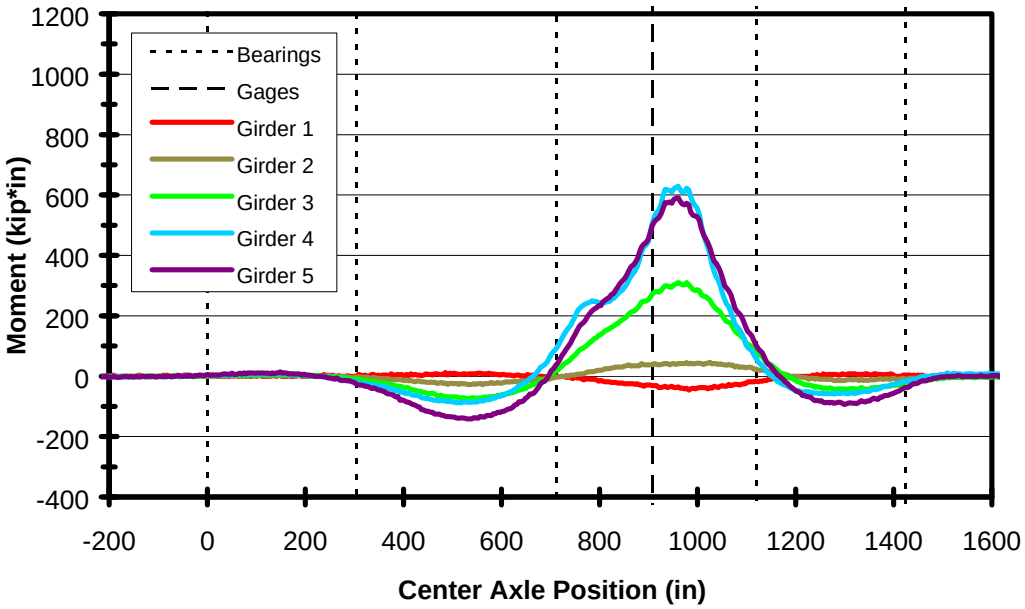

Figure 5-29 Moment Influence Lines, Wheel Line 5, Positive Moment Region

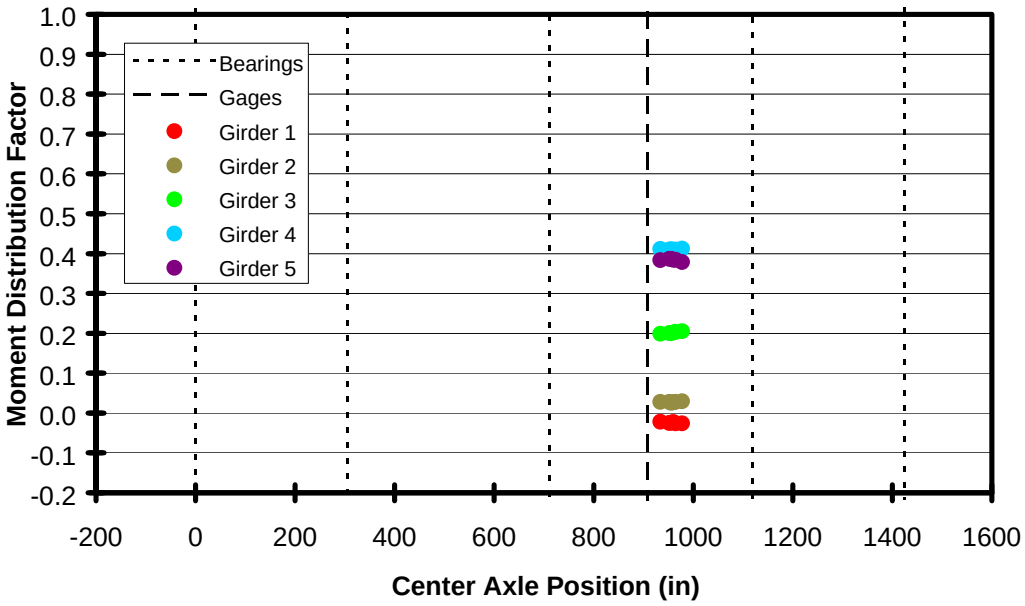

Figure 5-30 Moment Distribution Factors, Wheel Line 5, Positive Moment Region

Figures 5-21, 5-23, 5-27, and 5-29 show that the exterior girder farthest from the truck bent in reverse flexure from the primary girder, when the truck was on any wheel line except for wheel line 3. Although the magnitude of the reverse flexure was small, this behavior indicates that the superstructure was fairly flexible in the lateral direction and not very efficient at distributing the moment away from the primary girder. The moment distribution behavior of the bridge might improve if lateral braces are installed between the girders to increase the lateral and torsional stiffness of the superstructure. This would force all of the girders to flex in the same direction regardless of which wheel line is loaded.

Table 5-3 shows the maximum moment effect in each girder, for the cross section at 908 inches, for all five wheel lines. The table was generated using the data from Figures 5-21, 5-23, 5-25, 5-27, and 5-29. The largest maximum moment in each girder is shown in bold. The table shows that the largest moments were produced in each girder when the test truck was on the corresponding wheel line. Due to reverse flexure, the maximum moment effects in girders 1 and 5 were negative when the truck was placed on wheel lines on the far side of the bridge.

Maximum Moment Effect (kip-inches)	**Wheel Line 1**	**Wheel Line 2**	**Wheel Line 3**	**Wheel Line 4**	**Wheel Line 5**
Girder 1	**1117**	767	166	-29	-46
Girder 2	553	**633**	487	142	46
Girder 3	204	384	**716**	511	310
Girder 4	8	61	301	**656**	628
Girder 5	-29	-28	39	338	**591**

Table 5-3 Maximum Moment Effects in the Positive Moment Region at 908 Inches

Table 5-4 shows the corresponding moment distribution factors in each girder, for all five wheel lines. This table was generated using the data from Figures 5-22, 5-24,

5-26, 5-28 and 5-30 by calculating the average value of each plotted data set. The largest moment distribution factor for each girder is shown in bold. The table shows that the largest moment distribution factor for girder 4 was produced when the truck was on wheel line 5.

Moment Distribution Factors*	Wheel Line 1	Wheel Line 2	Wheel Line 3	Wheel Line 4	Wheel Line 5
Girder 1	**0.605**	0.424	0.099	-0.016	-0.024
Girder 2	0.295	**0.342**	0.282	0.086	0.028
Girder 3	0.112	0.214	**0.418**	0.315	0.202
Girder 4	0.002	0.033	0.179	0.406	**0.411**
Girder 5	-0.013	-0.014	0.022	0.208	**0.384**

* Does not include noncomposite flexure of the deck

Table 5-4 Moment Distribution Factors for the Positive Moment Region at 908 Inches

5.2.2 Negative Moment Region

In the negative moment region, the flexural behavior of the girders was similar, regardless of the wheel line, so the results from each wheel line are presented together. Figures 5-31, 5-33, 5-35, 5-37, and 5-39 are plots of the moment influence lines for all five girders, with the test truck moving on wheel lines 1, 2, 3, 4, and 5, respectively. The figures show that, in general, the responses of the girders closest to the truck were larger than the responses of the other girders.

The maximum negative moment in each girder occurred when the truck was near the middle of span 2, with values ranging from -301 kip-inches in girder 5 to -441 kip-inches in girder 1. In Figures 5-37 and 5-39, the behavior of girders 4 and 5 was particularly interesting. When the truck was on wheel line 5, the maximum moment in girder 4 was -419 kip-inches. However, when the truck was on wheel line 4, the maximum moment in girder 4 was only -409 kip-inches, slightly less than for wheel line 5. In addition, the moment in girder 4 was 1.39 times larger than the moment in

girder 5, when the truck was on wheel line 5. The moment in girder 4 seemed to be too large when the truck was on wheel line 5, since both girders were behaving in a noncomposite manner.

Figures 5-32, 5-34, 5-36, 5-38, and 5-40 show the moment distribution behavior for all five girders, with the test truck moving on wheel lines 1, 2, 3, 4, and 5, respectively. Each figure is shown on the same page as the corresponding plot of moment influence lines. In the figures, the moment distribution factors were plotted when the magnitude of the sum of the measured moments in the girders was larger than 700 kip$\frown$inches.

The test data was not sufficient to explain the moment carrying behavior of girder 4, as shown in Figure 5-39. However, the excess moment in girder 4 was probably caused by the behavior of girder 5. Figure 5-20, above, shows the neutral axis offset results for the negative moment region on girder 5. These results are significantly more scattered than the neutral axis offset results from any of the other cross sections. The scatter in Figure 5-20 may indicate that of out-of-plane bending or local buckling is taking place in girder 5, at this location. Because of the out-of-plane effect, the strain profile through the girder is no longer linear (an assumption used in the neutral axis calculations), and the results from the gage pairs becomes scattered. If this is the case then it is probable that the out of plane effect is caused by a lack of bracing at bearing 2, possibly because of unseen cracking in the deck or bearing support. The result is a loss of stiffness in girder 5, as it bends out of plane. Since the girder is less stiff, it does not develop as much moment as the other girders, resulting in a ‘shedding’ of moment over to girder 4, the nearest girder. This behavior could be confirmed by placing vertically-oriented strain gages on the webs of girders 3, 4, and 5, to measure the degree of out of plane bending in girder 5 as compared to the other girders.

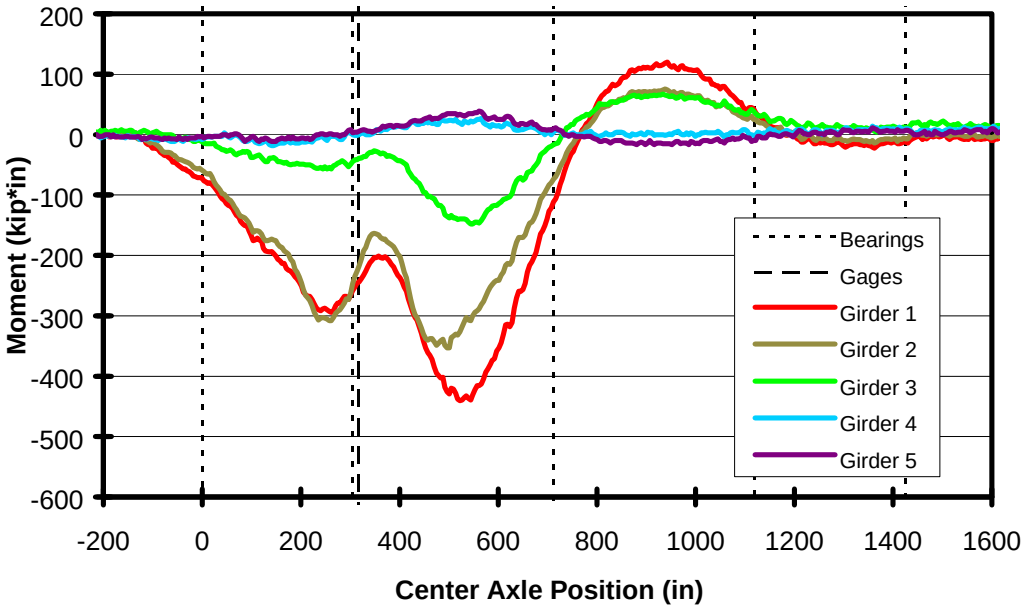

Figure 5-31 Moment Influence Lines, Wheel Line 1, Negative Moment Region

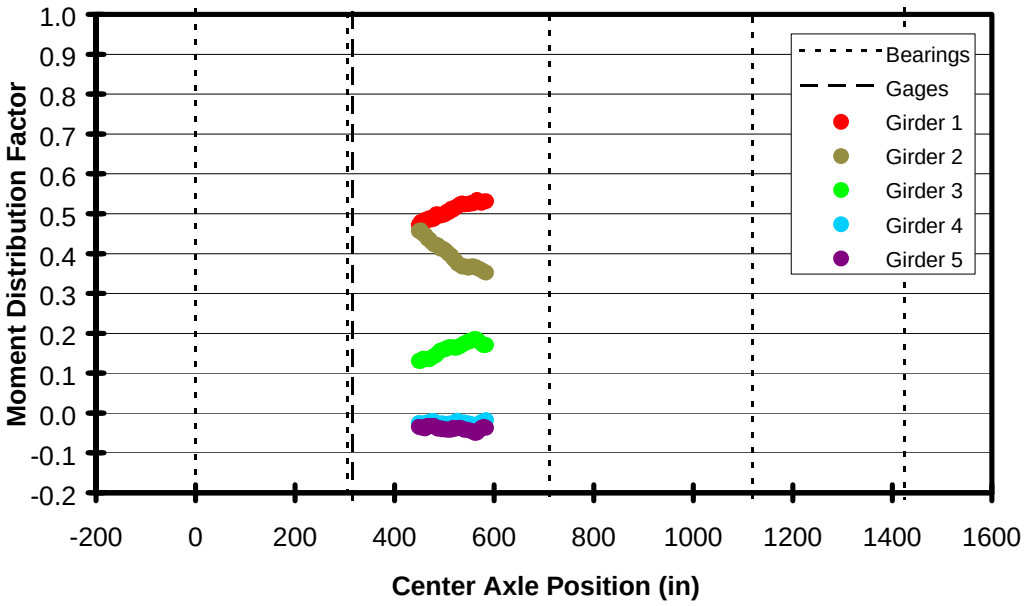

Figure 5-32 Moment Distribution Factors, Wheel Line 1, Negative Moment Region

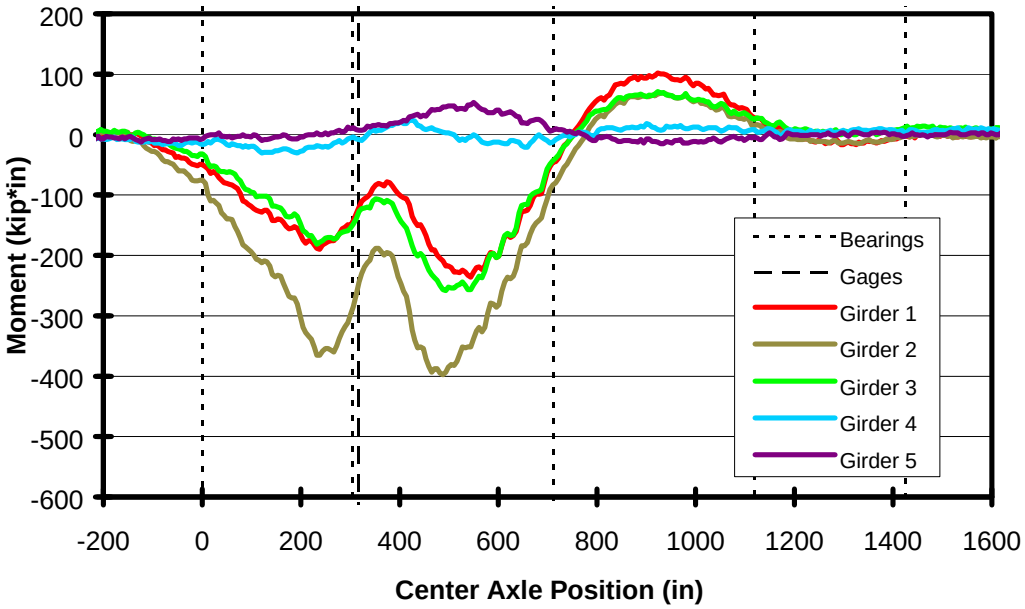

Figure 5-33 Moment Influence Lines, Wheel Line 2, Negative Moment Region

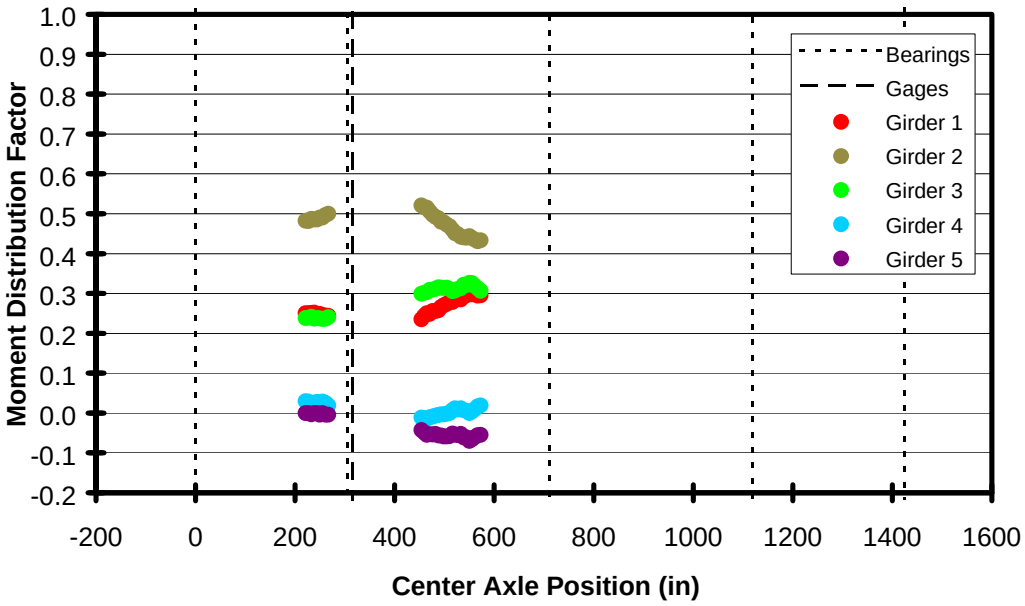

Figure 5-34 Moment Distribution Factors, Wheel Line 2, Negative Moment Region

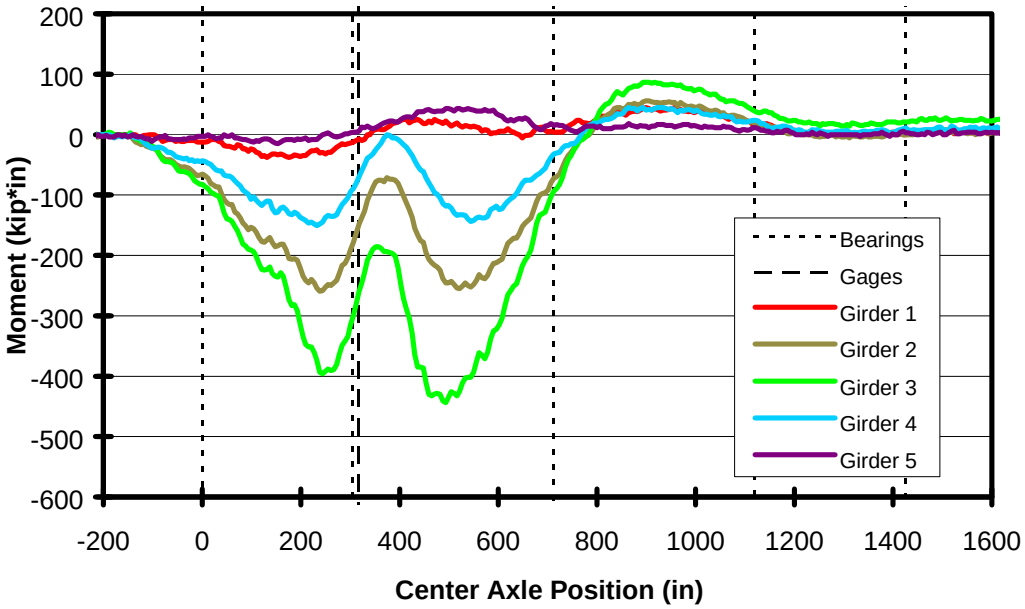

Figure 5-35 Moment Influence Lines, Wheel Line 3, Negative Moment Region

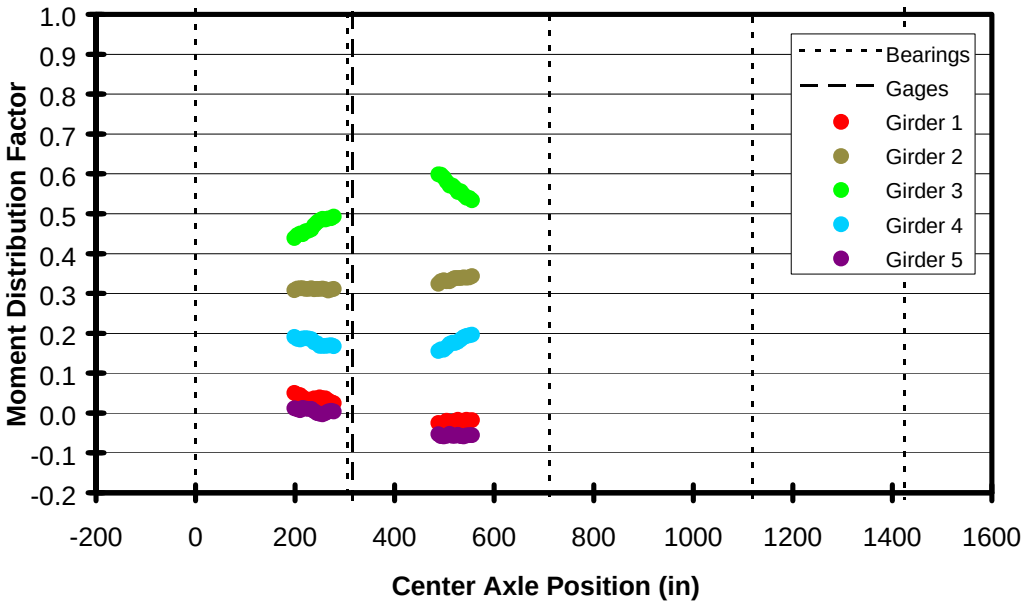

Figure 5-36 Moment Distribution Factors, Wheel Line 3, Negative Moment Region

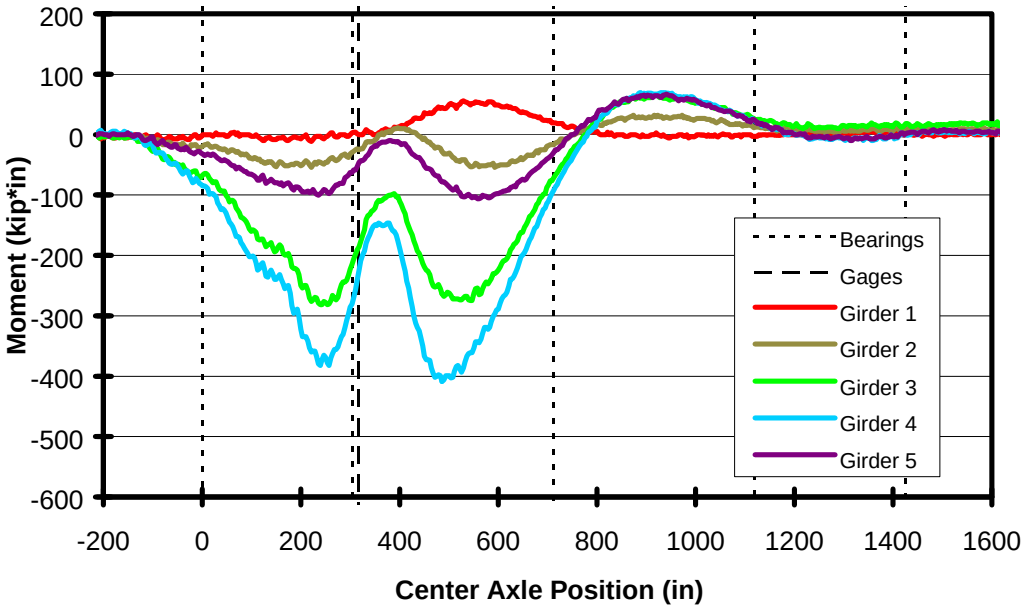

Figure 5-37 Moment Influence Lines, Wheel Line 4, Negative Moment Region

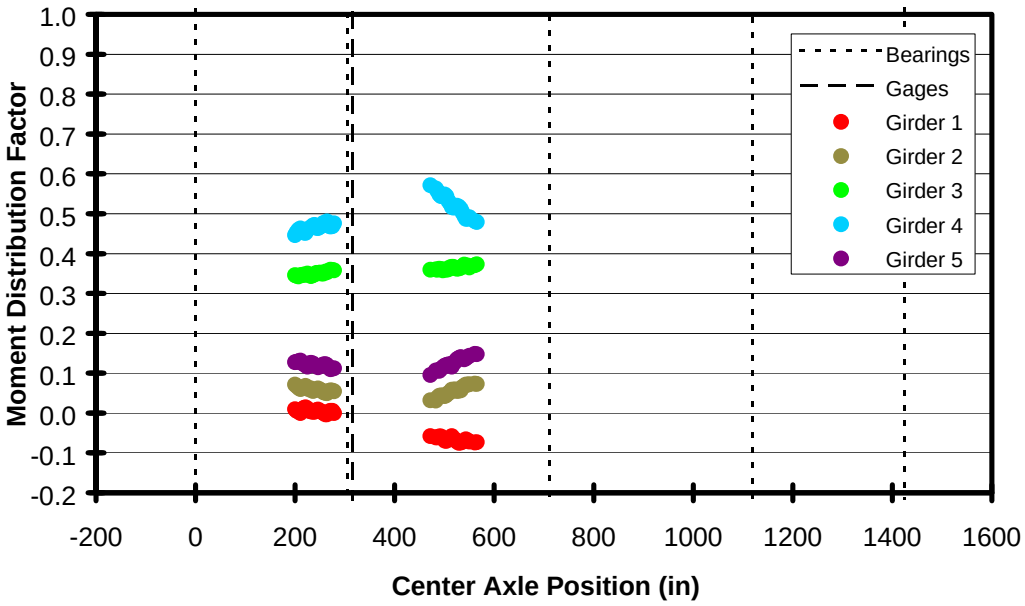

Figure 5-38 Moment Distribution Factors, Wheel Line 4, Negative Moment Region

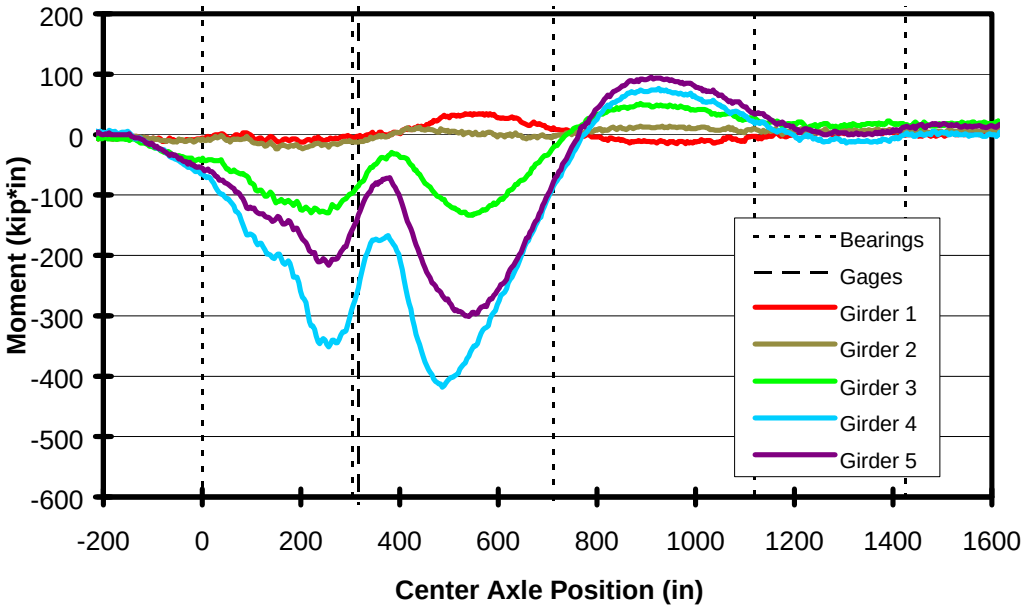

Figure 5-39 Moment Influence Lines, Wheel Line 5, Negative Moment Region

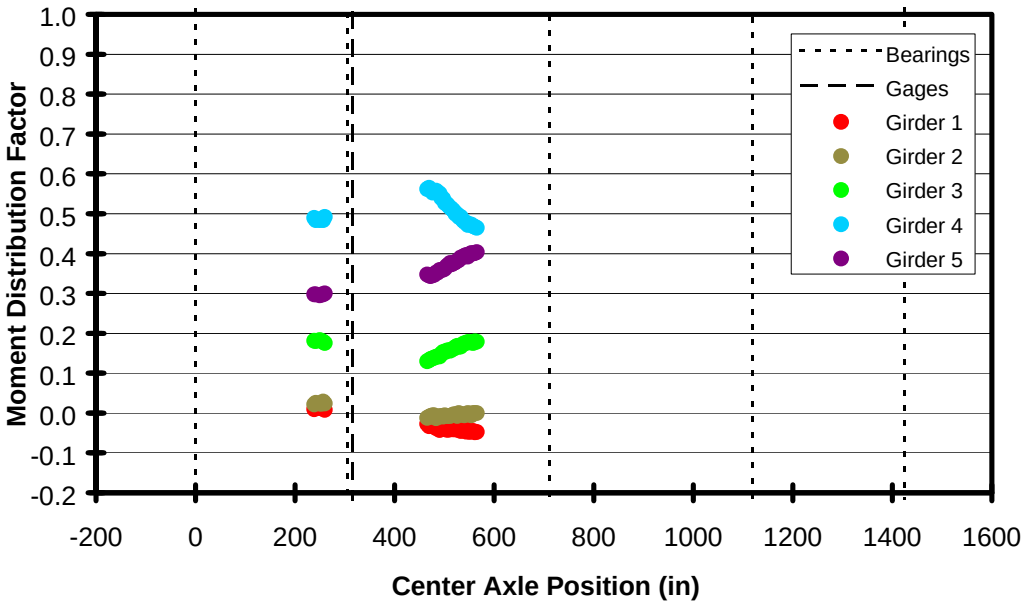

Figure 5-40 Moment Distribution Factors, Wheel Line 5, Negative Moment Region

Figures 5-31, 5-33, 5-37, and 5-39 show that the exterior girder farthest from the truck bent in reverse flexure from the primary girder. Furthermore, in Figure 5-35 both exterior girders bent in reverse flexure, while the truck was on wheel line 3. Although the magnitude of the reverse flexure was small, this behavior indicates that the superstructure was fairly flexible in the lateral direction and not very efficient at distributing the moment away from the primary girder. As with the distribution behavior in the positive moment region, the negative moment distribution behavior of the bridge might improve if lateral braces are installed between the girders to increase the lateral and torsional stiffness of the superstructure, forcing all of the girders to flex in the same direction regardless of which wheel line is loaded.

Table 5-5 shows the maximum moment effects in each girder, for the cross section at 316 inches, for all five wheel lines. The table was generated using the data from Figures 5-31, 5-33, 5-35, 5-37, and 5-39. The largest maximum moment in each girder is shown in bold. The table shows that the largest moments were produced in each girder when the test truck was on the corresponding wheel line, except for girder 4. The maximum moment in girder 4 was produced when the test truck was on wheel line 5. Due to reverse flexure, the maximum moment effects in girders 1, 2, 4, and 5 were positive when the truck was on wheel lines on the far side of the bridge.

Maximum Moment Effect (kip-inches)	**Wheel Line 1**	**Wheel Line 2**	**Wheel Line 3**	**Wheel Line 4**	**Wheel Line 5**
Girder 1	**-441**	-236	45	56	35
Girder 2	-353	**-398**	-259	-54	14
Girder 3	-148	-258	**-444**	-282	-134
Girder 4	27	24	-151	-409	**-419**
Girder 5	39	53	43	-106	**-301**

Table 5-5 Maximum Moment Effects in the Negative Moment Region at 316 Inches

Table 5-6 shows the corresponding moment distribution factors in each girder, for all five wheel lines. This table was generated using the data from Figures 5-32, 5-34, 5-36, 5-38 and 5-40 by calculating the average values of the data sets from span 2. The data from span 1 was not used, because it did not reflect the behavior of the bridge at maximum load. The largest moment distribution factor for each girder is shown in bold. The table shows that although the largest moment in girder 4 occurred when the truck was on wheel line 5, the moment distribution factor for girder 4 was largest when the truck was on wheel line 4.

Moment Distribution Factors*	Wheel Line 1	Wheel Line 2	Wheel Line 3	Wheel Line 4	Wheel Line 5
Girder 1	**.508**	.275	-.021	-.067	-.040
Girder 2	.397	**.468**	.336	.055	-.006
Girder 3	.160	.313	**.565**	.364	.159
Girder 4	-.026	.001	.177	**.522**	.513
Girder 5	-.039	-.056	-.056	.126	**.374**

* Does not include noncomposite flexure of the deck

Table 5-6 Negative Moment Distribution Factors for the Negative Moment Region at 316 Inches

5.2.3 Summary of Girder Moments and Moment Distribution

The maximum moments and moment distribution factors for both positive moment and negative moment in each girder are shown in Table 5-7. In the positive moment region, the composite behavior of girder 1 is evident, because of the large maximum moment and correspondingly large moment distribution factor for this girder. The moment distribution factor for girder 2 is small, because girder 1 is very stiff and carries a lot of the applied moment. Although the moment distribution factors for girders 3, 4, and 5 are similar, the maximum moments recorded in girders 3, 4, and 5, decrease significantly towards the exterior of the superstructure. This effect is due to increased

flexural participation of the deck as the truck is positioned closer to wheel line 5. This phenomenon is investigated more thoroughly in Section 5.3.

In the negative moment region, the maximum moments and moment distribution factors for each of the girders are similar, except for girder 5. The maximum moment and moment distribution factor are both smaller in girder 5. This effect may be caused by a lack of stiffness in girder 5, in this region, due to the out of plane effects discussed in Section 5.2.2.

Girder	Maximum Positive Moment (kip-in)	Positive Moment Distribution Factor*	Maximum Negative Moment (kip-in)	Negative Moment Distribution Factor*
1	1117	**.605**	-441	**.508**
2	633	**.342**	-398	**.468**
3	716	**.418**	-444	**.565**
4	656	**.406**	-419***	**.522**
5	591	**.411****	-301	**.374**

* Does not include noncomposite flexure of the deck
** Test truck on wheel line 4
*** Test truck on wheel line 5

Table 5-7 Maximum Moments and Corresponding Moment Distribution Factors

The moment distribution factors shown in Table 5-7 do not include the effects of noncomposite flexure in the deck. They only serve to indicate the portion of load carried by the primary girder, in relation to the other girders. Therefore, these moment distribution factors are not appropriate for use in rating or analysis. Total moment distribution factors, including the flexural participation of the deck are determined in the following section.

5.3 Total Moment Distribution

The sum of the moments measured in each girder were generally less than the actual moment applied to the superstructure. The difference between the applied moment and the measured moment is evidence that some portions of the superstructure, other than the girders, were helping to resist the weight of the test truck. In the Big Creek Relief Bridge, the only other structural element available to resist the additional moment was the deck. Therefore, the moment in the deck was determined by calculating the difference between the applied moment and the sum of the moments measured in the girders.

In chapter 3, a line girder analysis procedure was used to determine moment influence lines for the test vehicle. These moment influence lines are analogous to the total moment influence of the test vehicle on the superstructure and were compared directly with the sum of the measured moments in each girder. Plots of the moment at a cross section vs. the position of the test truck were generated, showing influence lines of the total applied moment from analysis, 'analysis total moment,' the total measured girder moment from the load tests, 'girder total moment,' and the difference between them, 'noncomposite deck moment.' The procedure used to generate these plots is presented in detail in the Appendix.

Total moment distribution factors for each girder were calculated by dividing the moment measured in each girder by the total moment applied to the bridge, as determined by the line girder analysis. A moment distribution factor for the deck was also determined in this manner. The results of the total moment distribution calculations were only considered when the sum of the measured moments was large. The rest of the results were excluded, because they did not represent the behavior of the superstructure under heavy loads. A more detailed description of the moment distribution calculations is presented in the Appendix.

After the total moment distribution factors for each girder were determined, the two-lane moment distribution factors were determined by combining the total moment distribution factors for each wheel line and girder through linear interpolation. The two-

lane moment distribution factors were used in the revised load rating calculations, replacing the AASHTO LRFD two-lane moment distribution factors.

5.3.1 Total Moment Distribution in the Positive Moment Region

In the positive moment region, the moment distribution behavior of the superstructure was similar for each wheel line. Therefore, the results from each wheel line are presented together. Figures 5-41, 5-42, 5-43, 5-44, and 5-45 are plots of the influence lines for the analysis total moment, girder total moment, and noncomposite deck moment, with the truck on wheel lines 1 through 5, respectively. The influence line for the analysis total moment is the same in each plot, because it was calculated, not measured. The influence lines for the girder total moments are similar, having the same general shape and similar maximum values. The influence lines for the noncomposite deck moment were calculated by subtracting the girder total moment from the analysis total moment.

The maximum moments from each plot were compared. The largest maximum girder total moment was 1851 kip∿inches, as shown in Figure 5-41, with the truck on wheel line 1. The smallest maximum girder total moment was 1535 kip∿inches, as shown in Figure 5-45, with the truck on wheel line 5. The other maximum girder total moments decreased in order as the truck was positioned on wheel lines 1 through 5, respectively. The influence lines for the noncomposite deck moment showed an opposite trend. The largest maximum noncomposite deck moment was 1060 kip∿inches, as shown in Figure 5-45, with the truck on wheel line 5. The smallest maximum noncomposite deck moment was 709 kip∿inches, as shown in Figure 5-41, with the truck in wheel line 1. The other maximum noncomposite deck moments increased in order as the truck was positioned on wheel lines 1 through 5, respectively.

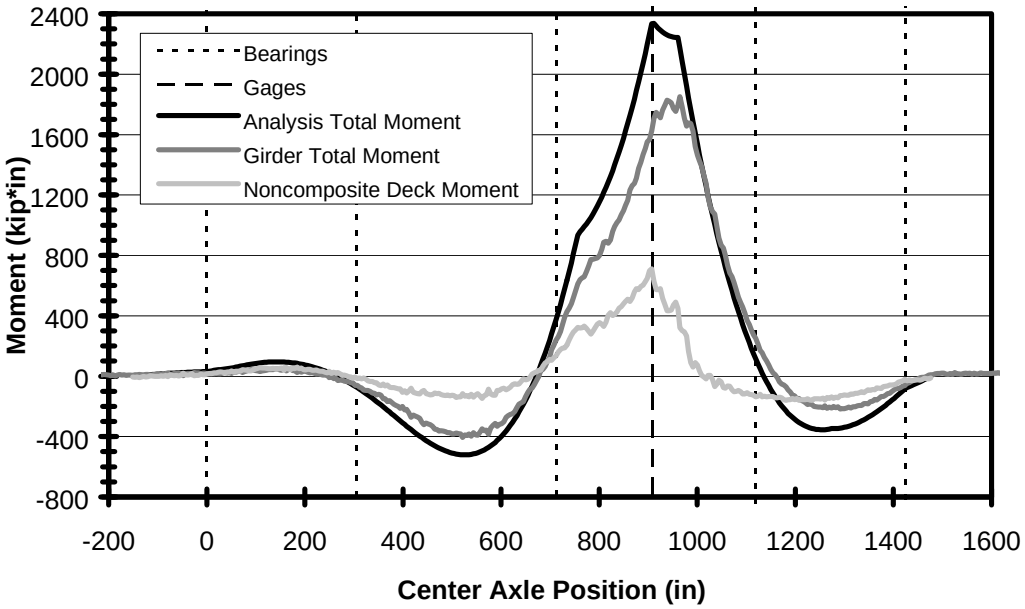

Figure 5-41 Applied, Measured, and Deck Moment Influence Lines, Wheel Line 1, Positive Moment Region

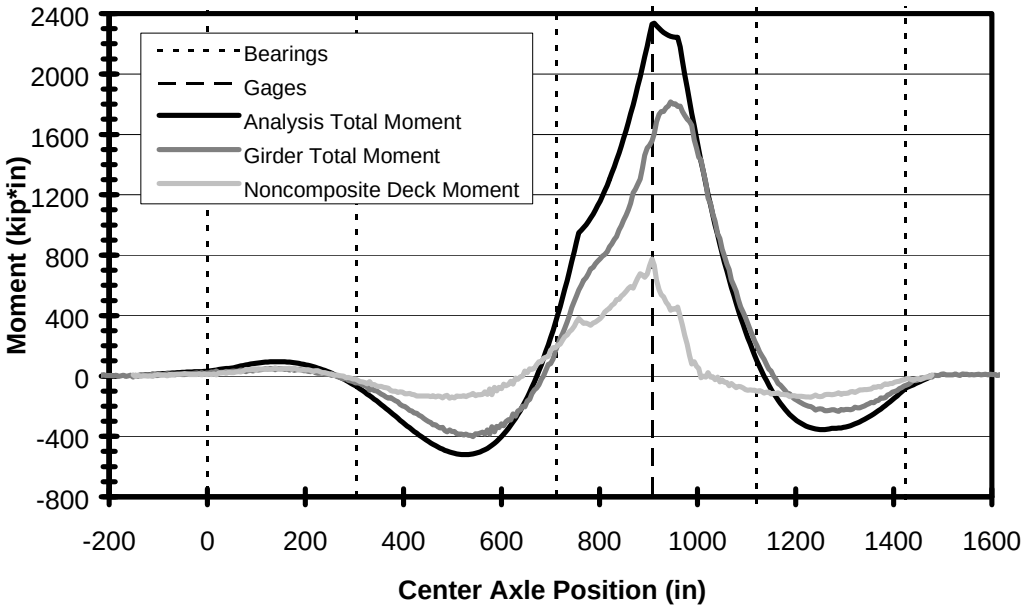

Figure 5-42 Applied, Measured, and Deck Moment Influence Lines, Wheel Line 2, Positive Moment Region

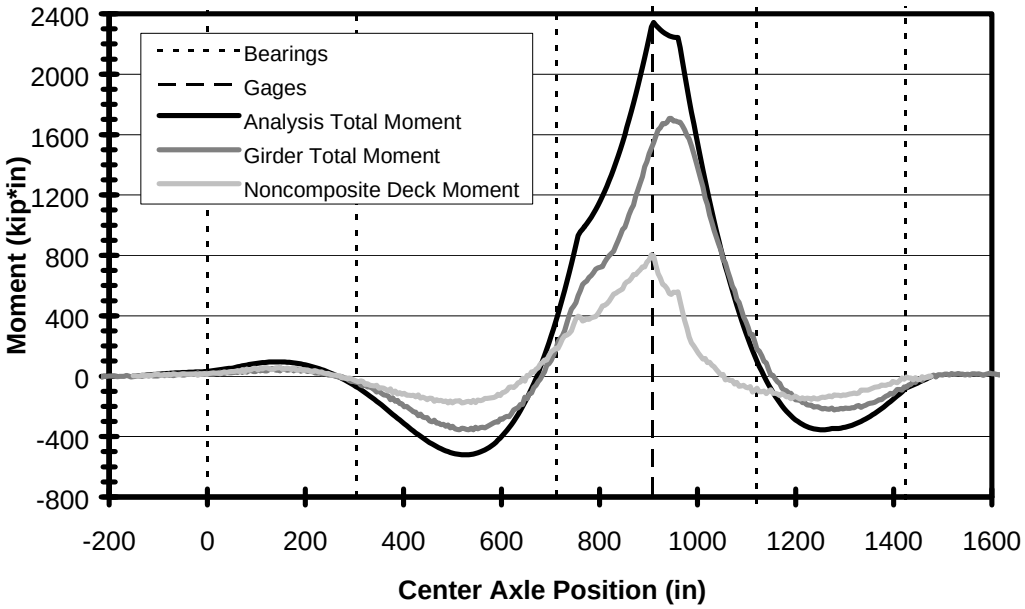

Figure 5-43 Applied, Measured, and Deck Moment Influence Lines, Wheel Line 3, Positive Moment Region

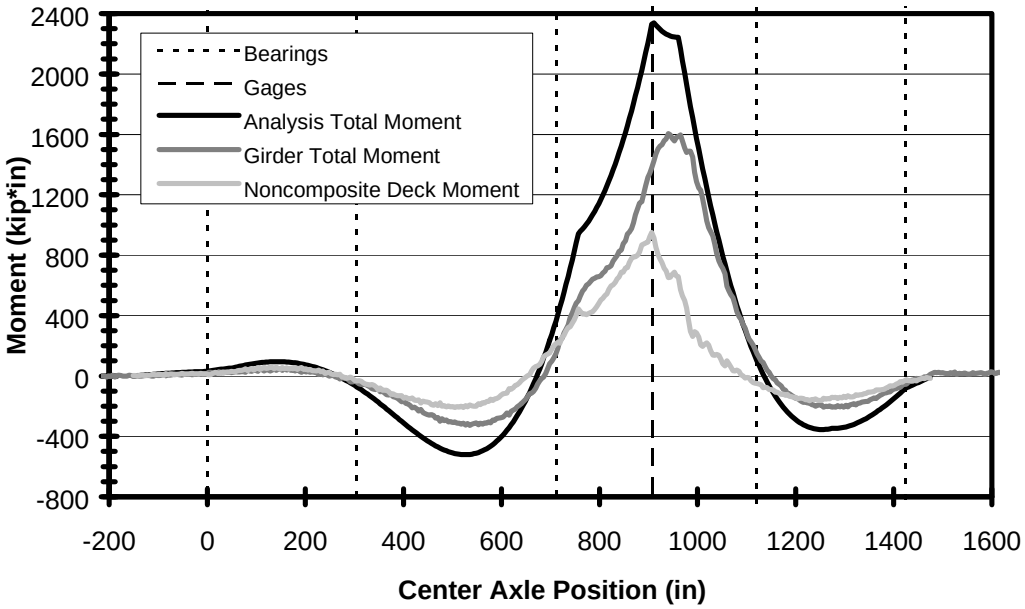

Figure 5-44 Applied, Measured, and Deck Moment Influence Lines, Wheel Line 4, Positive Moment Region

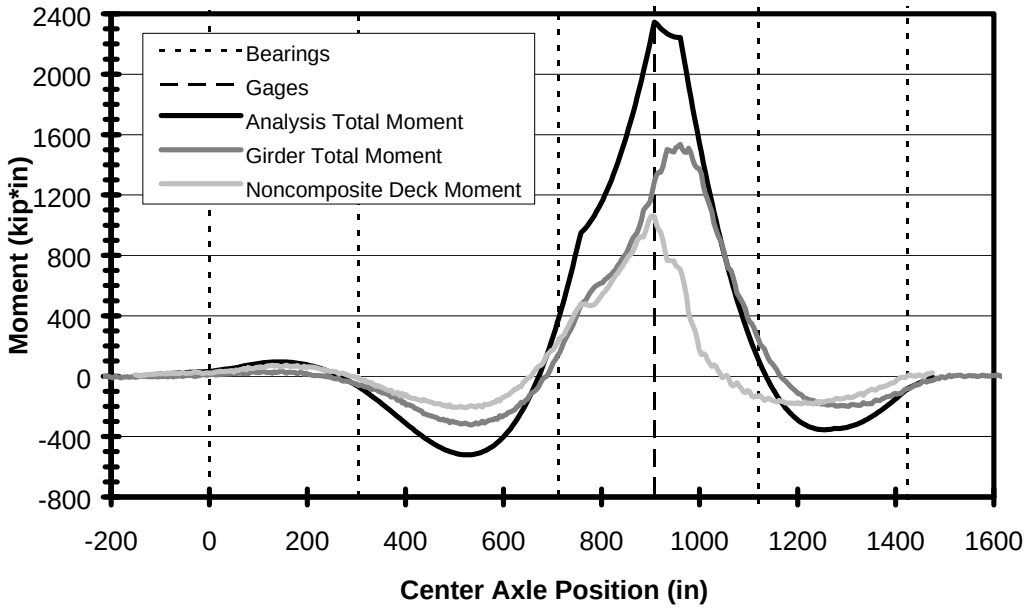

Figure 5-45 Applied, Measured, and Deck Moment Influence Lines, Wheel Line 5, Positive Moment Region

Figures 5-41 through 5-45 show that the maximum noncomposite deck moment occurred when the truck crossed over the gaged cross section, while the maximum girder total moment occurred a few inches farther along span 3. Although the maximum moments did not occur at the same location, the magnitudes of the maximum moments in the girders and the deck were compared. Table 5-8 presents the maximum girder total moment and the maximum noncomposite deck moment for each wheel line. As noted in the results from Section 5.1, girder 1 is the only composite girder. As the truck was positioned farther away from the composite girder, the maximum moment in the girders decreased while the maximum moment in the deck increased. This pattern confirms the noncomposite flexural participation of the deck, because the deck carried more moment when the noncomposite side of the superstructure was loaded.

Wheel Line	Maximum Girder Total Moment (kip∽inches)	Maximum Noncomposite Deck Moment (kip∽inches)	Ratio of Girders to Deck
1	1851	709	2.61
2	1815	773	2.35
3	1707	804	2.12
4	1605	951	1.69
5	1535	1060	1.45

Table 5-8 Maximum Girder and Maximum Noncomposite Deck Moments, Positive Moment Region

The ratio of maximum girder total moment to maximum noncomposite deck moment is shown in Table 5-8. When the truck was on wheel line 1, the girders held 2.61 times as much moment at the deck. However, when the truck was on span 5, the girders held only 1.45 times as much moment at the deck.

Figures 5-46, 5-47, 5-48, 5-49, and 5-50 show the stress distribution factors, girder moment distribution factors, and total moment distribution factors for each wheel line. The data in these plots was calculated from the moment data shown in Figures 5-21, 5-23, 5-25, 5-27, and 5-29, and from the stress data used to calculate the moments. Only the data recorded when the total girder moment was larger than 1500 kip∽inches was used, because the rest of the data did not reflect the moment distribution behavior of the bridge under heavy loads.

The effect of the composite behavior in girder 1 can be seen in Figures 5-46 and 5-47, where the moment distribution factor for girder 1 is significantly greater than the stress distribution factor. At the same time, the moment distribution factors for girders 2 through 5 were less than the stress distribution factors. In Figures 5-48 through 5-50, the composite behavior of girder 1 had little effect on the moment distribution behavior of the bridge, because girder 1 was not heavily loaded.

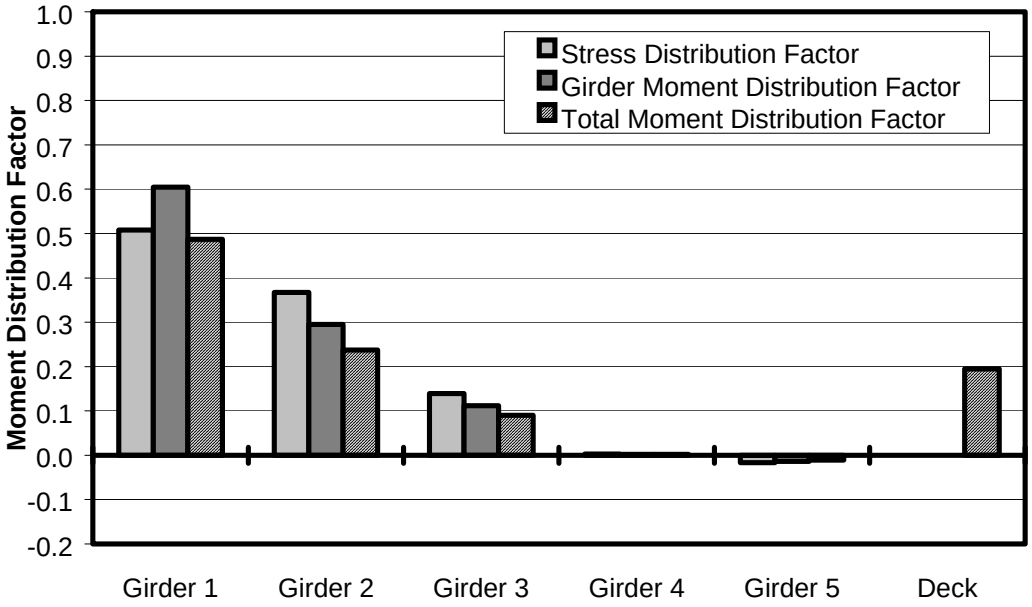

Figure 5-46 Stress, Girder Moment, and Total Moment Distribution Factors, Wheel Line 1, Positive Moment Region

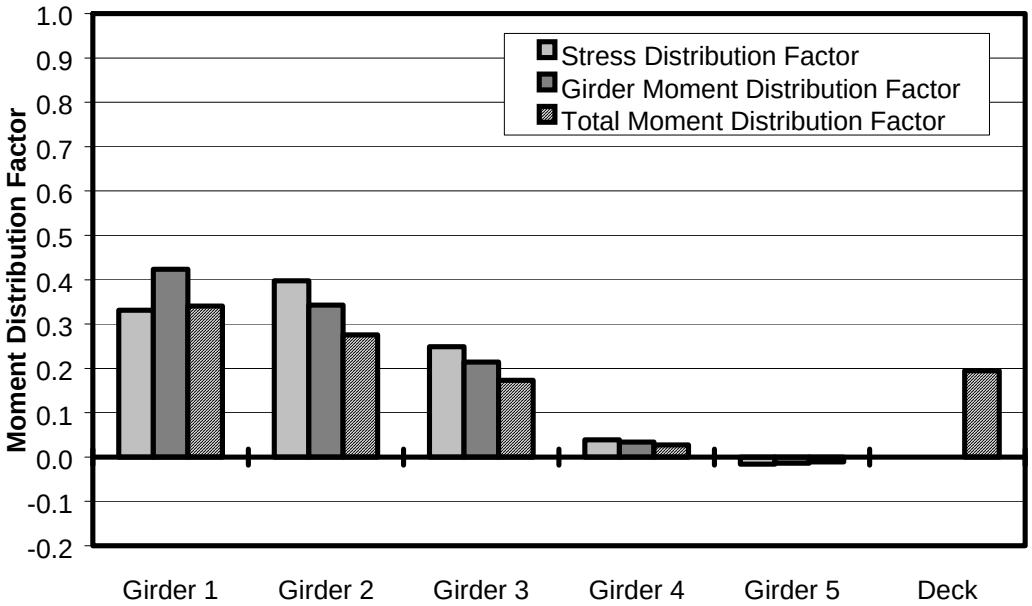

Figure 5-47 Stress, Girder Moment, and Total Moment Distribution Factors, Wheel Line 2, Positive Moment Region

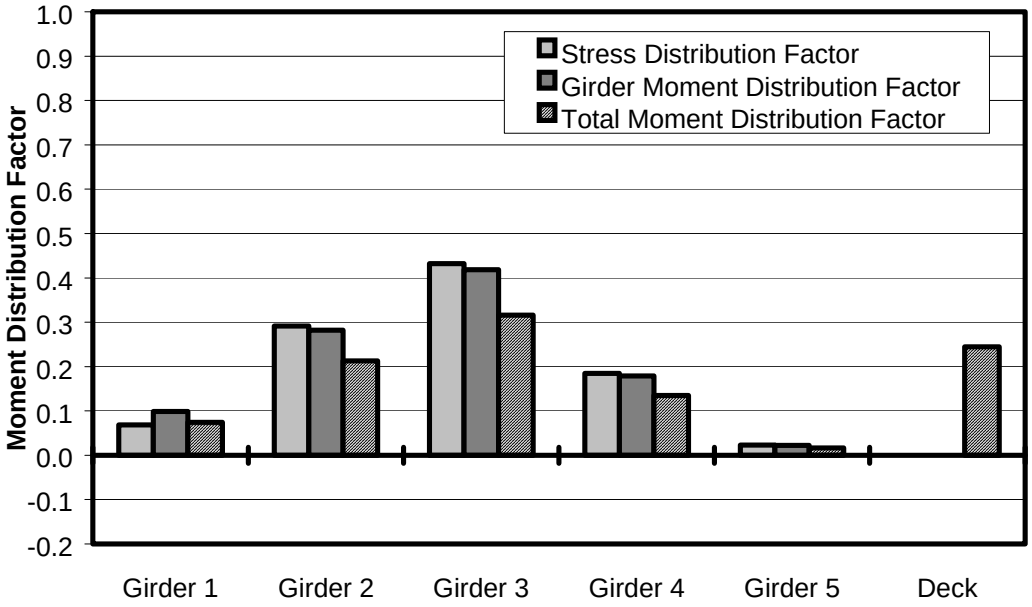

Figure 5-48 Stress, Girder Moment, and Total Moment Distribution Factors, Wheel Line 3, Positive Moment Region

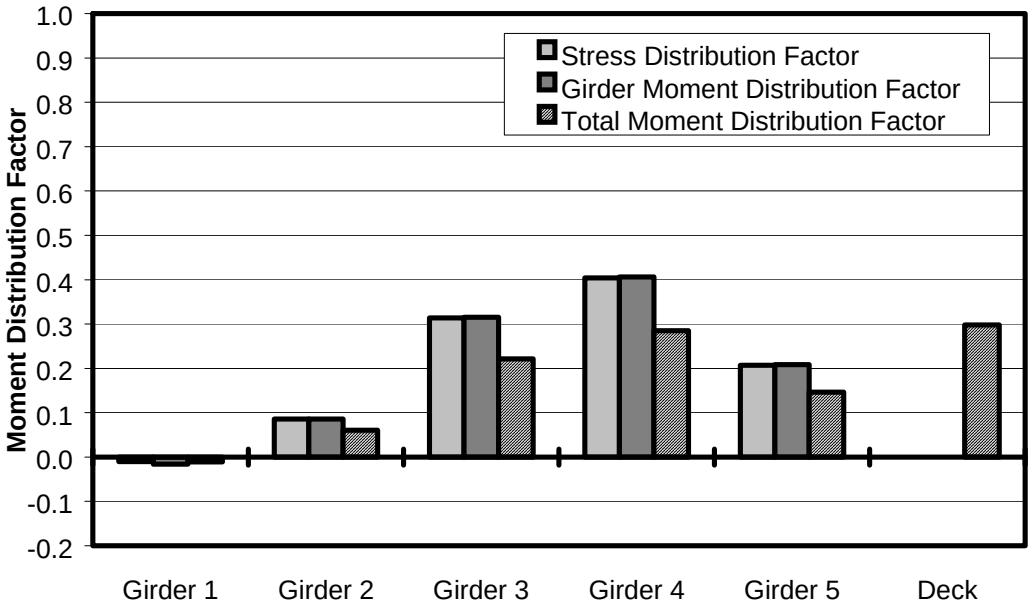

Figure 5-49 Stress, Girder Moment, and Total Moment Distribution Factors, Wheel Line 4, Positive Moment Region

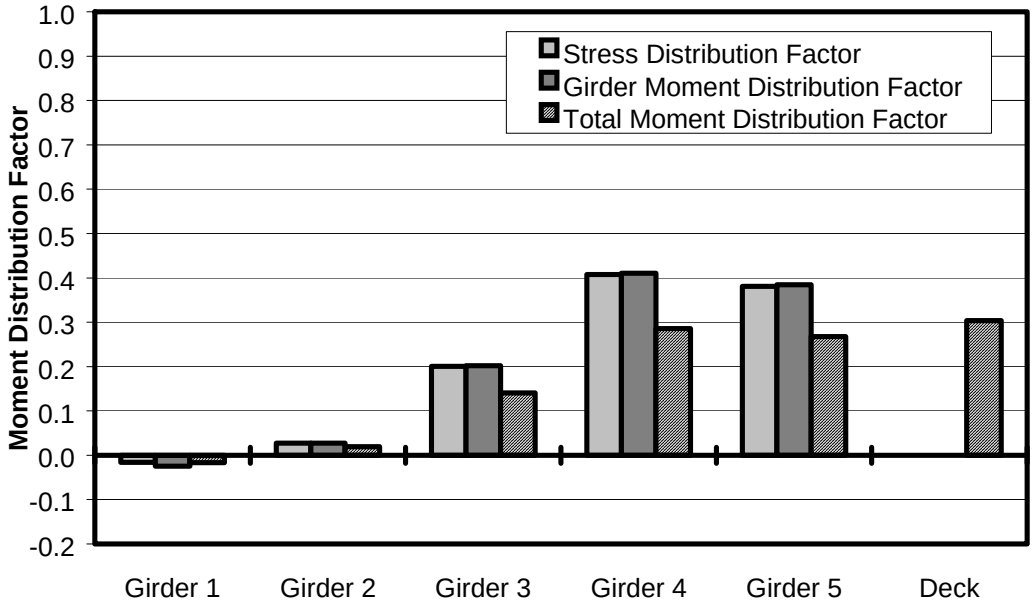

Figure 5-50 Stress, Girder Moment, and Total Moment Distribution Factors, Wheel Line 5, Positive Moment Region

Figures 5-46 through 5-50 show that the portion of the applied moment resisted by noncomposite flexure of the deck increased as the truck's position varied from wheel line 1 to wheel line 5. When the truck was on wheel line 1, the deck resisted 19.5 percent of the applied moment. However, when the truck was on wheel line 5, the deck resisted 30.4 percent of the applied moment, more than any of the girders.

Table 5-9 presents a summary of the total moment distribution factors for each girder and the deck, for all five wheel lines. The largest moment distribution factor for each girder is shown in bold. The table shows that, in general, the moment distribution factor for each girder was largest when the truck was on the closest wheel line.

The behavior of girder 5 was interesting. When the test truck was positioned on wheel line 5, as close to girder 5 as possible, the total moment distribution factor for girder 4 was larger. The total moment distribution factor for the deck was larger, as well. This suggests that girder 5 is a "soft" girder. For whatever reason, girder 5 is not capable of developing moments as large as it should. The moments that should have been carried by girder 5 were distributed to the deck and to girder 4, instead.

Total Moment Distribution Factors	Wheel Line 1	Wheel Line 2	Wheel Line 3	Wheel Line 4	Wheel Line 5
Girder 1	**.487**	.341	.075	-.011	-.017
Girder 2	.238	**.276**	.213	.060	.019
Girder 3	.090	.173	**.316**	.221	.141
Girder 4	.002	.027	.135	.285	**.286**
Girder 5	-.011	-.011	.017	.146	**.267**
Deck	.195	.195	.245	.298	.304

Table 5-9 Total Moment Distribution Factors for the Positive Moment Region at 908 Inches

The data in Table 5-9 is analogous to the single-lane moment distribution factors specified in the AASHTO LRFD code, because the data represents the behavior of the bridge under the weight of one vehicle. However, the Big Creek Relief Bridge was load rated for two design lanes, because the roadway was 30 feet wide. The data from Table 5-9 was used to create two-lane moment distribution factors for the bridge, by combining the effect of different wheel lines through linear interpolation. This procedure is explained in detail in the Appendix.

Table 5-10 presents the two-lane moment distribution factors for the bridge. The trucks' positions in each of the design lanes are also presented. The largest two-lane moment distribution factor was 0.539 for girder 1, and the smallest was 0.279 for girder 5. The discrepancy between the distribution factors for girder 1 and girder 5 was due to the composite behavior of girder 1 and the soft behavior of girder 5. The two lane moment distribution factors for the other three girders were similar, ranging from 0.388 to 0.460.

	Truck 1	Truck 2	Two-Lane Moment Distribution Factor
Girder 1	100% Wheel Line 1	69% Wheel Line 3 31% Wheel Line 4*	**.539**
Girder 2	43% Wheel Line 1 57% Wheel Line 2	69% Wheel Line 3 31% Wheel Line 4	**.426**
Girder 3	54% Wheel Line 2 46% Wheel Line 3	100% Wheel Line 4	**.460**
Girder 4	31% Wheel Line 2 69% Wheel Line 3	100% Wheel Line 5	**.388**
Girder 5	31% Wheel Line 2* 69% Wheel Line 3	100% Wheel Line 5	**.279**

* Not considered because of a negative contribution due to reverse flexure

Table 5-10 Two-Lane Moment Distribution Factors for the Positive Moment Region at 908 Inches

The values in Table 5-10 were used to reevaluate the load rating of the bridge, because they represent the actual moment distribution behavior of span 3 under an applied positive moment. They are analogous to the AASHTO LRFD two lane moment distribution factors for positive flexure in spans 2 and 3. The reevaluation of the bridge's load rating is presented in Chapter 6.

Figures showing the position of the trucks used to determine the two-lane moment distribution factors are shown in Section 5.3.3, below. To avoid repetition, the figures are not shown here, because, coincidentally, the positions of the trucks were the same for the positive moment and negative moment regions.

5.3.2 Total Moment Distribution in the Negative Moment Region

In the negative moment region, the moment distribution behavior of the superstructure was similar for each wheel line. Thus, the results from each wheel line are presented together. Figures 5-51, 5-52, 5-53, 5-54, and 5-55 are plots of the influence lines for the analysis total moment, girder total moment, and noncomposite deck moment, with the truck on wheel lines 1 through 5, respectively. The influence line for the

analysis total moment is the same in each plot, because it was calculated, not measured. The influence lines for the girder total moments are similar, having the same general shape and similar maximum values. The influence lines for the noncomposite deck moment were calculated by subtracting the girder total moment from the analysis total moment.

The maximum moments from each plot were compared. The largest maximum girder total moment was -862 kip⁄inches, as shown in Figure 5-51, with the truck on wheel line 1. The smallest maximum girder total moment was -757 kip⁄inches, as shown in Figure 5-53, with the truck on wheel line 3. In general, the maximum total girder moments were larger when the truck was on the exterior wheel lines. The largest maximum noncomposite deck moment was -625 kip⁄inches, as shown in Figure 5-53, with the truck on wheel line 3. The smallest maximum noncomposite deck moment was -479 kip⁄inches, as shown in Figure 5-51, with the truck in wheel line 1.

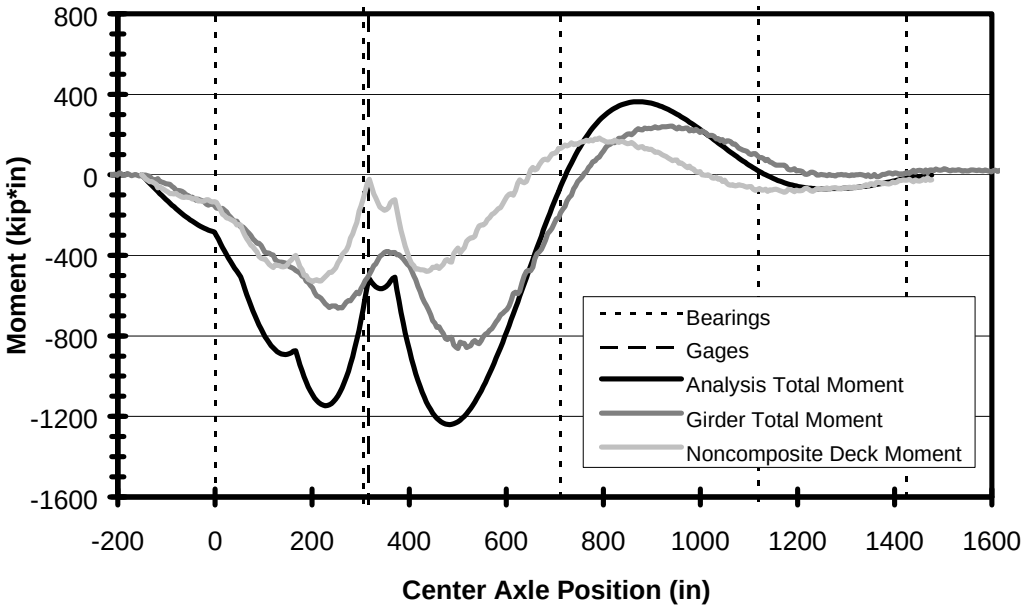

Figure 5-51 Analysis, Girder, and Deck Moment Influence Lines, Wheel Line 1, Negative Moment Region

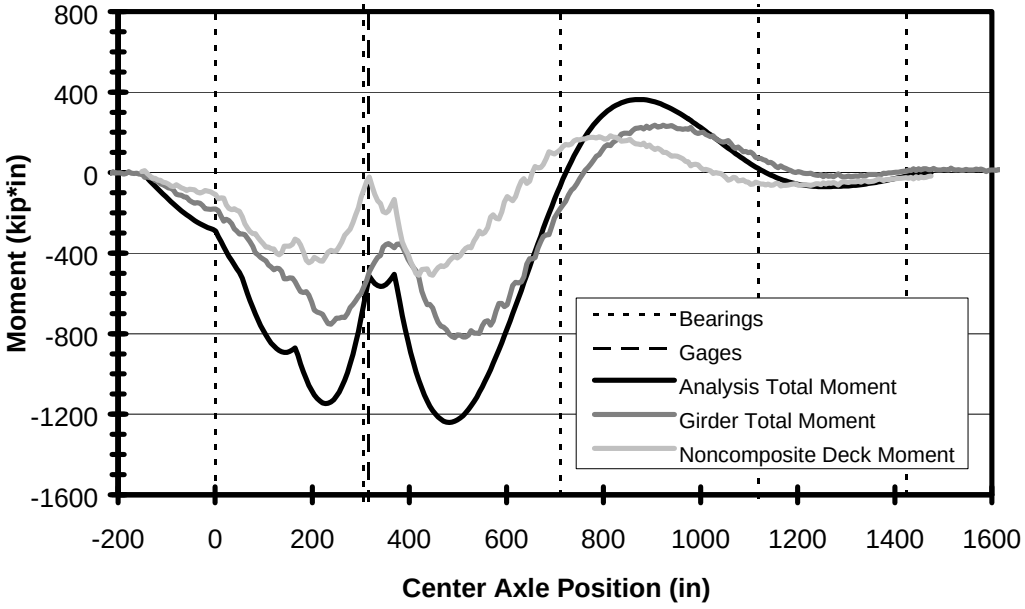

Figure 5-52 Analysis, Girder, and Deck Moment Influence Lines, Wheel Line 2, Negative Moment Region

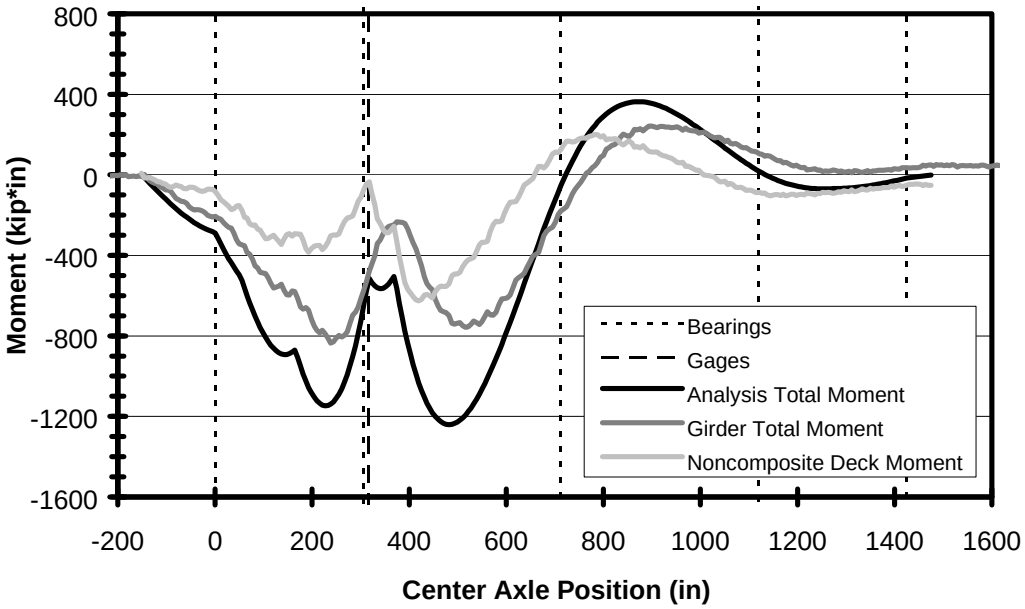

Figure 5-53 Analysis, Girder, and Deck Moment Influence Lines, Wheel Line 3, Negative Moment Region

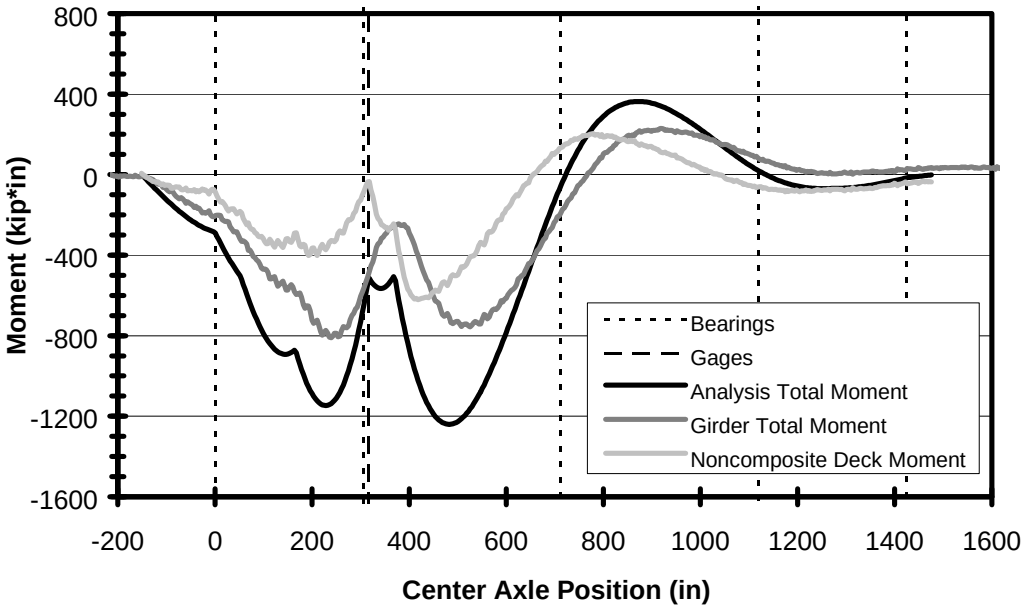

Figure 5-54 Analysis, Girder, and Deck Moment Influence Lines, Wheel Line 4, Negative Moment Region

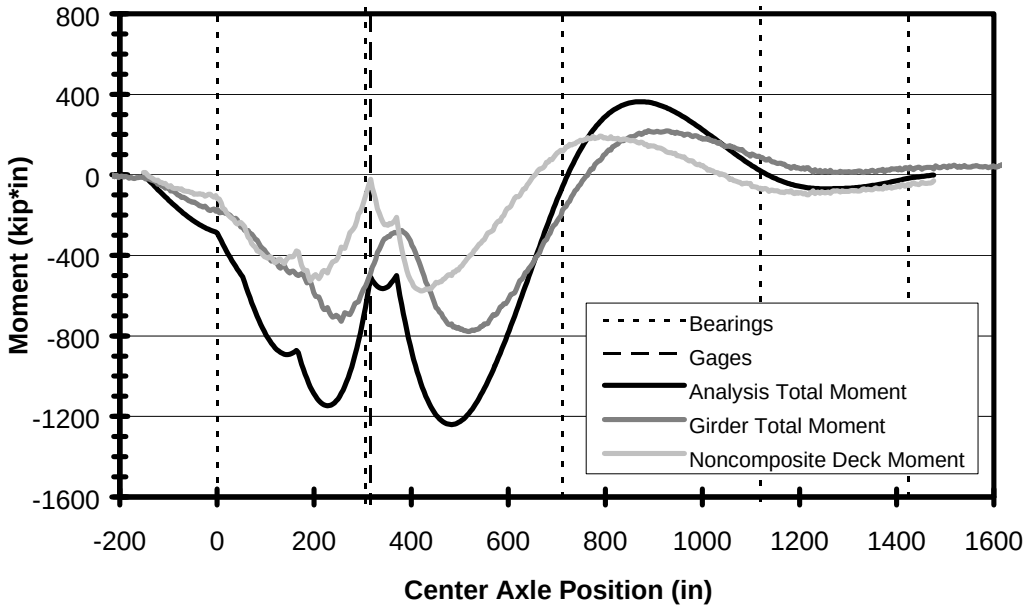

Figure 5-55 Analysis, Girder, and Deck Moment Influence Lines, Wheel Line 5, Negative Moment Region

Figures 5-51 through 5-55 show that the maximum noncomposite deck moment occurred when the truck was about one third of the way across span 2, but the maximum girder total moment occurred when the truck was near midspan. Although the maximum moments did not occur at the same location, the magnitudes of the maximum moments in the girders and the deck were compared. Table 5-11 presents the maximum girder total moment and the maximum noncomposite deck moment for each wheel line. In general, the maximum girder total moments were larger when the truck was on the exterior wheel lines, and smaller when the truck was near the midline of the bridge.

The ratio of maximum girder total moment to maximum nonncomposite deck moment is shown in Table 5-11. When the truck was on wheel line 1, the girders held 1.80 times as much moment at the deck. However, when the truck was on span 5, the girders held only 1.21 times as much moment at the deck.

Wheel Line	Maximum Girder Total Moment (kip-inches)	Maximum Noncomposite Deck Moment (kip-inches)	Ratio of Girders to Deck
1	-862	-479	1.80
2	-816	-509	1.60
3	-757	-625	1.21
4	-756	-621	1.22
5	-778	-576	1.35

Table 5-11 Maximum Girder and Maximum Noncomposite Deck Moments, Negative Moment Region

Figures 5-56, 5-57, 5-58, 5-59, and 5-60 show the stress distribution factors, girder moment distribution factors, and total moment distribution factors for each wheel line. The data in these plots was calculated from the moment data shown in Figures 5-31, 5-33, 5-35, 5-37, and 5-39, and from the stress data used to calculate the moments. Only the data recorded when the total girder moment was larger than -700 kip-inches was used, because the rest of the data did not reflect the moment distribution behavior of the bridge under heavy loads.

In the negative moment region, all of the girders behaved in a noncomposite manner. Therefore, the stress distribution and moment distribution factors for each girder were identical. However, the noncomposite flexural participation of the deck greatly affected the total moment distribution behavior of the girders. Figures 5-56 through 5-60 show that the percentage of the applied moment resisted by noncomposite flexure of the deck ranged from a minimum of 28.9 percent for wheel line 1 to a maximum of 36.7 percent for wheel line 4.

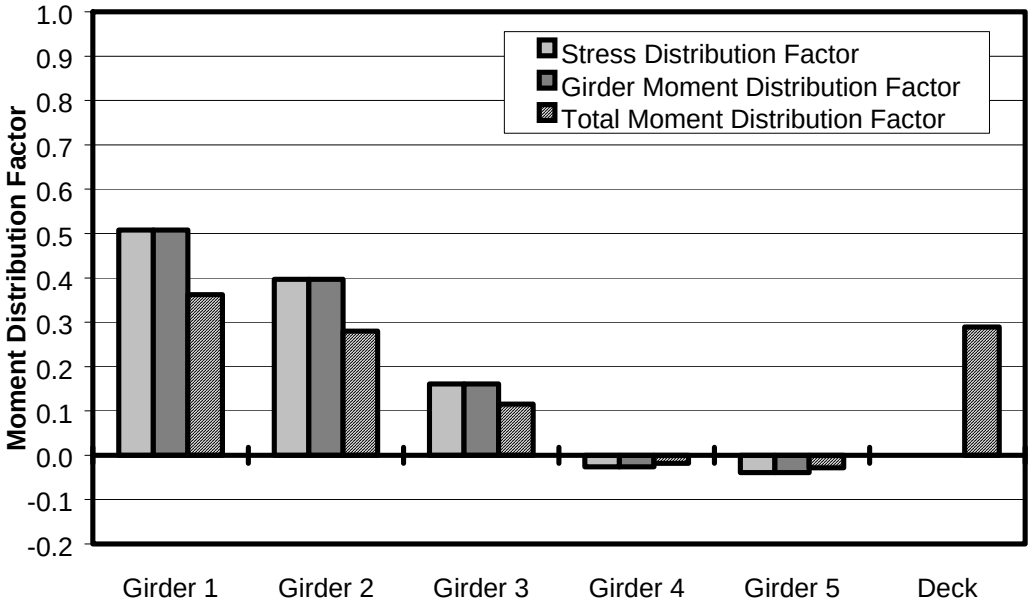

Figure 5-56 Stress, Girder Moment, and Total Moment Distribution Factors, Wheel Line 1, Negative Moment Region

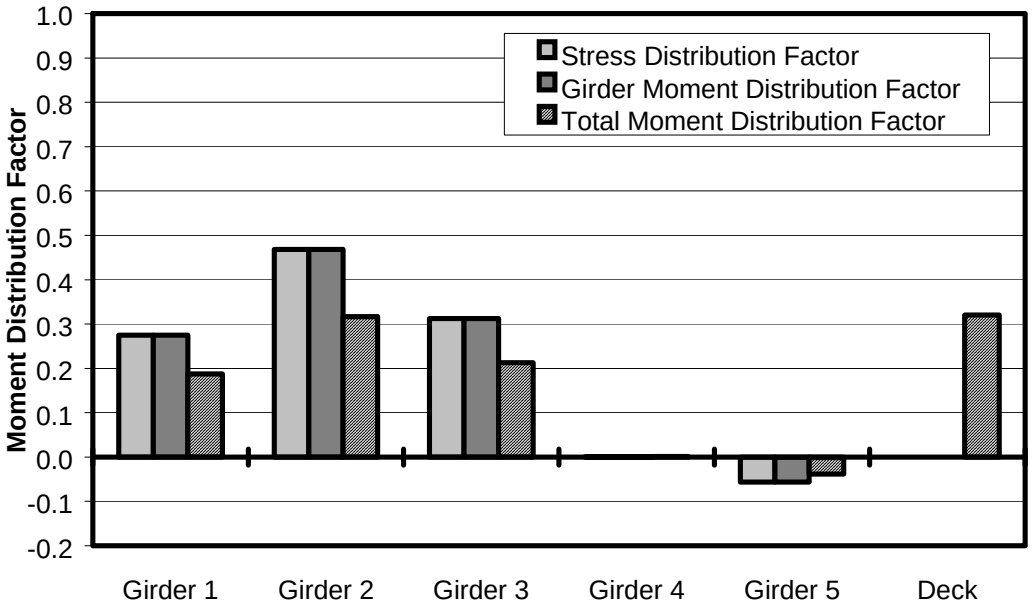

Figure 5-57 Stress, Girder Moment, and Total Moment Distribution Factors, Wheel Line 2, Negative Moment Region

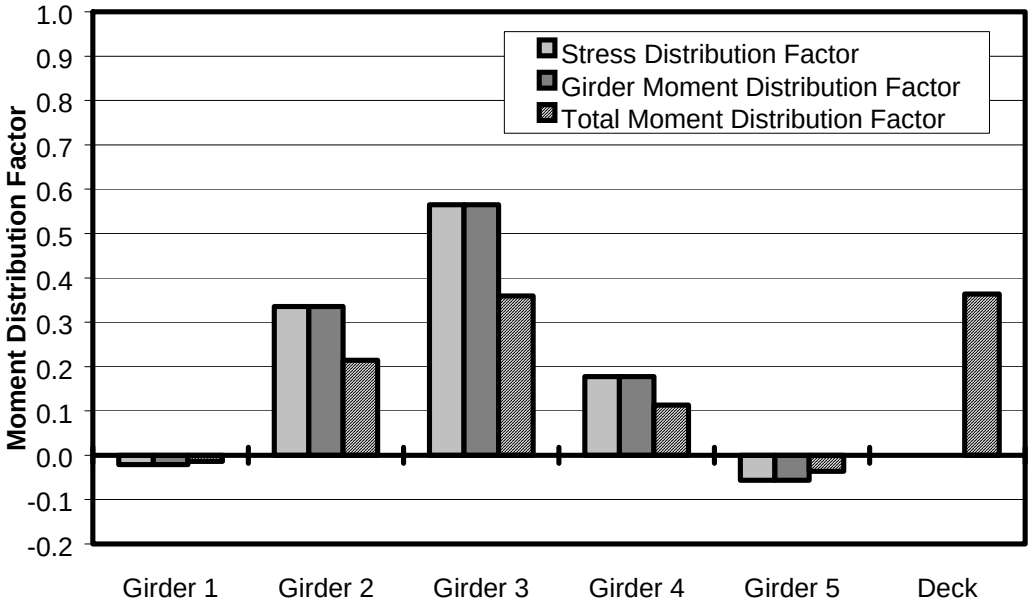

Figure 5-58 Stress, Girder Moment, and Total Moment Distribution Factors, Wheel Line 3, Negative Moment Region

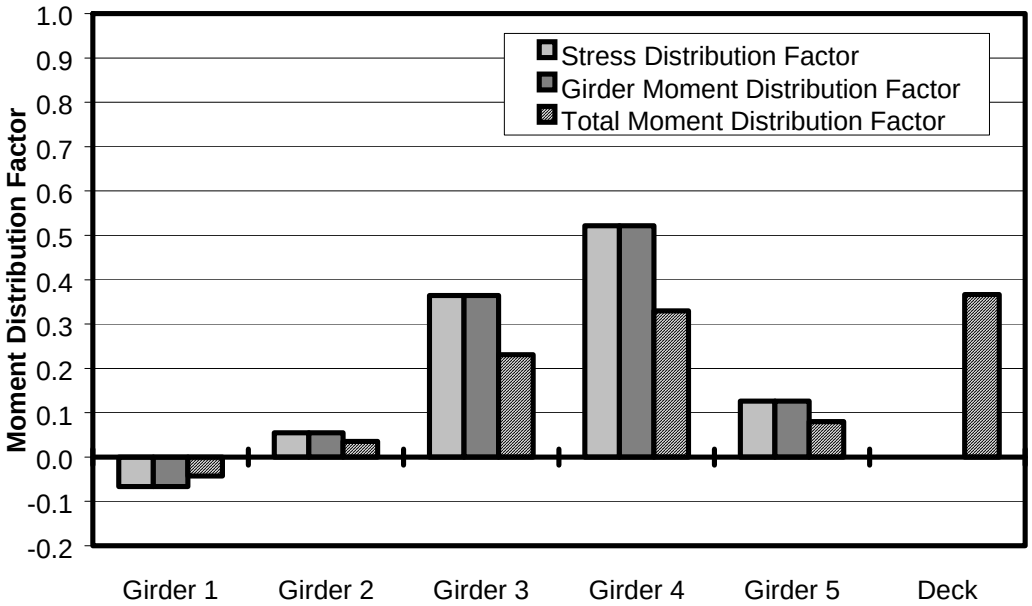

Figure 5-59 Stress, Girder Moment, and Total Moment Distribution Factors, Wheel Line 4, Negative Moment Region

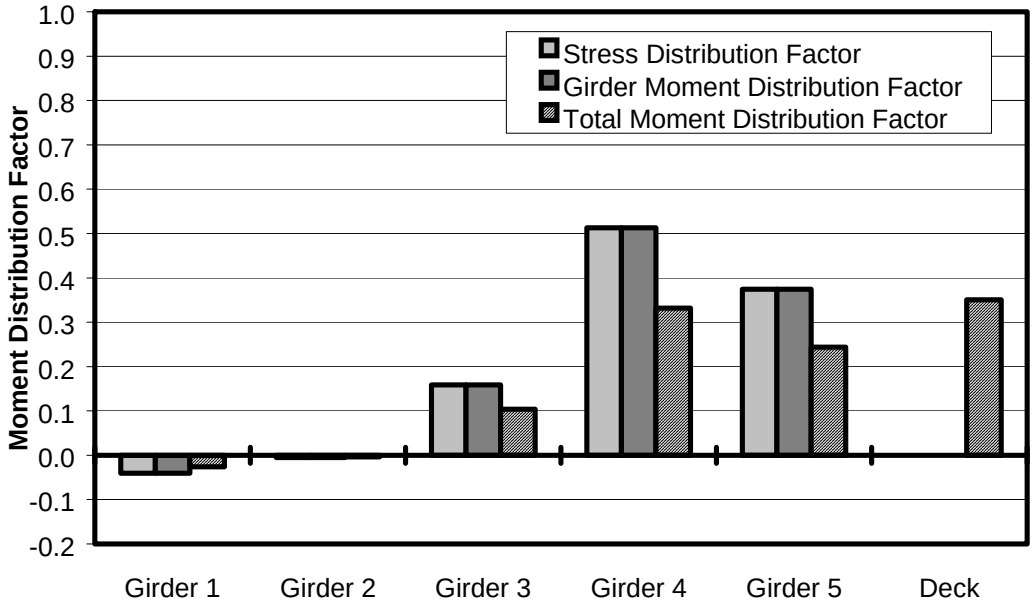

Figure 5-60 Stress, Girder Moment, and Total Moment Distribution Factors, Wheel Line 5, Negative Moment Region

Table 5-12 presents a summary of the total moment distribution factors in each girder and the deck, for all five wheel lines. The largest moment distribution factor for each girder is shown in bold. The table shows that, in general, the moment distribution factor for each girder was largest when the truck was on the closest wheel line.

As in the positive moment region, the behavior of girder 5 was interesting. When the test truck was positioned on wheel line 5, as close to girder 5 as possible, the total moment distribution factor for girder 4 was larger. The total moment distribution factor for the deck was larger as well. This suggests that girder 5 is a "soft" girder. For whatever reason, girder 5 is not capable of developing moments as large as it should. The moments that should have been carried by girder 5 were distributed to the deck and to girder 4 instead.

Total Moment Distribution Factors	Wheel Line 1	Wheel Line 2	Wheel Line 3	Wheel Line 4	Wheel Line 5
Girder 1	**.362**	.187	-.014	-.043	-.026
Girder 2	.280	**.317**	.214	.035	-.003
Girder 3	.115	.213	**.359**	.231	.104
Girder 4	-.018	.001	.113	.329	**.332**
Girder 5	-.028	-.038	-.036	.080	**.244**
Deck	.289	.320	.363	.367	.351

Table 5-12 Total Moment Distribution Factors for the Negative Moment Region at 316 Inches

The data in Table 5-12 is analogous to the single-lane moment distribution factors specified in the AASHTO LRFD code, because the data represents the behavior of the bridge under the weight of one vehicle. However, the Big Creek Relief Bridge was load rated for two design lanes, because the roadway was 30 feet wide. The data from Table 5-12 was used to create two-lane moment distribution factors for the bridge, by combining the effect of different wheel lines through linear interpolation. This procedure is explained in detail in the Appendix.

Table 5-13 presents the two-lane moment distribution factors for the bridge. The trucks' positions in each of the design lanes are also presented. The largest two-lane moment distribution factor was 0.511 for girder 3, and the smallest was 0.244 for girder 5. In general, the moment distribution factors decreased as the truck was positioned closer to the exterior girders. Because of the reverse flexure in the farthest three girders when the truck was on wheel lines 1 and 5, the two-lane moment distribution factors for girders 1 and 5 are the same as the single-lane moment distribution factors.

	Truck 1	Truck 2	Two Lane Moment Distribution Factor
Girder 1	100% Wheel Line 1	69% Wheel Line 3* 31% Wheel Line 4*	**.362**
Girder 2	43% Wheel Line 1 57% Wheel Line 2	69% Wheel Line 3 31% Wheel Line 4	**.460**
Girder 3	54% Wheel Line 2 46% Wheel Line 3	100% Wheel Line 4	**.511**
Girder 4	31% Wheel Line 2 69% Wheel Line 3	100% Wheel Line 5	**.411**
Girder 5	31% Wheel Line 2* 69% Wheel Line 3*	100% Wheel Line 5	**.244**

* Not considered because of a negative contribution due to reverse flexure

Table 5-13 Two-Lane Moment Distribution Factors for the Negative Moment Region at 316 Inches

The values in Table 5-13 were used to reevaluate the load rating of the bridge, because they represent the actual moment distribution behavior near bearing 2 under an applied negative moment. They are analogous to the AASHTO LRFD two-lane moment distribution factors for negative flexure at bearings 2 and 4. The reevaluation of the bridge's load rating is presented in Chapter 6.

Figures showing the position of the trucks used to determine the two-lane moment distribution factors are shown in Section 5.3.3, below. To avoid repetition, the figures are not shown here, because, coincidentally, the positions of the trucks were the same for the positive moment and negative moment regions.

5.3.3 Summary of Total Moment Distribution

Table 5-14 presents a summary of the single-lane moment distribution factors and two-lane moment distribution factors, determined through field testing. In the exterior girders, the moment distribution factors in the positive moment region were larger than the moment distribution factors in the negative moment region. However, in

the interior girders, the moment distribution factors in the negative moment region were larger than the moment distribution factors in the positive moment region.

Moment Distribution Factors	Single-Lane Positive Moment	Two-Lane Positive Moment	Single-Lane Negative Moment	Two-Lane Negative Moment
Girder 1	.487	.539	.362	.362
Girder 2	.276	.426	.317	.460
Girder 3	.316	.460	.359	.511
Girder 4	.286	.388	.332	.411
Girder 5	.267	.279	.244	.244

Table 5-14 Summary of the Moment Distribution Factors Determined Through Field Testing

The position of the trucks used to determine the two-lane moment distribution factors for both the positive moment and negative moment regions are shown in Figures 5-61, 5-62, 5-63, and 5-64. The figures show the positions of both trucks, relative to the nearest curb face, and the portions of the deck allocated to each design lane. Because of the soft response of girder 5, the maximum moment distribution factors for girders 4 and 5 both occurred with the trucks in the same positions. It is a coincidence of the test data that the truck positions corresponding to the maximum two-lane moment distribution factor for each girder were the same for the positive and negative moment regions. Also, it is a coincidence of the test data that the maximum moment distribution factor for girder 3 occurred with one truck exactly on wheel line 4.

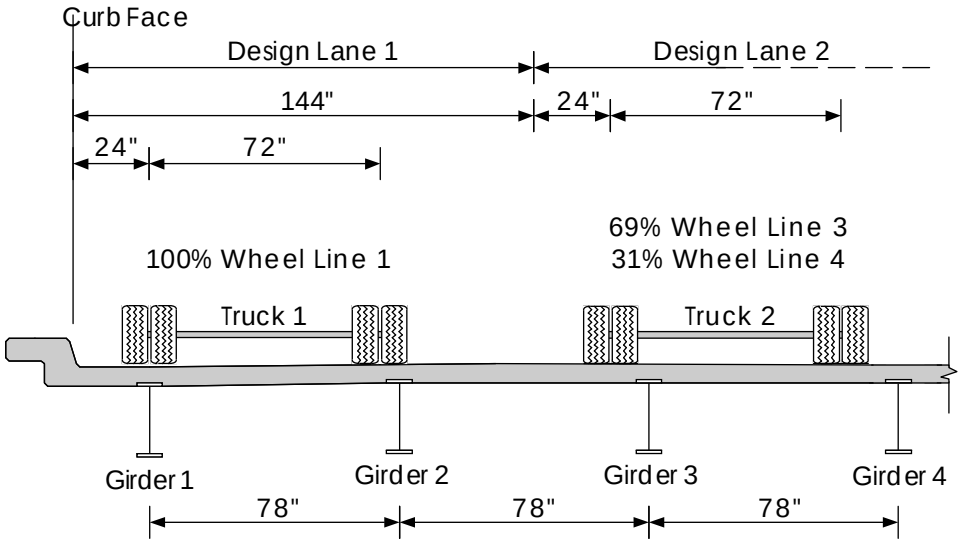

Figure 5-61 Truck Positions Used to Determine the Two-Lane Moment Distribution Factor for Girder 1

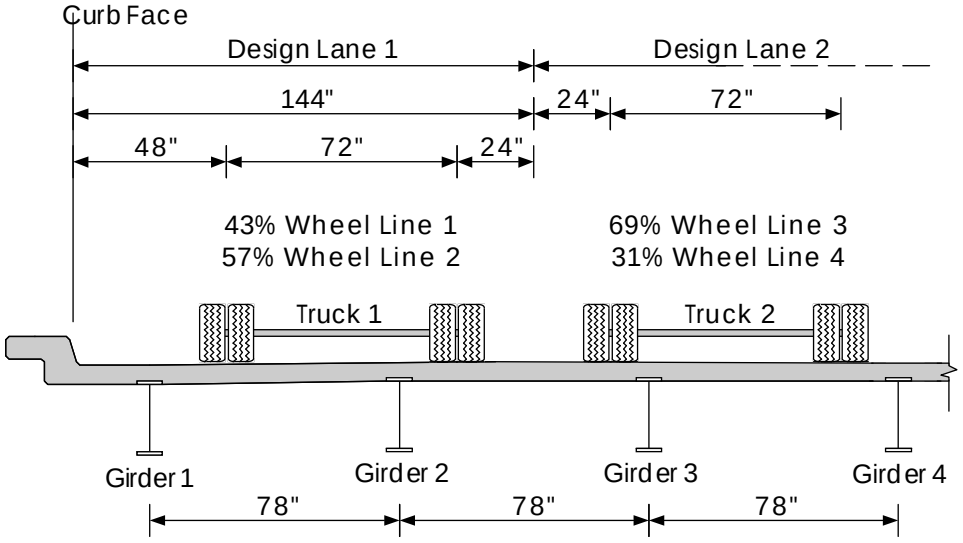

Figure 5-62 Truck Positions Used to Determine the Two-Lane Moment Distribution Factor for Girder 2

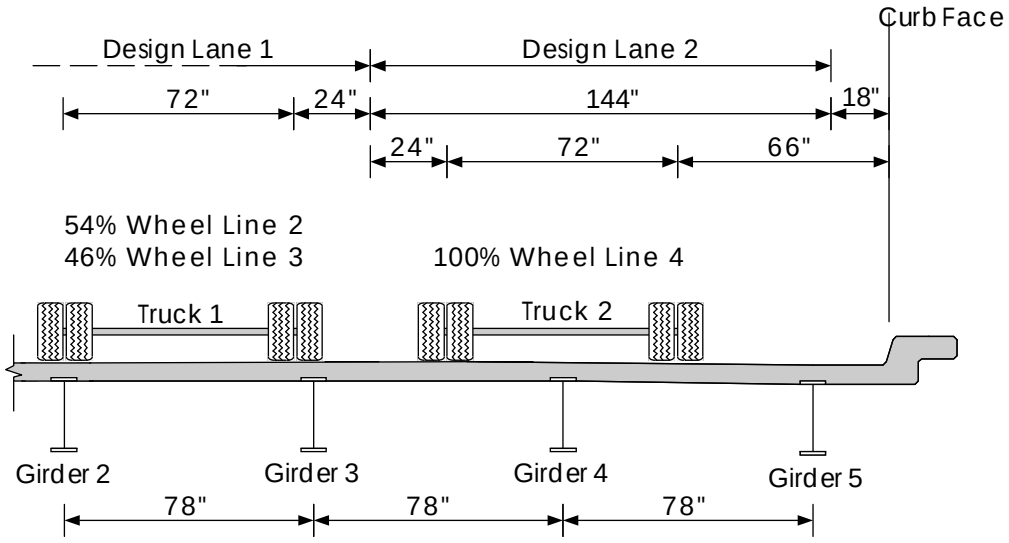

Figure 5-63 Truck Positions Used to Determine the Two-Lane Moment Distribution Factor for Girder 3

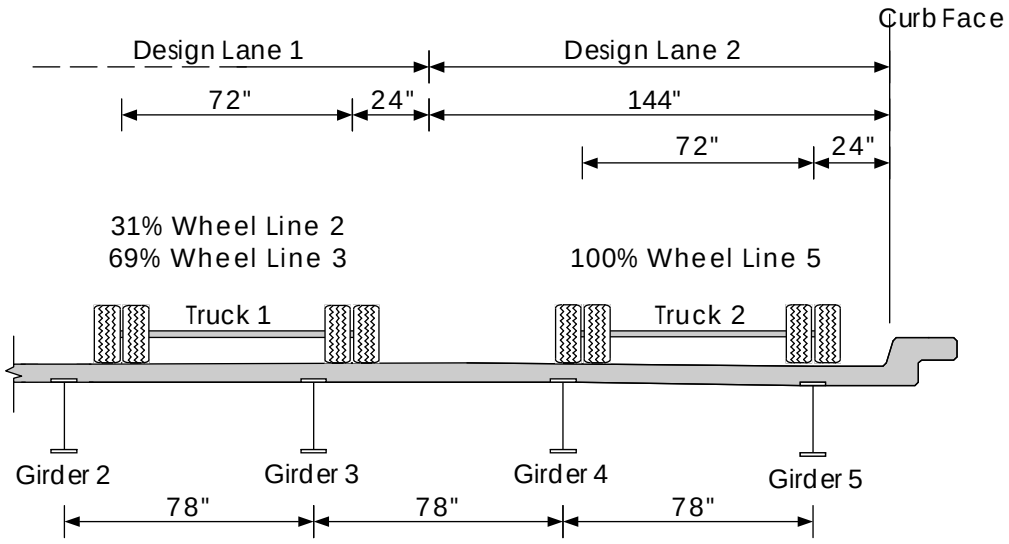

Figure 5-64 Truck Positions Used to Determine the Two-Lane Moment Distribution Factors for Girders 4 and 5

The results of the field tests were compared to the values provided by the AASHTO LRFD code. The field test single-lane moment distribution factors for positive moment and negative moment in all five girders are shown in Tables 5-15 and 5-16, respectively. The corresponding AASHTO LRFD single-lane moment distribution factors for positive moment and negative moment are also provided, along with the ratios of the field test values to the AASHTO LRFD values.

	Field Test Single-Lane MDF's	AASHTO LRFD Single-Lane MDF's	Ratio of Field Test to AASHTO
Girder 1	.487	.538	.905
Girder 2	.276	.403	.685
Girder 3	.316	.403	.784
Girder 4	.286	.403	.710
Girder 5	.267	.538	.496

Table 5-15 Comparison of Field Test Single-Lane Total Moment Distribution Factors and AASHTO LRFD Single-Lane Moment Distribution Factors for the Positive Moment Region

	Field Test Single-Lane MDF's	AASHTO LRFD Single-Lane MDF's	Ratio of Field Test to AASHTO
Girder 1	.362	.538	.673
Girder 2	.317	.422	.751
Girder 3	.359	.422	.851
Girder 4	.332	.422	.787
Girder 5	.244	.538	.454

Table 5-16 Comparison of Field Test Single-Lane Total Moment Distribution Factors and AASHTO LRFD Single-Lane Moment Distribution Factors for the Negative Moment Region

Tables 5-15 and 5-16 show that, in all cases, the moment distribution factors determined by field testing were lower than the AASHTO LRFD single-lane moment distribution factors. In the positive moment region, the moment distribution factors for girder 1 showed the least variation. The field test result was 0.905 times the AASHTO value. In the negative moment region, girder 3 showed the least variation. The field test result was 0.851 times the AASHTO value. In both the positive and negative moment regions, girder 5 showed the most variation. The field test results were 0.496 and 0.454 times the AASHTO values for the positive moment and negative moment regions, respectively.

The field test two-lane moment distribution factors for positive moment and negative moment in all five girders are shown in Tables 5-17 and 5-18, respectively. The corresponding AASHTO LRFD two-lane moment distribution factors for positive moment and negative moment are also provided, along with the ratios of the field test values to the AASHTO LRFD values.

	Field Test Two-Lane MDF's	**AASHTO LRFD Two-Lane MDF's**	**Ratio of Field Test to AASHTO**
Girder 1	**.539**	.608	.887
Girder 2	**.426**	.615	.693
Girder 3	**.460**	.615	.748
Girder 4	**.388**	.615	.631
Girder 5	**.279**	.608	.459

Table 5-17 Comparison of Field Test Two-Lane Moment Distribution Factors and AASHTO LRFD Two-Lane Moment Distribution Factors for the Positive Moment Region

	Field Test Two-Lane MDF's	AASHTO LRFD Two-Lane MDF's	Ratio of Field Test to AASHTO
Girder 1	**.362**	.630	.575
Girder 2	**.460**	.637	.722
Girder 3	**.511**	.637	.802
Girder 4	**.411**	.637	.645
Girder 5	**.244**	.630	.387

Table 5-18 Comparison of Field Test Two-Lane Moment Distribution Factors and AASHTO LRFD Two-Lane Moment Distribution Factors for the Positive Moment Region

Tables 5-17 and 5-18 show that, in all cases, the two-lane moment distribution factors determined by field testing were lower than the AASHTO LRFD two-lane moment distribution factors. In the positive moment region, the moment distribution factors for girder 1 showed the least variation. The field test result was 0.887 times the AASHTO value. In the negative moment region, girder 3 showed the least variation. The field test result was 0.802 times the AASHTO value. In both the positive and negative moment regions, girder 5 showed the most variation. The field test results were 0.459 and 0.387 times the AASHTO values for the positive moment and negative moment regions, respectively.

5.4 Strain Transducer Feasibility Study

Five removable strain transducers were placed on the bridge. The output of the transducers was examined to determine each transducer's ability to replicate the data recorded by nearby strain gages. A description of the removable strain transducers, including their placement and specifications, is presented in Chapter 4. The data recorded by the transducers was processed is a similar manner as the data from the foil gages. A description of the numerical methods used to process the foil gage strain data is presented in the Appendix.

The transducers were located on the top surface of the bottom flange of each girder, in the positive moment region at 908 inches. The transducer positions were labeled T1 through T5 and were located on girders 1 through 5, respectively. The output from the transducers was compared to the output from strain gages SB1 through SB5, respectively.

Figures 5-65, 5-66, 5-67, 5-68, and 5-69 are plots of stress vs. truck position for the transducers and foil gages on girders 1 through 5, respectively. In each plot the test truck was positioned on the wheel line closest to the girder, except for Figure 5-69 where the truck was positioned on wheel line 4.

In each figure, the output from the transducer closely resembled the output from the strain gage. The closest agreement was seen on girder 4, where the two influence lines are practically on top of each other. The worst agreement was seen on girder 1.

Figure 5-70 is a bar graph showing the ratio of transducer output to strain gage output for each girder. The ratios are compared to an ideal ratio of 1.00, where the transducer's output is exactly equal to the strain gage's output. The data from Figures 5-65 through 5-69 was used to determine the ratios shown in Figure 5-70, by calculating the average ratio for all of the data recorded when the strain in the strain gage was greater than 1.5 ksi. The rest of the strain data was not considered, to reduce the errors introduced by electronic noise in the data acquisition system.

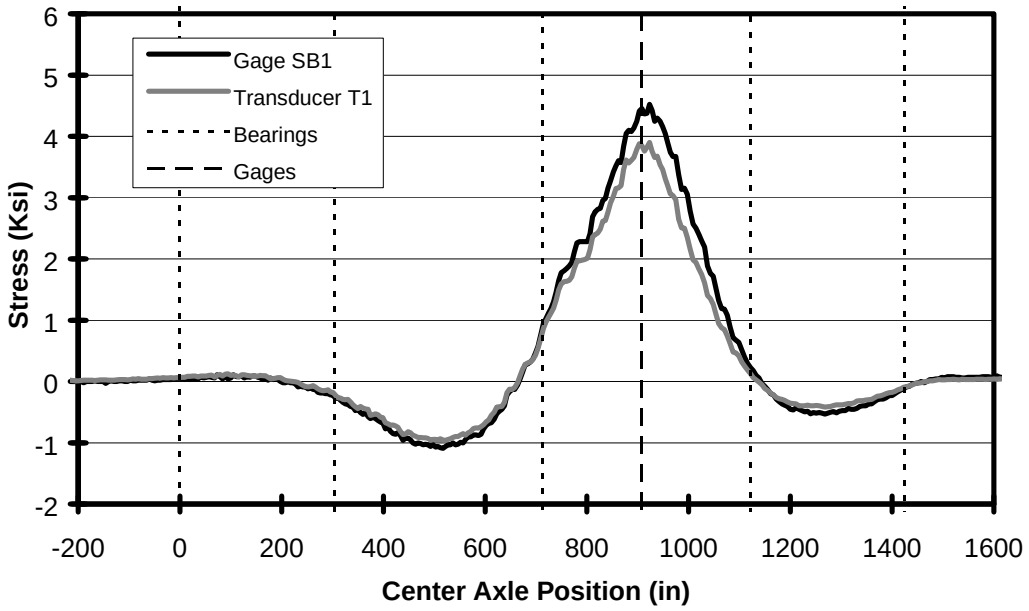

Figure 5-65 Stress Influence Lines for Girder 1, Wheel Line 1

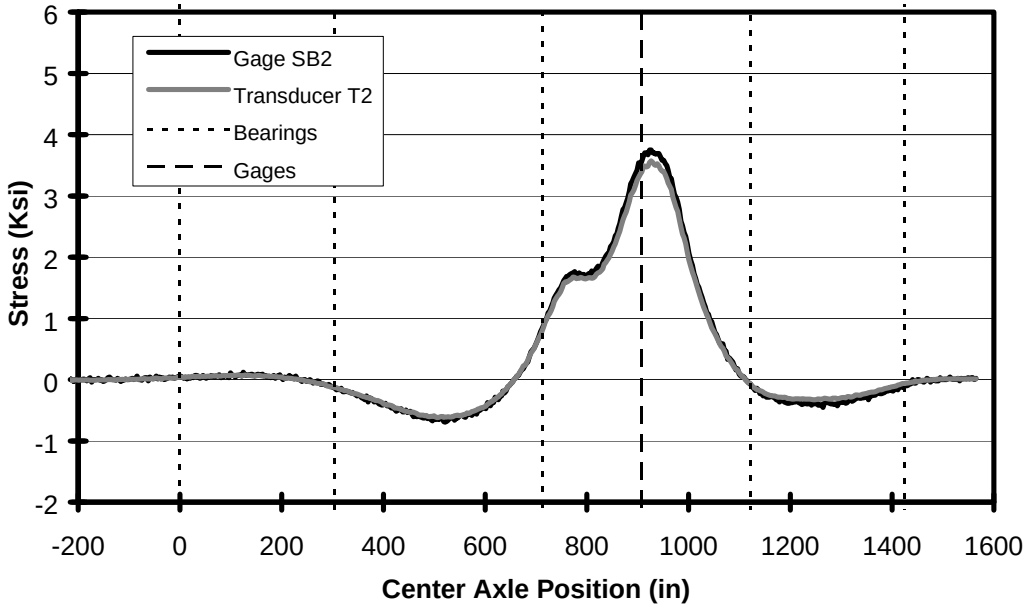

Figure 5-66 Stress Influence Lines for Girder 2, Wheel Line 2

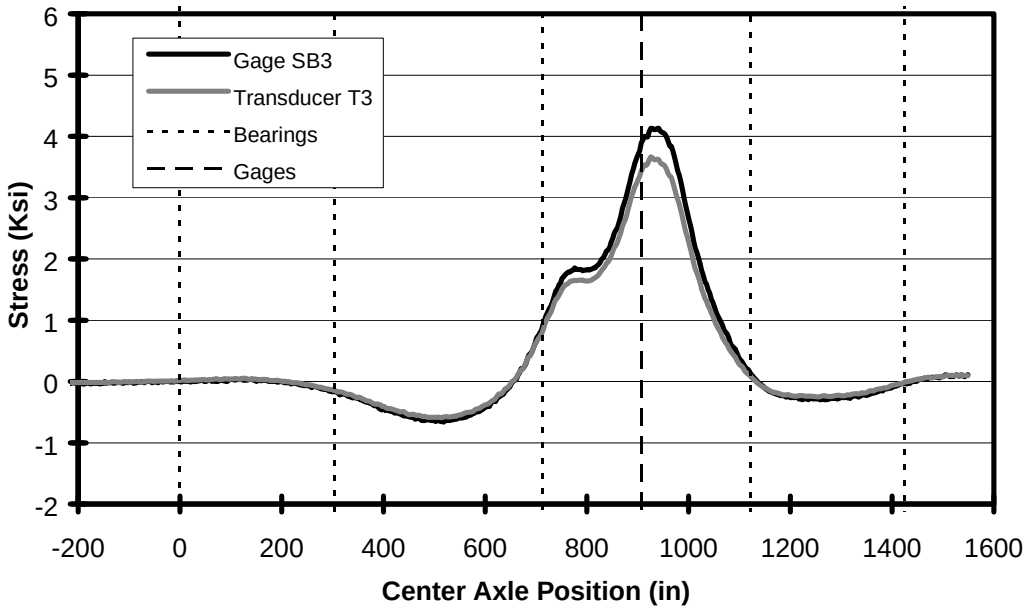

Figure 5-67 Stress Influence Lines for Girder 3, Wheel Line 3

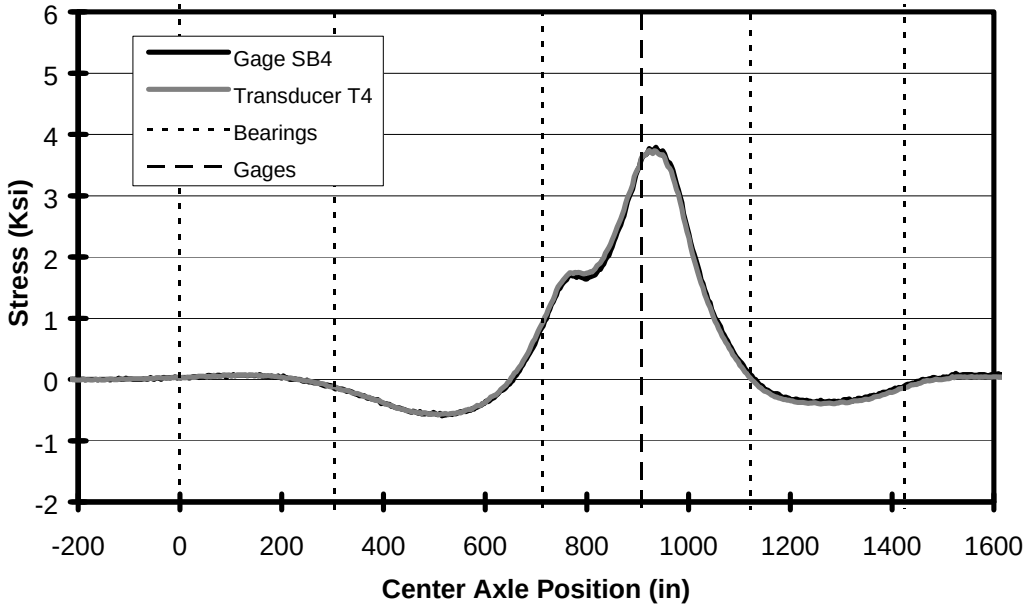

Figure 5-68 Stress Influence Lines for Girder 4, Wheel Line 4

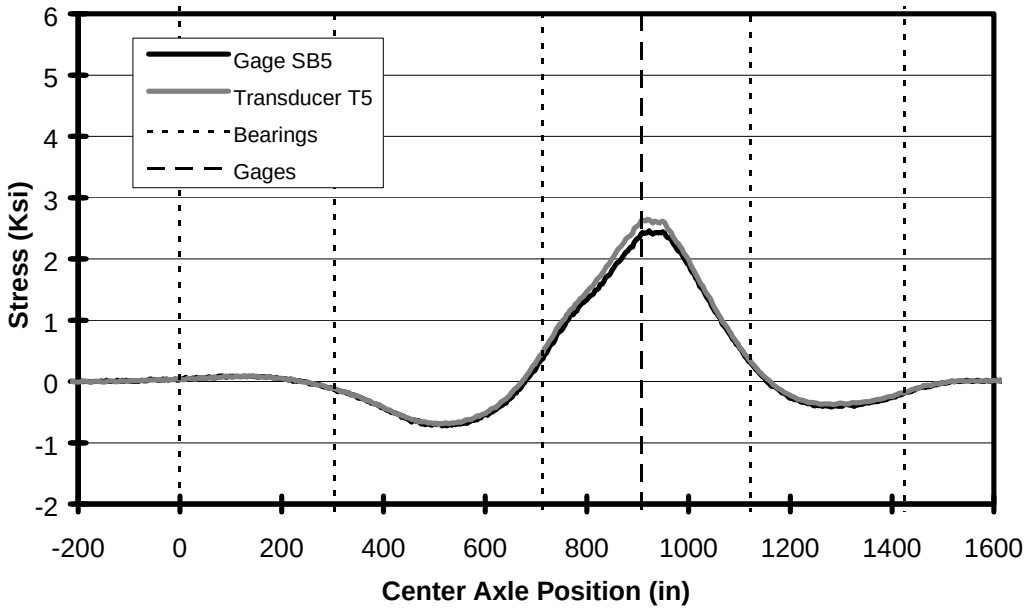

Figure 5-69 Stress Influence Lines for Girder 5, Wheel Line 4

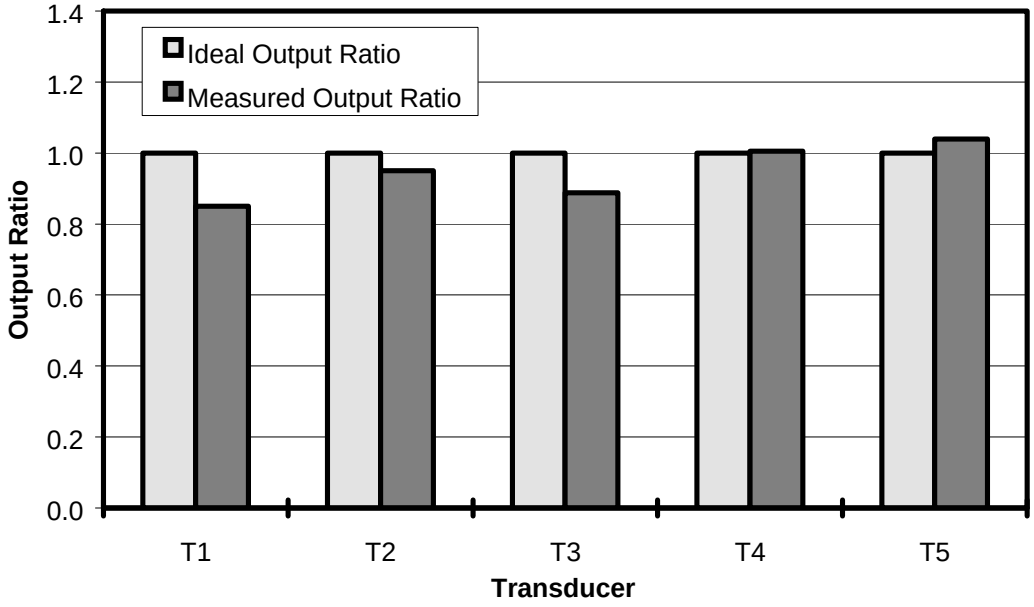

Figure 5-70 Ratio of Transducer Output to Strain Gage Output for Each of the Transducers

Figure 5-70 shows that the ability of the transducers to replicate the strain gage data varied from transducer to transducer. Transducer T4 performed the best, with a ratio of 1.01. Transducer T1 performed the worst, with a ratio of 0.85. The performance of each of the transducers is summarized in Table 5-19.

Transducer	Output Ratio: Transducer / Strain Gage	Error, as Percent of Strain Gage
T1	0.85	-15%
T2	0.95	-5%
T3	0.89	-11%
T4	1.01	1%
T5	1.04	4%

Table 5-19 Transducer Output Ratios and Errors

Several factors contributed to the varying degrees of accuracy in each of the transducers. First, the transducers were located on the opposite side of the web from the strain gages. Differences in the thickness and width of each half of the lower flange could have produced a slightly biaxial moment in the cross section, because the cross section was not perfectly symmetrical in both directions. Second, improper handling and installation of the transducers could have placed enough stress on the delicate center section of the transducers to affect the calibration factors. Finally, the calibration procedure may not be representative of the field conditions, since the calibration was performed in the lab using a tensile coupon, not a flexural member.

In Figures 5-65 through 5-69, the transducer's output appears to be a scaled version of the strain gage's output. Therefore, slip at the interface of the transducer and the girder was not a likely source of error. If the transducer was slipping, then the results would have shown less agreement as the truck moved across the bridge, rather than less agreement as the level of stress increased.

In summary, the transducer output was as precise as the strain gage output, but not very accurate. Each of the transducers displayed varying levels of error, when compared to the output from the strain gages. If the transducer data had been used in place of the strain gage data, the errors would have affected many of the calculations performed on the test data, especially the neutral axis offset and moment distribution calculations. Therefore, the removable strain transducers used in this study were not sufficient for field testing and load rating the bridge.

However, the transducer output was sufficient to determine the amplitude of stress applied to the bridge and was able to reproduce the shape of the stress influence line. Therefore, the transducers may be useful for applications such as fatigue analysis, where stress cycles and amplitudes and counted, but not for diagnostic load testing.

CHAPTER 6
Revised Load Rating

In Chapter 3, a preliminary load rating of the Big Creek Relief Bridge was presented. This analysis showed that the bridge had a deficient AASHTO LFD inventory rating, and a barely acceptable AASHTO LFD operating rating, controlled by negative moment at bearings 2 and 4 on the interior girders. To understand better the behavior of the bridge and improve its inventory and operating ratings, field tests were performed. The results of the field tests were presented in Chapter 5.

In this chapter, the results of the field tests are used to revise the inventory and operating ratings of the bridge. The capacity of girder 1 is recalculated, to account for the composite behavior recorded during the field tests. Also, the revised moment distribution behavior of the bridge and the noncomposite flexural participation of the deck are used to recalculate the live load moments applied to the bridge.

The revised load rating calculations assume that the load test vehicle produced moments in the superstructure that approximated the moment envelope for the HS-20 rating vehicle. However, the 10 cubic yard truck's moment envelope was not as large as the HS-20 rating vehicle's. Therefore the behavior of the bridge may have differed from its behavior under the HS-20 loading. In section 6.2, the limits of extrapolating the test data are discussed.

6.1 Revised HS-20 LFD Load Rating

The AASHTO LFD load rating of the five girders on the Big Creek Relief Bridge was revised to reflect the results of the field tests. New operating and inventory ratings were calculated using Equation 6-1, a revised version of the AASHTO LFD rating equation.

$$RF' = \frac{C' - A_1 \cdot D}{A_2 \cdot L'_{DF+I}} \qquad (6\text{-}1)$$

where

RF′ is the revised AASHTO LRFD rating factor,

C' is the revised capacity of the girder, in kip∿inches,

D is the dead load moment in the girder, in kip∿inches,

L'_{DF+I} is the revised live load moment in the girder, including the effects of lateral moment distribution and impact, in kip∿inches,

A_1 is the LFD rating coefficient for dead load, 1.3 for both inventory and operating ratings, and

A_2 is the LFD rating coefficient for live load, 1.3 for operating rating and 2.17 for inventory rating.

Equation 6-1 is the same as Equation 3-1 in Chapter 3, except that the capacity, live load plus impact, and rating factor are revised to reflect the results of the load tests. The dead load moment remains unchanged, as do the rating coefficients. As with the initial rating calculations, rating factors less than one indicate that the bridge is not capable of safely supporting the rating vehicle's load.

6.1.1 Revised Dead Load

The dead loads used during the initial load rating remained unchanged in the revised load rating. The various components of the superstructure were measured and inspected prior to the initial load rating, and no further information about the dead load moments was determined during the field tests. Table 6-1 shows a summary of the dead load moments used in the initial and revised rating calculations.

Case	Dead Load Moment (kip∿inches)
Positive Moment on Spans 2 and 3	431
Negative Moment at Bearing 3	-869
Negative Moment at Bearings 2 and 4	-767

Table 6-1 Dead Load Moments Used for the Initial and Revised Rating

6.1.2 Revised Live Load

In the initial load rating, the live load moments in the bridge were determined by calculating a moment envelope for the HS-20 vehicle and then scaling the moment envelope by the appropriate AASHTO LRFD two-lane lateral moment distribution factor. The maximum live load positive and negative moments in the envelope were then used to rate the bridge.

During the field tests, the actual two-lane moment distribution factors for each girder were determined. The revised maximum live load positive and negative moments in each girder were then calculated using Equation 6-2

$$M' = M \cdot \frac{MDF'}{MDF} \tag{6-2}$$

where

M′ is the revised maximum moment, used in the revised load rating,

M is the initial maximum moment, used in the initial load rating,

MDF′ is the revised two-lane lateral moment distribution factor, determined through field testing, and

MDF is the initial two-lane lateral moment distribution factor, determined using the provisions of the AASHTO LRFD code.

Tables 6-2, 6-3, and 6-4 present the initial and revised moments and lateral moment distribution factors for spans 2 and 3, bearings 2 and 4, and bearing 3, respectively. For bearing 3, the revised lateral moment distribution factors for bearings 2 and 4 were used, because no data was collected at bearing 3 during the load tests.

	Initial Two-Lane MDF's	Revised Two-Lane MDF's	Initial Max. Moment (kip-inches)	Revised Max. Moment (kip-inches)
Girder 1	.608	.539	2043	**1812**
Girder 2	.615	.426	2067	1432
Girder 3	.615	.460	2067	**1546**
Girder 4	.615	.388	2067	1304
Girder 5	.608	.279	2043	938

Table 6-2 Initial and Revised Moment Distribution Factors and Maximum Moments for Positive Moment on Spans 2 and 3

In Table 6-2, the controlling live load positive moments are 1812 kip-inches in girder 1 and 1546 kip-inches in girder 3. Both values were considered, because girder 1 behaved compositely in the positive moment region while the other four girders behaved noncompositely. These two moments were used in the revised load rating calculations.

	Initial Two-Lane MDF's	Revised Two-Lane MDF's	Initial Max. Moment (kip-inches)	Revised Max. Moment (kip-inches)
Girder 1	.630	.362	-1841	-1058
Girder 2	.637	.460	-1861	-1344
Girder 3	.637	.511	-1861	**-1493**
Girder 4	.637	.411	-1861	-1201
Girder 5	.630	.244	-1841	-713

Table 6-3 Initial and Revised Moment Distribution Factors and Maximum Moments for Negative Moment at Bearings 2 and 4

In Table 6-3, the controlling live load negative moment is -1493 kip-inches in girder 3. This moment was used in the revised load rating calculations.

	Initial Two-Lane MDF's	Revised Two-Lane MDF's	Initial Max. Moment (kip-inches)	Revised Max. Moment (kip-inches)
Girder 1	.608	.362	-1879	-1119
Girder 2	.615	.460	-1901	-1422
Girder 3	.615	.511	-1901	**-1580**
Girder 4	.615	.411	-1901	-1270
Girder 5	.608	.244	-1879	-754

Table 6-4 Initial and Revised Moment Distribution Factors and Maximum Moments for Negative Moment at Bearing 3

In Table 6-4, the controlling live load negative moment is -1580 kip-inches in girder 3. This moment was used in the revised load rating calculations.

6.1.3 Revised Capacity

In the initial load rating, the capacity of the girders was found to be the yield moment, for both positive moment and negative moment. The lateral bracing of the girders was insufficient to develop the full plastic moment. Since all of the girders were composed of the same steel section and were designed to behave in a noncomposite manner, the capacity of each girder was the same. However, the field tests indicated that girder 1 was behaving compositely in the positive moment region of spans 2 and 3. Therefore, girder 1 had a larger capacity than the value used in the initial load rating.

The revised positive moment capacity of girder 1 was taken as the yield moment of the composite section. The lack of shear connectors on the Big Creek Relief Bridge was ignored. Normally, in composite design, shear connectors are required to "lock" the girder and the deck together and allow for the transfer of shear across the deck-girder interface. Because a mechanical shear connection was not present, the composite behavior in girder 1 was most likely due to bonding between the steel and the concrete. Unfortunately, the strength of the bond could not be determined from the results of the field test. In order to proceed with the revised rating calculations, it was assumed that the

girder would behave compositely up to the onset of yield at the outer fiber of the composite section. The validity of this assumption is discussed in section 6.2.

The yield moment of girder 1 was defined as the moment causing first yield of the composite girder at the top of the deck or at the bottom of the steel girder. The yield moment was determined using Equation 6-3, the following equation:

$$M_n = F_y \cdot S \qquad (6\text{-}3)$$

where

M_n is the yield moment capacity of the composite girder, in kip∽inches,

F_y is the yield strength of the steel or concrete, in ksi, and

S is the elastic section modulus of the girder, in inches^3.

However, the section moduli for the top and bottom fibers of the composite girder needed to be calculated before Equation 6-3 could be used.

Figure 6-1 shows a diagram of the transformed section of the composite girder. Through field testing, the location of the composite girder's neutral axis was determined to be 9.36 inches above the center of gravity of the steel girder. The effective width of the transformed slab, b_t, was determined by calculating the effective width that resulted in a neutral axis offset of 9.36 inches.

Table 6-5 shows the dimensions, areas, centroidal offsets, first moments, second moments, and moments of inertia for the components of the composite girder. In the table, the center of gravity of the steel girder was used as a baseline. Because the transformed section of the deck was modeled as a rectangle, the top flange of the girder overlapped with the deck material. This overlap is accounted for in the table, and subtracted out.

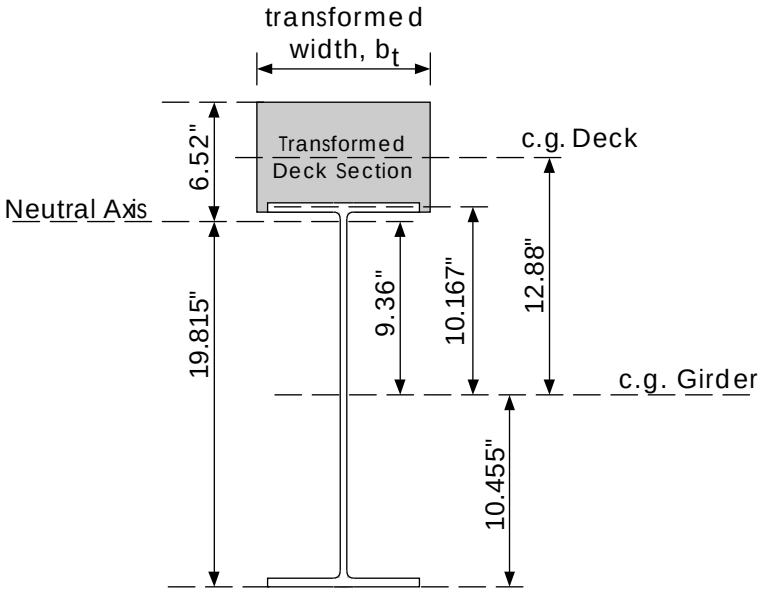

Figure 6-1 Transformed Cross Section of the Composite Girder

	Height (in)	Width (in)	Area, A (in^2)	Offset, y (in)	Ay (in^3)	Ay^2 (in^4)	I_o (in^4)
Slab	6.0	b_t	$6 b_t$	12.88	$77.28 b_t$	$995.4 b_t$	$18 b_t$
Girder	---	---	17.36	0	0	0	1246.8
Overlap	-0.575	0.809	-0.465	10.17	-4.73	-48.09	-0.01
Total	---	---	$6 b_t$ +16.90	---	$77.28 b_t$ -4.73	$995.4 b_t$ -48.09	$18 b_t$ +1246.8

Table 6-5 Dimensions, Areas, Centroidal Offsets, First Moments, Second Moments, and Moments of Inertia for the Various Components of the Composite Girder

In Table 6-5, the width of the overlap section was determined by calculating the transformed width of the flange-filled void in the concrete deck. The yield strength of the steel girder was 30 ksi., and the modulus of the steel was 29,000 ksi. These values were determined through material tests of the bridge, as described in Chapter 2. The compressive strength of the concrete was assumed to be 2.5 ksi., based on the age of the bridge. The elastic modulus of the concrete was determined using Equation 6-4, the following equation:

$$E_c = 57\sqrt{f'_c} \tag{6-4}$$

where

E_c is the elastic modulus of the concrete, in ksi., and

f'_c is the compressive strength of the concrete, in psi.

The elastic modulus of the concrete deck was determined as follows:

$$E_c = 57\sqrt{2500} = 2850 \text{ ksi.}$$

The width of the overlap section was determined using Equation 6-5, the following equation:

$$b_{overlap} = b_f \cdot \frac{E_c}{E_s} \tag{6-5}$$

where

$b_{overlap}$ is the width of the overlap section, in inches,

b_f is the flange width, in inches, and

E_s is the elastic modulus of the steel, in ksi.

The overlap width was determined as follows:

$$b_{overlap} = 8.23 \cdot \frac{2850}{29{,}000} = 0.809 \text{ inches}$$

Equation 6-6 shows the relationship between the composite section's neutral axis offset and its total area and total first moment.

$$\bar{y} = \frac{Ay}{A} \qquad (6\text{-}6)$$

where

$\bar{y}$ is the neutral axis offset, in inches,

Ay is the total first moment of the cross section, and

A is the total area of the cross section.

During the field tests, the neutral axis offset was determined to be 9.36 inches. The data from Table 6-5 and Equation 6-6 were used to solve for b_t, as follows:

$$9.36 = \frac{77.28 \cdot b_t - 4.73}{6 \cdot b_t + 16.90} \Rightarrow b_t = 7.71$$

The moment of inertia of the composite section about the center of gravity of the steel girder was calculated using Equation 6-7, the following equation:

$$I_s = I_o + Ay^2 \qquad (6\text{-}7)$$

where

I_s is the moment of inertia of the composite section about the center of gravity of the steel girder, in inches^4,

I_o is the total moment of inertia of each of the components of the composite section about their own centers of gravity, in inches^4, and

Ay^2 is the total second moment of each of the components of the composite section about the center of gravity of the steel girder, in inches^4.

Using the values from Table 6-5, and substituting 7.71 inches for b_t, the moment of inertia of the composite section about the center of gravity of the steel section was determined as follows:

$$I_s = (18 \cdot 7.71 + 1246.8) + (995.4 \cdot 7.71 - 48.09) = 9012 \text{ inches}^4$$

The moment of inertia of the composite section about the composite neutral axis was found using Equation 6-8, the following equation:

$$I_c = I_s - A\bar{y}^2 \tag{6-8}$$

where

I_c is the moment of inertia of the composite section about the composite neutral axis, in inches^4, and

$A\bar{y}^2$ is the second moment of the composite section about the neutral axis offset, in inches^4.

Using the results from Equations 6-6 and 6-7, the moment of inertia of the composite section about the composite neutral axis was determined as follows:

$$I_c = 9012 - (6 \cdot 7.71 + 16.90) \cdot 9.36^2 = 3479 \text{ inches}^4$$

The composite moment of inertia was used to determine the section moduli for the top of the deck and the bottom of the girder, using Equations 6-9 and 6-10, the following equations:

$$S_c^{top} = \frac{I_c}{y_c^{top}} \tag{6-9}$$

$$S_c^{bot} = \frac{I_c}{y_c^{bot}} \tag{6-10}$$

where

S_c^{top} is the section modulus for the top fiber of the composite girder, in inches^3,

S_c^{bot} is the section modulus for the bottom fiber of the composite girder, in inches^3,

y_c^{top} is the distance from the composite neutral axis to the top of the deck, in inches, and

y_c^{bot} is the distance from the composite neutral axis to the bottom of the girder, in inches.

The values of S_c^{top} and S_c^{bot} were determined as follows:

$$S_c^{top} = \frac{3479}{6.52} = 534 \text{ inches}^3$$

$$S_c^{bot} = \frac{3479}{19.815} = 176 \text{ inches}^3$$

Finally, the yield moment was determined by calculating the moment causing yield in the top of the deck and the moment causing yield in the bottom of the girder using Equation 6-3, above, as follows:

$$M_n^{deck} = \frac{29{,}000}{2850} \cdot 2.5 \cdot 534 = 13{,}584 \text{ kip} \cdot \text{inches}$$

$$M_n^{girder} = 33 \cdot 176 = 5284 \text{ kip} \cdot \text{inches}$$

The yield moment capacity of the composite girder was controlled by yielding of the steel girder at the bottom flange. The moment capacity of 5284 kip-inches was used for girder 1 in the revised load rating calculations.

Table 6-6 presents a summary of the girder capacities for each girder, for positive moment on spans 2 and 3, negative moment at bearing 3, and negative moment at bearings 2 and 4. Except for girder 1 in the positive moment region, the capacities are the same as in the initial load rating.

Moment Capacity (kip-inches)	Positive Moment on Spans 2 and 3	Negative Moment at Bearing 3	Negative Moment at Bearings 2 and 4
Girder 1	5284	-4587	-3578
Girders 2, 3, 4, and 5	3578	-4587	-3578

Table 6-6 Moment Capacities Used for the Revised Load Rating

6.1.4 Revised Load Rating Calculations

Revised inventory and operating ratings were determined using equation 6-1, above, for positive moment on spans 2 and 3, negative moment at bearing 3, and negative moment at bearings 2 and 4. The overall lowest revised rating factor was taken as the revised rating factor for the bridge. Table 6-7 shows the live load moment, dead load moment, and capacity used to determine the revised rating factor for each possible case. The four cases shown in bold, positive moment on spans 2 and 3 of girder 1, positive moment on spans 2 and 3 of girder 3, negative moment at bearing 3 of girder 3, and negative moment at bearings 2 and 4 of girder 3 are the four most critical cases.

Case	Yield Moment Capacity (kip-inches)	Dead Load Moment (kip-inches)	Live Load Moment (kip-inches)
	Girder 1		
+M, Spans 2 and 3	**5284**	**431**	**1812**
-M, Bearing 3	-4587	-869	-1119
-M, Bearings 2 and 4	-3578	-767	-1058
	Girder 2		
+M, Spans 2 and 3	3578	431	1432
-M, Bearing 3	-4587	-869	-1422
-M, Bearings 2 and 4	-3578	-767	-1344
	Girder 3		
+M, Spans 2 and 3	**3578**	**431**	**1546**
-M, Bearing 3	**-4587**	**-869**	**-1580**
-M, Bearings 2 and 4	**-3578**	**-767**	**-1493**
	Girder 4		
+M, Spans 2 and 3	3578	431	1304
-M, Bearing 3	-4587	-869	-1270
-M, Bearings 2 and 4	-3578	-767	-1201
	Girder 5		
+M, Spans 2 and 3	3578	431	938
-M, Bearing 3	-4587	-869	-754
-M, Bearings 2 and 4	-3578	-767	-713

Table 6-7 Yield Moment Capacity, Dead Load Moment, and Live Load Moment for Every Girder and Each Load Case

The four critical load cases from Table 6-7 were evaluated using Equation 6-1. However, for positive moment in spans 2 and 3 on girder 1, Equation 6-1 was modified to reflect the order in which loads were placed on the bridge. The dead load was applied to girder 1 during construction, when only the steel girder was available to resist the dead load, but the live load was applied when the whole composite section was available to resist the applied load. Therefore, Equation 6-11, the following equation, was used to determine the revised rating factor for positive moment on spans 2 and 3 for girder 1. The section moduli for the bottom fiber of the girder are used in this equation, because the yield capacity of the composite section is controlled by yielding of the bottom flange of the girder.

$$RF' = \frac{C' - A_1 \cdot D \cdot \frac{S_c^{bot}}{S_g^{bot}}}{A_2 \cdot L'_{DF+I}} \qquad (6\text{-}11)$$

where

RF' is the revised AASHTO LRFD rating factor,

C' is the revised capacity of the girder, in kip∿inches,

D is the dead load moment in the girder, in kip∿inches,

L'_{DF+I} is the revised live load moment in the girder, including the effects of lateral moment distribution and impact, in kip∿inches,

S_c^{bot} is the section modulus for the bottom fiber of the composite girder, in inches^3,

S_g^{bot} is the section modulus for the bottom fiber of the steel girder alone, in inches^3,

A_1 is the LFD rating coefficient for dead load, 1.3 for both inventory and operating ratings, and

A_2 is the LFD rating coefficient for live load, 1.3 for operating rating and 2.17 for inventory rating.

The section modulus for the bottom fiber of the steel girder alone was found using Equation 6-12, the following equation:

$$S_g^{bot} = \frac{I_g}{y_g^{bot}} \qquad (6\text{-}12)$$

where

y_g^{bot} is the distance from the composite neutral axis to the top of the deck, in inches, and

I_g is the moment of inertia of the steel girder alone, in inches^4.

For a moment of inertia of 1246.8 inches^4 and an arm of 10.455 inches, the section modulus for the bottom fiber of the steel girder alone was determined as follows:

$$S_g^{bot} = \frac{1246.8}{10.455} = 119 \text{ inches}^3$$

Using Equation 6-11, the revised inventory and operating ratings for positive moment on spans 2 and 3 of girder 1 were determined as follows:

$$RF' = \frac{(5284) - 1.3 \cdot (431) \cdot \left(\frac{176}{119}\right)}{2.17 \cdot (1812)} = 1.133 \qquad \text{inventory rating factor}$$

$$RF' = \frac{(5284) - 1.3 \cdot (431) \cdot \left(\frac{176}{119}\right)}{1.3 \cdot (1812)} = 1.891 \qquad \text{operating rating factor}$$

Using Equation 6-1, the revised inventory and operating ratings for positive moment on spans 2 and 3 of girder 3 were determined as follows:

$$RF' = \frac{(3578) - 1.3 \cdot (431)}{2.17 \cdot (1546)} = 0.900 \qquad \text{inventory rating factor}$$

$$RF' = \frac{(3578) - 1.3 \cdot (431)}{1.3 \cdot (1546)} = 1.501 \qquad \text{operating rating factor}$$

The inventory and operating ratings for negative moment at bearing 3 of girder 3 were determined as follows:

$$RF' = \frac{(-4587) - 1.3 \cdot (-869)}{2.17 \cdot (-1580)} = 1.008 \qquad \text{inventory rating factor}$$

$$RF' = \frac{(-4587) - 1.3 \cdot (-869)}{1.3 \cdot (-1580)} = 1.683 \qquad \text{operating rating factor}$$

The inventory and operating ratings for negative moment at bearings 2 and 4 of girder 3 were determined as follows:

$$RF' = \frac{(-3578) - 1.3 \cdot (-767)}{2.17 \cdot (-1493)} = 0.797 \qquad \text{inventory rating factor}$$

$$RF' = \frac{(-35787) - 1.3 \cdot (-767)}{1.3 \cdot (-1493)} = 1.330 \qquad \text{operating rating factor}$$

The revised HS-20 load rating of the Big Creek Relief Bridge was controlled by negative moment at bearings 2 and 4 on girder 3. This was the same location that controlled the initial load rating. Table 6-8 presents a summary of the HS-20 ratings for the bridge.

	Initial Rating Factor	**Initial HS-20 Rating**	**Revised Rating Factor**	**Revised HS-20 Rating**	**Ratio of Revised / Initial**
Inventory Level	0.639	HS-12.8	0.797	HS-15.9	1.25
Operating Level	1.067	HS-21.3	1.330	HS-26.6	1.25

Table 6-8 Initial and Revised LFD Load Ratings of the Big Creek Relief Bridge, Controlled by Negative Moment at Bearings 2 and 4 on Girder 3

Bridge ratings are often expressed as a multiple of the rating vehicle's designation. Since the revised inventory rating factor was for the bridge was 0.797 and

the HS-20 vehicle was used to apply the live load, the bridge had a HS-15.9 revised inventory rating. Similarly the revised operating rating for the bridge was HS-26.6.

The revised inventory rating factor of 0.797 indicated that the bridge could not carry traffic loads equivalent to the HS-20 vehicle for an indefinite period of time, and the revised operating rating factor of 1.330 suggested that HS-20 loads would be permissible on a limited-use basis, only.

Although the inventory rating factor remained below one, the ratio of the revised rating factor to the initial rating factor shows that field testing can lead to a significant level of improvement in the bridge's load rating. In this case, the load rating of the Big Creek Relief Bridge was improved by a factor of 1.25.

6.2 Reliability and the Limits of Extrapolation

The 10 cubic yard truck, used in the field tests, did not produce moments as large as the theoretical HS-20 rating vehicle. Therefore, the results of the revised load rating rely on the assumption that the behavior of the bridge under the test truck's load can be extrapolated to the level of load applied by the HS-20 vehicle. In this section, the reliability of the extrapolation is discussed, as it pertains to unintended composite action, increased load distribution, and noncomposite flexure of the deck.

6.2.1 Unintended Composite Action

In composite construction, the girders and the deck of the bridge are "locked" together using shear studs, or other mechanical means, allowing for the transfer of shear forces along the deck-girder interface. However, the load tests showed that girder 1 was behaving in a composite manner even though there were no shear studs present. Because the deck was cast in place, the composite behavior was probably due to bond between the steel girder and the concrete deck.

The strength of the steel-concrete bond could not be determined from the load test data. Furthermore, the steel-concrete bond was likely to release suddenly when the bond strength was exceeded, leading to sudden failure of the composite behavior of the girder and a sudden drop in the girder's capacity. Therefore, the reliability of the

moment capacity of girder 1 was highly suspect when live load moments greater than the moment applied by the 10 c.y. truck were applied to the girder.

The reliability of the revised load rating calculations was investigated by comparing the moments produced by the 10 c.y. truck and the HS-20 rating vehicle. Also, the horizontal shear forces at the deck-girder interface for the 10 c.y. and HS-20 vehicles were calculated. These shear forces were compared with the bond strength required to allow the composite section to develop the yield moment used in the revised load rating.

6.2.1.1 Moment Comparison

The live load moment applied by the 10 c.y. test vehicle was less than the HS-20 rating live load moment for two reasons. First, the 10 c.y. vehicle's axle weights and spacing produced smaller moments. Second, the load rating calculations were performed for two design lanes, with an HS-20 vehicle in each lane, but only one 10 c.y. truck was ever placed on the bridge during field testing.

In the revised load rating, the live load moment applied by the HS-20 vehicle was 1812 kip∽inches, as shown in Table 6-7, above. However, in Chapter 5, it was shown that the maximum live load moment measured in girder 1 was 1117 kip∽inches, only 0.62 times the revised rating moment.

The difference between the rating live load moment and the applied live load moment is substantial. Based on this comparison, it would be advisable to re-test the bridge using a heavier vehicle. To that end, girder 1 is a perfect candidate for proof testing. The ability of the girder to carry the HS-20 load could be proven by placing incrementally larger vehicle loads on the bridge until the full HS-20 load was applied. Unfortunately a proof test was beyond the scope and means of this study.

6.2.1.2 Horizontal Shear Comparison

The load test data was insufficient to determine the bond strength between the steel girder and the concrete deck. However, the horizontal shear stress at the deck-girder interface was calculated for the live load applied by the 10 c.y. and HS-20 trucks.

The bond strength required to reach the yield strength of the composite section was also determined, for comparison.

The neutral axis of the composite girder is located just below the bottom surface of the top flange of the steel girder. Therefore, when the composite girder is loaded with a positive moment, the concrete deck is placed in compression, and the majority of the steel girder is placed in tension. Figure 6-2 shows a free body diagram of a section of the transformed composite girder. The transformed section is used so that the deck and the girder have the same modulus of elasticity. The left side of the free body diagram is a cut through the location of maximum live load moment. The linear distribution of stress and the resultant tensile and compressive forces are shown. The right side of the free body diagram is a cut through the nearest inflection point. By definition, there are no normal forces due to flexure at the inflection point, so the stress block and resultant forces are equal to zero at this end. The shear forces at the deck-girder interface are also shown in the figure.

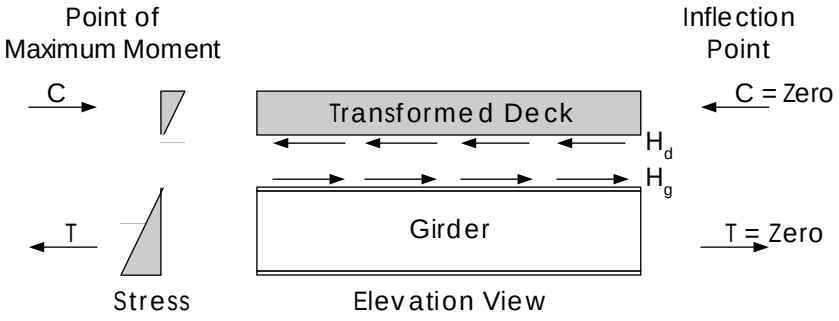

Figure 6-2 Free Body Diagram of the Transformed Composite Girder

Figure 6-2 shows that the compressive force in the deck, C, the shear force along the underside of the deck, H_d, the shear force along the top face of the girder, H_g, and the tensile force in the girder, T, are equal in magnitude. Therefore, the shear force along the deck-girder interface can be calculated by determining the compressive force in the deck, using stress blocks, as shown in Equation 6-13, the following equation:

$$H = C = \frac{\sigma_{top} + \sigma_{bot}}{2} \cdot b_t \cdot t \qquad (6\text{-}13)$$

where

H is the horizontal shear force along the deck-girder interface, in kips,

C is the compressive force in the deck, in kips,

σ_{top} is the transformed stress at the top of the deck section, in ksi.,

σ_{bot} is the transformed stress at the bottom of the deck section, in ksi.,

b_t is the transformed effective width of the deck section, in inches, and

t is the thickness of the deck section, in inches.

The transformed effective width of the deck was 7.71 inches, as determined above. The thickness of the deck section was 5.425 inches. The stress at the top of the deck section was calculated by dividing the maximum moment by the composite section modulus (534 inches^3, as determined above). Since the neutral axis location is known, the stress at the bottom of the deck section was calculated from the stress at the top of the deck, using the stress distribution diagram and similar triangles. The distance from the composite neutral axis to the top of the deck was 6.52 inches and the distance from the composite neutral axis to the bottom of the deck section was 1.095 inches.

For the 10 c.y. truck, the maximum moment in girder 1 was 1117 kip~inches. Using Equation 6-13, the horizontal shear force at the deck-girder interface was found as follows:

$$H = C = \frac{\left(\frac{1117}{534}\right) + \left(\frac{1.095}{6.52} \cdot \frac{1117}{534}\right)}{2} \cdot 7.71 \cdot 5.425 = 51 \text{ kips}$$

Similarly, for the HS-20 truck, the maximum moment in girder 1 was 1812 kip~inches. Using Equation 6-13, the horizontal shear force at the deck-girder interface was found as follows:

$$H = C = \frac{\left(\frac{1812}{534}\right) + \left(\frac{1.095}{6.52} \cdot \frac{1812}{534}\right)}{2} \cdot 7.71 \cdot 5.425 = 83 \text{ kips}$$

As with the maximum moments, the horizontal shear force due to the 10 c.y. truck was only 0.62 times the horizontal shear force due to the HS-20 vehicle.

The horizontal shear stress at the deck-girder interface was determined by dividing the horizontal shear force by the area of the contact surface at the deck-girder interface, as shown in Equation 6-14, the following equation:

$$\tau = \frac{H}{b_f \cdot L_{pos}} \tag{6-14}$$

where

τ is the horizontal shear stress at the deck-girder interface, in ksi.,

b_f is the width of the top flange of the steel girder, in inches, and

L_{pos} is the length of the positive moment region of the composite girder, in inches.

In the positive moment region of spans 2 and 3, the positive moment region usually occupied about 80 percent of the 34 foot span length. Therefore, the horizontal shear stresses for the 10 c.y. truck and HS-20 truck were determined, respectively, as follows:

$$\tau = \frac{51}{8.23 \cdot (34 \cdot 12 \cdot 0.8)} = 0.019 \text{ ksi} \qquad \text{10 c.y. truck}$$

$$\tau = \frac{83}{8.23 \cdot (34 \cdot 12 \cdot 0.8)} = 0.031 \text{ ksi} \qquad \text{HS-20 truck}$$

As with the maximum moments and horizontal shear forces, the horizontal shear stress due to the 10 c.y. truck was only 0.62 times the horizontal shear force due to the HS-20 vehicle. The ratios are the same, because it was assumed that there was no slip along the girder-deck interface and that the composite section behaved in a linear elastic manner.

In the revised load rating, the capacity of girder 1 was assumed to be the yield capacity of the composite section. In section 6.1, above, the yield moment capacity was found to be 5284 kip-inches. Equation 6-13 was used to determine the horizontal

shear force capacity required to develop the yield moment in the composite section, as follows:

$$H = C = \frac{\left(\frac{5284}{534}\right) + \left(\frac{1.095}{6.52} \cdot \frac{5284}{534}\right)}{2} \cdot 7.71 \cdot 5.425 = 242 \text{ kips}$$

The bond shear strength required to develop the yield moment in the composite section was then calculated using Equation 6-14, as follows:

$$\tau = \frac{242}{8.23 \cdot (34 \cdot 12 \cdot 0.8)} = 0.090 \text{ ksi}$$

For comparison, the ratio of the 10 c.y. applied horizontal shear stress to the horizontal shear stress capacity was 0.21 (= 0.019 / 0.090). Therefore, there was no reason to assume that girder 1 would be able to develop the composite yield moment, used in the revised load rating, because the 10 c.y. truck did not apply a comparable level of shear to the deck-girder interface.

Since the load test results were inadequate for confirming the yield moment capacity of girder 1, used in the revised load rating, alternate means of calculating the moment capacity of girder 1 were investigated. A brief literature review on the topic of steel-concrete bond strength turned up one reference. A research study by Rabbat and Russell (1984) showed that the push-off shear strength due to bonding between a steel plate and a cast-in-place concrete block ranged from 0.025 ksi to 0.089 ksi., just less than the shear capacity of 0.090 ksi. required to develop the yield moment. Table 6-9 shows a summary of the horizontal shear stresses and bond strengths calculated in this section.

Case	Horizontal Shear (ksi.)
Applied Live Load Shear, 10 c.y. Load Test	0.019
Applied Live Load Shear, HS-20 Revised Load Rating	0.031

Assumed Shear Capacity, Revised Load Rating	0.090
Reasonable Shear Capacity, Rabbat and Russell (1984)	0.025 to 0.089

Table 6-9 Review of Horizontal Shear Stresses and Bond Strengths for the Deck-Girder Interface

Although the results of Rabbat and Russell's study suggest that the assumed shear capacity of 0.090 ksi. is too large, girder 1 may still be able to develop the yield moment, for two reasons. First, the top flange of the girder is embedded in the deck, not just flush with it, providing additional surface area and confinement. Second, the dead load of the concrete deck, wearing surface, and railings provides a normal force at the deck-girder interface to help confine the bond surface. Therefore, the shear strength in girder 1 may be greater than the range provided by Rabbat and Russell (1984).

Nevertheless, the large shear strength required to develop the yield moment in girder 1 affects the reliability of the revised load rating calculations. Fortunately, the rating of the bridge was controlled by negative moment at bearings 2 and 4, and not by positive moment in spans 2 and 3 of girder 1, so the exact moment capacity of girder 1 did not need to be determined. In order for the positive moment in spans 2 and 3 of girder 1 to avoid control of the load rating, the capacity of the composite girder would have to be at least 3963 kip-inches. This moment capacity corresponds with a required bond strength of 0.067 ksi., well within the range suggested by Rabbat and Russell (1984).

Rather than trying to calculate the moment capacity of girder 1, the solution to the problem is proof testing. If a live load moment of 3963 kip-inches was actually applied to girder 1, with no loss of composite behavior, it would prove that the moment capacity of girder 1 does not control the load rating of the bridge. However, the danger of proof testing is that the heavy load may break the steel-concrete bond on girder 1. In this case, girder 1 will behave noncompositely, just like the other four girders. The loss of composite behavior on girder 1 would significantly change the bridge's lateral

moment distribution behavior as well as the level of noncomposite flexural participation in the deck. As a result, a new round of diagnostic load testing would be required for the bridge.

Rabbat and Russell's results also show why girder 1 was able to behave compositely during the load tests. The maximum horizontal shear caused by the 10 c.y. truck was 0.019 ksi., significantly less than the minimum push-off bond strength of 0.025 ksi. Perhaps all of the girders on the Big Creek Relief Bridge used to behave compositely, at one time, but the stress of heavy vehicle loads broke the bond between the steel and the concrete on girders 2 through 5 long before the load testing began.

6.2.2 Increased Moment Distribution

The field test data was not sufficient to determine whether the lateral moment distribution behavior of the Big Creek Relief Bridge was dependent on the weight of the test vehicle. In order to determine a relationship between lateral moment distribution and vehicle weight, the bridge would have to be load tested using another vehicle, either heavier or lighter than the first.

In lieu of additional testing, the provisions of the AASHTO LRFD (1994) code were considered, since these provisions were derived for numerous research projects and load tests. Although they account for many structural variables, such as girder spacing and stiffness, the AASHTO LRFD moment distribution equations do not include a term for the weight of the vehicle. This suggests that vehicle weight does not affect the load distribution behavior of the bridge, at least for the range of vehicle weights commonly used in design and load rating.

In the positive moment region, however, the unintended composite behavior in girder 1 influenced the lateral moment distribution behavior of the Big Creek Relief Bridge, because the additional stiffness of girder 1 allowed it to carry significantly more moment than the other girders. If the composite behavior of girder 1 was lost, by breaking the bond between the girder and the deck, the moment distribution behavior of the whole bridge would change. The moment distribution factor for girder 1 would decrease, and the moment distribution factors for the other girders would increase,

especially the factor for girder 2. Therefore, the weight of the test vehicle could influence the moment distribution behavior of the bridge, indirectly, by damaging girder 1.

As mentioned in the previous section, proof testing of girder 1 is the surest method for determining the reliability of the moment distribution behavior of the bridge. Until then, the moment distribution factors, as determined through load testing, were assumed to be reliable, as long as girder 1 continued to behave in a composite manner.

In the negative moment regions, all of the girders behaved in a noncomposite manner. Therefore, the lateral moment distribution factors, as determined through field testing, were likely to be reliable at higher levels of load.

6.2.3 Noncomposite Flexure of the Deck

The results of the load test showed that the deck was carrying a significant portion of the applied moment, through noncomposite flexure. In the positive moment region of span 3, the noncomposite deck moment was as large as 1060 kip⌒inches, 30.4 percent of the moment applied by the 10 c.y. truck. In the negative moment region at bearing 2, the noncomposite deck moment was as large as -625 kip⌒inches, 36.3 percent of the applied moment. Because the moments in the deck were so large, the noncomposite portions of the deck were considered to be a major source of strength in the bridge.

The reliability of the noncomposite flexure of the deck was investigated by determining the moments produced by the HS-20 vehicle and comparing them with the moments produced by the 10 c.y. truck and with the ultimate capacity of the deck. The moment and capacity calculations are shown in the following sections.

In the positive moment region, the amount of noncomposite flexure in the deck is dependent on the composite behavior of girder 1. If the bond between girder 1 and the deck is broken, more of the deck will be available to resist the noncomposite moment. However, the portion of the moment carried by the deck will increase, as well, since girder 1 will lose stiffness. Therefore, if the bond on girder 1 is broken, the bridge will need to be load tested again to reevaluate the noncomposite flexural behavior of the deck.

Once again, proof testing of girder 1 is the best way to determine if the bridge's behavior can be extrapolated to the HS-20 vehicle's load.

6.2.3.1 HS-20 Noncomposite Deck Moment

In Chapter 5, the single-vehicle moment distribution factors for each girder and wheel line were combined to determine a set of two-design-lane moment distribution factors for each girder. This procedure was repeated for the moments in the deck. Table 6-10 shows the maximum moment distribution factors in the deck for each wheel line, for both the positive and negative moment regions.

	Wheel Line 1	Wheel Line 2	Wheel Line 3	Wheel Line 4	Wheel Line 5
Deck, Positive Moment Region	.195	.195	.245	.298	.304
Deck, Negative Moment Region	.289	.320	.363	.367	.351

Table 6-10 Moment Distribution Factors for the Noncomposite Portion of the Deck

The moment distribution factors from Table 6-10 were combined, as shown in Table 6-11, to determine the two-lane moment distribution factors for the deck.

	Truck 1	Truck 2	Two-Lane MDF
Deck, Positive Moment Region	31% Wheel Line 2 69% Wheel Line 3	100% Wheel Line 5	**0.534**
Deck, Negative Moment Region	31% Wheel Line 2 69% Wheel Line 3	57% Wheel Line 4 43% Wheel Line 5	**0.710**

Table 6-11 Two-Lane Moment Distribution Factors for the Noncomposite Portion of the Deck

In Chapter 3, the maximum live load positive moment in spans 2 and 3, applied by the HS-20 vehicle, was found to be 2532 kip∽inches. The maximum live load negative moment at bearing 3 was -2324 kip∽inches, and the maximum live load negative moment at bearings 2 and 4 was -2196 kip∽inches. In addition, the AASHTO dynamic load impact factor for the bridge was taken as 1.33.

The maximum moments in the deck were determined by multiplying the HS-20 maximum moments by the two-lane moment distribution factors and by the impact factor. The results of this calculation are shown in Table 6-12, along with the maximum moments produced by the 10 c.y. truck.

Case	10 c.y. Applied Moment (kip∽inches)	HS-20 Rating Moment (kip∽inches)	Ratio of 10 c.y. to HS-20
Positive Moment, Spans 2 and 3	1060	1798	0.590
Negative Moment, Bearing 3	-589*	-2195	0.268
Negative Moment, Bearings 2 and 4	-625	-2074	0.301

* Scaled from negative moment at bearings 2 and 4, using Chapter 3 data.

Table 6-12 Maximum Live Load Moments in the Noncomposite Portion of the Deck

Table 6-12 shows that the moments applied by the HS-20 vehicle are significantly larger that the moments applied by the 10 c.y. truck. However, the noncomposite behavior of the deck, as determined through field testing, is likely to remain the same at the HS-20 load, as long as girder 1 continues to behave compositely.

6.2.3.2 Noncomposite Deck Capacity

The moment capacity of the noncomposite portion of the deck was checked to see if the deck was able to support the moment applied by the HS-20 vehicle. Two assumptions were made to simplify the calculations. In the negative moment region, the

entire 30 foot width of the deck was modeled as a single flexural member. In the positive moment region, where girder 1 was behaving compositely, 80 percent of the deck was assumed to participate in noncomposite flexure. The moment contribution of the curbs was neglected.

The main reinforcement in the deck was placed in a transverse direction to the flow of traffic. This reinforcement was detailed in Chapter 2. In addition, longitudinal reinforcement was provided in the deck. This reinforcement, running parallel to the girders, helped to resist the moments applied to the deck through noncomposite flexure. Figure 6-3 shows a detail of the secondary, longitudinal, reinforcement in the deck.

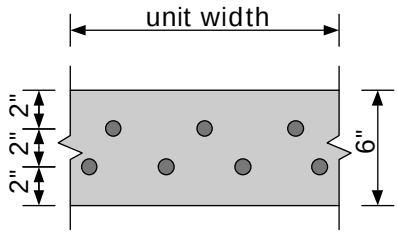

Figure 6-3 Cross Section of Longitudinal Reinforcement in the Deck

All of the longitudinal reinforcement is #5 rebar. The yield strength was assumed to be 40 ksi., as specified in the AASHTO Manual (1994b). As stated above, the compressive strength of the concrete was assumed to be 2500 psi.

In the 30-foot-wide section of the deck, there were 19 #5 bars in the top layer and 28 #5 bars in the bottom layer. A plastic analysis of the deck showed that, for both positive and negative flexure, the neutral axis was located 0.896 inches in from the extreme compressive fiber, and that all of the steel in both layers yielded in tension. The moment capacity of the 30-foot-wide negative moment region was found to be -1415 kip~inches. The moment capacity of the 24-foot-wide positive moment region (80 percent of the full width) was found to be 1310 kip~inches. Table 6-13 shows a comparison of the moment capacity of the noncomposite portion of the deck with the moments applied by the HS-20 rating vehicle.

Case	Moment Capacity (kip-inches)	HS-20 Rating Moment (kip-inches)	Ratio of Capacity to HS-20
Positive Moment, Spans 2 and 3	1310	1798	0.729
Negative Moment, Bearing 3	-1415	-2195	0.645
Negative Moment, Bearings 2 and 4	-1415	-2074	0.682

Table 6-13 Maximum Live Load Moments in the Noncomposite Portion of the Deck

Table 6-13 shows that the deck is not capable of supporting the moment applied by the HS-20 vehicle. Therefore, the behavior of the Big Creek Relief Bridge, under the HS-20 load is likely to differ from the behavior measured during field testing. The percentage of the applied moment carried by the deck is likely to drop, as the deck deforms under the weight of the HS-20 vehicle. At the same time, the percentage of the applied moment carried by each girder is likely to increase. Therefore, further diagnostic testing, with a heavier vehicle, is required to determine the percentage of the live load moment carried by noncomposite flexure of the deck at the HS-20 load.

6.3 Symmetrical Load Rating for the Positive Moment Region of Span 3

The field test results and the revised load rating calculations showed that the bridge behaved in a very unsymmetrical manner in the positive moment region of span 3. In particular, girder 1 behaved compositely, while the other 4 girders behaved noncompositely. As a result, the lateral moment distribution behavior of the bridge was skewed, with girder 1 carrying a disproportionately large portion of the applied moment.

If the composite bond on girder 1 were to brake, the lateral moment distribution behavior of the bridge would change, subsequently effecting the load rating of the bridge. This situation was investigated by recalculating the single-lane and two-lane lateral moment distribution factors, and the load rating, for positive moment on span 3.

Table 6-14 shows a summary of the single-lane lateral moment distribution factors for the positive moment regions of span 3, assuming symmetrical behavior. The factors shown in bold, mostly on wheel lines 4 and 5, were recorded during the field tests. The other factors are mirrored from the data for wheel lines 3, 4, and 5. The factors for the deck were determined by assuming that the factors for each wheel line add up to 1.00.

Symmetrical MDF's	Wheel Line 1	Wheel Line 2	Wheel Line 3	Wheel Line 4	Wheel Line 5
Girder 1	.267	.146	.017	**-.011**	**-.017**
Girder 2	.286	.285	.135	**.060**	**.019**
Girder 3	.141	.221	**.316**	**.221**	**.141**
Girder 4	.019	.060	**.135**	**.285**	**.286**
Girder 5	-.017	-.011	**.017**	**.146**	**.267**
Deck	.304	.298	.380	**.298**	**.304**

Table 6-14 Single-Lane Lateral Moment Distribution Factors for the Symmetrical Case for Positive Moment on Span 3

The single-lane lateral moment distribution factors from Table 6-14 were combined to produce two-lane lateral moment distribution factors. The results of this procedure are shown in Table 6-15. The maximum two-lane moment distribution factor was 0.486 for girder 3. This value was used to calculate the symmetrical load rating for positive moment on span 3.

	Truck 1	Truck 2	Two-Lane Moment Distribution Factor
Girder 1	100% Wheel Line 1	69% Wheel Line 3 31% Wheel Line 4*	**.279**
Girder 2	100% Wheel Line 1	69% Wheel Line 3 31% Wheel Line 4	**.398**
Girder 3	77% Wheel Line 2 23% Wheel Line 3	23% Wheel Line 3 77% Wheel Line 4	**.486**
Girder 4	31% Wheel Line 2 69% Wheel Line 3	100% Wheel Line 5	**.398**
Girder 5	31% Wheel Line 2* 69% Wheel Line 3	100% Wheel Line 5	**.279**

* Not considered because of a negative contribution due to reverse flexure

Table 6-15 Two-Lane Moment Distribution Factors for the Positive Moment Region of Span 3, Assuming Symmetrical Behavior

The live load positive moment for the symmetrical load rating was calculated using Equation 6-2, shown above. For an initial-rating live load moment of 2067 kip∽inches and an initial lateral moment distribution factor of 0.615, the live load positive moment was calculated as follows:

$$2067 \cdot \frac{0.486}{0.615} = 1633 \text{ kip} \cdot \text{inches}$$

The dead load moment of 431 kip∽inches from the initial and revised load ratings was also used in the symmetrical load rating. Furthermore, the noncomposite yield moment capacity of 3578 kip∽inches was used. Table 6-16 presents a summary of the moments used in the symmetrical load rating. These values represent the most critical load case for the symmetrical load rating for span 3.

Case	Yield Moment Capacity (kip-inches)	Dead Load Moment (kip-inches)	Live Load Moment (kip-inches)
Positive Moment on Girder 3, Span 3	3578	431	1633

Table 6-16 Yield Moment Capacity, Dead Load Moment, and Live Load Moment Assuming Symmetrical Behavior

Using Equation 6-1, shown above, the symmetrical inventory and operating ratings for positive moment on spans 2 and 3 were determined as follows:

$$RF' = \frac{(3578) - 1.3 \cdot (431)}{2.17 \cdot (1633)} = 0.852 \qquad \text{inventory rating factor}$$

$$RF' = \frac{(3578) - 1.3 \cdot (431)}{1.3 \cdot (1633)} = 1.389 \qquad \text{operating rating factor}$$

Table 6-17 presents a comparison of the revised and symmetrical load ratings for positive moment in girder 3. The results suggest that the loss of composite behavior in girder 1 would result in a reduction in the load rating for girder 3, by a factor of 0.947. However, the load rating of the bridge is still controlled by negative moment at bearings 2 and 4 of girder 3, where the revised inventory-level load rating factor is 0.797, as shown in section 6.1.

	Revised Rating Factor for Girder 3	Symmetrical Rating Factor for Girder 3	Ratio of Symmetrical / Revised
Inventory Level	0.900	0.852	0.947
Operating Level	1.501	1.389	0.947

Table 6-17 Comparison of the Revised and Symmetrical Load Ratings for Positive Moment in Girder 3

The symmetrical rating factors represent a more pessimistic evaluation of the behavior of span 3, since they were calculated under the assumption that the composite behavior of girder 1 is only temporary. However, the symmetrical rating factors may be a more accurate assessment of the behavior of span 2, since no instrumentation was placed in the positive moment region of span 2 and it is possible that girder 1 only behaved compositely on span 3.

The symmetrical load rating was determined by making some rather general assumptions about the bridge's behavior, and therefore should be taken lightly. For example, in Table 6-14 the factors for girders 2 and 4 for wheel line 3 seem to be too low. This is reflected in the unusually high lateral moment distribution factor for the deck for wheel line 3. In addition, in Table 6-15 the two-lane factors for girders 2 and 4 are significantly lower than the two-lane factor for girder 3. The actual two-lane lateral moment distribution factors for these girders are probably closer in value, and the symmetrical load rating for span 3 is probably closer to the revised load rating than Table 6-17 suggests. At any rate, the results of the symmetrical load rating suggest that the loss of composite behavior in girder 1 has a moderate effect on the load rating of span 3, since the load rating only changed by a factor of 0.947.

6.4 Summary of the Revised Load Rating

The results of the field test with the 10 c.y. truck were used to reevaluate the load rating of the Big Creek Relief Bridge. As a result, the bridge's operating and inventory ratings improved by a factor of 1.25. However, the unintended composite behavior of girder 1 in the positive moment region and the deficient noncomposite moment capacity of the deck indicated that the behavior of the bridge at the HS-20 load would differ from the behavior that was measured during the field tests. Therefore, the bridge needs to be retested with a vehicle heavier than the 10 c.y. truck, in order for the results of the revised load rating to be considered reliable.

CHAPTER 7
Conclusions

The field test of the Big Creek Relief Bridge was a success. The instrumentation used during the field test was found to be capable of diagnosing the presence of unintended composite behavior in the girders, improved lateral moment distribution in the superstructure, and noncomposite flexure in the deck. Analysis of these behaviors resulted in an improvement in the bridge's AASHTO LFD load rating, by a factor of 1.25. This improved load rating was not a surprise, since many previous research studies have shown that field testing can lead to an improvement in the bridge's load rating, or at least to a better understanding of the bridge's structural deficiencies.

Furthermore, the test procedure was found to be reliable. Multiple passes on the same wheel line produced virtually identical results. In addition, the use of three foil gages on each girder's cross section highlighted the varying reliability of the neutral axis calculations, because the results from separate gage pairs showed favorable agreement when the strains in the gages were large and wild disagreement when the strains in the gages were small.

However, analysis of the test data showed that the weight of the test vehicle was not sufficient for determining the behavior of the bridge under an AASHTO HS-20 vehicle loading. Therefore, further diagnostic or proof testing of the bridge is required, using a heavier test vehicle, in order to confirm the reliability of the improved load rating. Nevertheless, the test procedure was capable of producing results that aided in understanding the bridge's behavior.

The evaluation of the removable strain transducers did not agree with other research findings (Chajes et al. 1997; Schultz et al. 1995). In the field tests of the Big Creek Relief Bridge, the transducers were found to be moderately capable of reproducing the data recorded by the foil gages, except when the data was required for use in the neutral axis calculations. In this case, the transducer data was not sufficiently accurate. In addition, it was found that the transducer calibration and installation procedure was

not significantly less cumbersome than the foil gage installation procedure. Therefore, the use of removable strain transducers, in place of foil gages, could not be justified.

The test results showed that the girders on the Big Creek Relief Bridge did not exhibit a symmetrical response. For example, girder 1 exhibited composite behavior in the positive moment region, while all of the other girders behaved noncompositely. The variety of response exhibited by each girder illustrated the need to place instrumentation on every girder, instead of assuming that the structure will behave in a symmetrical manner. Furthermore, the composite behavior measured in girder 1 in the positive moment region of span 3 was no indication of the behavior of girder 1 in the other positive moment regions. Additional instrumentation would be required to determine the girder's response on the other three spans.

In closing, the success of the Big Creek Relief Bridge load test indicates that the strain instrumentation, test procedure, and analysis methods used in this study are appropriate for diagnosing the behavior of a concrete-slab-on-steel-girder bridge and possibly improving the bridge's load rating.

APPENDIX A

Methods of Data Analysis

This chapter contains a description of the data files recorded by the 21X and a description of the calculations performed on the data. Portions of the load test data from the Big Creek Relief Bridge are used to provide sample calculations. The full set of data from the load tests on the Big Creek Relief Bridge is presented and discussed in Chapter 5.

A.1 Raw Data File Description

A 21X datalogger was used to measure the output and excitation voltages in the strain gage circuits. After each pass, the voltage data was downloaded to the laptop computer and saved in a file. The raw data in the file was used to calculate strains, stresses, truck positions, neutral axis positions, stress distributions, and moment distributions.

Each data file contained hundreds of rows of data, arranged in nine columns. Table A-1 shows a portion of the data in a typical data file. In the table, the row numbers in the left column were added after the data was saved. The row numbers were not recorded by the 21X during the load test.

In the file, the first column was a memory pointer, used internally by the 21X to label and keep track of the data. The second through eighth columns contained the output voltage data from the strain gages on channels one through seven, respectively. The ninth column contained the excitation voltage data recorded on channel eight. The output voltages were recorded in millivolts, and the excitation voltage was recorded in volts.

The pointers in the first column specified which line in the 21X program issued the “sample data” command. The values of the pointers were useful for debugging the 21X’s data acquisition program, but they were not needed during the load tests. However, there was no way to prevent the 21X from recording them during a load test.

Row	Pointer	Output Ch 1 (mV)	Output Ch 2 (mV)	Output Ch 3 (mV)	Output Ch 4 (mV)	Output Ch 5 (mV)	Output Ch 6 (mV)	Output Ch 7 (mV)	Excitation Ch 8 (Volts)
...	...	...	...	...	...	...	...	...	...
271	303	0.388	0.231	0.118	0.004	-0.015	0.043	-0.022	4.900
272	303	0.396	0.239	0.120	0.005	-0.013	0.044	-0.023	4.900
273	303	0.418	0.257	0.122	0.002	-0.015	0.046	-0.024	4.901
274	303	0.426	0.269	0.124	0.002	-0.013	0.045	-0.024	4.901
275	303	0.440	0.283	0.129	0.003	-0.017	0.047	-0.024	4.900
276	303	0.452	0.295	0.127	0.003	-0.016	0.047	-0.024	4.900
277	303	0.461	0.310	0.128	0.003	-0.014	0.049	-0.023	4.900
278	303	0.464	0.319	0.130	0.002	-0.017	0.049	-0.026	4.901
...	...	...	...	...	...	...	...	...	...

Table A-1 Sample Raw Data File

Each row of data in the file shows the results of one scan of the eight measurement channels. During a scan, the 21X performed one voltage measurement at a time, reading each of the eight channels consecutively. During a load test, the 21X performed an eight-channel scan once every 62.5 milliseconds. This corresponded to a 16 hertz sample rate on each channel, and therefore 16 rows of data were added to the file every second. Because a load test on the Big Creek Relief Bridge took about 30 seconds, a typical data file contained about 480 rows of data.

A.2 Calculating Strain and Stress

The excitation and output voltages were used to calculate the strains in the steel girders. Equation A-1 shows the relationship between voltage and strain for the quarter bridge circuit used with the foil gages,

$$\frac{E_0}{E_i} = \frac{F_{gage}}{4} \cdot \varepsilon \qquad \text{(A-1)}$$

where

E_0 is the output voltage from the quarter bridge circuit, in volts,

E_i is the input voltage to the quarter bridge circuit, in volts,

F_{gage} is the gage factor, and

ε is the strain in the steel at the gage location.

Equation A-1 is commonly known as "the quarter bridge equation."

In Equation A-1, the output and excitation voltages are expressed in the same units. In the data files, however, the excitation was recorded in volts and the output was recorded in millivolts. For compatibility, the excitation data was converted into millivolts before using this equation.

The stresses at the gage locations were calculated from the strains using Hooke's law, as shown in Equation A-2,

$$\sigma = E \cdot \varepsilon \qquad \text{(A-2)}$$

where

σ is the stress in the steel,

ε is the strain in the steel, and

E is the modulus of elasticity.

The modulus of elasticity of the steel girders was found to be 29,000 ksi., based on tensile tests performed on two flame-cut specimens (Jauregui 1999).

Hooke's law is not valid after the stress in the steel reaches the yield point. For all of the field tests, the load applied to the bridge was not heavy enough to cause yielding of the steel in the girders. Thus Equation A-2 was valid for the range of data collected during the load tests.

A.3 Establishing an Artificial Zero for the Output Data

The quarter-bridge completion boxes did not contain a balancing circuit to compensate for the differences in the resistance of each arm of the quarter-bridge. Therefore, the output from each gage was not zero when there was no applied load. In the Big Creek Relief Bridge tests, the raw output from the unloaded foil gages was anywhere between -0.2 and +0.2 millivolts.

An artificial zero was imposed on the output voltages to provide a frame of reference for the strain data. Before the start of each pass, the unbalanced output from each gage was read 10 times. Then the average of the 10 readings was calculated and stored in the 21X's memory. The averages were called the "zero readings" of the gages.

Each foil gage had a different zero reading. During testing, the 21X subtracted the appropriate zero readings from the measured output voltages on each channel. As a result, each gage read zero volts at the start of a pass. The 21X recorded the "zeroed data" during each pass in the load test. As a result of the effects of bearing restraint and changes in temperature, the zero reading for each gage changed throughout the day. To correct for this problem, a new set of zero readings was recorded before each pass began.

A.4 Measurement Error and Electronic Noise

Electronic noise in the data acquisition circuitry produced errors in the voltage measurements made by the 21X. This section presents a description of the electronic noise in the 21X data acquisition system. The procedure used to evaluate the amount of electronic noise is described, and the techniques used to minimize the noise are presented.

A.4.1 Evaluating the Measurement Error

The amount of electronic noise in the 21X system was determined by recording baseline data and performing a statistical evaluation. In this process, all of the data channels were connected to gages on the bridge, with no vehicle load on the bridge, and the gages were "zeroed" using the procedure described in section A.3, above. Then, data was recorded for about 30 seconds. This data was called the "baseline data." Figure A-1 is a plot of the baseline data recorded on one channel. This plot is typical of the baseline data recorded on each channel in the data acquisition system.

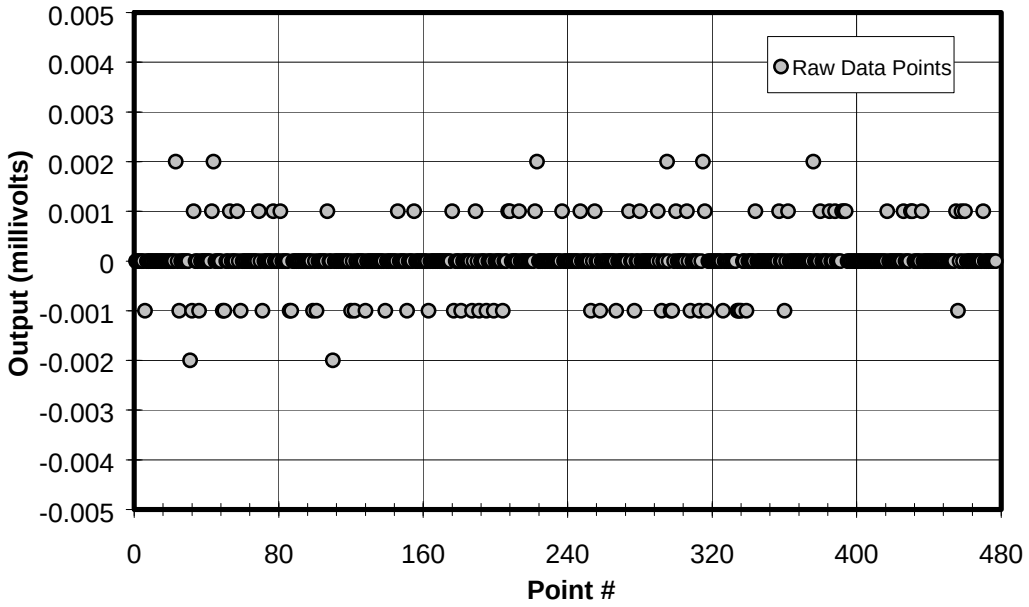

Figure A-1 Typical Baseline Output Data

Figure A-1 shows that there was a small amount of noise in the baseline data. The noise had a maximum amplitude of 0.002 millivolts. The 0.001 millivolt resolution of the 21X's voltage measurement caused the data to be arranged in discrete steps. Most of the baseline data points showed a reading of zero millivolts, with very little scatter.

In a noiseless data acquisition system, every baseline data point has a measured voltage equal to zero. The noise in the 21X system was evaluated by examining the frequency of occurrence of the non-zero data points. Table A-2 shows the frequency of occurrence for the range of output values in this baseline data sample.

A statistical analysis was performed on the baseline data. The analysis showed that the baseline data had an average value of 0.0000189 millivolts and a standard deviation of 0.0004954 millivolts. The standard deviation of the data was only half of the resolution of the voltage measurement, indicating that there was very little noise in the system.

Recorded Output Voltage (mV)	Number of Data Points	Percentage of Total Data Points
0.002	2	0.4%
0.001	42	8.8%
0.000	384	80.5%
-0.001	43	9.0%
-0.002	6	1.3%

Table A-2 Frequency of Occurrence for Baseline Output Data

The range, or dispersion, of the baseline data was too small, compared to the resolution of the voltage measurement, to determine a mathematical distribution for the baseline data. However, the data was fairly symmetrically distributed and appeared to follow a normal distribution. In the example presented in Table A-2, 80.5 percent of the data was contained within 1 standard deviation (as compared with 68.26% of the data within one standard deviation for the continuous normal distribution), 98.3 percent of the data was contained within 2.02 standard deviations deviation (as compared with 95.46% of the data within two standard deviations for the continuous normal distribution), and all of the data was contained within 4.04 standard deviations.

In a statistical analysis, it is common to exclude data that lies outside of 3 standard deviations, which for normally distributed data would be the 0.26% that are the extreme values. This criterion was applied to the baseline output data. The maximum amplitude of the data within 3 standard deviations was ±1 microvolt. For the strain gages in our data acquisition system, this corresponded to a measurement error of ±0.3791 microstrain, or ±0.0110 Ksi in the calculated steel stress. The measurement error due to electronic noise was used to determine tolerances for the neutral axis and moment distribution calculations.

A.4.2 Reducing the Measurement Error

Precautions were taken to minimize the extent of noise in the data acquisition system and thereby reduce the measurement errors in the test data. The laptop, 21X, 12 volt batteries, and 120-volt generator were connected to the same ground lead. This prevented a ground loop from forming in the system. Moreover, the connections to the gages were made using shielded cable of the shortest possible length, to prevent the data cables from acting like antennae and picking up radio and microwave signals. Finally, the number of soldered and terminal block connections was kept to a minimum to reduce the noise caused by changes in resistance.

The noise in the system was checked briefly when the gages were zeroed before each pass. When excess noise was detected in the system, it was often the result of loose terminal blocks or frayed connections. The problems were quickly fixed by tightening the screws on the terminal blocks and by re-soldering the worn connections.

A.5 Lag Error

Non-instantaneous measurements contribute a source of error. For example, the information in the data files was arranged in a table, where each line in the table represented one scan of the eight data channels. In analyzing the data, it was assumed that all eight channels were read simultaneously. However, this assumption was not true, since the channels were read by the 21X in series. The slight change in voltage during the delay between measurements was a source of error affecting the accuracy of the calculations. This error, called the lag error, affected the results of the neutral axis and stress distribution calculations, because these calculations used data from more than one gage at a time. Calculations requiring the use of only one gage's output, such as stress vs. truck position, were unaffected by lag.

Figure A-2 is a scheduling diagram for the tasks performed by the 21X during one scan of the eight data channels. In the figure, the duration and timing of each task is indicated. The total time elapsed in the scan is shown at the bottom of the figure. The output voltage measurements on channels one through seven took 3.185 milliseconds per channel, and the excitation voltage measurement on channel 8 took about 7.45

milliseconds, for a total of 29.75 milliseconds of voltage measurements per scan. Another 32.75 milliseconds were used to perform zeroing calculations, store the data in the 21X's memory, and initiate the next scan. Each scan required a total of 62.5 milliseconds to complete, indicating a sample rate of 16 Hz. per channel.

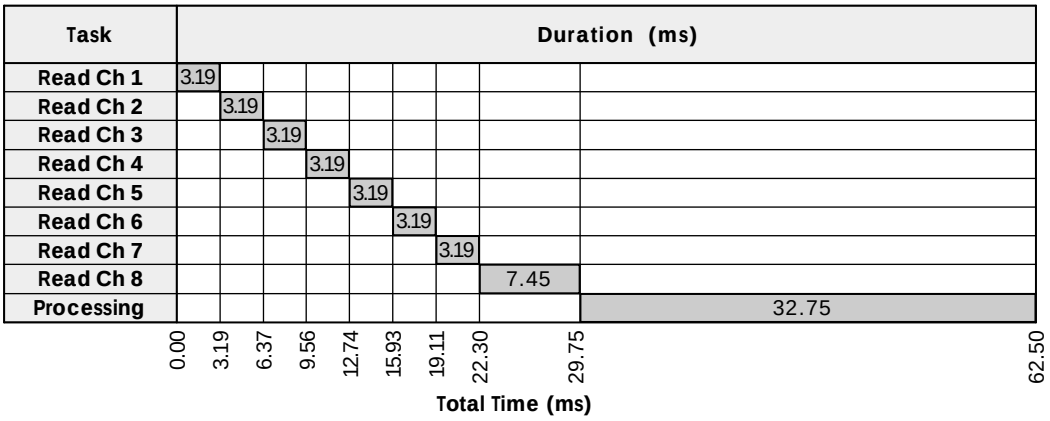

Figure A-2 Scheduling Diagram for One Cycle of 21X Voltage Measurements

A.5.1 Evaluating the Lag Error

Two conditions must be present in order for lag error to occur. First, the strain on each channel must be changing. Second, there must be a time delay between the measurements made on different channels during a scan.

An analysis of the strain data was performed to determine the magnitude of the lag error. The maximum probable change in strain was found by performing a statistical analysis. Then, the maximum probable change in strain was used to calculate the maximum probable lag error. The magnitude of the maximum probable lag error was compared with the magnitude of the measurement error, to determine whether the lag error was large enough to account for it in this study.

A.5.1.1 Determining the Maximum Probable Change in Strain

Figure A-3 is a frequency diagram for the change in strain between measurements for the bottom flange strain gage on girder 1. The strain data used to

produce this frequency diagram was recorded on channel 1 during one pass of the truck. This set of data was chosen because, on this pass, this gage recorded the largest range of strain out of all of the gages used in all of the field tests. Therefore, the data from this gage represents the worst case for evaluating the effects of the rate of change in strain on the lag error.

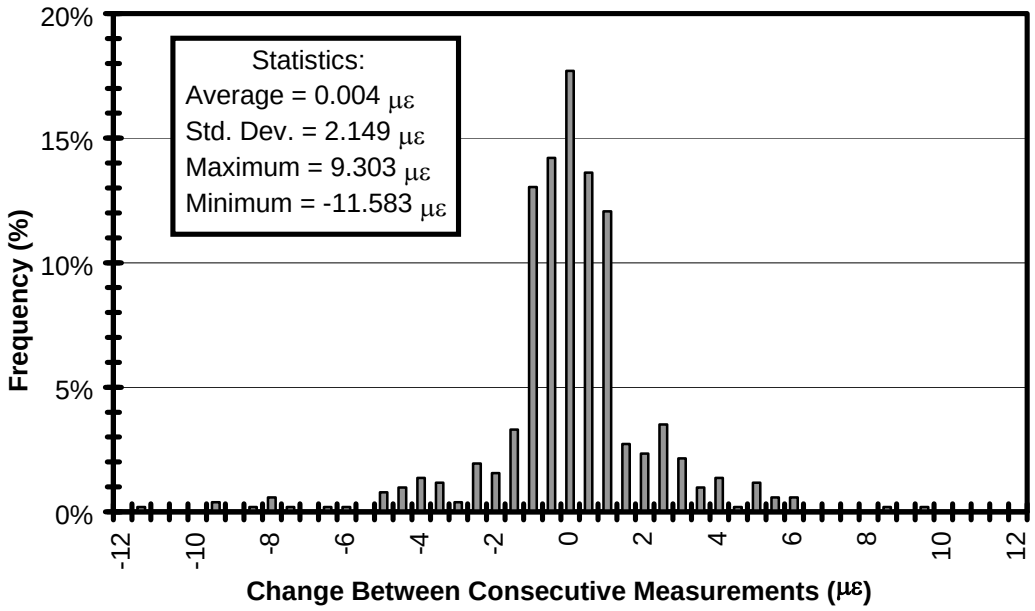

Figure A-3 Frequency Diagram for the Change in Strain Between Consecutive Strain Measurements

A statistical analysis was performed on the data from Figure A-3. The most common change in strain between measurements was zero microstrain, the average was 0.004 microstrain, and the standard deviation was 2.149 microstrain. The maximum and minimum changes in strain between measurements were 9.303 microstrain and -11.583 microstrain, respectively.

In the frequency diagram, the data resembles a normal distribution. 82.5 percent of the data was within one standard deviation, 94.4 percent was within two standard deviations, and 98.1 percent was within 3 standard deviations. The data outside of three standard deviations was regarded as statistically insignificant and excluded. Thus the

maximum probable change in strain between measurements was found to be 3 times the standard deviation, or ±6.447 microstrain.

A.5.1.2 Determining the Maximum Probable Lag Error

Figure A-4 shows an example plot of the strain measured at three gage locations vs. time. In this example, the three gages are located on the bottom flange, mid-web, and top flange of a girder, and the data acquisition system recorded the gage output consecutively on channels 1, 2, and 3, respectively. The recorded data points are shown as circles in the figure. The time line at the bottom of Figure A-4 shows that the strain was measured in the bottom flange gage at the start of a scan, in the mid-web gage at 3.19 microseconds, and in the top flange gage at 6.37 microseconds. The measurement sequence repeated 62.50 microseconds later, at the start of the next scan.

To highlight the rate of change in strain for each gage, straight lines are drawn through the consecutive strain measurements on each channel. The slope of the line indicates the rate of change in strain for the gage on that channel. The lines are straight because the rate of change in strain in each gage is assumed to be constant. This is a reasonable approximation due to the 21X's high sample rate.

In Figure A-4, the top flange strain measurement (on channel 3) was chosen as a baseline. The strains in the other gages, at the time that the top flange strain was measured, are plotted as squares in the figure and labeled "baseline data points." The lag error is defined as the difference in strain between the recorded data points and their corresponding baseline data points. For simplicity, only the lag time and lag error between channels 1 and 3 are shown in the figure.

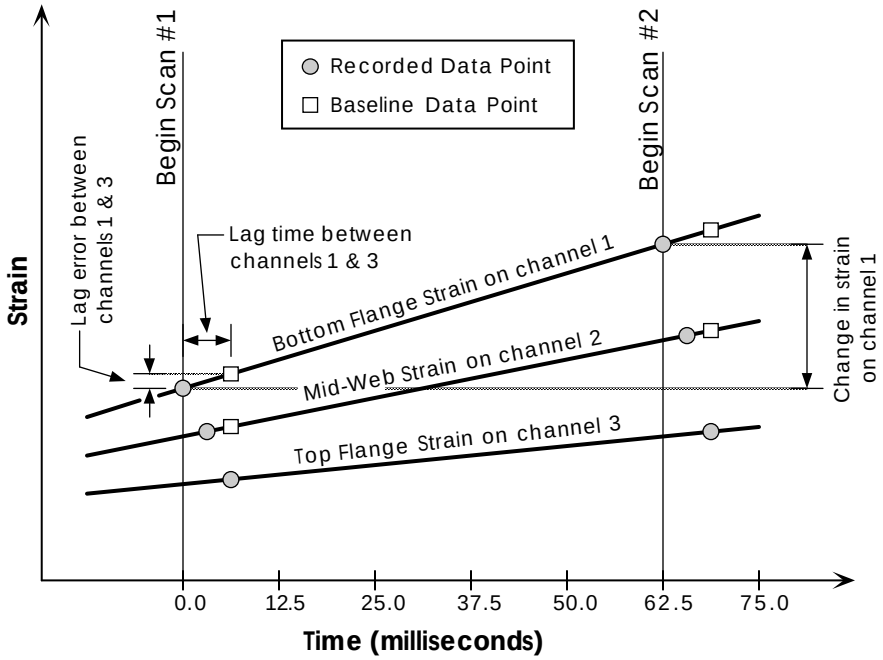

Figure A-4 Example of Lag Time and Lag Error, Showing Data from Three Gages Recorded on Three Consecutive Channels

The magnitude of the lag error is unique for each strain measurement and each pair of gages. The lag error between the top flange and bottom flange gages is greater than the lag error between the top flange and mid-web gages, because of the larger lag time between the two gages and the larger rate of change in strain in the bottom flange gage. The lag error for channel 3 is zero, because channel 3 was used for the baseline.

The magnitude of the lag error depends on the gage chosen for use as a baseline. In Figure A-4, the output from the top flange gage was chosen as a baseline, because the rates of change in strain in the other gages are large in comparison to the rate of change in strain in the top flange gage. If the bottom flange gage had been chosen for the baseline, then the lag errors would have appeared to be much smaller.

In section A.5.1.1 the maximum probable change in strain was found to be ±6.447 microstrain. Dividing this number by the time between measurements, 62.50 milliseconds, resulted in the maximum probable rate of change in strain of ±0.1032

microstrain per millisecond. The maximum probable rate of change in strain is analogous to the steepest probable slope for the lines drawn in Figure A-4.

The lag error between two gages depends on the lag time between them and the rate of change of strain. Multiplying the maximum rate of change in strain by the lag time between two consecutive channels, gives the maximum probable lag error per channel of separation: ±0.3288 microstrain.

For the neutral axis calculations, the necessary data was recorded on three consecutive channels. Thus, there were, at most, two channels of separation in the data. Therefore, as an upper bound, the maximum probable lag error in the neutral axis calculations was 2 times the lag error per channel, or ±0.6576 microstrain. Similarly, the maximum probable lag error for the strain distribution calculations, which used the data from 5 gages, was taken as 4 times the lag error per channel, or ±1.3151 microstrain.

In comparison, the measurement error in the data was ±0.3791 microstrain. Because the magnitude of the lag error was similar to the magnitude of the measurement error, the effects of lag were not considered negligible. Therefore, lag error was accounted for when assessing the errors in the data.

A.5.2 Reducing the Lag Error

The neutral axis calculations used data from three strain gages on each girder. To minimize the lag error in the neutral axis calculations, the three strain gages on each girder were read from top to bottom on consecutive output channels. That way, the lag time between the top flange and bottom flange gages was only 6.37 milliseconds.

The strain distribution calculations used data from five strain gages, one on each girder. Compared with the neutral axis calculation, the lag error in the strain distribution data was larger because of the number of gages required. Even when the five gages were read consecutively, the lag time between the first and last measurements was 12.74 milliseconds.

Despite the larger lag errors in the strain distribution data, the strain distribution calculations were not as sensitive to lag errors as the neutral axis calculations. Consequently, in the load tests where both strain distribution data and neutral axis data

were recorded, the gages recording the neutral axis data were read consecutively. This arrangement minimized the lag errors in the neutral axis data at the expense of the strain distribution data.

As an additional measure, the speed of the truck was kept as slow as possible. This minimized the rate of change in strain in the gages. Consequently, slow truck speeds helped to reduce the lag error.

A.6 Converting Raw Data to Position-Referenced Data

An electronic switch was used to record the longitudinal position of the truck in the test data. The switch was connected to channel 8 on the 21X and was operated by a person standing on the deck of the bridge. The truck's position was recorded by interrupting the signal to channel 8 every time the truck's front axle crossed a bearing.

All of the data files from the Big Creek Relief Bridge contained five interruptions on channel 8. Table A-3 shows a portion of a typical raw data file, including an interruption that began in row number 108. The first zero in the interruption indicated when the truck's front axle was positioned over the bearing. The other zero was recorded before the switch was released.

In a typical data file, each interruption on channel 8 was between two and four rows long. In all cases, the leading edge of the interruption indicated the truck's position over a bearing. During an interruption, the excitation voltage was assumed to be the same as the last excitation recorded. For the data file shown in Table A-3, the excitation of 4.901 volts, as recorded in row 107, was used to calculate strain for the output data in rows 107, 108 and 109.

Row	Output Ch 1 (mV)	Output Ch 2 (mV)	Output Ch 3 (mV)	Output Ch 4 (mV)	Output Ch 5 (mV)	Output Ch 6 (mV)	Output Ch 7 (mV)	Excitation Ch 8 (Volts)
...	...	...	...	...	...	...	...	...
105	0.013	0.007	0.004	0.002	0.002	0.003	0.000	4.901
106	0.012	0.007	0.004	0.002	0.003	0.004	0.000	4.901
107	0.009	0.007	0.004	0.003	0.003	0.001	-0.004	4.901
108	**0.010**	**0.006**	**0.002**	**0.002**	**0.004**	**0.002**	**-0.003**	**0.000**
109	0.012	0.008	0.006	0.004	0.003	0.001	-0.001	0.000
110	0.009	0.005	0.004	0.000	0.002	0.002	-0.002	4.901
111	0.011	0.005	0.003	0.004	0.003	0.002	-0.003	4.900
112	0.010	0.005	0.004	0.005	0.005	0.003	-0.003	4.901
...	...	...	...	...	...	...	...	...

Table A-3 Portion of a Typical Raw Data File, Including an Interruption of Channel 8

Figure A-5 shows a simplified plot of an excitation voltage signal. In the figure, the leading edges of the first three interruptions are labeled, along with the corresponding front axle positions. The data used to create Figure A-5 came from the file used to create Table A-3. The last two interruptions in the file are not shown in Figure A-5.

The leading edge of the first interruption occurred in row 40, indicating that row 40 was recorded as the front axle passed bearing 1. The leading edge of the second interruption occurred in row 108, and the leading edge of the third interruption occurred in row 200. Although not shown in the figure, the leading edges of the fourth and fifth interruptions occurred in rows 293 and 362, respectively.

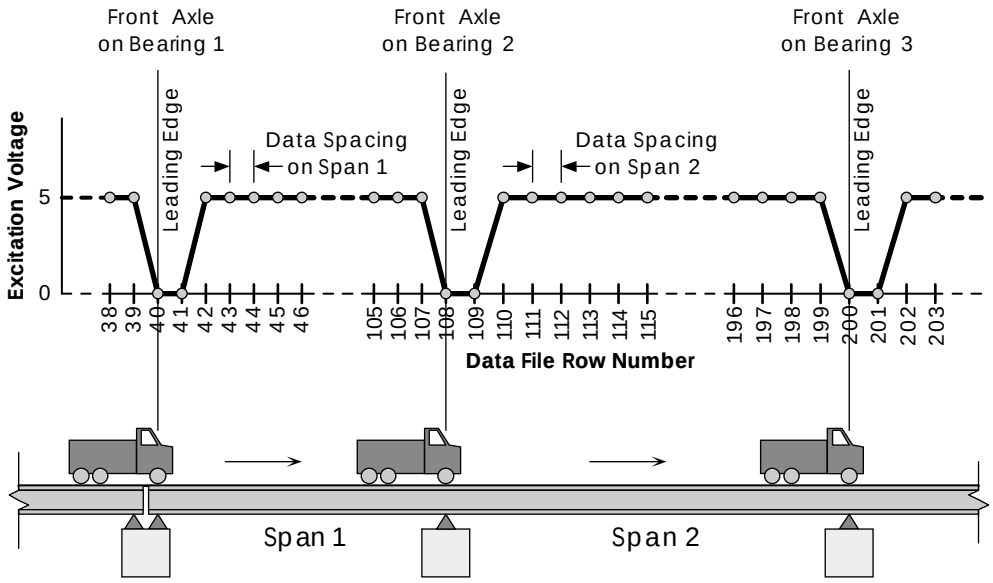

Figure A-5 Typical Excitation Signal and Corresponding Front Axle Positions

When the truck's front axle was not over one of the bearings, the position of the front axle was estimated by calculating the average spacing between the data points. For example, in the data file used to create Figure A-5, the front axle was on bearing 1 in row 40 and on bearing 2 in row 108. There were 67 rows of data between row 40 and row 108, and therefore there were 68 spaces between the rows of data. The distance between bearing 1 and bearing 2 was 304.5 inches. Thus, the average spacing between each row of data was 304.5 inches divided by 68 spaces, or 4.478 inches per space. In other words, the position of the front axle increased by 4.478 inches for each consecutive row of data recorded while the front axle was on span 1.

The data spacing and front axle positions on spans 2, 3, and 4 were all calculated in the same way as they were for span 1. The spacing of the data collected before the front axle reached bearing 1 was assumed to be the same as the spacing on span 1 and the spacing of the data collected after the front axle passed bearing 5 was assumed to be the same as the spacing on span 4.

Table A-4 shows the number of data points on each span, for the example data file. The table also shows the span length, data spacing, and average truck speed for each

span. The information shown in Table A-4 is typical of all of the data files. The truck's average velocity was calculated (in inches per second) by dividing the data spacing by the 21X's scan rate of 0.0625 seconds per scan. The velocity results were converted to miles per hour using two conversion factors: 63,360 inches per mile and 3600 seconds per hour.

Front Axle Position	Span Length (in)	Number of Data Points on Span	Data Spacing (in)	Avg. Truck Velocity (in/sec)	Avg. Truck Velocity (Mph)
Approaching Span 1	---	39	4.478*	71.7*	4.0*
On Span 1	304.5	67	4.478	71.7	4.07
On Span 2	408.0	92	4.387	70.2	4.03
On Span 3	408.0	91	4.435	71.0	3.99
On Span 4	304.5	68	4.413	70.6	4.01
After Exiting Span 4	---	107	4.413**	70.6**	4.01**

* Extrapolated from the data spacing or average truck speed on span 1.
** Extrapolated from the data spacing or average truck speed on span 4.

Table A-4 Data Spacing and Truck Velocity for a Typical Data File

In calculating the average data spacing, the truck was assumed to maintain a constant velocity on each span. However, the results shown in Table A-4 indicate that the velocity of the truck varied by up to 1.0 percent, from span to span. Therefore, the actual data spacing was not constant. The error in the data spacing was ignored in this study, because the variation in the truck's velocity was small.

Table A-5 shows a sample of position-referenced data. The stresses in the table were calculated by converting the voltages from Table A-3 into stresses, using the procedure from section A.2. In the table, the front axle position in row 108 was known, because the data file was marked by the vehicle position sensor. The other front axle positions were calculated by adding or subtracting the appropriate data spacing from the

front axle position established for row 108, using the data spacing information for span 1 and span 2, shown in Table A-4.

Row	Stress Ch 1 (Ksi)	Stress Ch 2 (Ksi)	Stress Ch 3 (Ksi)	Stress Ch 4 (Ksi)	Stress Ch 5 (Ksi)	Stress Ch 6 (Ksi)	Stress Ch 7 (Ksi)	Front Axle Position (in)	Center Axle Position (in)
...	...	...	...	...	...	...	...	...	...
105	0.146	0.079	0.045	0.022	0.022	0.034	0.000	291.07	140.07
106	0.135	0.079	0.045	0.022	0.034	0.045	0.000	295.54	144.54
107	0.101	0.079	0.045	0.034	0.034	0.011	-0.045	300.02	149.02
108	**0.112**	**0.067**	**0.022**	**0.022**	**0.045**	**0.022**	**-0.034**	**304.50**	**153.50**
109	0.135	0.090	0.067	0.045	0.034	0.011	-0.011	308.89	157.89
110	0.101	0.056	0.045	0.000	0.022	0.022	-0.022	313.27	162.27
111	0.123	0.056	0.034	0.045	0.034	0.022	-0.034	317.66	166.66
112	0.112	0.056	0.045	0.056	0.056	0.034	-0.034	322.05	171.05
...	...	...	...	...	...	...	...	...	...

Table A-5 Portion of a Typical Position-Referenced Data File

The 10 cubic yard truck was used to create the data file shown in this example. The distance from the front axle to the center axle was 151 inches. In Table A-5, the center axle's position was calculated by subtracting 151 inches from the front axle's position. Shifting the position data to reference the heavier center axle was useful for understanding the bridge behavior as well as for comparing the bridge's response to different trucks.

Figure A-6 is a sample plot of some position-referenced data. The data from the first 5 channels in the file used to create Table A-5 is shown. In this plot, the bearing locations are marked with five short-dashed vertical lines, and the location of the active gages is marked with a long-dashed vertical line. Plots like this, showing data from all five girders, were used to determine the stress distribution behavior of the bridge. The position-referenced format helped to make sense of the data, by showing where the truck

was in relation to the bearings and gages. Because of the position reference, the stress data shown here is actually a series of stress influence lines for the truck.

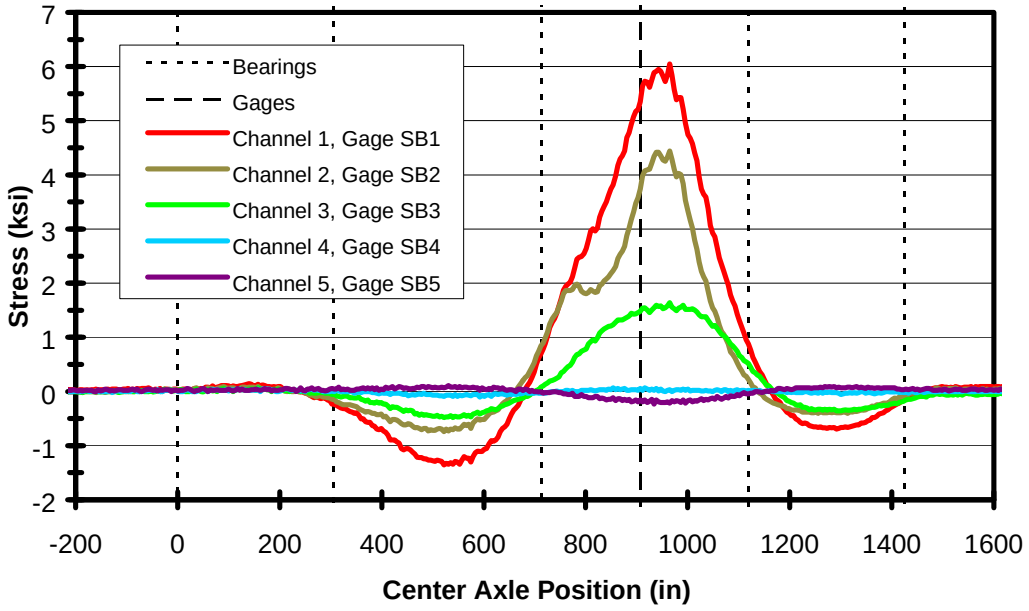

Figure A-6 Plot of a Typical Position-Referenced Data File

A.7 Comparing Data Files

This section presents the technique used to compare data that was recorded in different files. An example comparison is presented. Furthermore, the limitations of the comparison technique are explained.

Some aspects of the bridge's response could not be evaluated by examining the data from only one pass of the truck. For example, a study of the influence of lateral truck position on the stress in girder 1 required data from five passes of the truck, one on each wheel line. The position-referencing technique from section A.6 was used to determine the truck's position for each row of data in the files. Then the data from girder 1 in each file was combined and plotted on a single graph, using the truck's position as the independent variable.

Figure A-7 is a plot of the bottom flange stress in girder 1, for five different wheel lines, vs. the longitudinal position of the truck's center axle. The location of each bearing is shown, along with the location of the active strain gage. Because the truck's position is used for the independent variable, the data from each pass can be compared easily, as if the data from all five wheel lines had been recorded in the same file. Figure A-7 is typical of the graphs produced by comparing data from different files.

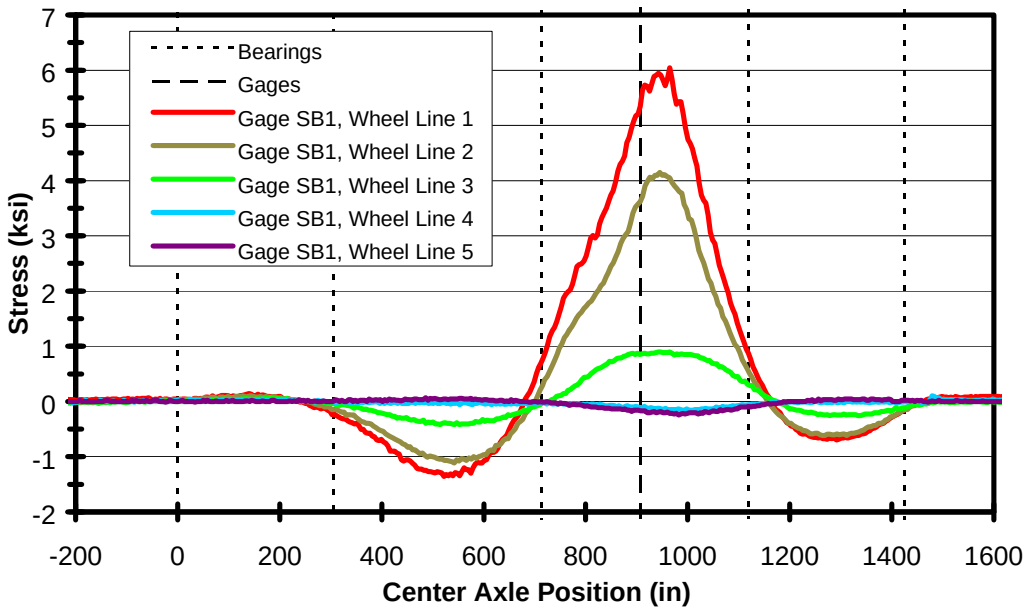

Figure A-7 Sample of Combined Data From Five Position-Referenced Files

In contrast, Figure A-8 shows the original, raw, data from each of the five files. The independent variable in Figure A-8 is the row number for each data point. The information in Figure A-8 is not position referenced, and therefore there is no basis for comparison between wheel lines. As a result, Figure A-8 is not useful for understanding the behavior of the bridge.

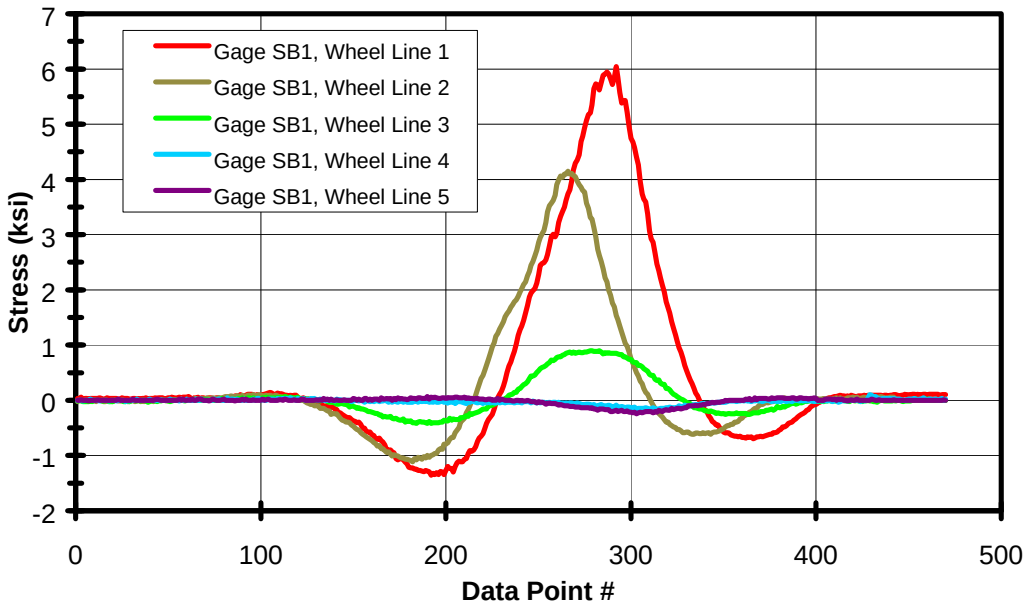

Figure A-8 Sample of Combined Data From Five Raw Data Files

The position-reference technique was useful for combining and comparing the data from different files. However, it did not allow calculations to be performed on the combined data, because the truck positions did not line up exactly from file to file. In most calculations the truck's position was assumed to be the same for each data point. Thus, interpolation of the data was necessary, to reduce the errors caused by misalignment, before calculations could be performed.

Figure A-9 shows an illustration of the data spacing for the position-referenced data from two files, "Data File 1" and "Data File 2." In this figure, the position data references the truck's front axle. The truck was moving faster when Data File 2 was recorded, and therefore Data File 2 has a larger data spacing than Data File 1. The figure shows that the different data spacing in each file causes misalignment of the data when the front axle is between the bearings. The data in the files is aligned when the front axle is over a bearing, however, because the bearings were used as a reference point for marking the position of the truck.

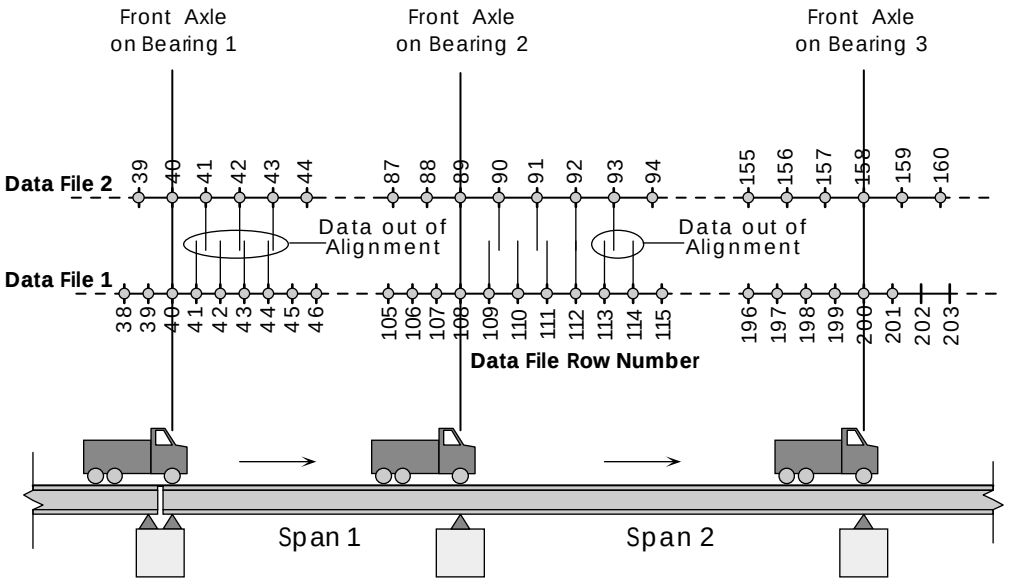

Figure A-9 Misaligned Position Data from Two Data Files

To avoid performing calculations on data from separate files, and thereby introducing interpolation errors into the analysis, all of the data necessary for a calculation was recorded in the same file. For example, when the data from three gages was used to determine the location of the neutral axis in a girder, the data from all three gages was recorded at the same time. In all cases, it was easier and more accurate to perform an additional test to record the data for a particular calculation in one file, than it was to interpolate between several data files. In this study, files were combined for comparison of the data, but no calculations were performed on the combined files.

A.8 Calculating the Neutral Axis Position

Three strain gages were placed on each girder's cross section. Data from the gages was used to calculate the position of the neutral axis and determine the extent of composite behavior in the girders, using data from two gages at a time. In this section, the technique used to determine the location of the neutral axis in each girder is presented, and the accuracy of the neutral axis calculations is discussed.

Figure A-10 shows a sample plot of strain vs. truck position, for gages SB1, SM1, and ST1. The figure shows that the girder was behaving in a composite manner, because the strain in the top flange was almost zero while the strain in the bottom flange was very large. The data from the three gages shows good agreement, because the mid-web strain curve was situated approximately halfway between the other two curves and the shapes of the bottom flange and mid-web curves were identical.

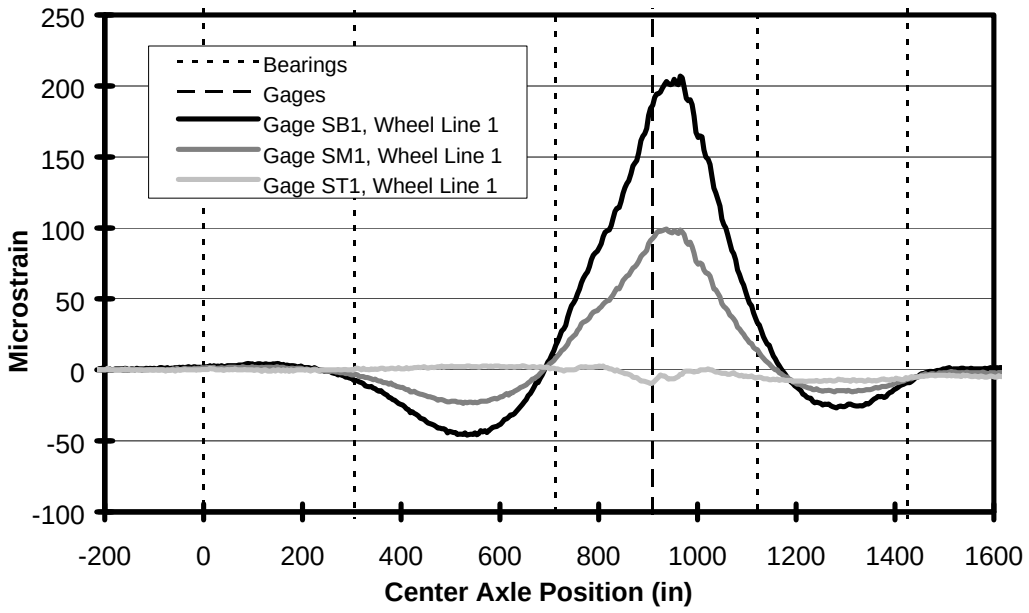

Figure A-10 Sample Plot of Strain Data from a Composite Girder

In contrast, a plot of strain vs. truck position for a noncomposite girder looks very different than Figure A-10. In a noncomposite girder, the strains in the top flange and the bottom flange are equal and opposite. Moreover, the strain at mid-web is approximately zero.

Ideally, the output from the three strain gages would indicate a linear strain profile through the depth of the girder. An ideal strain profile is shown in Figure A-11. The strain measured by the top flange gage is labeled ε_t, the mid-web strain is labeled ε_m, and the bottom flange strain is labeled ε_b. The offset between the center of gravity of the

steel alone and the composite girder's neutral axis is labeled N. The vertical distance between gages is labeled C.

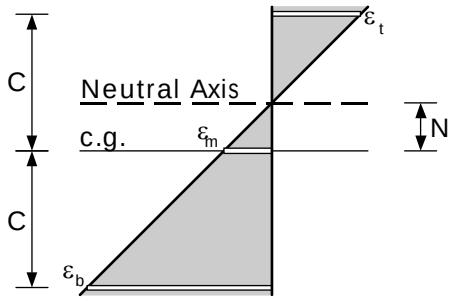

Figure A-11 Ideal Strain Profile in a Composite Girder

The value of N was calculated for three pairs of gages. Equations A-3, A-4, and A-5 show the formulas used to calculate the value of N, for each pair. In this study, these equations are referred to as the neutral axis equations. All three of the equations were derived from Figure A-11, using similar triangles. Positive values of strain indicate tension, and N is positive when the neutral axis is above the center of gravity of the steel girder.

Neutral Axis Equations

$$N_{mb} = C \cdot \frac{\varepsilon_m}{\varepsilon_b - \varepsilon_m} \qquad \text{(A-3)}$$

$$N_{tb} = C \cdot \frac{\varepsilon_b + \varepsilon_t}{\varepsilon_b - \varepsilon_t} \qquad \text{(A-4)}$$

$$N_{tm} = C \cdot \frac{\varepsilon_m}{\varepsilon_m - \varepsilon_t} \qquad \text{(A-5)}$$

where

N is the position of the neutral axis. (gage pair indicated by subscript),

ε_b is the strain measured in the bottom flange gage,

ε_m is the strain measured in the mid-web gage,

ε_t is the strain measured in the top flange gage, and

C is the vertical distance between gages.

Figure A-12 is a plot of the neutral axis offset, N, vs. truck position. The results shown in Figure A-12 were calculated using Equations A-3, A-4, and A-5, and the strain data shown in Figure A-10. The scatter of the results in Figure A-12 was surprising, considering that all of the data shown in Figure A-10 seemed to indicate a consistent neutral axis location. Unfortunately, the scattered results shown in Figure A-12 are typical of the results of the neutral axis calculations, for all of the test data.

The neutral axis equations produced scattered results when the truck was crossing each bearing and when the truck was on spans 1 or 4. These were the truck positions that produced little or no strain in the gages. When the measured strains were small, the measurement and lag errors in the data were large in comparison to the measured strains. The scatter in the neutral axis results occurred because the neutral axis equations were sensitive to the errors in the strain data, at low levels of strain.

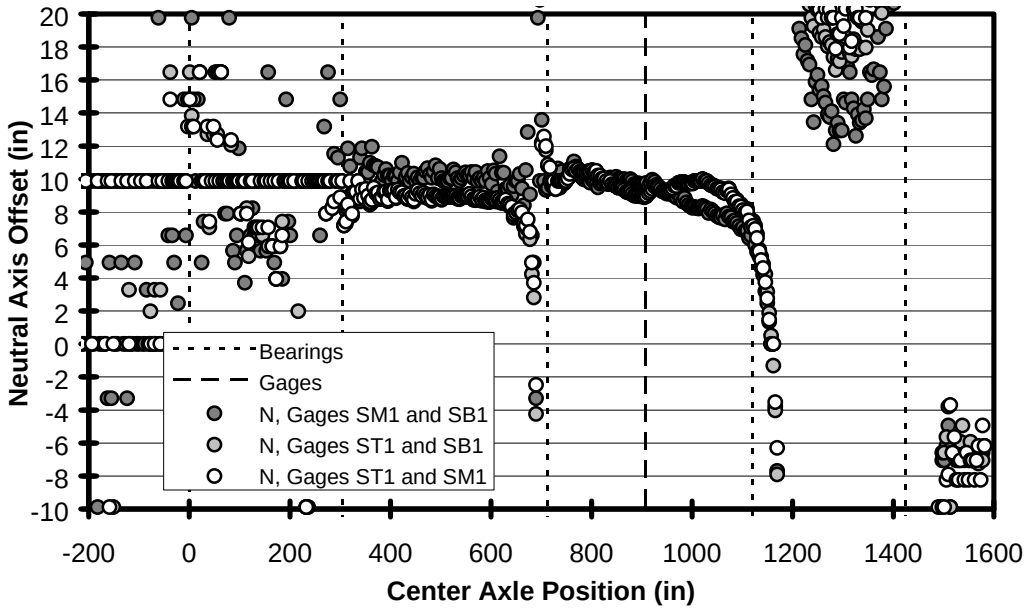

Figure A-12 Sample Plot of Neutral Axis vs. Truck Position

A.8.1 Evaluating the Accuracy of the Neutral Axis Calculations

For each of the three neutral axis equations, the relationship between errors in strain measurement and errors in calculating N was determined. Equations A-6 and A-7 are the partial derivatives of Equation A-4 with respect to strain in the mid-web and bottom flange gages. Equations A-8 and A-9 are the partial derivatives of Equation A-5 with respect to strain in the top flange and bottom flange gages, and Equations A-10 and A-11 are the partial derivatives of Equation A-6 with respect to strain in the top flange and mid-web gages.

Partial Derivatives of Equation A-3, N_{mb}

$$\frac{\delta N_{mbm}}{\delta \varepsilon_m} = C \cdot \frac{\varepsilon_b}{\left(\varepsilon_b - \varepsilon_m\right)^2} \tag{A-6}$$

$$\frac{\delta N_{mbb}}{\delta \varepsilon_b} = C \cdot \frac{-\varepsilon_m}{\left(\varepsilon_b - \varepsilon_m\right)^2} \tag{A-7}$$

where

ε_b is the strain in the bottom flange gage,

ε_m is the strain in the mid-web gage,

$\delta\varepsilon_b$ is the total error in strain measurement for the bottom flange gage,

$\delta\varepsilon_m$ is the total error in strain measurement for the mid-web gage,

C is the vertical distance between gages, 9.88 inches,

δN_{mbm} is the error in N_{mb} due to $\delta\varepsilon_m$, and

δN_{mbb} is the error in N_{mb} due to $\delta\varepsilon_b$.

Partial Derivatives of Equation A-4, N_{tb}

$$\frac{\delta N_{tbt}}{\delta \varepsilon_t} = 2 \cdot C \cdot \frac{\varepsilon_b}{\left(\varepsilon_b - \varepsilon_t\right)^2} \tag{A-8}$$

$$\frac{\delta N_{tbb}}{\delta \varepsilon_b} = 2 \cdot C \cdot \frac{-\varepsilon_t}{\left(\varepsilon_b - \varepsilon_t\right)^2} \tag{A-9}$$

where

ε_t is the strain in the top flange gage,

$\delta\varepsilon_t$ is the total error in strain measurement for the top flange gage,

δN_{tbt} is the error in N_{tb} due to $\delta\varepsilon_t$, and

δN_{tbb} is the error in N_{tb} due to $\delta\varepsilon_b$.

Partial Derivatives of Equation A-5, N_{tm}

$$\frac{\delta N_{tmt}}{\delta \varepsilon_t} = C \cdot \frac{\varepsilon_m}{\left(\varepsilon_t - \varepsilon_m\right)^2} \tag{A-10}$$

$$\frac{\delta N_{tmm}}{\delta \varepsilon_m} = C \cdot \frac{-\varepsilon_t}{\left(\varepsilon_t - \varepsilon_m\right)^2} \tag{A-11}$$

where

δN_{tmt} is the error in N_{tm} due to $\delta\varepsilon_t$ and

δN_{tmm} is the error in N_{tm} due to $\delta\varepsilon_m$.

The right side of Equations A-6 through A-11 is composed of three variables, ε_b, ε_m, and ε_t, and a constant, C. The values of ε_b, ε_m, and ε_t were recorded as data, and the value of C was 9.88 inches. Thus, the value of the right side of each equation could be calculated from the recorded strain data.

The value of $\delta\varepsilon$ was determined by combining the measurement error and the lag error into one number, the total error. The total error was estimated using the square root of the sum of the squares method, shown in Equation A-12. This method is often referred to as the SRSS method. The SRSS method is valid for assessing the combined error due to lag time and noise, because the lag error and the measurement error are independent of each other.

$$\left|\delta\varepsilon\right| = \sqrt{\delta\varepsilon_{measure}{}^2 + \delta\varepsilon_{lag}{}^2} \tag{A-12}$$

where

$\delta\varepsilon_{measure}$ is the measurement error, in microstrain,

$\delta\varepsilon_{lag}$ is the lag error, in microstrain, and

$\delta\varepsilon$ is the total error, in microstrain.

The value of $\delta\varepsilon_{measure}$ was found to be ±0.3791 microstrain, as presented above in section A.4.1. The value of $\delta\varepsilon_{lag}$ was calculated for every strain measurement, on each of the gages, using Equation A-13.

$$\delta\varepsilon_{lag} = \frac{\varepsilon_{next} - \varepsilon_{prev}}{2 \cdot t_{scan}} \cdot \Delta_{ch} \cdot t_{lag} \qquad \text{(A-13)}$$

where

ε_{prev} is the strain measured in that gage in the previous scan,

ε_{next} is the strain measured in that gage in the next scan,

t_{scan} is the scan time, 62.5 milliseconds,

t_{lag} is the lag time for consecutive channels, 3.185 milliseconds,

Δ_{ch} is the number of channels separating the pertinent gages, and

$\frac{\varepsilon_{next} - \varepsilon_{prev}}{2 \cdot t_{scan}}$ is the average rate of change in strain over 2 scan intervals.

For the error analysis of Equations A-3 and A-5, the value of Δ_{ch} was 1, because the gages used in these equations were read consecutively. However, for the error analysis of Equation A-4, the value of Δ_{ch} was 2, because the gages used in this equation were separated by the mid-web gage's channel. Therefore, the lag error in the top flange and bottom flange gages was twice as large when applied to Equation A-4 than when the same data was applied to Equations A-3 and A-5.

In Equations A-6 through A-11, the value of δN was determined by calculating the appropriate value of $\delta\varepsilon$ and plugging in the recorded strain data. The values of δN_{mbm} and δN_{mbb} from Equations A-6 and A-7 were used to calculate the error in N_{mb} from Equation A-3, using the SRSS combination shown in Equation A-14.

Accuracy of Equation A-3, N_{mb}

$$\left|\Delta N_{mb}\right| = \sqrt{\delta N_{mbm}{}^2 + \delta N_{mbb}{}^2} \qquad \text{(A-14)}$$

where

ΔN_{mb} is the accuracy of N_{mb} in Equation A-3.

The errors in N_{tb} and N_{tm} from Equations A-4 and A-5 were calculated in the same manner. Equation A-15 shows the procedure used to determine the accuracy of N_{tb} in Equation A-4, and Equation A-16 shows the procedure used to determine the accuracy of N_{tm} in Equation A-5.

Accuracy of Equation A-4, N_{tb}

$$\left|\Delta N_{tb}\right| = \sqrt{\delta N_{tbt}{}^2 + \delta N_{tbb}{}^2} \qquad \text{(A-15)}$$

where

ΔN_{tb} is the accuracy of N_{tb} in Equation A-4.

Accuracy of Equation A-5, N_{tm}

$$\left|\Delta N_{tm}\right| = \sqrt{\delta N_{tmt}{}^2 + \delta N_{tmm}{}^2} \qquad \text{(A-16)}$$

where

ΔN_{tm} is the accuracy of N_{tm} in Equation A-5.

The effect of errors in strain measurement on the magnitude of ΔN was examined by calculating ΔN for Equations A-3, A-4, and A-5, for every line of data in a sample data file. Table A-6 shows the accuracy of Equations A-3, A-4, and A-5, for three lines of data from the sample file.

In Table A-6, the first set of strain data was recorded when the truck was near the middle of span 1 and the strain in the gages was small. In this case, the errors in the neutral axis calculations were large, ranging from ±2.15 to ±3.05 inches. The second set of strain data was recorded when the truck was near the middle of span 2 and the strain in the gages was moderate. In this case, the errors in the neutral axis calculations were small, ranging from ±0.13 to ±0.37 inches. Finally, the third set of strain data was recorded when the truck was near the middle of span 3 and the strain in the gages was large. In this case, the errors in the neutral axis calculations were very small, ranging from ±0.04 to ±0.07 inches.

The results from Table A-6 suggest that when the measured strains were large, the measurement and lag errors were negligible. In these cases the results of the neutral axis calculation were more accurate. The relationship between strain magnitude and the accuracy of N was used to clean-up the neutral axis vs. truck position plots, by identifying the most accurate data and excluding the rest.

Gage Pair	ε_b ($\mu\varepsilon$)	ε_m ($\mu\varepsilon$)	ε_t ($\mu\varepsilon$)	N (in)	δN (in)	δN (in)	ΔN (in)
SM1&SB1	2.690	0.759	0.379	3.95 (eq A-3)	2.72 (eq A-6)	-0.78 (eq A-7)	±2.83 (eq A-14)
ST1&SB1				7.41 (eq A-4)	-2.13 (eq A-8)	0.31 (eq A-9)	±2.15 (eq A-15)
ST1&SM1				6.59 (eq A-5)	-2.16 (eq A-10)	2.15 (eq A-11)	±3.05 (eq A-16)
SM1&SB1	-45.97	-23.17	2.690	10.05 (eq A-3)	-0.33 (eq A-6)	0.17 (eq A-7)	±0.37 (eq A-14)
ST1&SB1				8.78 (eq A-4)	0.15 (eq A-8)	-0.01 (eq A-9)	±0.15 (eq A-15)
ST1&SM1				8.85 (eq A-5)	0.13 (eq A-10)	-0.01 (eq A-11)	±0.13 (eq A-16)
SM1&SB1	206.9	98.45	-3.103	8.966 (eq A-3)	-0.07 (eq A-6)	-0.03 (eq A-7)	±0.07 (eq A-14)
ST1&SB1				9.589 (eq A-4)	-0.04 (eq A-8)	0.00 (eq A-9)	±0.04 (eq A-15)
ST1&SM1				9.579 (eq A-5)	-0.04 (eq A-10)	0.00 (eq A-11)	±0.04 (eq A-16)

Table A-6 Sample Neutral Axis Error Calculations

Figure A-13 is a reduced plot of N vs. truck position, showing only the results of the neutral axis calculations when the calculation had an error, ΔN, of ±0.21 inches, or less. The tolerance of ±0.21 inches was chosen arbitrarily. This value was equivalent to

1 percent of the girder depth, a nice round figure, and seemed adequate for removing the scattered data from the plots of neutral axis vs. truck position.

Figure A-13 is easier to interpret than Figure A-12, because the less-accurate information has been removed. The reduced neutral axis data shows that the girder is behaving in a composite manner. Moreover, in this case, the neutral axis of the composite girder is located about 9 inches above the center of gravity of the steel alone.

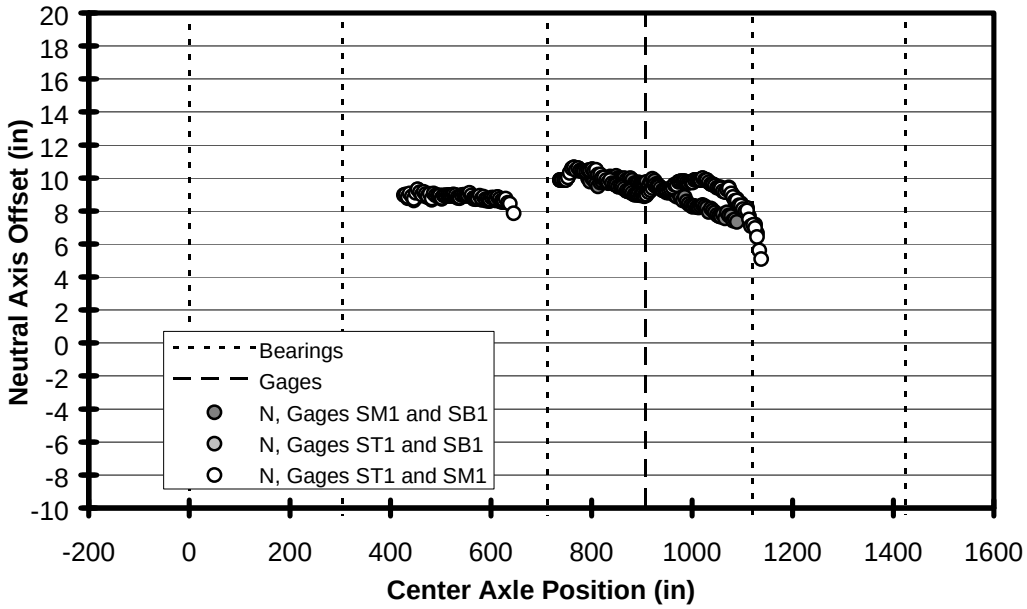

Figure A-13 Sample Plot of Neutral Axis vs. Truck Position, Reduced by the Differential Equation Method

A.8.2 A Simplified Method for Reducing the Neutral Axis Results

The differential equation method, used to determine the error in Equations A-3, A-4, and A-5, and reduce the set of neutral axis results, was impractical because it was computationally intense. A simpler method, called the strain difference method, was developed to approximate the differential equation method.

In the strain difference method, the neutral axis calculation was only performed when the difference in strain between the gages was sufficiently large. Figure A-14 shows a reduced set of neutral axis results, determined using the strain difference

method. In this figure, the set of neutral axis results was reduced by excluding the results of Equation A-3 when the difference between the bottom flange strain and the mid-web strain was less than 17.25 microstrain. Moreover, the results of Equation A-4 were excluded when the difference between the top flange and bottom flange strain was 34.50 microstrain. Finally, the results of Equation A-5 were excluded when the difference between the top flange and mid-web strains was less than 17.25 microstrain. The limiting strain difference applied to Equation A-4 was twice as large, because the top and bottom flange gages were separated by twice the vertical distance of the gages used in the other equations.

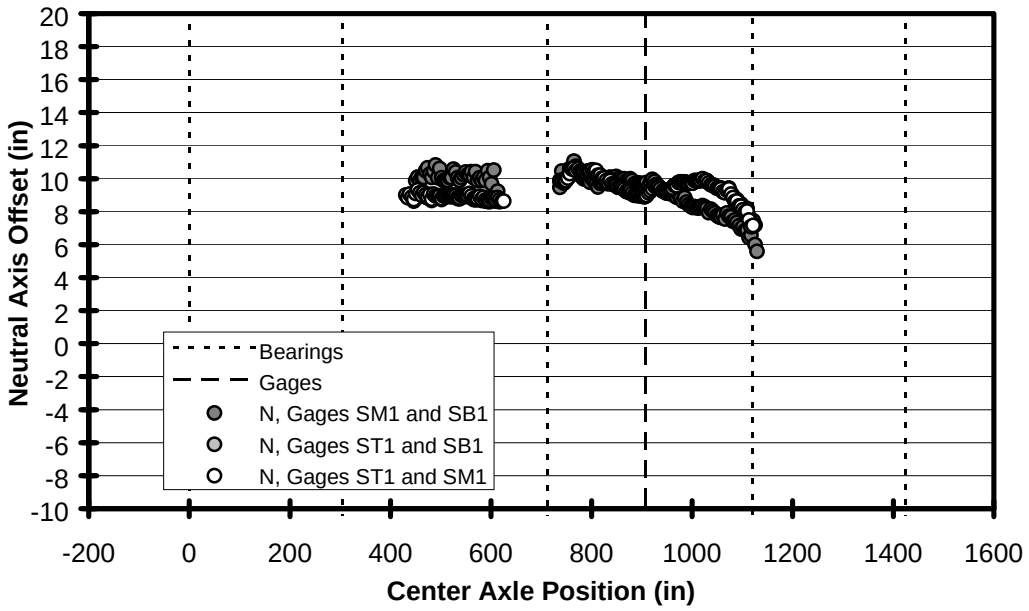

Figure A-14 Sample Plot of Neutral Axis vs. Truck Position, Reduced by the Strain Difference Method

The cutoff limit of 17.25 microstrain was chosen arbitrarily, because it corresponded to a stress of 0.5 ksi. in the steel and it worked well for approximating the results shown in Figure A-13. Table A-7 shows a tally of the number of data points in Figures A-13 and A-14, by neutral axis equation, and the number of points in common between the two figures.

The results shown in Table A-7 indicate that the strain difference method was extremely good at approximating the results of the differential equation method, for Equations A-4 and A-5. However, for Equation A-3, the strain difference method included a large group of results which were excluded using the differential equation method.

Neutral Axis Equation	# of Data Points: Differential Eq. Method, Figure A-13	# of Data Points: Strain Difference Method, Figure A-14	# of Data Points in Common
A-3	75	140	75
A-4	148	144	144
A-5	156	147	147

Table A-7 Comparison of the Results Sets Produced by the Differential Equation Method and the Strain Difference Method

The strain difference method approximated the differential equation method well, because it eliminated the results of the neutral axis equations when the measured strains were small. However, the strain difference method did not evaluate the accuracy of the neutral axis calculations. Instead, it worked by eliminating the results of the neutral axis equations when the slope of the strain profile in the girder was too flat.

The strain difference method did not work as well for Equation A-3 as for the other two equations, because neither of the gages used in Equation A-3 were close to the neutral axis. Even when the slope of the strain profile was steep, the vertical distance between the mid-web gage and the neutral axis was large enough to allow for larger errors in the neutral axis calculation.

The results of the neutral axis calculations are presented in Chapter 5, for all of the load tests. In Chapter 5, the results of Equations A-3, A-4, and A-5 were reduced using the strain difference method, because the strain difference method was simpler and approximated the differential equation method well.

When the girder was behaving in a noncomposite manner and the neutral axis was near the mid-web gage, the results of Equation A-4 were as accurate as the results of Equations A-3 and A-5. Equation A-4 did not suffer from the same problem as Equation A-3. This suggests that more-accurate data was recorded when the neutral axis was between the gages, and less-accurate data was recorded when the neutral axis was outside the gages.

A.9 Moment and Stress Distribution

The procedures used to determine the lateral stress distribution and lateral moment distribution behavior of the bridge are presented in this section. The differences between moment distribution and stress distribution are discussed. A detailed explanation of moment distribution is presented above in Chapter 1.

Loads applied to the bridge were distributed among all of the girders. The girders underneath the load resisted a larger portion of the load than the girders farther away from the load. The stress distribution in the bridge was measured by recording strain data from the bottom flanges of all five girders, at the same longitudinal position, simultaneously, and converting the measured strains into stresses. Then, the stress distribution factor for each girder was calculated by comparing the stress in that girder to the sum of the stresses in all of the girders.

The stress distribution factor for each girder was calculated using Equation A-17.

$$SDF_i = \frac{\sigma_i}{\sum_{j=1}^{n} \sigma_j} \qquad \text{(A-17)}$$

where

SDF_i is the stress distribution factor for girder i,

σ_i is the stress in girder i, and

n is the total number of girders.

The stress distribution data was also used to determine the moment distribution behavior of the bridge. The moment in each girder was determined from the measured stresses, using equation A-18.

$$M = \sigma \cdot \frac{I}{c} = \sigma \cdot S \qquad \text{(A-18)}$$

where

M is the moment in the girder, in kip-inches,

σ is the stress at the gage's location, in ksi,

I is the girder's moment of inertia, in inches^4,

c is the distance from the gage to the girder's neutral axis, in inches, and

S is the section modulus of the girder, in inches^3.

After determining the moment in each girder, the moment distribution factors were calculated using Equation A-19.

$$MDF_i = \frac{M_i}{\sum_{j=1}^{n} M_j} \qquad \text{(A-19)}$$

where

MDF_i is the moment distribution factor for girder i,

M_i is the moment in girder i, and

n is the total number of girders.

In the negative moment region, all of the girders exhibited noncomposite behavior. The moment of inertia for a noncomposite girder was simply the moment of inertia for the steel section, 1246.8 inches^4, and the value of c was equal to the separation of the gages, 9.88 inches. These values, and the bottom flange stresses, were used in Equation A-18 to determine the moment in each girder.

In the positive moment region, the girders exhibited varying degrees of composite behavior, because the location of the neutral axis, determined using the procedures from section A.8, was different for each girder. In a girder designed to

behave in a composite manner, the moment of inertia can be calculated using Equation A-20.

$$I_{comp} = I_g + A_g \cdot d_g^{\,2} + \left(I_s + A_s \cdot d_s^{\,2}\right) \cdot \frac{1}{n} \qquad \text{(A-20)}$$

where

I_{comp} is the moment of inertia of the composite section,

I_g is the moment of inertia of the steel girder,

A_g is the area of the steel girder,

d_g is the distance from the center of gravity of the steel girder to the center of gravity of the composite section,

I_s is the moment of inertia of the effective portion of the concrete slab,

A_s is the effective area of the concrete slab,.

d_s is the distance from the center of gravity of the transformed concrete slab to the center of gravity of the composite section, and

n is the modular ratio of the steel to the concrete, E_s/E_c, used to transform the concrete into an equivalent area of steel.

However, the girders in the Big Creek Relief Bridge were not designed to behave in a composite manner. The AASHTO LRFD code (1994a) specifies a method for determining the effective slab width for composite girders, but the equations used to determine the effective slab width are based on the assumption that the transfer of horizontal shear forces between the steel girder and the concrete slab are developed using shear studs or other mechanical means, which were not present on the bridge. Consequently, the effective slab width and composite moment of inertia could not be determined analytically, and Equation A-18 could not be used to determine the moment in any of the composite girders. An alternate method for calculating M was required, in order to determine the moment distribution in the positive moment region.

A.9.1 Calculating Moments from Measured Stresses

In the positive moment region, the stress profile and neutral axis offset in each girder were used to determine the forces in the flanges and in the web. Then, the force in the deck was calculated from equilibrium of the composite section. Finally, the moment in the girder was calculated by multiplying the forces in the flanges, web, and deck by their distance from the neutral axis. This method of determining the moment in the girder was called the "equilibrium" method.

Figure A-15 shows a cross section of a composite girder, including the strain and stress profiles through the girder depth, and the resulting forces in the flanges, web, and deck. Because the exact shapes of the strain and stress profiles in the deck were not known, the strain and stress profiles are shown with dashed lines in the figure. For simplicity, the force in the deck was assumed to act through a point two-thirds of the way up through the deck.

In Figure A-15, the stress on the inside of the top flange is labeled σ_t, and the stress on the outside of the top flange is labeled σ_{t2}. The stress on the inside of the bottom flange is labeled σ_b, and the stress on the outside of the bottom flange is labeled σ_{b2}.

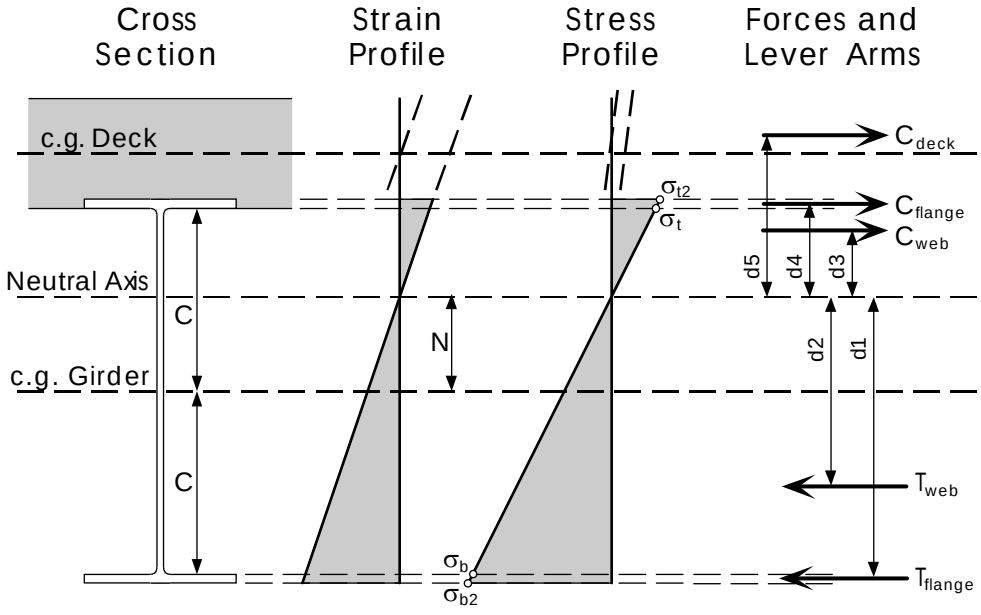

Figure A-15 Composite Girder Cross Section, Showing the Strain Profile, Stress Profile, Measured Stresses, Resulting Forces, and Lever Arms

For each girder, the value of σ_b was defined as the stress at the bottom flange gage. Equations A-21, A-22, and A-23 were used to determine the values of σ_{b2}, σ_t, and σ_{t2}. All three equations were determined from the geometry of Figure A-15, using similar triangles.

$$\sigma_{b2} = \sigma_b \cdot \frac{C + N + t_f}{C + N} \tag{A-21}$$

$$\sigma_t = \sigma_b \cdot \frac{C - N}{C + N} \tag{A-22}$$

$$\sigma_{t2} = \sigma_b \cdot \frac{C - N + t_f}{C + N} \tag{A-23}$$

where

N is the neutral axis position, in inches,

C is the vertical distance between each strain gage, 9.88 inches, and

t_f is the steel flange thickness, 0.575 inches.

The stresses in the bottom flange, lower web, upper web, and top flange were resolved into forces by determining the volume of stress blocks. Equations A-24, A-25, A-26, and A-27 were used to determine the forces in the composite section. These equations are only valid when the neutral axis is located in the web of the steel section.

$$T_{flange} = \left(\frac{\sigma_b + \sigma_{b2}}{2} \right) \cdot b_f \cdot t_f \tag{A-24}$$

$$T_{web} = \left(\frac{\sigma_b}{2} \right) \cdot t_w \cdot (C + N) \tag{A-25}$$

$$C_{web} = \left(\frac{\sigma_t}{2} \right) \cdot t_w \cdot (C - N) \tag{A-26}$$

$$C_{flange} = \left(\frac{\sigma_t + \sigma_{t2}}{2} \right) \cdot b_f \cdot t_f \tag{A-27}$$

where

b_f is the steel flange width, 8.230 inches,

t_w is the steel web thickness, 0.390 inches,

T_{flange} is the force in the bottom flange,

T_{web} is the force in the lower web,

C_{web} is the force in the upper web, and

C_{flange} is the force in the top flange.

The force in the deck, C_{deck}, was assumed to act two thirds of the way up through the deck. This assumption was conservative, as long as the neutral axis of the composite section was in the web of the steel section. The magnitude of C_{deck} was found by equilibrium, using Equation A-28.

$$C_{deck} = T_{flange} + T_{web} - C_{flange} - C_{web} \tag{A-28}$$

The lever arm for each force was determined by calculating the distance from the centroid of each stress block to the neutral axis of the composite girder. Equations A-29, A-30, A-31, A-32, and A-33 were used to determine the lever arm for each of the forces.

$$d1 = \left[\frac{\left(\sigma_b\right)\cdot\frac{1}{2} + \left(\sigma_{b2} - \sigma_b\right)\cdot\frac{2}{3}}{\sigma_{b2}}\right]\cdot t_f + C + N \tag{A-29}$$

$$d2 = \left(C + N\right)\cdot\frac{2}{3} \tag{A-30}$$

$$d3 = \left(C - N\right)\cdot\frac{2}{3} \tag{A-31}$$

$$d4 = \left[\frac{\left(\sigma_t\right)\cdot\frac{1}{2} + \left(\sigma_{t2} - \sigma_t\right)\cdot\frac{2}{3}}{\sigma_{t2}}\right]\cdot t_f + C - N \tag{A-32}$$

$$d5 = C - N + t_f + \left(t_{slab}\right)\cdot\frac{2}{3} \tag{A-33}$$

where

d1 is the lever arm for the force in the bottom flange, T_{flange},

d2 is the lever arm for the force in the lower web, T_{web},

d3 is the lever arm for the force in the upper web, C_{web},
d4 is the lever arm for the force in the top flange, C_{flange},
d5 is the lever arm for the force in the deck, C_{deck}, and
t_{slab} is the slab thickness, 6 inches.

Finally, the moment in the girder was calculated by adding up the moment from each force, using Equation A-34. In the positive moment region, Equation A-34 was used to calculate M, in lieu of Equation A-18.

$$M = \left(T_{flange} \cdot d1\right) + \left(T_{web} \cdot d2\right) + \left(C_{web} \cdot d3\right) + \left(C_{flange} \cdot d4\right) + \left(C_{deck} \cdot d5\right) \qquad \text{(A-34)}$$

The equilibrium method was used to determine the moment in each girder, regardless of the degree of composite behavior, because this method did not require any knowledge about the effective flange width or the modulus of the concrete. However, the unknown stress profile in the deck, and the potential for slip between the deck and the girder, prevented the determination of the exact length of the lever arm for the force in the deck. This resulted in a small error in the moment calculation.

A.9.2 Evaluating the Assumed Stress Profile in the Deck

In Equation A-33, the force in the deck was assumed to act through a point two thirds of the way up through the deck. Placing the resultant force in this position implied that stress profile in the girder was triangular in shape, and that the neutral axis was located at the bottom of the deck. Figure A-16 shows a detail of the triangular stress profile.

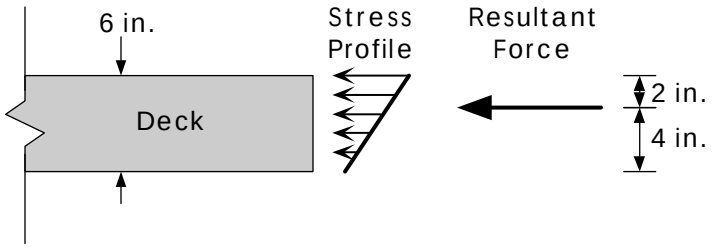

Figure A-16 Triangular Stress Profile in the Deck of a Composite Girder, and the Resultant Force in the Deck

The test data from the Big Creek Relief Bridge indicated that the neutral axis was always located in the web of the steel section. Therefore, Figure A-16 represents the highest possible line of action for the force in the deck. Using this position for the force in the deck led to overestimation of the moment in each girder, when the neutral axis was below the top of the web. This was a conservative approach, because overestimation of the moment in the girder led to overestimation of the girder's moment distribution factor.

An alternate stress profile was examined to determine the degree of conservativism in the triangular stress profile. When the neutral axis of the composite section was near the center of gravity of the steel section, the stress profile in the deck was trapezoidal, and the resultant force in the deck acted through a point just above the center of the deck's thickness. Figure A-17 shows a detail of the trapeziodal stress profile.

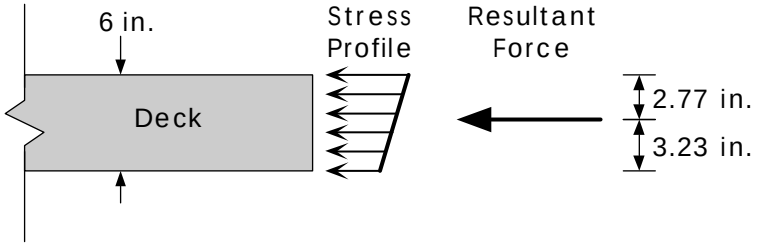

Figure A-17 Trapezoidal Stress Profile in the Deck of a Composite Girder, and the Resultant Force in the Deck

The test data indicated that the neutral axis was never located below the center of gravity of the steel section. Therefore, Figure A-17 represents the lowest possible line of action for the force in the deck. In this case, the line of action was only 0.77 inches lower than it was in the triangular profile. Thus, using the triangular stress profile for determining the moment in the girder never overestimated the length of the lever arm for the force in the deck by more than 0.77 inches. As a result, the triangular stress profile was selected for use in this study.

A.9.3 Comparing Moment Distribution and Stress Distribution

Moment distribution factors were used to assess the percentage of the applied moment carried by each girder. When the section modulus was the same in each girder, the moment distribution factor for each girder was equal to the stress distribution factor. This was the case in the negative moment region of the Big Creek Relief Bridge, where all of the girders were behaving noncompositely.

However, in the positive moment region, the girders exhibited varying degrees of composite behavior, and the section modulus was different for each girder. In this case, the moment distribution in the bridge differed from the stress distribution. The girders with a larger section modulus had a moment distribution factor that was greater than their stress distribution factor, while the girders with a smaller section modulus had a moment distribution factor that was less than their stress distribution factor.

A.10 Noncomposite Flexure of the Deck

The method used to determine the extent of noncomposite flexure in the deck is presented in this section. A detailed explanation of noncomposite deck flexure is presented above in Chapter 1.

In the positive moment region, the moment in each girder was determined, including the contributions of composite action between the girder and the deck, when appropriate. The total moment in a transverse section of the bridge was determined by adding up the moments resisted by each of the girders. In most cases, the total measured moment was less than the moment applied to the bridge. The difference between the

total measured moment and the applied moment was accounted for by flexure of the portions of the deck which were not acting compositely with any girder.

Figure A-18 shows a detail of the stress profile in the deck, for the portions of the deck which were flexing in a noncomposite manner. The stress profile in the deck shows that the deck is flexing about its own center of gravity. Moreover, the compression and tension stress blocks work together to create a moment.

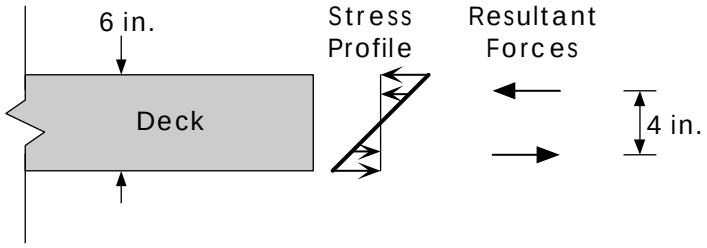

Figure A-18 Example of a Noncomposite Girder's Stress Profile and the Resultant Forces in the Bridge Deck

The magnitude of the noncomposite moment in the deck was determined using Equation A-35.

$$M_{deck} = M_{analysis} - \sum_{i=1}^{n} M_i \qquad \text{(A-35)}$$

where

M_{deck} is the noncomposite moment in the deck,

$M_{analysis}$ is the total moment applied to the bridge, by the test vehicle, as determined by analysis,

M_i is the moment measured in girder i, including possible contributions of composite action, and

n is the number of girders on the bridge.

Figure A-19 shows a sample bar graph of the stress distribution factors, girder moment distribution factors, and total moment distribution factors for all five girders and

the deck. Note that the first two distribution factors for the deck are zero, since the deck is not included in those calculations.

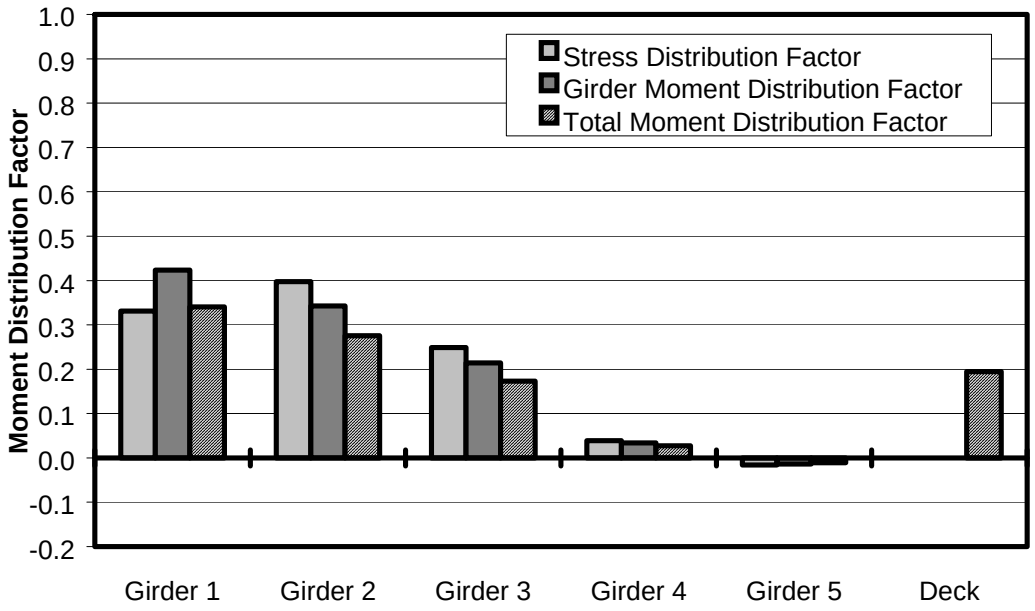

Figure A-19 Sample Bar Graph of the Stress, Girder Moment, and Total Moment Distribution Factors for All Five Girders and the Deck

In Figure A-19, girder 1 is behaving in a composite manner and the other four girders are behaving noncompositely. Therefore, girder 1 is stiffer than the other girders. As a result, the girder moment distribution factor for girder 1 is larger than the stress distribution factor. This trend is reversed in the other four girders.

The test truck was positioned on wheel line 2, over girder 2, when the data used to create Figure A-19 was recorded. Note that the stress distribution factor for girder 2 was the largest stress distribution factor, but the largest girder moment distribution factor occurred in girder 1. This shows that the composite behavior of individual girders can have a significant effect on the moment distribution behavior of the bridge.

The flexural participation of the deck also had a significant effect on the moment distribution behavior of the bridge. In Figure A-19, the deck carried almost 20 percent of

the applied moment, reducing the moment distribution factors for each of the girders by the same 20 percent.

A bar chart like Figure A-19 was plotted for every wheel line in both the positive and negative moment regions. These plots are shown in Chapter 5, as part of the test results.

A.11 Determining Two-Lane Moment Distribution Factors

During the field test, only one vehicle was placed on the bridge. However, the Big Creek Relief Bridge was load rated for two design lanes. Therefore, it was necessary to determine the moment distribution factors for each girder for a two-vehicle load.

During the field test, the 10 c.y. truck was placed on all five wheel lines, and moment distribution factors for each girder and each wheel line were determined. Two-lane moment distribution factors were determined from the single-vehicle moment distribution factors test data by superimposing the results from separate wheel lines.

The lateral position of each vehicle was adjusted in 1 inch increments until the maximum moment distribution factor for each girder was found. The positions of the vehicles were subject to the following rules, in accordance with the AASHTO LRFD code (1994a):

1. The bridge contained two design lanes.
2. One vehicle was placed in each design lane.
3. Each design lane was 12 feet wide, with no overlap.
4. The centerline of each wheel was placed no closer than 2 feet from the edges of the design lane.
5. The design lanes did not extend beyond either curb face.

When a vehicle was placed directly on one of the wheel lines, the lateral moment distribution factor for that vehicle was equal to the lateral moment distribution factor for that wheel line, as determined in the field test. When a vehicle was placed between any two wheel lines, the lateral moment distribution factor for that vehicle was determined by

linearly interpolating between the lateral moment distribution factors for the nearest two wheel lines. The two-lane lateral moment distribution factor was determined by adding together the lateral moment distribution factors for each vehicle.

For example, the single-lane lateral moment distribution factors for the positive moment region of span 3 on girder 3 are shown in Table A-8. The maximum lateral moment distribution factor was recorded when the test vehicle was on wheel line 3, and the other lateral moment distribution factors decreased as the test vehicle was positioned farther away from wheel line 3. Therefore, the largest two-lane lateral moment distribution factor occurred when both vehicles were positioned close to wheel line 3.

	Wheel Line 1	**Wheel Line 2**	**Wheel Line 3**	**Wheel Line 4**	**Wheel Line 5**
Girder 3 Single-Lane MDF's	.090	.173	.316	.221	.141

Table A-8 Single-Lane Moment Distribution Factors for Girder 3

Figure A-20 shows the design lane dimensions and vehicle positions resulting in the maximum two-lane lateral moment distribution factor for girder 3. The single-lane lateral moment distribution factors for each wheel line are also plotted in the figure.

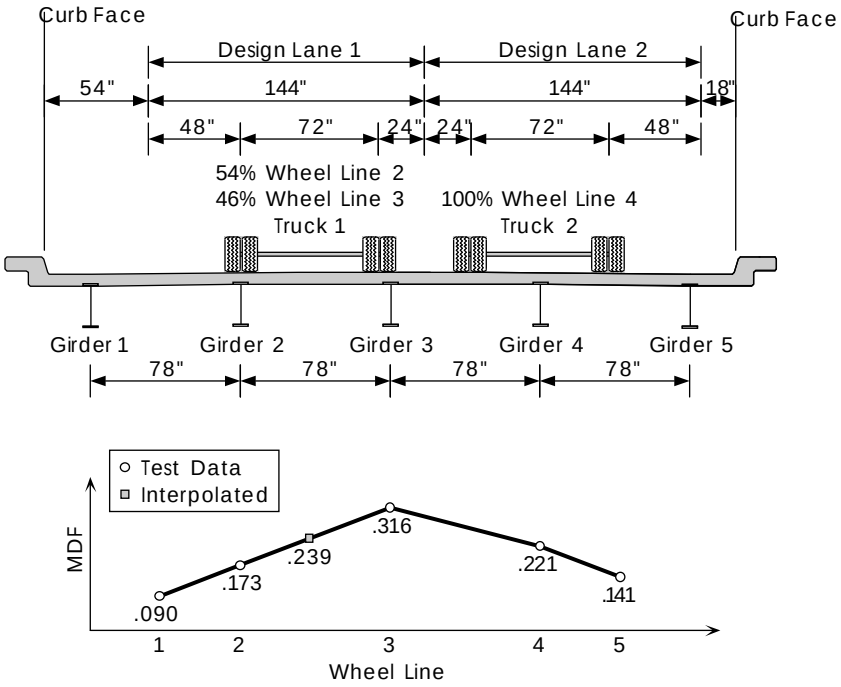

Figure A-20 Sample Two-Lane Truck Position Diagram, including the Corresponding Single-Lane Lateral Moment Distribution Factors

In this example, the maximum two-lane lateral moment distribution factor for girder 3 occurred when truck 2 was on wheel line 4 and truck 1 was between wheel lines 2 and 3. The two-lane lateral moment distribution factor for girder 3 was determined using Equations A-36 and A-37, the following equations:

$$MDF_{2-lane} = MDF_{truck1} + MDF_{truck2} \quad \text{(A-36)}$$

where

$MDF_{2\text{-}lane}$ is the two-lane lateral moment distribution factor,

MDF_{truck1} is the lateral moment distribution factor for truck 1, and

MDF_{truck2} is the lateral moment distribution factor for truck 2.

$$MDF_{truck} = \left(P_{left} \cdot MDF_{left}\right) + \left(P_{right} \cdot MDF_{right}\right) \quad \text{(A-37)}$$

where

MDF_{truck} is the lateral moment distribution factor for the truck under consideration,

P_{left} is the portion of the left wheel line's lateral moment distribution factor, based on the position of the truck,

P_{right} is the portion of the right wheel line's lateral moment distribution factor, based on the position of the truck,

MDF_{left} is the single-lane lateral moment distribution factor for the left wheel line, and

MDF_{right} is the single-lane lateral moment distribution factor for the right wheel line.

To complete this example, the two-lane moment distribution factor for span 3 on girder 3 was determined as follows:

$$MDF_{truck1} = (0.54 \cdot 0.173) + (0.46 \cdot 0.316) = 0.239$$

$$MDF_{truck2} = (1.00 \cdot 0.221) + (0.00 \cdot 0.141) = 0.221$$

$$MDF_{2-lane} = 0.239 + 0.221 = 0.460$$

The two-lane lateral moment distribution factor was found to be 0.460.

This procedure was followed for all of the two-lane lateral moment distribution factor calculations. However, when the lateral moment distribution factor for a wheel line was negative, due to reverse flexure of the deck, the contribution of that wheel line was neglected in Equation A-37. This modification prevented the two-lane lateral moment distribution factor from being less than the single lane moment distribution factor in a few instances.

APPENDIX B

Data Acquisition Hardware and Software

The data acquisition system used in the load tests of the Big Creek Relief Bridge is described in detail in this appendix. The electronic layout of the hardware and instrumentation is documented in section B.1. The software program used to control the datalogger is presented and explained in section B.2.

The information presented in this appendix is written with the assumption that the reader is already familiar with the Campbell Scientific model 21X datalogger and its operation. Prior reading of Post et al. (1988) is also highly recommended, since Post's data acquisition system, described therein, was salvaged for use in the load tests of the Big Creek Relief Bridge. However, the wiring of Post's system was substantially altered to take advantage of faster computer connections and better control software.

B.1 Data Acquisition System

Figure B-1 shows an overview of the data acquisition system. The Campbell Scientific model 21X datalogger is the heart of the system. The 21X is programmed and monitored using a PC compatible laptop computer. A communications cable links the laptop's serial port with the 21X unit. An SC32A optically isolated adapter is used to establish communication between the serial port on the laptop and the serial port on the 21X. The laptop is powered by a 120-volt generator, and the 21X is powered by a 12-volt deep-cycle marine battery. The gages and transducers on the bridge are excited externally using a 12-to-5-volt DC reducer.

The 21X, SC32A, and DC voltage reducer are contained in a protective field case. Connections to the field case are made using "military style" amphenol connectors. Weather resistant, durable, four-wire cable is used to connect the data channels on the field case with the transducers, full-bridge completion boxes, and vehicle position sensor. The completion boxes are positioned near the foil gages, to reduce errors from leadwire resistance.

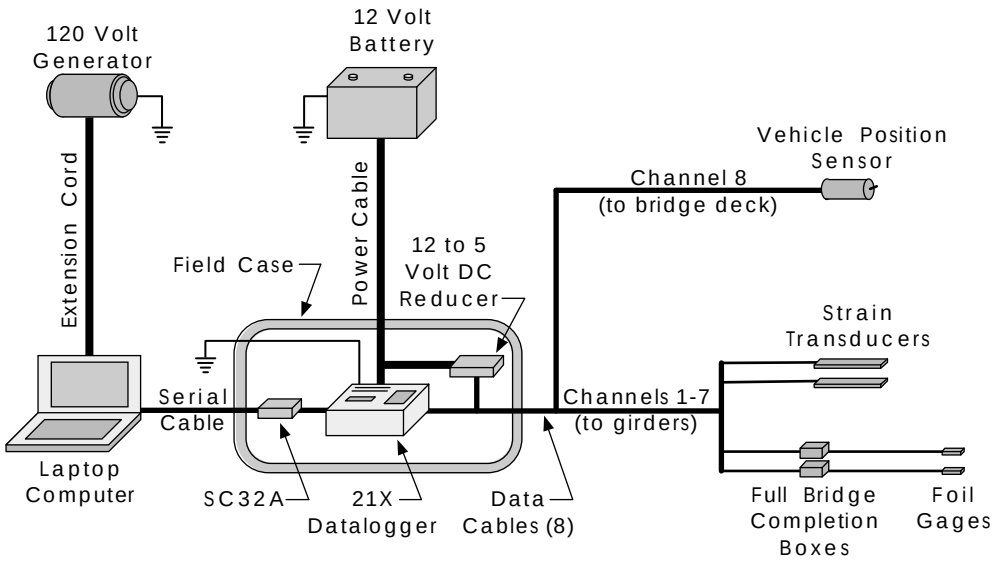

Figure B-1 Overview of the Data Acquisition System

The 120-volt generator, 12-volt battery, and 21X unit are all connected to the same ground lead. In the field, a wire-brushed 5-foot-long piece of #6 rebar was driven four feet into the ground, to establish a clean ground connection. The ground wires were connected to the rebar using alligator clips.

B.1.1 Field Case

The 21X datalogger, 12 to 5 volt DC transformer, and SC32A unit are installed in a protective field case. The case is made from 3/16 inch thick aluminum and measures 25 x 10 x 11 inches on the outside. The case protects the delicate electronics from severe weather and rough handling during testing. The top of the case is removable and bolts into place. The lid is oversized to provide ventilation for the heat produced by the electronics.

Figure B-2 shows a picture of the front of the field case. There are 8 five-pin amphenol plugs on the front of the case, used for connecting the gages, transducers and vehicle position sensor. Each amphenol plug is connected to one input channel on the

21X. The input channels are numbered sequentially from left to right, with channels 1 through 4 on the bottom row and channels 5 through 8 on the top row.

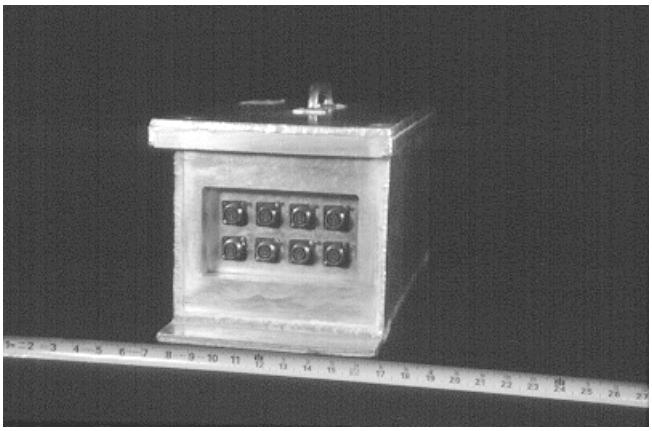

Figure B-2 Front View of the Field Case

Figure B-3 shows a picture of the back of the field case. Both of the lower plugs on the back side of the case are two-pin amphenol plugs for connecting the 12-volt batteries. The plugs are wired in parallel, so that a new battery can be 'switched in' without interrupting power to the unit. The upper plug is a five-pin amphenol plug for connecting the communication cable from the laptop to the SC32A unit.

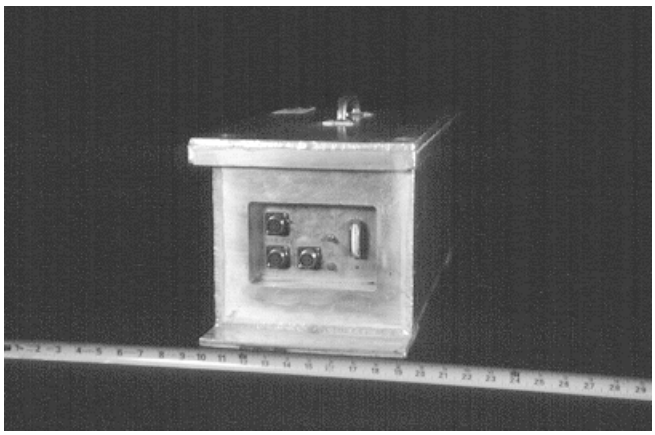

Figure B-3 Back View of the Field Case

Figure B-4 shows a diagram of the wiring in the 21X unit. The amphenol plugs on the front of the field case each contain five pins. Only four of the pins are used by the data acquisition system. In Figure B-4, the excitation and ground pins are labeled E+ and E-, respectively, and the high and low pins for the output signal are labeled H and L.

There are two terminal strips on the top of the 21X unit. On the upper terminal strip, each input channel is connected to one of the eight amphenol plugs on the front side of the field case. On the lower terminal strip, the power supply terminals are connected to both of the two-pin plugs on the back of the field case.

The 12-to-5-volt DC reducer is wired in parallel with the 21X's power supply. The reducer supplies 5 volts of power, in parallel, to all of the amphenol plugs on the front of the field case. The ground leads on the 5 volt and 12 volt sides of the reducer are connected to stabilize the ground potential of the gage circuits.

The circuit containing the 21X's serial port and the SC32A is not directly connected to the rest of the wiring in the field case. The only link between the two circuits is that they share a common ground potential through the ground wires on the 21X and the laptop. The 9-pin male port on the SC32A unit is connected to the 9-pin female port on the 21X using a straight-through 9-pin serial cable with one male and one female end. The connection between the SC32A and the laptop is more complicated. Table B-1 presents a pinout diagram for the connections from the 25-pin male connector on the SC32A to the 9-pin male serial port on the laptop.

Pin Assignment	SC32A 25-Pin Connector	9-Pin Serial Port (RS232)
Receive	3	2
Transmit	2	3
Data Terminal Ready	20	4
Ground	7	5

Table B-1 Serial Port Pinout Diagram for the SC32A Connection

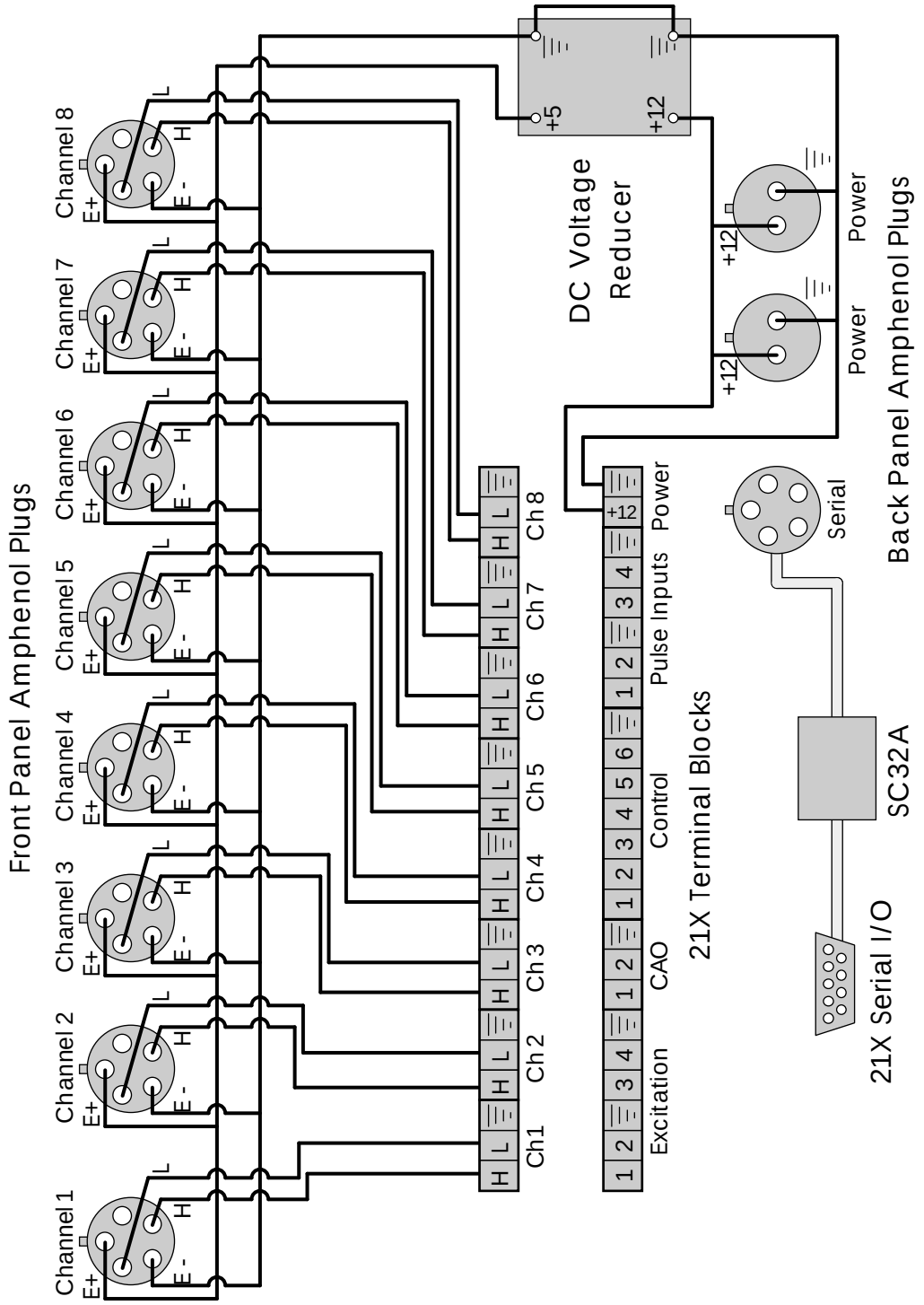

Figure B-4 Field Case Wiring Diagram

B.1.2 Vehicle Position Sensor

The test vehicle's position was recorded by shorting out the 5-volt excitation signal to the 21X when the test vehicle crossed each bearing line on the bridge. This was accomplished using a device called the vehicle position sensor, or VPS. The VPS is a weatherproof PVC tube, housing a double-pole double-throw switch on one end and a five-pin amphenol plug on the other. It is connected to channel 8 on the datalogger, using the same data cables as the gages and transducers. Figure B-5 shows a wiring diagram for the VPS circuit.

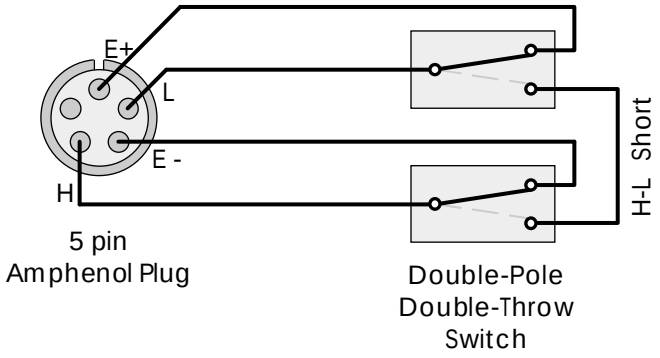

Figure B-5 Vehicle Position Switch Wiring Diagram

The switch on the VPS is spring-loaded. It returns to the position shown in Figure B-5 when released. In the released position, the excitation leads are connected to the high and low leads for input channel 8. This allows the 21X to record the excitation voltage in the circuit. When the switch is pressed, the high and low leads are shorted together, and the 21X reads zero volts on channel 8.

The excitation leads are not connected to each other in the circuit, so the VPS has an extremely high resistance (corresponding to the resistance of the 21X input channel) and does not draw current from the 5-volt external power source. Therefore, the position of the switch does not change the current demand on the circuit or the excitation voltage to the gages and transducers.

B.1.3 Full-Bridge Completion Boxes

Full-bridge completion boxes were used to complete the wheatstone bridge circuit for the foil gages. Each completion box contains three precision 120 ±0.012 ohm resistors, and is designed to attach to a three-wire lead from a 120-ohm foil gage. The completion boxes only support the use of 120-ohm foil gages. Figure B-6 shows a diagram of the completion box circuit, including an attached foil gage.

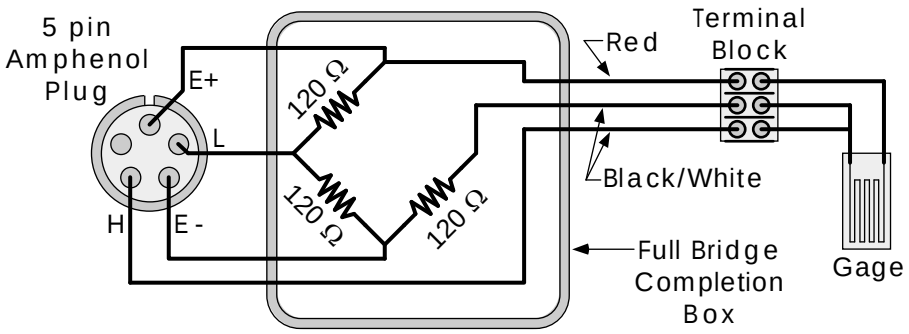

Figure B-6 120-Ohm Full-Bridge Completion Box Wiring Diagram

The completion boxes are sealed to protect the electronics from moisture. On one end of the completion box, the bridge circuit is wired to a 5-pin amphenol plug. This plug connects to the data cables coming from the field case. On the other end of the box, three terminals connect the completion box to the three-wire foil gages. The red wire connects to the single-wire side of the gage.

B.1.4 Transducers

The transducers contain a 350-ohm full-bridge circuit and do not require the use of a completion box. A five-pin amphenol plug is wired into the transducer's full-bridge circuit. The transducers connect directly to the field case, using the same data cables as the completion boxes and vehicle position sensor. The full-bridge circuit and five-pin connection is shown in Figure B-7.

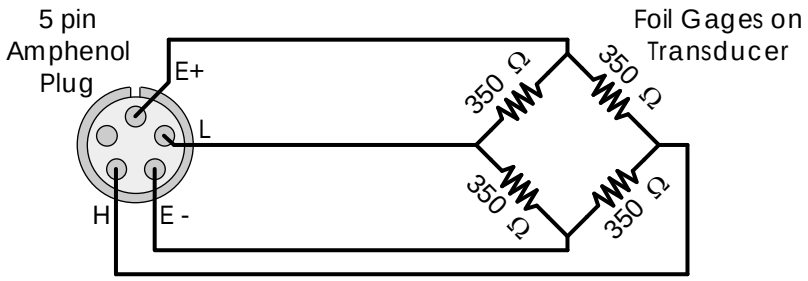

Figure B-7 350-Ohm Full-Bridge Transducer Wiring Diagram

B.1.5 Data Cables

Fifteen weatherproof data cables were made for use with this data acquisition system. The cables connect the transducers, foil gages, and vehicle position sensor to the data channels on the front of the field case, using the five-pin amphenol plugs. All of the cables are interchangeable, and they consist of three different lengths: 4 ninety-two foot cables, 10 fifty foot cables, and 1 thirty-five foot cable.

The male end of the data cable connects to the field case, and the female end connects to the completion box, transducer, or vehicle position sensor. The data cables are labeled A through O on both ends to reduce confusion in the field. Letters were chosen to differentiate the cable names from the 21X input channel numbers.

B.1.6 Battery Boxes

A pair of twelve-volt deep-cycle marine batteries are used to power the 21X datalogger and instrumentation. The batteries are contained in weatherproof aluminum cases, similar to the 21X field case. Each battery case measures 20 x 14 x 11 inches on the outside. A power cable connects each battery to the power plugs on the back of the 21X field case. Only one battery is needed at a time. The other battery can be recharged and 'switched in,' by attaching it to the other power plug on the field case. This way, constant power can be supplied to the 21X, allowing it to run indefinitely. Inside the battery box, a 0.5 amp fuse is connected to the positive battery terminal. The fuse protects the 21X from excess current.

B.2 21X Data Acquisition Program

The 21X was controlled using a PC-compatible laptop computer. The software program PC208E, supplied with the 21X unit, was used to establish communication with the 21X, upload the data acquisition program, control the data acquisition program, and download the test data. The 21X data acquisition program is explained in this section. The operation of the PC208E program itself is explained in the documentation provided with the 21X. It is assumed that the reader is familiar with the basic operation of the 21X unit and the PC208E program.

B.2.1 Program Tables

The data acquisition program is organized around two modes of operation. In mode 1, zeroed data is recorded from the gages. This mode is used to collect data during the load test. In mode 2, baseline data is measured for each gage and used to determine a zero reading for each gage. This mode is used before each pass to re-zero the gages.

In the 21X's memory, the data acquisition program's code is contained in memory blocks called program tables, numbered 1 through 3. The code for mode 1, data acquisition, is stored in program table 1, and the code for mode 2, zeroing, is stored in program table 2. Program tables 1 and 2 call many subroutines, stored in program table 3. Table B-2 presents a summary of the 21X's program tables.

Table	Content
1	Mode 1: data acquisition code
2	Mode 2: gage zeroing code
3	Subroutine code

Table B-2 21X Program Tables

B.2.2 User Flags and Program Operation

The user interacts with the data acquisition program by toggling the value of eight user flags, using the PC208E communication program on the laptop computer.

Table B-3 presents a description of each user flag. The flags can be set either 'high' or 'low.' Most of the flags specify no action when set low, except for flag 5.

Flag	Toggle
1	Record data continuously from the gages when **high**.
2	Record four samples of data from the gages when **high**.
3	Normalize the voltage data when **high**.
4	Zero the voltage data when **high**.
5	Bypass program table 1 when **high**, and bypass program table 2 when **low**.
6	Measure the gage zeros when **high**.
7	Check the 21X battery voltage when **high**.
8	Hold the gage output when **high**.

Table B-3 21X Program Control Flags

After uploading the data acquisition program to the 21X, all of the user flags are initially set low. Therefore, program table 1 is running, the gages are being read, no zeroing is taking place, and no data is being recorded. Before recording data, zero readings for each gage must be determined.

In order to zero the gages, set flag 5 high and then set flag 6 high. The 21X will execute program table 2 and record zero readings for each gage. At this point, flag 6 will return to low. The average, maximum and minimum values for ten readings on each channel have now been recorded. The range between the maximum and minimum

readings can be examined to evaluate the level of electronic noise in the system. Set flag 5 low to return to data acquisition mode.

Before recording data, set flag 4 high to zero the data. To begin recording data, set flag 1 high. The 21X will record data for all eight channels at a rate of 16 hertz per channel. Set flag 1 low to stop recording data. Download the data to the laptop between each pass: the 21X does not have enough memory to hold more than 1 pass of data at a time, and it will overwrite the oldest data in its memory with no warning.

When flag 5 is low and no data is being recorded, set flag 7 high to check the voltage from the marine battery. This voltage should not be allowed to drop below 10.5 volts, or the 21X may behave erratically and even turn off.

Flags 2, 3, and 8 were used during program development. They are still operational, but may only provide limited utility during a load test.

B.2.3 Memory Allocation

While the 21X is running the data acquisition program, voltage data and program variables are stored in sixty-five memory locations. Table B-4 presents a summary of these variables.

The PC208E program can display the values stored in any of the 21X's memory locations in "real time." During the load test, memory locations 1 through 8, and 10 should be displayed. This allows the computer operator to continuously monitor the gage output and battery voltage. During the gage zeroing process, memory locations 11 through 18, 21 through 28, and 31 through 38 should be displayed, allowing the computer operator to check for electronic noise in the system.

Memory Location	Assignment
1-7	Output voltage from channels 1 through 7.
8	Input voltage from channel 8.
9	Reciprocal of the input voltage.
10	2 uses: (1) gage pointer, used during zeroing, and (2) battery voltage.
11-17	Gage zeros: average baseline values from channels 1 through 7.
18	Average baseline value from channel 8.
19	Not used.
20	Statistical memory pointer.
21-28	Minimum baseline values from channels 1 through 8.
29	Not used.
30	Baseline data memory pointer.
31-38	Maximum baseline values from channels 1 through 8.
39	Not used.
40	Sample data counter.
41-48	Hold data from channels 1 through 8.
49	Hold data counter.
50-59	Baseline statistical data.
60	Average value result.
61	Average value pointer.
62	Minimum value result.
63	Minimum value pointer.
64	Maximum value result.
65	Maximum value pointer.

Table B-4 21X Program Memory Assignments

B.2.4 Execution Intervals

In the 21X unit, program execution is clocked in 0.0125 second units (1/80 of a second). Therefore, the code in program tables 1 and 2 is executed over and over in some multiple of 0.0125 seconds. For the data acquisition program, program table 1 is executed every 0.0625 seconds (5/80 of a second), and program table 2 is executed every 2 seconds.

Program execution intervals are specified in the code for program tables 1 and 2. The execution interval for table 2 is specified as 2 seconds, as expected. However, the execution interval for program table 1 is specified as 0.0125 seconds, even though the code takes almost 0.0625 seconds to run. Therefore, program 1 overruns its 0.0125 second execution interval and restarts on the next available clock tick. Overrunning the 0.0125 second interval always produced a sample rate of 16 hertz, while setting the execution interval to 0.0625 seconds produced varying sample rates from 15.5 hertz to 16 hertz. This indicated that overrunning the 0.0125 second interval was a more stable method of program execution, since the sample rate was the same every time. No explanation was found for this phenomenon.

B.2.5 Data Acquisition Program Code

Annotated code for the data acquisition program is presented below. A commentary is provided to aid in understanding the program flow. The 21X code is presented in .CSI format, the format used by EDLOG, the editor provided with the PC208E communications program. EDLOG can be used to convert the .CSI files to the .DLD file format used by PC208E and the 21X.

The most common modification to the data acquisition program is to adjust the voltage range for each channel to correct for the different output levels from different types of instrumentation, such as removable strain transducers. This can be done by modifying the read differential voltage instructions, contained in subroutine 9 in program table 3. However, adding additional differential voltage instructions may increase the program's execution time and thereby reduce the sample rate below 16 hertz per channel.

21X Code

```
*Table 1 Program
 01: .0125      Execution Interval (sec.)

1:  If Flag/Port (P91)
 1: 15       Do if Flag 5 is High
 2: 0        Go to end of Program Table

2:  If Flag/Port (P91)
 1: 11       Do if Flag 1 is High
 2: 22       Set Flag 2 Low

3:  If Flag/Port (P91)
 1: 11       Do if Flag 1 is High
 2: 23       Set Flag 3 Low

4:  If Flag/Port (P91)
 1: 11       Do if Flag 1 is High
 2: 28       Set Flag 8 Low

5:  If Flag/Port (P91)
 1: 12       Do if Flag 2 is High
 2: 23       Set Flag 3 Low

6:  If Flag/Port (P91)
 1: 12       Do if Flag 2 is High
 2: 28       Set Flag 8 Low

7:  If Flag/Port (P91)
 1: 16       Do if Flag 6 is High
 2: 26       Set Flag 6 Low


8:  If Flag/Port (P91)
 1: 28       Do if Flag 8 is Low
 2: 30       Then Do

    9:  Z=F (P30)
     1: 0.0      F
     2: 49       Z Loc [H_RepC]

    10:  Do (P86)
     1: 9        Call Subroutine 9

    11:  If Flag/Port (P91)
     1: 14       Do if Flag 4 is High
     2: 4        Call Subroutine 4
```

Comments

Begin table 1.

Skip the rest of table 1 if flag 5 is high.

In order to record data at 16 hertz, the amount of processing had to be kept to a minimum. Therefore, when flag 1 is high, and data is being recorded continuously, the data sample, normalize, and hold functions are switched off by setting their flags low.

The same procedure is followed for flag 2, however, the record continuous data option (flag 1) takes precedence over the sample data option (flag 2).

Flag 6 is used to run the statistical subroutine that determines the zero reading for each gage. This feature is only used in table 2.

If flag 8 is low and data gathering is not on hold, then...

set the data hold counter to zero,

read all eight channels,

zero the data on channels 1 through 7, and

21X Code	Comments
12: If Flag/Port (P91) 1: 13 Do if Flag 3 is High 2: 3 Call Subroutine 3	normalize the data on channels 1 through 7.
13: End (P95)	
14: If Flag/Port (P91) 1: 18 Do if Flag 8 is High 2: 8 Call Subroutine 8	If flag 8 is high, hold data gathering.
15: If Flag/Port (P91) 1: 17 Do if Flag 7 is High 2: 7 Call Subroutine 7	If flag 7 is high, read the battery voltage.
16: If Flag/Port (P91) 1: 11 Do if Flag 1 is High 2: 1 Call Subroutine 1	If flag 1 is high, write the current voltage data to final storage.
17: If Flag/Port (P91) 1: 12 Do if Flag 2 is High 2: 2 Call Subroutine 2	If flag 2 is high, write the current voltage data to final storage.
	End table 1.
*Table 2 Program 02: 2.0 Execution Interval (sec.)	Begin table 2.
1: If Flag/Port (P91) 1: 25 Do if Flag 5 is Low 2: 0 Go to end of Program Table	Skip the rest of table 2 if flag 5 is low.
2: If Flag/Port (P91) 1: 15 Do if Flag 5 is High 2: 21 Set Flag 1 Low	Turn off data recording, normalizing, zeroing, battery read, and data hold.
3: If Flag/Port (P91) 1: 15 Do if Flag 5 is High 2: 22 Set Flag 2 Low	
4: If Flag/Port (P91) 1: 15 Do if Flag 5 is High 2: 23 Set Flag 3 Low	
5: If Flag/Port (P91) 1: 15 Do if Flag 5 is High 2: 24 Set Flag 4 Low	

21X Code	Comments
6: If Flag/Port (P91) 1: 15 Do if Flag 5 is High 2: 27 Set Flag 7 Low	
7: If Flag/Port (P91) 1: 15 Do if Flag 5 is High 2: 28 Set Flag 8 Low	
8: Z=F (P30) 1: 60 F 2: 61 Z Loc [Z_AvgP]	Set average, minimum, and maximum pointers. They keep track of where the current results of the average, maximum, and minimum value calculations are stored.
9: Z=F (P30) 1: 62 F 2: 63 Z Loc [Z_MinP]	
10: Z=F (P30) 1: 64 F 2: 65 Z Loc [Z_MaxP]	
11: If Flag/Port (P91) 1: 16 Do if Flag 6 is High 2: 30 Then Do	If flag 6 is high, get new zeroes for each channel.
12: Z=F (P30) 1: 0 F 2: 10 Z Loc [Z_GageP]	Set the gage pointer equal to zero.
13: Beginning of Loop (P87) 1: 0 Delay 2: 8 Loop Count	Loop eight times, one time for each channel.
14: Z=Z+1 (P32) 1: 10 Z Loc [Z_GageP]	Increment the gage pointer.
15: Z=F (P30) 1: 50 F 2: 20 Z Loc [Z_StatP]	Set the statisistical pointer to memory location 50.
16: Beginning of Loop (P87) 1: 0 Delay 2: 10 Loop Count	Loop ten times, one time for each voltage measurement.
17: Do (P86) 1: 9 Call Subroutine 9	Read the voltage on all eight channels.

21X Code

```
   18:  Indirect Move (P61)
    1: 10      Source Loc [Z_GageP]
    2: 20      Destination Loc [Z_StatP]


   19:  Z=Z+1 (P32)
    1: 20      Z Loc [Z_StatP]

20:  End (P95)



21:  Z=X+F (P34)
 1: 10      X Loc [Z_GageP]
 2: 10      F
 3: 30      Z Loc [Z_DataP]

22:  Spatial Average (P51)
 1: 10      Swath
 2: 50      First Loc [Stat1]
 3: 60      Avg Loc [Z_AvgV]

23:  Indirect Move (P61)
 1: 61      Source Loc [Z_AvgP]
 2: 30      Destination Loc [Z_DataP]


24:  Z=X+F (P34)
 1: 10      X Loc [Z_GageP]
 2: 20      F
 3: 30      Z Loc [Z_DataP]

25:  Spatial Mimimum (P50)
 1: 10      Swath
 2: 50      First Loc [Stat1]
 3: 62      Min Option [Z_MinV]

26:  Indirect Move (P61)
 1: 63      Source Loc [Z_MinP]
 2: 30      Destination Loc [Z_DataP]


27:  Z=X+F (P34)
 1: 10      X Loc [Z_GageP]
 2: 30      F
 3: 30      Z Loc [Z_DataP]
```

Comments

Move the value stored in the location specified by the gage pointer to the location specified by the statistical pointer

Increment the statistical pointer

End the inner loop. At this point ten values from the gage specified by the gage pointer are stored in memory locations 50 through 59.

Set the data pointer to the gage pointer's value plus 10.

Calculate the average value of memory locations 50 through 59 and store in memory location 60.

Move the value in the location specified by the average value pointer to the location specified by the data pointer.

Set the data pointer to the gage pointer's value plus 20.

Calculate the minimum value of memory locations 50 through 59 and store in memory location 62.

Move the value in the location specified by the minimum value pointer to the location specified by the data pointer.

Set the data pointer to the gage pointer's value plus 30.

21X Code	Comments
28: Spatial Maximum (P49) 1: 10 Swath 2: 50 First Loc [Stat1] 3: 64 Max Option [Z_MaxV]	Calculate the maximum value of memory locations 50 through 59 and store in memory location 64.
29: Indirect Move (P61) 1: 65 Source Loc [Z_MaxP] 2: 30 Destination Loc [Z_DataP]	Move the value in the location specified by the maximum value pointer to the location specified by the data pointer.
30: End (P95)	End the outer loop. At this point data from each gage has been read in series.
31: Do (P86) 1: 26 Set Flag 6 Low	Stop calculating zeroes for each channel.
32: End (P95)	End if flag 6 is high, then calculate zeros.
	End Table 2.
*Table 3 Subroutines	Begin Table 3.
1: Beginning of Subroutine (P85) 1: 1 Subroutine 1	Begin Subroutine 1.
2: If Flag/Port (P91) 1: 14 Do if Flag 4 is High 2: 30 Then Do	If zeroing is turned on, turn on the output flag in line 303, so that 303 is written to the first column of the data file.
3: Do (P86) 1: 10 Set Output Flag High	
4: End (P95)	
5: If Flag/Port (P91) 1: 24 Do if Flag 4 is Low 2: 30 Then Do	If zeroing is turned off, turn on the output flag in line 306, so that 306 is written to the first column of the data file.
6: Do (P86) 1: 10 Set Output Flag High	
7: End (P95)	

21X Code

```
    8:  Sample (P70)
     1: 8        Reps
     2: 1        Loc [EOut_1]

9:  End (P95)

10:  Beginning of Subroutine (P85)
 1: 2        Subroutine 2

    11:  If Flag/Port (P91)
     1: 14       Do if Flag 4 is High
     2: 30       Then Do

        12:  Do (P86)
         1: 10       Set Output Flag High

    13:  End (P95)

    14:  If Flag/Port (P91)
     1: 24       Do if Flag 4 is Low
     2: 30       Then Do

        15:  Do (P86)
         1: 10       Set Output Flag High

    16:  End (P95)

    17:  Sample (P70)
     1: 8        Reps
     2: 1        Loc [EOut_1]

    18:  Z=Z+1 (P32)
     1: 40       Z Loc [Sample_C]

    19:  IF (X<=>F) (P89)
     1: 40       X Loc [Sample_C]
     2: 3        >=
     3: 4        F
     4: 30       Then Do

        20:  Do (P86)
         1: 22       Set Flag 2 Low

        21:  Z=F (P30)
         1: 0        F
         2: 40       Z Loc [Sample_C]

22:  End (P95)
```

Comments

Write the current voltage data from channels 1 through 8 to final storage.

End subroutine 1.

Begin subroutine 2.

If zeroing is turned on, turn on the output flag in line 312, so that 312 is written to the first column of the data file.

If zeroing is turned off, turn on the output flag in line 315, so that 315 is written to the first column of the data file.

Write the current voltage data from channels 1 through 8 to final storage.

Increment the sample counter.

If four samples have been recorded...

set flag 2 low to turn off recording, and

reset the sample counter.

23: End (P95)

24: Beginning of Subroutine (P85)
1: 3 Subroutine 3

25: Z=1/X (P42)
1: 8 X Loc [EInput]
2: 9 Z Loc [R_EInput]

26: Z=X*Y (P36)
1: 1 X Loc [EOut_1]
2: 9 Y Loc [R_EInput]
3: 1 Z Loc [EOut_1]

27: Z=X*Y (P36)
1: 2 X Loc [EOut_2]
2: 9 Y Loc [R_EInput]
3: 2 Z Loc [EOut_2]

28: Z=X*Y (P36)
1: 3 X Loc [EOut_3]
2: 9 Y Loc [R_EInput]
3: 3 Z Loc [EOut_3]

29: Z=X*Y (P36)
1: 4 X Loc [EOut_4]
2: 9 Y Loc [R_EInput]
3: 4 Z Loc [EOut_4]

30: Z=X*Y (P36)
1: 5 X Loc [EOut_5]
2: 9 Y Loc [R_EInput]
3: 5 Z Loc [EOut_5]

31: Z=X*Y (P36)
1: 6 X Loc [EOut_6]
2: 9 Y Loc [R_EInput]
3: 6 Z Loc [EOut_6]

32: Z=X*Y (P36)
1: 7 X Loc [EOut_7]
2: 9 Y Loc [R_EInput]
3: 7 Z Loc [EOut_7]

33: End (P95)

34: Beginning of Subroutine (P85)

Comments

End subroutine 2.

Begin subroutine 3.

Calculate the reciprocal of the input voltage on channel 8.

Multiply the output voltages on channels 1 through 7 by the reciprocal of the input voltage. Multiplying is much faster than dividing. This step saves about 7.9 milliseconds, reducing the program's execution time by 13 percent.

End subroutine 3.

Begin subroutine 4.

21X Code	Comments
35: Z=X-Y (P35) 1: 1 X Loc [EOut_1] 2: 11 Y Loc [AVG_1] 3: 1 Z Loc [EOut_1]	Zero the output voltage data on channels 1 through 7 by subtracting the zero reading for each channel.
36: Z=X-Y (P35) 1: 2 X Loc [EOut_2] 2: 12 Y Loc [AVG_2] 3: 2 Z Loc [EOut_2]	
37: Z=X-Y (P35) 1: 3 X Loc [EOut_3] 2: 13 Y Loc [AVG_3] 3: 3 Z Loc [EOut_3]	
38: Z=X-Y (P35) 1: 4 X Loc [EOut_4] 2: 14 Y Loc [AVG_4] 3: 4 Z Loc [EOut_4]	
39: Z=X-Y (P35) 1: 5 X Loc [EOut_5] 2: 15 Y Loc [AVG_5] 3: 5 Z Loc [EOut_5]	
40: Z=X-Y (P35) 1: 6 X Loc [EOut_6] 2: 16 Y Loc [AVG_6] 3: 6 Z Loc [EOut_6]	
41: Z=X-Y (P35) 1: 7 X Loc [EOut_7] 2: 17 Y Loc [AVG_7] 3: 7 Z Loc [EOut_7]	
42: End (P95)	End subroutine 4.
43: Beginning of Subroutine (P85) 1: 7 Subroutine 7	Begin subroutine 7.
44: Batt Voltage (P10) 1: 10 Loc [Z_GageP]	Check battery voltage.
45: Do (P86) 1: 27 Set Flag 7 Low	Set flag 7 low.
46: End (P95)	End subroutine 7.

1: 9 Call Subroutine 9

47: Beginning of Subroutine (P85)
1: 8 Subroutine 8

48: IF (X<=>F) (P89)
1: 49 X Loc [H_RepC]
2: 1 =
3: 0 F
4: 30 Then Do

49: Z=F (P30)
1: 0.0 F
2: 41 Z Loc [Hold_1]

50: Z=F (P30)
1: 0.0 F
2: 42 Z Loc [Hold_2]

51: Z=F (P30)
1: 0.0 F
2: 43 Z Loc [Hold_3]

52: Z=F (P30)
1: 0.0 F
2: 44 Z Loc [Hold_4]

53: Z=F (P30)
1: 0.0 F
2: 45 Z Loc [Hold_5]

54: Z=F (P30)
1: 0.0 F
2: 46 Z Loc [Hold_6]

55: Z=F (P30)
1: 0.0 F
2: 47 Z Loc [Hold_7]

56: Z=F (P30)
1: 0.0 F
2: 48 Z Loc [Hold_8]

57: Beginning of Loop (P87)
1: 0 Delay
2: 4 Loop Count

58: Do (P86)

Comments

Begin subroutine 8.

If the hold counter is equal to zero, reset the hold data memory locations and start the collect-new-hold-data routine.

Begin data collection loop. All eight channels are read four times and the sum of the readings is stored in the hold data memory locations.

Read all eight channels.

21X Code	Comments
59: Z=X+Y (P33) 1: 41 X Loc [Hold_1] 2: 1 Y Loc [EOut_1] 3: 41 Z Loc [Hold_1]	
60: Z=X+Y (P33) 1: 42 X Loc [Hold_2] 2: 2 Y Loc [EOut_2] 3: 42 Z Loc [Hold_2]	
61: Z=X+Y (P33) 1: 43 X Loc [Hold_3] 2: 3 Y Loc [EOut_3] 3: 43 Z Loc [Hold_3]	
62: Z=X+Y (P33) 1: 44 X Loc [Hold_4] 2: 4 Y Loc [EOut_4] 3: 44 Z Loc [Hold_4]	
63: Z=X+Y (P33) 1: 45 X Loc [Hold_5] 2: 5 Y Loc [EOut_5] 3: 45 Z Loc [Hold_5]	
64: Z=X+Y (P33) 1: 46 X Loc [Hold_6] 2: 6 Y Loc [EOut_6] 3: 46 Z Loc [Hold_6]	
65: Z=X+Y (P33) 1: 47 X Loc [Hold_7] 2: 7 Y Loc [EOut_7] 3: 47 Z Loc [Hold_7]	
66: Z=X+Y (P33) 1: 48 X Loc [Hold_8] 2: 8 Y Loc [EInput] 3: 48 Z Loc [Hold_8]	
67: End (P95)	End data collection loop.
68: Z=X*F (P37) 1: 41 X Loc [Hold_1] 2: 0.25 F 3: 41 Z Loc [Hold_1]	Calculate the average of the four readings on each channel by multiplying the values in the hold data memory locations by 0.25.

21X Code	Comments
69: Z=X*F (P37) 1: 42 X Loc [Hold_2] 2: 0.25 F 3: 42 Z Loc [Hold_2]	
70: Z=X*F (P37) 1: 43 X Loc [Hold_3] 2: 0.25 F 3: 43 Z Loc [Hold_3]	
71: Z=X*F (P37) 1: 44 X Loc [Hold_4] 2: 0.25 F 3: 44 Z Loc [Hold_4]	
72: Z=X*F (P37) 1: 45 X Loc [Hold_5] 2: 0.25 F 3: 45 Z Loc [Hold_5]	
73: Z=X*F (P37) 1: 46 X Loc [Hold_6] 2: 0.25 F 3: 46 Z Loc [Hold_6]	
74: Z=X*F (P37) 1: 47 X Loc [Hold_7] 2: 0.25 F 3: 47 Z Loc [Hold_7]	
75: Z=X*F (P37) 1: 48 X Loc [Hold_8] 2: 0.25 F 3: 48 Z Loc [Hold_8]	
76: Block Move (P54) 1: 8 No. of Values 2: 41 First Source Loc [Hold_1] 3: 1 Source Step 4: 1 First Destination Loc [EOut_1] 5: 1 Destination Step	Move the values in the hold data memory locations to the channel 1 through 8 memory locations.
77: If Flag/Port (P91) 1: 14 Do if Flag 4 is High 2: 4 Call Subroutine 4	Zero the data on channels 1 through 7.

21X Code	Comments
78: If Flag/Port (P91) 1: 13 Do if Flag 3 is High 2: 3 Call Subroutine 3	Normalize the data on channels 1 through 7.
79: Z=F (P30) 1: 1 F 2: 49 Z Loc [H_RepC]	Set the hold counter equal to 1 so that no new data will be read until the user turns off hold.
80: End (P95)	End the collect new hold data routine.
81: End (P95)	End subroutine 8.
82: Beginning of Subroutine (P85) 1: 9 Subroutine 9	Begin subroutine 9.
83: Volt (Diff) (P2) 1: 7 Reps 2: 12 15 mV Fast Range 3: 1 In Chan 4: 1 Loc [EOut_1] 5: 1.0 Mult 6: 0.0 Offset	Read channels 1 through 7 on a ±15 millivolt range. This range is valid for the foil gages only. For the removable strain transducers, use the ±50 millivolt range. Note that these ranges apply to the raw channel voltages, not to the zeroed or the normalized voltages.
84: Volt (Diff) (P2) 1: 1 Reps 2: 15 5000 mV Fast Range 3: 8 In Chan 4: 8 Loc [EInput] 5: 0.001 Mult 6: 0.0 Offset	Read channel 8 on a ±5000 millivolt range, because channel 8 is carrying the 5-volt excitation signal.
85: End (P95)	End subroutine 9.
	End program table 3.
End Program	End data acquisition program.

REFERENCES

American Concrete Institute, Committee 318 (ACI-318). 1995. *Building code requirements for structural concrete and commentary.* ACI 318-95. Farmington Hills, Mich.: American Concrete Institute.

American Institute of Steel Construction (AISC). 1953. *AISC iron and steel beams catalog.* Chicago: American Institute of Steel Construction.

American Institute of Steel Construction (AISC). 1994. *Load & resistance factor design.* 2nd Ed. Vol. 1. Chicago: American Institute of Steel Construction.

American Association of Highway Transportation Officials (AASHTO). 1992. *Standard specifications for highway bridges.* 15th Ed. Washington D.C.: American Association of Highway Transportation Officials.

American Association of Highway Transportation Officials (AASHTO). 1994a. *AASHTO LRFD bridge design specifications.* U.S. Customary Units 1st Ed. Washington D.C.: American Association of Highway Transportation Officials.

American Association of Highway Transportation Officials (AASHTO). 1994b. *Manual for condition evaluation of bridges.* Washington D.C.: American Association of Highway Transportation Officials.

Bakht, B., and L. G. Jaeger. 1990. Bridge testing ✂ a surprise every time. *Journal of Structural Engineering* 116(5): 1370-83.

Burdette, E.G., and D. W. Goodpasture. 1988. *Correlation of bridge load capacity estimates with test data.* NCHRP report 306. Washington D.C.: Transportation Research Board, National Research Council.

Chajes, M. J., D. R. Mertz, and B. Commander. 1997. Experimental load rating of a posted bridge. *Journal of Bridge Engineering* 2(1): 1-10.

Commander, B. C. 1989. An improved method of bridge evaluation: comparison of field test results with computer analysis. Master's thesis, University of Colorado at Boulder.

Commander, B. C., M. M. McMullen, and M. Mohseni. 1994. An integrated approach to load rating. In *Proceedings of the 11th annual international bridge conference.* IBC-94-63: 1-7. Pittsburgh, Pa.: Engineers' Society of Western Pennsylvania.

Jauregui, D. 1999. Load Testing of Highway Bridges. Ph.D. diss., University of Texas at Austin.

Lichtenstein, A. G. 1993. *Bridge rating through nondestructive load testing.* NCHRP project 12-28(13)A, final draft. Washington D.C.: Transportation Research Board, National Research Council.

Moses, F., and D. Verma. 1987. *Load capacity evaluation of existing bridges.* NCHRP report 301. Washington D.C.: Transportation Research Board, National Research Council.

Pinjarkar, S. G., O. C. Gudelhofer, B. J. Smith, and R. W. Kritzler. 1990. *Nondestructive load testing for bridge evaluation and rating.* NCHRP project 12-28(13), final report. Washington D.C.: Transportation Research Board, National Research Council.

Post, G. Jeff, Karl H. Frank, and Bahram (Alec) Tahmassebi. 1988. *Estimating residual fatigue life of bridges.* CTR research report 464-1F. Austin, Tx.: Center for Transportation Research, Bureau of Engineering Research, University of Texas at Austin.

Rabbat, B. G., and H. G. Russell. 1985. Friction coefficient of steel on concrete or grout. *Journal of Structural Engineering* 111(3): 505-15.

Salmon, Charles G., and John E. Johnson. 1990. *Steel structures: design and behavior.* 3rd Ed. New York: Harper Collins.

Schultz, J. L., B. Commander, G. G. Goble, and D. M. Frangopol. 1995. Efficient field testing and load rating of short and medium span bridges. *Structural Engineering Review* 7(3): 181-94.

Tonias, Demetrios E. 1995. *Bridge engineering: design, rehabilitation, and maintenance of modern highway bridges.* New York: McGraw-Hill.

Wang, Chu-Kia, and Charles G. Salmon. 1992. *Reinforced concrete design.* 5th ed. New York: Harper Collins.